

Metal Organic Frameworks as Dual Functional
Adsorbent/Catalysts for Plasma Air Purification Systems

Mitra Bahri

A Thesis

in

the Department of

Building, Civil and Environmental Engineering

Presented in Partial Fulfillment of the Requirements

For the Degree of Doctor of Philosophy at

Concordia University

Montreal, Quebec, Canada

December 2016

© Mitra Bahri, 2016

CONCORDIA UNIVERSITY
SCHOOL OF GRADUATE STUDIES

This is to certify that thesis prepared

By: Mitra Bahri

Entitled: Metal Organic Frameworks as Dual Functional
Adsorbent/Catalysts for Plasma Air Purification Systems

and submitted in partial fulfillment of the requirements for the degree of
Doctor of Philosophy

complies with the regulations of the University and meets the accepted standards with respect to originality and quality.

Signed by the final examining committee:

Dr. W. Ghaly Chair

Dr. Z. Hashisho External Examiner

Dr. A. Dolatabadi External to Program

Dr. C. Mulligan Examiner

Dr. L. Wang Examiner

Dr. F. Haghghat Thesis Co-Supervisor

Dr. S. Rohani Thesis Co-Supervisor

Approved by

Chair of Department or Graduate Program Director

December 2016

Dean of Faculty

Abstract

Metal Organic Frameworks as Dual Functional Adsorbent/Catalysts for Plasma Air Purification Systems

Mitra Bahri, Ph.D.

Concordia University, 2016

Indoor air pollution is responsible for the annual premature death of millions of people worldwide. Volatile organic compounds (VOCs) are among these pollutants with proven detrimental effects on occupants' health. Plasma-based methods' capabilities for VOCs degradation have motivated designers to employ these methods for purifying indoor air environment. It has been demonstrated that utilizing a dual functional adsorbent/catalyst (DFA/C) in a plasma system can significantly enhance the VOCs removal and the system's energy efficiency. However, selecting an appropriate DFA/C has remained a challenge.

For the first time, this research attempted to utilize metal organic frameworks (MOFs) as DFA/Cs for a plasma-driven catalytic reactor. Accordingly, three different MOFs, MIL-101 (MIL: Material Institute Lavoisier), MIL-53, and CPM-5 (CPM: Crystalline Porous Material-5) were synthesized through microwave and solvothermal methods. Furthermore, for the first time, a mechanochemical method was developed to synthesize CPM-5. To test the performance of the developed MOFs, a non-thermal plasma dielectric barrier discharge (DBD) system was designed, set-up and calibrated. Several adsorption and oxidation experiments were performed to study the physical and chemical behaviors of these MOFs for the removal of toluene and isobutanol. Also, the effect of the presence of humidity on the adsorption/oxidation capacities of MOFs was investigated.

Further analyses were carried out to study the surface characteristic of the developed MOFs using X-ray diffraction (XRD), scanning electron microscopy (SEM), BET surface area analysis, and thermogravimetric analysis (TGA). The results for microwave-synthesized MIL-53 and CPM-5 and also solvothermal-synthesized MIL-101 showed a good crystallinity, very high specific surface area (S_{Langmuir} : 1275-3747 m²/g), and acceptable thermal stability. In the case of mechanochemical-synthesized CPM-5, the TGA analysis showed a similar thermal stability

compared to the microwave-synthesized CPM-5. However, the SEM micrographs showed a formation of different morphology of crystallites. Also, the surface area of the mechanochemical-synthesized CPM-5 was lower than the one synthesized by the microwave method.

The adsorption isotherms of toluene and isobutanol demonstrated the physisorption of these MOFs. This result was also confirmed by TGA characterization of samples before and after toluene adsorption. In addition, oxidation evaluation studies exhibited VOCs removal potential over these MOFs. MIL-101 and MIL-53 exhibited superior adsorption and oxidation ability than CPM-5 in most cases. Results also showed higher adsorption capacity of MIL-101 than MIL-53 in dry conditions but almost the same oxidation efficiency. Nevertheless, adsorption/oxidation capacities of MIL-53 surpassed MIL-101 in the presence of 30% relative humidity. Moreover, Fourier transform infrared spectroscopy (FTIR) showed the stable structure of the examined MOFs after plasma-catalytic reactions, which indicated they were easy to be regenerated.

During the course of plasma-catalytic oxidation of toluene and isobutanol, different organic by-products and ozone were detected. Results showed utilization of a MOF as catalyst in the plasma system can reduce the downstream ozone concentration. Moreover, the presence of humidity suppressed the amount of ozone generation.

In conclusion, results demonstrated the potential capacity of MIL-53 and MIL-101 as DFA/Cs in plasma-catalyst air purification system.

Dedication

To:

My beloved parents, Eissa and Rouhangiz

For their unconditional love and support from the very first day and their warmest spiritual support in the toughest days of my life

My dearest love, Alireza

For his endless love, ongoing encouragement to follow my dreams, always being by my side, and his heartfelt assistance throughout all arisen hardships

My amazing siblings, Amir, Mehrab and Maryam

For being the first and best friends of my life and for their continuous support, spiritually and materially

And

My little angel, Jina

The most fabulous gift of God to my life

Acknowledgment

First and foremost, I would like to express my sincere gratitude to my supervisor, Professor Fariborz Haghighat, for accepting me as a member of his Energy & Environment research team. He assured me of his full support to work on this interdisciplinary project and gave me intellectual freedom in the research path that I had chosen. He kept his office door open whenever I needed his precious advice and I continuously benefited from his wise guidance.

I am deeply grateful to Professor Sohrab Rohani who accepted to co-supervise this research. He offered me an opportunity to use the resources and facilities in his research labs in the Department of Chemical and Biochemical Engineering at Western University. The time that I spent there consolidated my primary steps throughout the research.

My sincere gratitude also goes to Professor Hossein Kazemian, who enlightened the first glance of research on green the chemistry, which I used for a part of my work. His warm encouragement, scientific knowledge and invaluable comments were always helpful and a motivation engine for me.

I owe a debt of gratitude to Dr. Chang-Seo Lee for her valuable suggestions and useful feedback during the course of my research. She provided a friendly atmosphere in the lab and I benefited a lot from the stimulating discussions during our meetings.

I am indebted to Mr. Luc Demers, Mr. Josef Hrib, and Ms. Hong Guan, the experienced technicians of the Department of Building, Civil & Environmental Engineering at Concordia University. My job would have undoubtedly been more difficult without their constant technical assistance, advice and valuable supports.

My gratitude also goes to Professor Michelle Nokken and Professor Maria Elektorowicz who allowed me to utilize some of the facilities in their research Lab.

My very sincere thanks to Professor Pierre-Luc Girard-Lauriault and Professor Sylvain Coulombe from the Department of Chemical Engineering at McGill University, who helped me with their great scientific knowledge in plasma science throughout my study.

During the five-year-period of my study, I was fortunate to work with valuable colleagues and amazing friends: Dr. Ali Gholizadeh Touchei, Dr. Lexuan Zhong, Dr. Salman Bukhari, Esmael Kariminezhed, Donya Farhanyan, Alireza Aghighi, Zahra Shayegan, Alireza Haghghatmamaghani, Zahra Jandaghian, Oluchi Okoro, and lots of other friends who motivated and helped me during my research.

I appreciate the technical help and assistance of Dr. Bahareh Khalili Najafabadi and Jenna Marie Skieneh at Western University, and also, Mr. Armando R. Garcia and Dr. Daniel J. Burnett from Surface Measurement Systems during the DVS experiments.

I acknowledge the funding I received towards my PhD from Concordia University, Natural Sciences and Engineering Research Council of Canada (NSERC), and Circul-Aire, Inc., and l'Institut de recherche Robert-Sauvé en santé et en sécurité du travail (IRSST) through different grants and programs.

Finally, I would like to sincerely thank my thesis committee Dr. Catherine Mulligan, Dr. Leon Wang, Dr. Ali Dolatabadi, and Dr. Zaher Hashisho for their interest in my work and their very constructive questions and insightful comments.

Contribution of Authors

Chapters 1 and 2

Article Title: Plasma-Based Indoor Air Cleaning Technologies: State of the Art-review
Authors: Mitra Bahri, Fariborz Haghighat
Article Status: Published, CLEAN-Soil, Air, Water
Description: Mitra Bahri compiled and wrote the paper. Professor Fariborz Haghighat supervised the research and revised various drafts of the paper. The content of this paper is used as a part of chapters 1, 2 and 7.
Bahri, Mitra, and Fariborz Haghighat. "Plasma-Based Indoor Air Cleaning Technologies: The State of the Art-Review." <i>CLEAN-Soil, Air, Water</i> 42, No. 12 (2014): 1667-1680.

Chapter 3

Article Title: Impact of Design Parameters on the Performance of Non-Thermal Plasma Air Purification System
Authors: Mitra Bahri, Fariborz Haghighat, Sohrab Rohani, Hossein Kazemian
Article Status: Published, Chemical Engineering Journal
Description: Mitra Bahri performed the experiments, analyzed the data and wrote the paper. Professor Fariborz Haghighat and Professor Sohrab Rohani supervised the research. Various drafts of the paper were reviewed by Professor Fariborz Haghighat, Professor Sohrab Rohani and Professor Hossein Kazemian.
Bahri, Mitra, Fariborz Haghighat, Sohrab Rohani, and Hossein Kazemian. "Impact of design parameters on the performance of non-thermal plasma air purification system." <i>Chemical Engineering Journal</i> , 302 (2016): 204-212.

Chapter 4

Article Title: Mechanochemical synthesis of CPM-5: A Green Method
Authors: Mitra Bahri, Hossein Kazemian, Sohrab Rohani, Fariborz Haghighat
Article Status: In Press, Chemical Engineering Journal
Description: Mitra Bahri conducted the experiments and wrote the paper. Professor Fariborz Haghighat and Professor Sohrab Rohani supervised the research. Professor Hossein Kazemian advised on methods of experiments and characterization. Professor Hossein Kazemian, Professor Fariborz Haghighat and Professor Sohrab Rohani revised the content of various drafts.
Bahri, Mitra, Hossein Kazemian, Sohrab Rohani, and Fariborz Haghighat. "Mechanochemical synthesis of CPM-5: A Green Method." <i>Chemical Engineering & Technology</i> 40, No.1 (2017): 88-93.

Chapter 5

Article Title: A Comparative Study on Metal Organic Frameworks for Indoor Environment Application: Adsorption Evaluation
Authors: Mitra Bahri, Fariborz Haghighat, Hossein Kazemian, Sohrab Rohani
Article Status: In Press, Chemical Engineering Journal
Description: Mitra Bahri performed experiments, analyzed the samples and data, and wrote the paper. Professor Hossein Kazemian advised on methods of experiments and contributed in performing a part of tests. The research was supervised by Professor Fariborz Haghighat and Professor Sohrab Rohani. Various drafts of the paper were reviewed by Professor Fariborz Haghighat, Professor Sohrab Rohani and Professor Hossein Kazemian.
Bahri, Mitra, Fariborz Haghighat, Hossein Kazemian, and Sohrab Rohani. "A Comparative Study on Metal Organic Frameworks for Indoor Environment Application: Adsorption Evaluation." <i>Chemical Engineering Journal</i> (2016), http://dx.doi.org/10.1016/j.cej.2016.10.004 .

Chapter 6

Article Title: Metal Organic Frameworks for Gas-Phase VOCs Removal in a NTP-Catalytic Reactor
Authors: Mitra Bahri, Fariborz Haghighat, Sohrab Rohani, Hossein Kazemian
Article Status: Submitted for possible publication in Chemical Engineering Journal
Description: Mitra Bahri performed the experiments and wrote the paper. The research was supervised by Professor Fariborz Haghighat and Professor Sohrab Rohani. Various drafts of the paper were reviewed by Professor Fariborz Haghighat, Professor Sohrab Rohani, and Professor Hossein Kazemian.
Bahri, Mitra, Fariborz Haghighat, Hossein Kazemian, and Sohrab Rohani. "Metal Organic Frameworks for Gas-Phase VOCs Removal in a NTP-Catalytic Reactor." <i>Chemical Engineering Journal</i> (Submitted, November, 2016).

Table of Contents

List of Tables	xiv
List of Figures	xv
Nomenclature	xviii
List of Abbreviations	xviii
List of Symbols	xx
Chapter 1.....	1
1. Introduction	1
1.1 Problem Statement.....	1
1.2 Techniques for VOC Abatement	2
1.2.1 Adsorption.....	2
1.2.2 Photocatalytic oxidation (PCO)	2
1.2.3 Plasma-based methods.....	4
1.3 Motivation and Objective	5
1.4 Approach and Methodology	6
1.5 Boundary of the Research.....	7
1.6 Statement of Novelty.....	8
1.7 Thesis Outline and Organization	8
Chapter 2.....	10
2. Literature Review	10
2.1 Part 1: Plasma-based Air cleaners.....	10
2.1.1 Introduction	10
2.1.2 Thermal Plasma.....	10
2.1.3 Non-thermal Plasma (NTP)	11
2.1.4. Plasma Catalyst	20

2.2 Part 2: Metal Organic Frameworks	35
2.2.1 Introduction	35
2.2.2 Structure of MOFs.....	36
2.2.3 MOFs as Adsorbent.....	38
2.2.3 MOFs as Catalyst.....	46
2.2.4 Synthesis of MOFs.....	47
2.3 Summary and Research Direction.....	48
Chapter 3.....	50
3. Impact of Design Parameters on the Performance of Non-Thermal Plasma Air Purification System	50
Connecting Statement	50
3.1 Introduction	50
3.2 Experimental Setup and Apparatus	53
3.3. Results and Discussion.....	56
3.3.1 Effect of residence time	56
3.3.2 Effect of electrode configuration.....	59
3.3.3 Effect of reactor size	62
3.4 Conclusion.....	64
Chapter 4.....	66
4. Mechanochemical synthesis of CPM-5: A Green Method	66
Connecting Statement	66
4.1 Introduction	67
4.2 Materials and Methods.....	68
4.3. Results and Discussion.....	69
4.3.1 The effect of metal balls/reactant ratio.....	69
4.3.2 The effect of oscillation parameters	70
4.3.3 Effect of thermal condition	71

4.3.4 Effect of washing.....	73
4.3.5 Further characteristic analysis	74
4.4 Conclusion.....	76
Chapter 5.....	78
5. A Comparative Study on Metal Organic Frameworks for Indoor Environment Application: Adsorption Evaluation.....	78
Connecting statement.....	78
5.1 Introduction	79
5.2 Experimental.....	81
5.2.1 Synthesis and Preparation of Materials.....	81
5.2.2 Materials characterization	84
5.2.3 Apparatus and method	84
5.2.4 Efficiency Evaluation	87
5.3 Result and Discussion.....	87
5.3.1 MOF Characterization	87
5.3.2 Adsorption isotherms	90
5.3.3 Breakthrough curves and influence of relative humidity on adsorption capacity	95
5.3.4 Thermo-gravimetric analysis (TGA) characterization.....	99
5.4 Conclusion.....	101
Chapter 6.....	102
6. Metal Organic Frameworks for Gas-Phase VOCs Removal in a NTP-Catalytic Reactor	102
Connecting statement.....	102
6.1 Introduction	102
6.2 Experimental.....	104
6.2.1 Experimental set-up and measurement apparatus	104
6.2.2 Catalysts and reagents	108

6.2.3 Catalytic performance evaluation for VOCs adsorption and oxidation	108
6.2.4 Catalyst Characterization	109
6.3 Results and Discussion	110
6.3.1 Adsorption capacities of catalysts	110
6.3.2 VOCs removal efficiency at dry condition.....	111
6.3.3 Effect of relative humidity on VOCs removal efficiency	112
6.3.4 Organic by-products formation and effect of humidity.....	115
6.3.5 Ozone as by-product and the effect of humidity.....	117
6.3.6 Catalyst characterization	121
6.4 Conclusion.....	123
Chapter 7.....	125
7. Conclusions and Recommendations	125
7.1 Conclusion	125
7.2 Recommendation for Future Work.....	128
Bibliography	130
Appendix A.....	153
A. Repeatability of the system	153
Appendix B.....	154
B. Detailed values of standard deviation	154

List of Tables

TABLE 1.1 THE MAXIMUM EXPECTED CONCENTRATION, INDOOR SOURCES AND POTENTIAL HEALTH EFFECTS OF SOME VOCS	3
TABLE 2.1 RESULTS OF VOC REMOVAL, CO ₂ SELECTIVITY, ENERGY EFFICIENCY AND BY-PRODUCT FORMATION IN NTP REACTORS	18
TABLE 2.2 RESULTS OF VOC REMOVAL, CO ₂ SELECTIVITY, RESIDENCE TIME, ENERGY EFFICIENCY AND BY-PRODUCT FORMATION IN PLASMA CATALYST REACTORS	28
TABLE 2.3 COMPARISON OF VOC CONVERSION (50 PPM) BY UV/TiO ₂ , TiO ₂ AND UV IN A PPC REACTOR	31
TABLE 2.4 AN OVERVIEW OF STUDIES ON THE CSD PLASMA PROCESS.....	34
TABLE 2.5 GENERAL CHARACTERISTIC OF DIFFERENT ADSORBENTS AND/OR CATALYSTS IN PLASMA STUDIES	36
TABLE 2.6 THE EFFECT OF THE LENGTH OF ORGANIC LINKER ON THE SPECIFIC SURFACE AREA AND OPENING SIZE OF THE SYNTHESIZED MOF [138].....	38
TABLE 2.7 CHARACTERISTICS OF THE BENCHMARK MOFS, [122]	39
TABLE 2.8 COMPARISON BETWEEN THE EQUILIBRIUM AMOUNT OF ADSORBED BENZENE ON MIL-101 AND OTHER ADSORBENTS; ADAPTED FROM [35]	45
TABLE 2.9 COMPARISON BETWEEN THE DIFFUSION PARAMETERS OF BENZENE WITHIN THE MIL-101 AND OTHER ADSORBENTS, ADAPTED FROM [35]	46
TABLE 3.1 SPECIFICATION OF THE REACTORS	54
TABLE 4.1 SPECIFICATION OF THE APPLIED METHOD FOR THE MC SYNTHESIS OF CPM-5; EFFECT OF OSCILLATION FREQUENCY AND TIME, BALL NUMBER: 30, THERMAL TREATMENT:150°C/3H	70
TABLE 4.2 SPECIFICATION OF THE APPLIED METHOD FOR THE MC SYNTHESIS OF CPM-5; EFFECT OF THERMAL CONDITION; OSCILLATION FREQUENCY: 90 HZ, OSCILLATION TIME: 30 MIN, BALL NUMBER: 30.....	72
TABLE 4.3 SPECIFICATION OF THE METHOD APPLIED FOR THE MC SYNTHESIS OF CPM-5; EFFECT OF WASHING WITH DIFFERENT SOLVENTS; OSCILLATION FREQUENCY: 90 HZ, , THERMAL TREATMENT:150°C/3H.....	73
TABLE 4.4 THE BET/ LANGMUIR SURFACE AREA OF THE SYNTHESIZED CPM-5 BEFORE AND AFTER WASHING	75
TABLE 5.1 PROPERTIES OF CHEMICAL COMPOUNDS USED TO SYNTHESIZE THE MOFS	82
TABLE 5.2 SOME PHYSICOCHEMICAL PROPERTIES OF THE SELECTED VOCS	86
TABLE 5.3 EXPERIMENTAL PARAMETERS OF THE ADSORPTION TESTS	86
TABLE 5.4 PORE STRUCTURE PARAMETERS OF THE SYNTHESIZED CPM-5, MIL-53, AND MIL-101	90
TABLE 5.5 THE MAXIMUM SORPTION CAPACITY OF TOLUENE AND ISOBUTANOL ON CPM-5, MIL-53 AND MIL-101 IN DRY AIR (RH=0%) AND HUMID AIR (RH=30%) CALCULATED ACCORDING TO EQUATION (2)	98
TABLE 6.1 DETECTED ORGANIC COMPOUNDS DOWNSTREAM OF THE PLASMA REACTOR DURING THE OXIDATION OF TOLUENE AND ISOBUTANOL IN DRY CONDITION (RH=0%) AND HUMID CONDITION (RH=30%)	117
TABLE B.1 STANDARD DEVIATION OF OZONE FOR DIFFERENT SIE (JL-1); IE SIZE: L, L/2, AND L/4; GE: SS-T, SS-F, AL, AND AG; REACTOR#1	155

List of Figures

FIGURE 2.1 CONFIGURATION OF THE MOST COMMON NTP REACTORS	12
FIGURE 2.2 SCHEMATIC DIAGRAM OF PLASMA REACTORS: (A) IN PLASMA CATALYST (IPC) REACTOR, AND (B) POST PLASMA CATALYST	20
FIGURE 2.3 SCHEME OF THE POSSIBLE REACTIONS IN (A) PLASMA ZONE AND (B) CATALYST ZONE ON THE SURFACE OF THE CATALYST.....	26
FIGURE 2.4 SCHEMATIC DIAGRAM FOR A CSD PLASMA CATALYTIC REACTOR	32
FIGURE 2.5 OPERATING DIAGRAM OF PLASMA DISCHARGE- TIME IN A CSD PLASMA REACTOR.....	33
FIGURE 2.6 BREAKTHROUGH CURVES OF (A) TETRAHYDROTHIOPHENE (THT), (B) BENZENE, (C) DICHLOROMETHANE (CH ₂ CL ₂), ETHYLENE OXIDE (ETO) ADAPTED FROM [122]	40
FIGURE 2.7 A VIEW OF THE THREE DIMENSIONAL, CAGE-WITHIN-CAGE ARCHITECTURE OF CPM-5, ADAPTED FROM [146].....	42
FIGURE 2.8 BREATHING PHENOMENON UPON THE HYDRATION/ DEHYDRATION OF MIL-53. LEFT: MIL-53 (HYDRATED), AND RIGHT: MIL-53 (DEHYDRATED), ADAPTED FROM [148]	43
FIGURE 2.9 LEFT: STRUCTURE OF THE MIL-101(CR), RIGHT: THE CORRESPONDING INORGANIC SUBUNIT OF MIL-53. METAL, OXYGEN, AND CARBON ATOMS ARE SHOWN IN GREEN, RED, AND BLACK, RESPECTIVELY, TERMINAL WATER MOLECULES AND FLUORINE ARE SHOWN IN GRAY. ADAPTED FROM [140]	44
FIGURE 3.1 SCHEMATIC DIAGRAM OF THE PLASMA SET-UP; (A) COMPRESSED AIR, (B) PRESSURE REGULATOR, (C) MASS FLOW CONTROLLER (MFC), (D) DBD REACTOR, (E) HIGH VOLTAGE GENERATOR ARRAY, (F) OZONE MONITOR, AND (G) EXHAUST	53
FIGURE 3.2 CONFIGURATION OF THE INNER ELECTRODES	54
FIGURE 3.3 LEFT PANEL: THE SCHEMATIC DIAGRAM OF THE HIGH VOLTAGE POWER SUPPLY; (A) AC POWER, (B) FUNCTION GENERATOR, (C) AC POWER AMPLIFIER, (D) HIGH VOLTAGE TRANSFORMER BOX, (E) OSCILLOSCOPE, (F) DBD REACTOR, AND (G) HIGH VOLTAGE PROBE. RIGHT PANEL: THE BLOCK DIAGRAM OF THE HIGH VOLTAGE TRANSFORMER BOX; (H) COIL, (I) 10 KΩ RESISTOR, (J) 530 KΩ RESISTOR, (K) 1 KΩ RESISTOR.....	55
FIGURE 3.4 EFFECT OF INCREASING THE RESIDENCE TIME (IE SIZE: L, L/2 AND L/4) ON THE REQUIRED POWER; GE: SS-T, SS-F, AL, AND AG; REACTOR#1	57
FIGURE 3.5 EFFECT OF INCREASING THE RESIDENCE TIME (IE SIZE: L, L/2, AND L/4) ON THE OZONE GENERATION; GE: SS-T, SS-F, AL, AND AG; REACTOR#1.....	58
FIGURE 3.6 EFFECT OF THE SPECIFIC INPUT ENERGY ON THE RATE OF OZONE GENERATION; IE SIZE: L, L/2 AND L/4, GE: SS-T, SS-F, AL, AND AG; REACTOR#1.....	60
FIGURE 3.7 FORMATION OF MICRO-DISCHARGES IN THE AIR-GAP INSIDE THE REACTOR, AS WELL AS CORONA DISCHARGES OUTSIDE OF THE REACTOR (A), AND THE EQUIVALENT ELECTRICAL CIRCUIT (B) DURING PLASMA GENERATION IN A DBD REACTOR	61
FIGURE 3.8 EFFECT OF INCREASING THE SIZE OF REACTOR ON THE RATE OF OZONE GENERATION; IE SIZE: L, AND L/4, GE: AG	62
FIGURE 3.9 EFFECT OF THE SPECIFIC INPUT ENERGY ON THE AMOUNT OF GENERATED OZONE; IE: 4L/3, L, L/2 AND L/4; GE: AL AND AG, REACTOR#2.....	63
FIGURE 3.10 COMPARISON BETWEEN THE AMOUNTS OF OZONE GENERATION IN REACTORS; IE: 4L/3, L, L/2 AND L/4; GE: AL AND AG; REACTOR#2.....	64
FIGURE 4.1 EFFECT OF BALL NUMBERS IN THE INTENSITY OF THE FORMED PEAKS; COMPARISON BETWEEN XRD PATTERNS OF SAMPLES #B-1, #B-2 AND #B-3, AND THE SIMULATED XRD PATTERN OF CPM-5.....	70
FIGURE 4.2 EFFECT OF BALL NUMBERS IN THE INTENSITY OF THE FORMED PEAKS IN THE RESULTED SAMPLES; COMPARISON BETWEEN XRDS OF SAMPLES #O-1, #O-2, #O-3, AND #O-4, AND THE SIMULATED XRD PATTERN OF CPM-5	71

FIGURE 4.3 EFFECT OF THERMAL CONDITION IN CHANGE PHASE OF PRECURSORS; COMPARISON BETWEEN XRDS OF FORMED SAMPLES IN 5 DIFFERENT STAGES: SAMPLES #T-AS, #T-3HR, #T-15H #T-FIN, AND #T-*, AND PRECURSORS: (IN(NO ₃) ₃ .XH ₂ O, AND TRIMESIC ACID).....	72
FIGURE 4.4 COMPARISON BETWEEN XRDS OF WASHED SAMPLES #W-1, #W-2, #W-3, #W-4, AND THE SIMULATED XRD PATTERN OF CM-5; EFFECT OF WASHING TREATMENT WITH DIFFERENT SOLVENTS ON THE FORMED CPM-5	74
FIGURE 4.5 THE SEM MICROGRAPHS OF CRYSTALLIZED CPM-5 SYNTHESIZED BY MC METHOD: SAMPLE #W-4	75
FIGURE 4.6 COMPARING THE TGA CURVES OF THE CPM-5 SAMPLES PREPARED BY MC AND MW METHODS.....	76
FIGURE 5.1 SCHEMATIC DIAGRAM OF THE ADSORPTION APPARATUS.....	85
FIGURE 5.2 XRD PATTERNS OF MIL-53, CPM-5, AND MIL-101	88
FIGURE 5.3 SEM IMAGES OF FULLY CRYSTALLIZED SYNTHESIZED PARTICLES; MIL-53 (UP) SCALE: 10 μM, CPM-5 (MIDDLE), SCALE: 5 μM; MIL-101 (DOWN), SCALE: 3 μM	89
FIGURE 5.4 N ₂ ADSORPTION ISOTHERMS OF CPM-5, MIL-53 AND MIL-101. DATA OBTAINED BY A BET ANALYZER ..	91
FIGURE 5.5 DYNAMIC ADSORPTION-DESORPTION ISOTHERMS OF ISOBUTANOL OVER CPM-5, MIL-53, AND MIL-101. RESULTS ARE OBTAINED BY DVS, ONE (1) CYCLE, AND STEP SIZE: 2H. 48 HOURS OF WAIT IS APPLIED BEFORE DESORPTION TO REACH EQUILIBRIUM.	93
FIGURE 5.6 DYNAMIC ADSORPTION-DESORPTION ISOTHERMS OF ISOBUTANOL OVER CPM-5, MIL-53, AND MIL-101; RESULTS ARE OBTAINED BY DVS; 2 CYCLES, STEP SIZE: 2H, AND 2H OF WAIT AFTER EACH ADSORPTION.	94
FIGURE 5.7 ADSORPTION BREAKTHROUGH CURVES OF ISOBUTANOL OVER MIL-101, MIL-53 AND CPM-5 IN DRY AIR	95
FIGURE 5.8 ADSORPTION BREAKTHROUGH CURVES OF TOLUENE OVER MIL-101, MIL-53 AND CPM-5 IN DRY AIR ..	95
FIGURE 5.9 BREAKTHROUGH BEHAVIOR OF TOLUENE ON MIL-101, MIL-53, AND CPM-5 IN THE ABSENCE OF HUMIDITY (DRY AIR) AND THE PRESENCE OF HUMIDITY (RH: 30%); T: 21°C, FLOW RATE: 0.6L/MIN, CAT: 0.2G.	96
FIGURE 5.10 BREAKTHROUGH BEHAVIOR OF ISOBUTANOL ON MIL-101, MIL-53, AND CPM-5 IN THE ABSENCE OF HUMIDITY (DRY AIR) AND THE PRESENCE OF HUMIDITY (RH: 30%); T: 21°C, FLOW RATE: 0.6L/MIN, CAT: 0.2 G.	97
FIGURE 5.11 TGA AND FIRST DERIVATIVE CURVES OF CPM-5, MIL-53, AND MIL-101 BEFORE AND AFTER TOLUENE ADSORPTION.....	100
FIGURE 6.1 SCHEMATIC DIAGRAM OF THE SET-UP; (A) COMPRESSED AIR, (B) REGULATOR, (C) CONTROL VALVE, (D) WATER BUBBLER, (E) MASS FLOW CONTROLLERS, (F) SYRINGE PUMP, (G) REACTOR, (H) ADSORPTION TUBES, (I) SAMPLING PUMP, (J) HUMIDITY CONTROLLER, (K) OZONE MONITOR	105
FIGURE 6.2 THE DBD REACTOR.....	107
FIGURE 6.3 SCHEMATIC OF THE HIGH VOLTAGE APPARATUS; (A) AC POWER, (B) FUNCTION GENERATOR, (C) AC POWER AMPLIFIER, (D) HIGH VOLTAGE TRANSFORMER BOX, (E) OSCILLOSCOPE, (F) DBD REACTOR, AND (G) HIGH VOLTAGE PROBE	107
FIGURE 6.4 ADSORPTION CAPACITY OF TOLUENE AND ISOBUTANOL OVER CPM-5, MIL-53 AND MIL-101 IN: DRY AIR (RH=0%), AND HUMID AIR (RH=30%).	110
FIGURE 6.5 REMOVAL EFFICIENCY OF TOLUENE OVER MIL-53, MIL-101, CPM-5, AND IN THE ABSENCE OF CATALYST (NTP)	112
FIGURE 6.6 REMOVAL EFFICIENCY OF ONE PPM TOLUENE OVER MIL-53, MIL-101, CPM-5 AS CATALYST IN HUMID AIR (RH=30%).	113
FIGURE 6.7 REMOVAL EFFICIENCY OF ONE PPM ISOBUTANOL OVER MIL-53, MIL-101, CPM-5 AS CATALYST IN HUMID AIR (RH=30%).	114
FIGURE 6.8 GC/MS CHROMATOGRAMS OF ORGANIC BY-PRODUCTS DURING PLASMA-CATALYST TREATMENT OF TOLUENE (UP) AND ISOBUTANOL (DOWN) OVER MIL-53, MIL-101, CPM-5, AND NTP ALONE.....	116
FIGURE 6.9 OZONE CONCENTRATION DOWNSTREAM OF THE REACTOR DURING THE PLASMA-CATALYST TREATMENT OF TOLUENE OVER MIL-53, MIL-101, CPM-5, AND NTP; INPUT VOLTAGE: 17.6±0.3 KVP-P	119

FIGURE 6.10 OZONE CONCENTRATION DOWNSTREAM OF THE REACTOR DURING PLASMA-CATALYST TREATMENT OF ISOBUTANOL OVER MIL-53, MIL-101, CPM-5, AND NTP; INPUT VOLTAGE: 16.8 ± 0.1 KVP-P	119
FIGURE 6.11 A COMPARISON BETWEEN THE OZONE REMOVAL PERFORMANCE OF FRESH AND SATURATED MIL-53 DURING A PLASMA-CATALYST TREATMENT OF ISOBUTANOL, RH=30%, INPUT VOLTAGE: 16.8 ± 0.1 KVP-P ...	120
FIGURE 6.12 FTIR SPECTRA OF MIL-53 BEFORE CATALYTIC REACTION (FRESH), AFTER 96 HOURS NTP-CATALYST TREATMENT OF ISOBUTANOL IN THE PRESENCE OF 30%RH (SATURATED), AND AFTER REGENERATION FOR 48 HOURS (REGENERATED).....	121
FIGURE 6.13 FTIR SPECTRA OF MIL-101 BEFORE CATALYTIC REACTION (FRESH), AFTER 96 HOURS NTP-CATALYST TREATMENT OF ISOBUTANOL IN THE PRESENCE OF 30%RH (SATURATED), AND AFTER REGENERATION FOR 48 HOURS (REGENERATED).....	122
FIGURE 6.14 FTIR SPECTRA OF CPM-5 BEFORE CATALYTIC REACTION (FRESH), AFTER 96 HOURS NTP-CATALYST TREATMENT OF ISOBUTANOL IN THE PRESENCE OF 30%RH (SATURATED), AND AFTER REGENERATION FOR 48 HOURS (REGENERATED).....	122
FIGURE A.1 THE RESULTS OF THE REPEATABILITY OF TESTS; REACTOR#1; SS-T MESH AS GROUND ELECTRODE; IE: L & L/2	153

Nomenclature

List of Abbreviations

<i>Abbreviations</i>	<i>Description</i>
AC	Activated carbon
AC	Alternating current
BDDT	Brunauer, Deming, Deming, and Teller
BET	Brunauer-Emmett-Teller
CCD	Crystallographic Data Centre
CPM-5	Crystalline porous material-5
CE	Conventional electrical
DFA/C	Dual functional adsorbent/catalyst
DMF	Dimethylformamide
DOH	Department of Health
DW	Deionized water
DVS	Dynamic vapor sorption
DW	Distilled water
DBD	Dielectric barrier discharge
DC	Direct current
DE	Dielectric
EPA	Environmental Protection Agency
ETSDR	Agency for Toxic Substances & Disease Registry
FTIR	Fourier transform infrared
GC/MS	Gas Chromatograph/Mass Spectrometer
GE	Ground electrode
HME	Health Metrics and Evaluation
HV	High voltage
IAQ	Indoor air quality
IB	Isobutanol

IPC	In plasma catalyst
IE	Inner electrode
L	Length
MIL-101	Materials of Institute Lavoisier-101
MIL-53	Materials of Institute Lavoisier-53
MOF	Metal organic framework
MC	Mechanochemical
MW	Microwave
NIOSH	National Institute for Occupational Safety and Health
NTP	Non-thermal plasma
OSHA	Occupational Safety & Health Administration standards
P	Power
PCO	Photocatalytic oxidation
PID	Photoionization detector
PPC	Post plasma catalyst
HV	High voltage
ppb	Parts per billion
ppm	Parts per million
RH	Relative humidity
SD	Surface discharge
SD	Standard deviation
SIE	Specific input energy
SSA	Specific surface area
T	Temperature
TGA	Thermo-gravimetical analysis
VOC	Volatile organic compound
WHO	World Health Organization
XRD	X-ray diffraction
SEM	Scanning electron microscopy
US	Ultrasound
UV	Ultra violet

List of Symbols

<i>English Symbol</i>	<i>Description</i>
Al	Aluminum
Ag	Silver paste
Conc.	Concentration ($\mu\text{g}/\text{m}^3$)
BTC	1,3,5-benzenetricarboxylate
C	Capacitance
C_{Total}	Total capacity
C_{down}	Downstream concentrations (mg m^{-3})
$C_{\text{Down,t}}$	Downstream concentrations (ppm)
C_{in}	Inlet concentration (ppm)
Cr	Chromium
C_s	Sorbent saturation capacity (%)
C_{up}	Upstream concentrations (mg m^{-3})
$C_{\text{Up,t}}$	Upstream concentrations (ppm)
D	Dipolar moment
DMF	N, N- dimethylformamide (DMF)
E_0	Field permittivity without dielectric
E	Field permittivity with the dielectric
E_c^{CSD}	Energy cost (kWhm^{-3})
EEc	Energy efficiency (kWhm^{-3})
EEi	Energy efficiency (g kWh^{-1})
eV	Electron volt
Fe	Iron
h	Hour
Hz	Hertz
H_2BDC	Benzene-1,4 dicarboxylic acid
I	Current (mA)
In	Indium

J	Joule
K	Kelvin
k	Kilo
M	Mega
M	Molar mass (g mol^{-1})
M _w	Molecular weight (g mol^{-1})
M _s	Total mass of sorbent (mg)
nm	Nanometer
P _{discharge}	Discharge power (kWh)
Q	Volumetric gas flow rate ($\text{m}^3\text{min}^{-1}$)
Q ₁	Flow rate in the storage step (m^3h^{-1})
q _s	Normalized adsorption capacity per area (mmol.m^{-2})
R(t)	Equivalent discharge resistance
R'(t)	Equivalent discharge resistance
S _{BET}	BET surface area ($\text{m}^2.\text{g}^{-1}$)
SIE	Specific input energy (J L^{-1})
SS-T	Stainless steel-Thick
SS-F	Stainless steel-Fine
t ₁	Storage period (h)
t ₂	Discharge period (h)
t _s	Time required to reach the defined breakthrough((min).
U	Voltage (kV)
V _{p-p}	Peak to peak voltage (kV)
W	watt
W _t	weight percent (wt%)

Greek Symbol

Description

Å	Angstrom
ε	Dielectric constant ($\epsilon = E_0/E$)
η	Conversion

μ	Micro
Ω	Ohm
ρ	Resistivity (Ω m)
\emptyset	Diameter (mm)
v	Bed volume
τ	Residence time
η_b	Adsorption capacity (mmol)
η_t	Single pass removal efficiency (%)
ν_{as}	Asymmetric vibrations (cm^{-1})
ν_s	Symmetric vibrations (cm^{-1})

Chapter 1

1. Introduction

1.1 Problem Statement

According to the March 2014 report of the World Health Organization (WHO), outdoor and household air pollution caused the premature death of more than seven million people worldwide in 2012, of which 4.3 million were the result of household pollutions. [1]. In other words, air pollution contributes to one-eighth of deaths in the world annually [2]. The statistics presented in a joint study in 2016 between the World Bank and the Institute for Health Metrics and Evaluation (IHME) also showed that air pollution was the fourth greatest fatal risk worldwide in 2013 and led to around US\$225 billion loss of labor income [3].

Since more than 60% of mortality is recorded annually from indoor air pollutions, there is a necessity for the purification of indoor environments, including residential buildings. A modern building ventilation system design, therefore, must take into account the health and comfort of the occupants. To reduce exposure to internal contaminants, outdoor air is brought into the building to dilute the contaminants and exhaust a portion to outdoors. However, the quantity of the outdoor air can have a direct negative effect on the building energy cost. There is a cost to heat, cool, humidify or dehumidify the outdoor air depending on the location and season.

A number of factors must be taken into consideration in selecting the most effective air cleaning system. They include long-term performance, minimum energy consumption, and minimum amount of unwanted by-products formation [4], [5]. Furthermore, the capability of the system to work in indoor conditions (ambient temperature, variable relative humidity and variety of pollutants) is an important parameter in selecting the system [6].

The system needs to protect occupants against chemical contaminants from numerous internal sources, as well as bio-contaminants from the occupants themselves. Among different pollutants,

volatile organic compounds (VOCs) are a group of biogenic/anthropogenic pollutants that can be emitted from several indoor sources [6]–[8]. The proven detrimental effects of these compounds to human health has been reported in several studies [9]–[11]. Table 1.1 shows the maximum expected concentration, indoor sources, and potential health effects of some VOCs.

1.2 Techniques for VOC Abatement

Although, the building mechanical ventilation and air conditioning system can provide a comfortable indoor environment, it is not capable of efficiently removing all chemical compounds present in indoor air when it is used alone. Therefore, other supportive techniques are needed to increase its performance. Thus far, several physical and chemical methods have been employed for the abatement of VOCs from indoor air. The application of the most common employed methods in indoor air is described as follows.

1.2.1 Adsorption

Adsorption is a physical technique in which the removal of VOCs is performed in the presence of an appropriate adsorbent [6], [12]. [13]. Activated carbon (AC) and zeolites are the most common adsorbents due to their high surface area and high storage capacity [14], [15]–[16]. Adsorption is a favorable method from the economical aspect of view; however, in this method VOCs removal is based on transferring the pollutants to solid phase rather than their destruction, which implies frequent replacement of the adsorbent medium [17].

1.2.2 Photocatalytic oxidation (PCO)

Photocatalytic oxidation (PCO), is one of the common chemical techniques used for destruction of VOCs [18]–[21]. In this process UV irradiance is employed to enhance the performance of a semiconductor, generally TiO_2 , as the catalyst so that different types of VOCs can be degraded to H_2O and CO_2 [17]. Despite the known advantages of PCO, generation of hazardous by-products, which can be even more harmful than the target pollutant (i.e. O_3 , CO and organic by-products), can be significant in this process[22]. Moreover, low efficiency and slow reaction rate are other deficiencies, which highlight the necessity of more studies to enhance the capability of this method for indoor environment application [23], [24].

Table 1.1 The maximum expected concentration, indoor sources and potential health effects of some VOCs

Compound	Formula	Indoor Conc. ($\mu\text{g}/\text{m}^3$)	Indoor Source	Potential Health Effect
Formaldehyde	HCHO	20	Pressed wood products (hardwood plywood wall paneling/article board, fiberboard), combustion sources and environmental tobacco smoke, other textiles, and glues, combustion gas	Eye, nose, and throat irritation; asthma; lung damage, nausea, wheezing and coughing; fatigue; skin rash; reactions. May cause cancer
1,2 Dichloroethane	$\text{CH}_2\text{Cl}=\text{CH}_2\text{Cl}$	1	Adhesives, cleaning products, paint/varnish/ finish removers, pesticides, wallpaper/ carpeting glue, paint/varnish/ finish removers	Drowsiness; nausea; dizziness and loss of consciousness; cumulative liver and kidney damage; immune system and nervous system toxicity
Trichloroethene	$\text{CHCl}=\text{CCl}_2$	1	Paint stripper, adhesive solvent, an ingredient in paints and varnishes	Narcosis; cumulative systemic toxicity; mutagen/Suspect carcinogen; Suspect teratogen; CNS damages, risk of reproductive and developmental health effects
Tetrachloroethene	$\text{CCl}_2=\text{CCl}_2$	10	Dry-cleaning of fabrics, paint and spot removers, water repellents, brake and wood cleaners, glues, and suede protectors	Cumulative liver and CNS damage; narcosis; reproductive effects including increased risks for spontaneous abortion, menstrual sperm disorders, and reduced fertility
Vinyl chloride	$\text{H}_2\text{C}=\text{CHCl}$	1	Production of polyvinyl chloride (PVC), water pipes, wire and cable coatings, packaging materials, furniture automobile upholstery, housewares and toys	Lung, liver and kidney cancer; Angiosarcoma; nervous system and immune system problems
Benzene	C_6H_6	5	Tobacco smoke, stored fuels and paint supplies, and automobile emissions in attached garages, certain plastics, glues, paints, furniture wax, resins, nylon and synthetic fibers, some types of rubbers, lubricants, dyes, detergents, drugs and pesticides	Human Carcinogen; leukemia; cumulative bone marrow damage; CNS depression; respiratory arrest; cardiovascular collapse; aplastic anemia; irritation

Compound	Formula	Indoor Conc. ($\mu\text{g}/\text{m}^3$)	Indoor Source	Potential Health Effect
Acetone	$(\text{CH}_3)_2\text{CO}$	60	Solvent in nail polish remover, particle board, paint removers, waxes, polishes, certain detergents and cleansers	Irritation of the eyes and respiratory tract; nervous system effects including headaches, lightheadedness, dizziness, unsteadiness and confusion; nervous system toxicity.
Toluene	$\text{C}_6\text{H}_5\text{CH}_3$	1	Paints, paint thinners, fingernail polish, lacquers, adhesives, rubber, some printing and leather tanning processes, tobacco smoke	Irritation of the eyes, respiratory tract, and skin; narcosis
Styrene	$\text{C}_6\text{H}_5\text{CH}=\text{CH}_2$	0.1–50	Emissions from building materials, consumer products, and tobacco smoke	Irritation of eyes, nose, throat, skin; CNS effects; narcosis; mutagen
Dichloromethane	CH_2Cl_2	5	Paint strippers, aerosol products, adhesives, spray paints, automotive cleaners, and varnish removers	Dizziness, headache, confusion, incoordination, drowsiness, adverse effects on the nervous system, risk for liver and kidney toxicity

Data are extracted from Department of Health (DOH), Environmental Protection Agency (EPA), Agency for Toxic Substances & Disease Registry (ATSDR), National Institute for Occupational Safety and Health (NIOSH) and Occupational Safety & Health Administration standards (OSHA) websites.

1.2.3 Plasma-based methods

In recent decades, the development of plasma-based methods, and their capabilities for VOCs destruction, has motivated their applications in indoor air purification. In a plasma process, a high electrical voltage is applied for the destruction of pollutants. However, incomplete oxidation and formation of harmful by-products (i.e. O_3 , CO , NO_x and other VOCs), and high level of energy consumption are the main disadvantages of this method [25], [26]. To solve this issue, a plasma catalytic process that incorporates the use of a catalyst in the plasma process is suggested. A higher VOCs removal efficiency and lower levels of by-product formation are the advantages of this method [27], [28]. Also, catalyst implementation in plasma reactors lowers the level of electricity consumption. Nevertheless, minimizing the by-products formation should still be considered very carefully. Due to a very low concentration of VOCs in indoor environment (usually in the order of sub ppm), energy optimization is an important challenge, when this technique is considered for

indoor air treatment [29]. In such condition, utilizing reactive adsorption processes can be a new approach to improve the performance of plasma air purification systems [30]. In this method, a medium with the ability of simultaneous adsorption and oxidation of VOCs is utilized in the plasma reactor. Such adsorber-oxidizers are not only favorable from an economic point of view, but they can also increase VOCs removal efficiency of the system [29].

1.3 Motivation and Objective

Selecting an appropriate medium with a high adsorption capacity and oxidation capability is an important challenge to achieve the best performance of VOCs removal in a plasma catalyst system. Significantly, more amounts of pollutants can be adsorbed on the catalyst surface as its storage capacity grows higher. Furthermore, the oxidation ability of the catalyst plays an important role in the VOCs removal performance. This suggests that an appropriate dual functional adsorbent/catalyst (DFA/C) is a good candidate for a plasma catalyst process.

As of now, different types of materials have been applied as DFA/Cs in plasma reactors [4], [28], [31]–[33], each of which has drawbacks including limited adsorption capacity, limitation in adsorbing different sizes and types of VOC molecules, inadequate catalytic properties, etc. These deficiencies have given rise to the use of new types of materials that can induce higher performance in plasma processes, especially at low concentration which exists in indoor environment.

Among several considered materials, metal organic frameworks (MOFs) are a new class of porous materials with uniform structures, high surface area, and high porosity [34] [35]. The application of MOFs in the adsorption of a wide range of differently structured and sized molecules has been studied [36] [34]. MOFs are also proposed to have the potential to be used as a catalyst in different applications [37], [38]. Yet, despite their unique characteristics, MOFs have not been considered for the oxidation of VOCs in air purifiers.

Based on the above-mentioned challenges, the main objective of this research is to develop MOFs as DFA/Cs with high adsorbent capacities and catalytic properties for a plasma-driven catalyst reactor. Accordingly, the following sub-objectives were specifically addressed in this research:

- 1) To design and implement a plasma-driven catalyst micro reactor set-up.
- 2) To synthesize three different MOFs with different methods.
- 3) To evaluate the adsorption capacity of VOCs on synthesized MOFs.
- 4) To evaluate the catalytic ability of MOFs in a plasma-catalytic reactor.

Toluene and isobutanol were selected as target VOCs in this study. Both of these compounds are commonly found in indoor environment and they may cause several health effects such as irritation of the eyes, nose skin, and respiratory system, narcosis, etc.

1.4 Approach and Methodology

To meet the aforementioned objectives of this research, the following approaches were applied in the course of the project:

Design and implement a plasma-driven catalyst micro reactor set-up.

- A high voltage plasma set-up with adjustable voltage and frequency was designed. Implementation, calibration and validation of the set-up were performed.
- The impact of different parameters including residence time, type and configuration of the electrodes, and reactor size on the energy density and the rate of ozone generation were studied.

Synthesize three different MOFs with different methods.

- Amongst several considered MOFs, three different MOFs, MIL-101 (MIL: Metal institute Lavoisier), MIL-53, and CPM-5 (CPM: Crystalline Porous Material-5), were identified and synthesized. Preparation of these catalysts was performed using hydrothermal and microwave methods. Beside the conventional techniques, a mechanochemical method was successfully developed for the CPM-5 preparation.
- To identify the type, specific surface area and thermal stability of the synthesized MOFs, characterization of synthesized samples was performed by means of different characterization methods, including X-ray Diffraction (XRD), Scanning Electron Microscopy (SEM), Thermogravimetric Analysis (TGA), and BET surface area and pore size analyzer.

Evaluate the adsorption capacity of VOCs on the synthesized MOFs.

- Adsorption isotherms and breakthrough behaviors of the synthesized MOFs were studied for one (1) ppm of two different VOCs including an aromatic compound (toluene) and an alcohol (isobutanol). The performed characterization tests were TGA, BET, XRD and SEM.
- The effect of the presence of humidity on the adsorption capacity of each MOF was investigated. Reversibility of the adsorption was also studied.

Evaluate the catalytic capacity of MOFs in the plasma-catalytic reactor.

- The removal efficiency of the prepared MOFs for the degradation of VOCs during plasma-catalytic reaction process was studied. The effect of humidity in the ability of MOFs for VOCs removal was investigated.
- Formation of organic by-products and ozone and also the ability of regeneration of the catalyst after a plasma-oxidation reaction were investigated.
- Different characterization and analytical instruments such as Fourier Transform Infrared Spectroscopy (FTIR), Gas Chromatograph/Mass Spectrometer (GC/MS), and VOCs Photoionization Detector (PID) were utilized during the experiments.

1.5 Boundary of the Research

- The objectives of this research were carried out in a small-scale (micro scale) reactor.
- Indoor environment contains a mixture of VOCs. Nevertheless, in this research, the removal performance of the DFA/C was considered for single VOCs.
- All experiments were performed under two conditions: at dry air and in the presence of 30% relative humidity.
- Energy optimization was not in the scope of this research.

1.6 Statement of Novelty

Although application of MOFs for VOCs adsorption and also in different catalytic reactions has been reported in previous studies, these materials have never been considered as DFA/Cs for removal of VOCs in air purifying systems. Here, developments viewed in isolation by earlier studies are considered together. Accordingly, for the first time three different MOFs were used as DFA/Cs and their adsorption and oxidation capacities were studied for removal of VOCs in a NTP-reactor.

Developing a new mechanochemical method for preparation of CPM-5 represents another main contribution of this study.

1.7 Thesis Outline and Organization

The present thesis is provided according to an article-integrated format, which is stipulated by the School of Graduate Studies at Concordia University. The structure consists of seven chapters based on one review paper and four research articles. The content of the literature review is used as a part of Chapters 1 and 2 and the four other research papers are presented as individual chapters.

Part 1 of Chapter 2 presents a comprehensive literature review on plasma-based methods, from thermal plasma to plasma-catalyst and their applications for VOCs removal in indoor environments. Different aspects such as reaction mechanisms, effect of the presence of humidity, advantages and deficiencies of each method are studied. Several types of reactors and catalysts are classified. Finally, the critical role of the presence of the catalyst is reviewed. In Part 2 of Chapter 2, pertinent literature on metal organic frameworks (MOFs) and general information about different structures of these materials, synthesis methods, characteristics and applications are presented.

Chapter 3 describes the design and implementation of a dielectric barrier discharge (DBD) plasma set-up. The impact of various design parameters such as reactor size, change in the residence time, configuration and type of electrodes on the energy performance of the system and ozone generation are investigated.

Chapter 4 presents the process of mechanochemical synthesizing of CPM-5. In this novel method, preparation of the catalyst is performed in the absence of solvent. The effect of several parameters such as oscillation frequency and time, and the number of metal balls used for milling, the thermal treatment of the samples after grinding and washing treatment of samples are intensively studied.

Chapter 5 reports synthesizing three target MOFs, MIL-101, MIL-53, and CPM-5 via conventional methods, hydrothermal and microwave methods. Characterization of these samples is performed and results are compared with previously reported studies. A comparative study in adsorption of one (1) ppm toluene and isobutanol as selected VOCs on these MOFs is performed. Adsorption isotherms, breakthrough behaviors, and adsorption reversibility of these MOFs are studied and the effect of the presence of humidity on the adsorption capacity of these MOFs is investigated.

Chapter 6 is dedicated to investigate the performance of MIL-101, MIL-53, and CPM-5 as DFA/Cs for gas-phase VOCs removal in a plasma-catalytic reactor. The adsorption and oxidation evaluations of these MOFs for the removal of one (1) ppm toluene and isobutanol are performed at both dry and humid conditions. Formation of ozone and different organic by-products are explored. And structural analysis of catalysts is performed before and after catalytic oxidation of VOCs to investigate the feasibility of the catalyst regeneration after the reaction.

Chapter 7 presents the outcome of all preformed experiments, analyses and the obtained results from this study. A summary of major findings is reported and recommendations for future work are proposed.

Chapter 2

2. Literature Review

2.1 Part 1: Plasma-based Air Cleaners

2.1.1 Introduction

Plasma-based methods refer to a series of processes in which a high voltage (HV) discharge is used for the destruction of pollutants [30], [39]–[42]. Development of plasma-based methods in recent decades has improved the performance of this technology and made it more cost-effective and applicable for applying as an air treatment method in sustainable and energy efficient buildings. This section reports the outcomes of a comprehensive literature review on the plasma-based air cleaner technologies, thermal to non-thermal plasma and plasma catalyst, and their application for VOCs removal in indoor environment. The reaction mechanism, effect of different parameters on the performance of the method, and abilities and limitations of these methods for indoor VOC removal are discussed. Different types of reactors and the most common used catalysts are classified. Finally, the role of the presence of the catalyst in VOCs decomposition and improving the non-thermal plasma efficiency is reviewed.

2.1.2 Thermal Plasma

In thermal plasma, a high electrical voltage and high current ($P \sim 1\text{kW}-50\text{MW}$) is applied to generate a plasma flame at atmospheric pressure in an active zone [41]. This HV discharge causes an initial excitation in the working gas, followed by ionization and generating of large amounts of reactive species, including ionized and dissociated radicals (>99% ionization). In this state, the temperature of the reactive species in the background gas can reach as high as 1000 K while the peak may reach up to 10,000 – 20,000 K ($T_{\text{peak}} \sim 1-2 \text{ eV}$) depending on the voltage, gas flow rate, and the source of plasma [43]–[45].

Thermal plasma is one of the processes for the removal of noxious compounds, especially VOCs, from industrial applications [44]. Using high electrical voltage and increasing the temperature results in generation of high fluxes of reactive species and consequently swift reaction rate and shorter response time for the reactor to start up. As a result, a smaller reactor could be used in thermal plasma technology [44]. Obtaining the full fragmentation of molecules and high specific activation are other advantages of thermal plasma [46]. However, consuming high amounts of electricity, which is an expensive source of energy, is a consideration against applying this method [44], [47]. On the other hand, in thermal plasma all particles including electrons, ions, atoms, and molecules in the background gas are at thermal equilibrium ($T_e \approx T_{ion} \approx T_{gas}$). Therefore, overheating the reaction media is inevitable [41]. Thermal plasma is applicable for wastes containing high concentration of organic components [44]. At low concentration levels however, this technology is not economical. As a result, the application of thermal plasma for indoor air treatment and its integration in the buildings mechanical ventilation system is practically impossible.

2.1.3 Non-thermal Plasma (NTP)

NTP technique, acts based on creating a quasi-neutral environment including, ions, radicals, electrons, neutrals and UV photons [48]. Because of the lower mass, electrons are accelerated selectively in the background. The temperature of these accelerated electrons can reach to about 10,000–250,000 K (1–25 eV) while the background gas is still at ambient temperature [49] ($T_e \gg T_{ion} \sim T_{gas}$). Therefore, the ionization of the molecules is significantly lower than thermal plasma (~1% ionization). The collision of electrons with molecules in the background gas, including oxygen, nitrogen and water vapor, results in producing excited bulk gas molecules (N_2^* , O_2^* , etc.). These excited molecules emit photon or heat to lose their energy. This energy forms reactive ions and radicals (i.e, $OH\cdot$ and $O\cdot$) which are unstable and contribute to the oxidation reactions [50].

Working in atmospheric pressure causes instability in NTP systems due to increase in the number of collisions and heat generation, which consequently leads the system to sparking and arcing. To prevent this problem, these systems commonly work in low pressure. Nevertheless, preventing the reaction media temperature from increasing, as a significant advantage of this method, has motivated scientists to develop NTPs for work in atmospheric pressure.

2.1.3.1 Non- thermal Plasma Reactors

Generally, classification of NTP reactors is based on the type of the employed discharge mode, such as dielectric barrier discharge (DBD), surface discharge (SD), direct current (DC) positive or negative corona discharge, pulsed corona discharge, ferroelectric pellet packed-bed reactor, plasma jet, etc. [49], [50]. Figure 2.1 illustrates the configuration of the most commonly used NTP reactors.

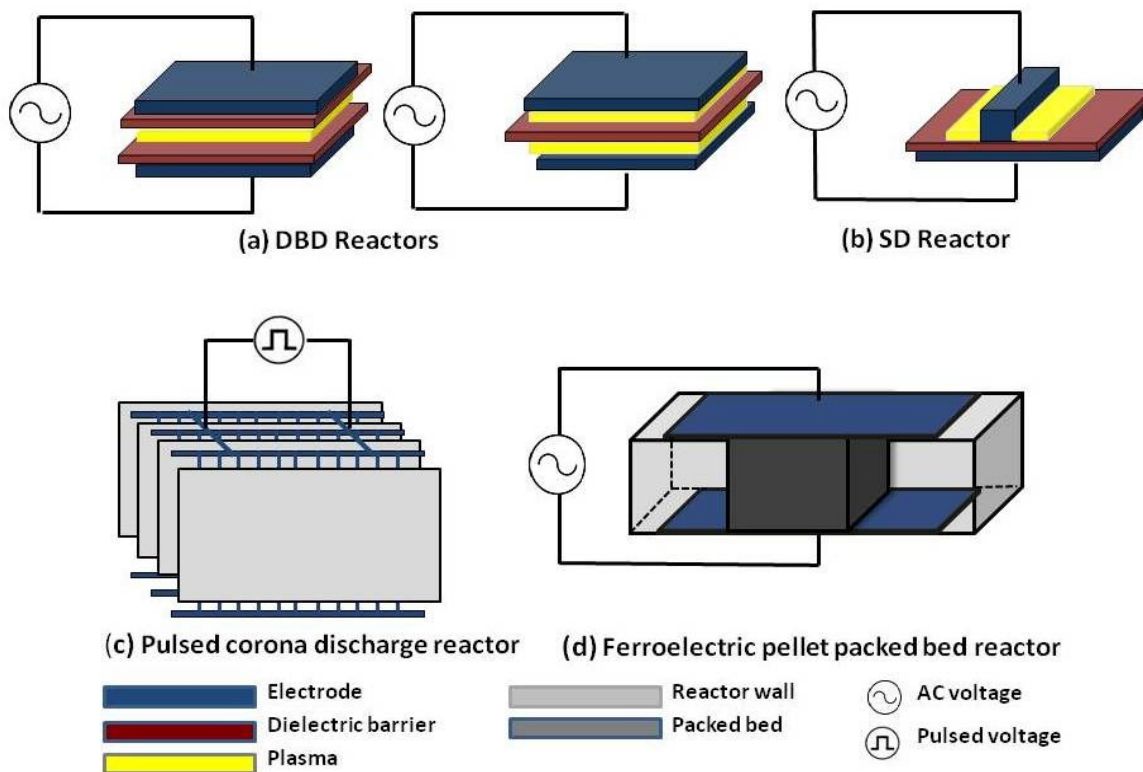


Figure 2.1 Configuration of the most common NTP reactors

Dielectric barrier discharge (DBD): DBD or silent discharge is one of the most common types of NTP reactors [51]–[54], (Figure 2.1.(a)). This reactor consists of at least one dielectric, such as glass, quartz, ceramic, alumina, teflon or mica between electrodes which plays a key role in the stabilizing NTP [52], [54]–[56]. Facile implementation, non-complicated reactor scale up, lower power consumption and higher energy efficiency are the most important advantages of this discharge mode compared to the other modes [52].

Surface discharge (SD): SD has a similar configuration to the DBD (Figure 2.1. (b)). Usually, in this type of reactor a dielectric barrier is attached to an electrode on one side and covered by a metallic cover on the other side [33]. Ceramic-based alumina can be used in this reactor. This reactor can be used for decomposition of VOCs; though, ozone accumulation without the possibility of its destruction restricts its application for the indoor environment [49].

Pulsed corona discharge: In this type of reactor voltage pulses applies in a fraction of a second between electrodes produces plasma [57], (Figure 2.1.(c)). The spark formation in this way can be prevented, which means a higher efficiency and longer lifetime of the reactor can be expected [50]. Pulse corona discharge can be applied for the indoor environment applications due to reduction of ozone formation [58].

Ferroelectric (dielectric) pellet packed-bed reactor: In this type of reactor, ferroelectric pellets (BaTiO₃, NaN₂O₂, MgTiO₄, CaTiO₃, SrTiO₃, PbTiO₃ and PbZrO₃-PbTiO₃) are used as packed-bed [59]–[61], (Figure 2.1.(d)). The efficiency of a dielectric to store more charge depends on the dielectric of used material. The ratio of the field permittivity without the dielectric (E_o) to the net field permittivity (E) with the dielectric is defined as dielectric constant ($\epsilon = E_o/E$). The larger the dielectric constant, the more charge can be stored. BaTiO₃ is the most commonly used metal oxide in this type of reactor due to its high dielectric constant ($2000 < \epsilon < 10,000$). The presence of packed bed makes a uniform distribution of gas and electrical discharge. However, pressure drop increase is a negative aspect that should be considered [50].

2.1.3.2 VOC Abatement in NTPs and Reaction Mechanism

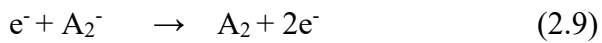
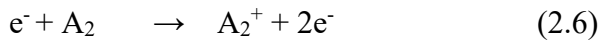
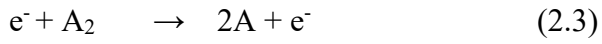
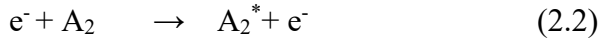
In a NTP process, in addition to the physical parameters (i.e. temperature, pressure, electron acceleration and mobility of ions), chemical reactions have a key role in the destruction of pollutants. As mentioned earlier, collision of accelerated electrons with background gaseous molecules generates reactive species as follows:



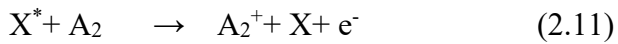
where X* represents different types of reactive species including N*, N₂*, O*, O₃*, OH*, etc. either in the form of radicals or ions. Eliasson and Kogelschatz (1991)[62] classified the main

plasma reactions between target pollutants (A, A₂, B) with the formed electrons and reactive species, as bellow:

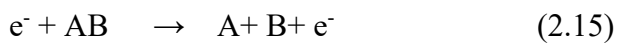
Electron/ Molecular reactions:



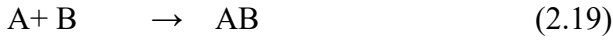
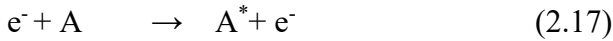
Atomic/Molecular reactions:



Decomposition reactions:



Synthesis reactions:



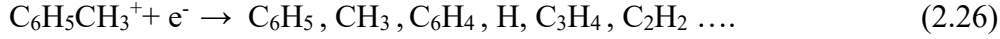
Chang and Chang [63] described the main destruction reactions of toluene in a NTP reactor with silent discharge mode in regards to reactions between toluene and reactive species in the following way:



Based on the reaction constant (k), the dominant pathway involved in toluene destruction, which leads to CO₂ and H₂O formation could be thought to be the reaction between toluene and OH radicals (eq. (2.22)) [41]. However, the concentration of the formed species also determine the kinetics of chemical reactions and thus the rate of toluene destruction. For instance, as the concentration of O₂ is expected to be several orders of magnitude higher than that of OH, the reaction between toluene and O₂ also plays an important role in toluene decomposition (eq. (2.23)). On the other hand, one can describe the reaction between toluene and the formed ions or electrons in the following way [42].

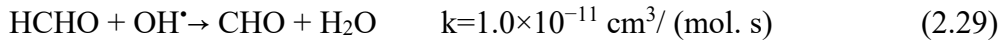
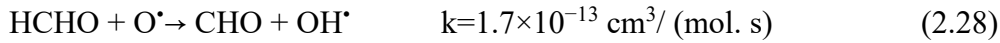
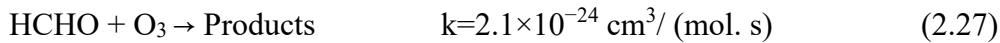


where X⁺ represents O⁺, O₂⁺, N⁺ or N₂⁺ ions. The density of these ions is much lower than radicals; nevertheless, because of their faster rates, ionic reactions have an important role in the VOCs degradation [42]. Furthermore, owing to high density of electrons, different types of radicals may be formed in the discharge zone [42]:



2.1.3.3 Impact of Humidity on the NTP Performance

Wan et al. [64], investigated the effects of the presence of relative humidity (0 to 70%) on the removal of 2.2 ppm formaldehyde (HCHO) in a DC corona discharge reactor. Results showed that despite the decrease in the formation of O₃, HCHO conversion increases as humidity increases. Accordingly, the most probable decomposition reactions of HCHO in the presence of oxidative plasma species (O₃, O[•], OH[•]) are:



According to the reaction constants, OH radicals play an important role in destruction of HCHO as compared to ozone. The same study for removal of 50 ppm toluene in a DBD Reactor showed that despite the positive role of the presence of water molecules in formation of OH radicals, increasing the relative humidity level (up to 80%) has a negative effect on the removal efficiency due to decreasing electron density and quenching of the reactive species in the reactor [56]. Therefore, humidity level plays a crucial role on the removal performance of NTP reactors.

2.1.3.4 Limitations of NTP Technology

The capability of NTP has been reported for abatement of a wide range of VOCs concentrations (1-10,000 ppm), acid gases (i.e NO_x, SO_x), particulate matters [65], and bacteria [66], [67] at ambient temperature. The main advantage of NTP are a lower energy requirement as compared to thermal plasma and high efficiency in removing particulate matters [32], [68], [69]. Table 2.1 summaries the VOCs removal and CO₂ selectivity in NTP reactors, the energy efficiency as well as by-product formation. The specific input energy (SIE, J L⁻¹) and energy efficiency (EE_i, g kWh⁻¹) are defined as:

$$\text{SIE} = \frac{60UI}{Q} \quad (2.30)$$

$$\text{EE}_i = \frac{3.6 C_{in} \cdot \eta \cdot M}{24.4 \text{ SIE}} \quad (2.31)$$

where, U is the applied voltage (kV); I is the discharge current (mA); Q is the gas flow rate (L min^{-1}); C_{in} and η are the inlet concentration (ppm) and the conversion of the compound, respectively; M indicates the compound molar mass (g mol^{-1}); 24.4 is the gas molar volume (L mol^{-1}) under the defined condition and finally 60 and 3.6 are the conversion coefficients.

As it can be seen from Table 2.1, despite the advantages of NTP, this method has poor energy efficiency especially for low VOCs concentrations. Relative humidity has a strong impact on the system performance. In addition, incomplete oxidation of target pollutants could result in formation of CO and some other organic by-products (i.e. formaldehyde) that are more hazardous to building's occupants than the target pollutant[25], [26]. Furthermore, the formation of NO_x and O_3 as a consequence of plasma inducing in NTP reactors is inevitable. These disadvantages have made this method impractical for indoor environment application

Table 2.1 Results of VOC removal, CO₂ selectivity, energy efficiency and by-product formation in NTP reactors

Ref.	Reactor type	Target pollutant	Carrier gas	Conc. (ppm)	Flow Rate (Lmin ⁻¹)	Removal efficiency (%)	CO ₂ yield (%)	SIE (J L ⁻¹)	EEi (g kWh ⁻¹)	Reported formed by-product	Concentration	
[70]	Corona	Toluene	Air	2000	1	90	N/A	N/A	26	Aerosol particles	N/A	
		Trichloroethylene				40			13	Aerosol particles, Cl ₂		
[71]	Wire cylinder puls	Toluene	Air	280	5	Up to 97	20	N/A	N/A	CO Aerosol	500 ppm N/A	
		Butyl acetate		120	20	Up to 75				CO	N/A	
[72]	Ferroelectric Pellet Packed-bed	Toluene	N ₂ + 20%O ₂	100	0.5	~85 ^a	~60 ^a	450 ^a	~2.6 ^c	For SIE _≥ 400J/L	CO	N/A
		CH ₂ Cl ₂		109		~85 ^a	~40 ^a		~2.6 ^c		CO, Formaldehyde, Acetic acid	
		Mix (Toluene+ CH ₂ Cl ₂)		100+109		N/A	~60 ^a		---		Chloroform (CHCl ₃) Benzene	
[73]	DBD	Toluene	N ₂ + O ₂	800	0.07	60	N/A	N/A	N/A	O ₃ , CO, CO ₂ , NOx (NO, NO ₂), Formic acid, Acetic acid, Benzene	N/A	
[64]	DC- Corona	Formaldehyde	Dry Air	2.2	6	42	N/A	80	0.05	O ₃	282 ppm	
			Air+ 30%RH			54			0.06		162 ppm	
			Air+ 70%RH			57			0.07		157 ppm	
[74]	DBD	Toluene	20% O ₂ + 80%N ₂	240	0.315	36	6	172	6.8 ^c	CO O ₃	8% 8 ppm	
[75]	DBD	Toluene	N ₂ , 5%O ₂	50	100	~ 52 ^a	61	600	0.6 ^c	CO	N/A	
			N ₂ , 5%O ₂ , 0.2%H ₂ O			73.1	72		0.8 ^c			
[76]	DBD	Acetone	Air+ N ₂	200	2.5	38	N/A	402	2.9	N/A	N/A	
		Benzene				56			5.8			
		Tetrachloroethylene				74			16.3			
		m-Xylene				98			13.9			
		Mix				N/A			29.3			

Ref.	Reactor type	Target pollutant	Carrier gas	Conc. (ppm)	Flow Rate (Lmin ⁻¹)	Removal efficiency (%)	CO ₂ yield (%)	SIE (J L ⁻¹)	EEi (g kWh ⁻¹)	Reported formed by-product	Concentration
[4]	DC-tooth wheel cylinder	BTX mix (Benzene, Toluene, p-Xylene)	Air	1.5	6	~ 60 ^a	~ 45 ^a	300	N/A	CO O ₃ NOx (NO, NO ₂ , N ₂ O, N ₂ O ₅) Formic acid, Benzaldehyde, Benzyl alcohol	>35% ^a 46.7 ppm (0, 1380 ppb, 0,0) N/A N/A
				1.4		~ 93 ^a					
				1.2		~ 100 ^a					
[69]	DC-Corona	Toluene	Dry air	0.5	10.8	70	N/A	60	0.09 ^c	O ₃ NO NO ₂	SE=10/L 49.9 ppm <10 ppb 1500 ppb
			Air+27% RH		10.8	~ 80 ^a	N/A		0.1 ^c	O ₃ NO NO ₂	
[77]	DC-Corona	Toluene	Dry air	0.5	10	46	N/A	28.8	0.12 ^c	For both dry and humid air Ozone Formic acid, Benzaldehyde Benzoic acid, Benzyl alcohol 4-Methyl-2-propyl furan 5-Methyl-2-Nitrophenol 3-Methyl-4-nitrophenol 4-Methyl-2-nitrophenol 4-Nitrophenol 2-Methyl-4,6-dinitrophenol	55-75 ppm ^a N/A
			Air+ 26%RH			57			0.15 ^c		
			Air+ 50%RH			26			0.07 ^c		

^a Approximate amounts extracted from graphs

^b Calculated by equation (28) data extracted from reference.

^c Calculated by equation (29) data extracted from reference.

2.1.4. Plasma Catalyst

To overcome the deficiencies of NTP, a combination of this method and catalyst, called plasma catalyst is proposed. In the plasma catalyst approach, the presence of catalyst and the synergic effect of plasma and catalyst enhances the removal efficiency and total oxidation of the components [27], [28]. This synergic effect results in higher removal efficiency compared to the sum of plasma and catalyst processes, when they are used separately [48], [71], [78], [79].

In a plasma catalyst reactor, catalyst and plasma can be combined in two different ways:

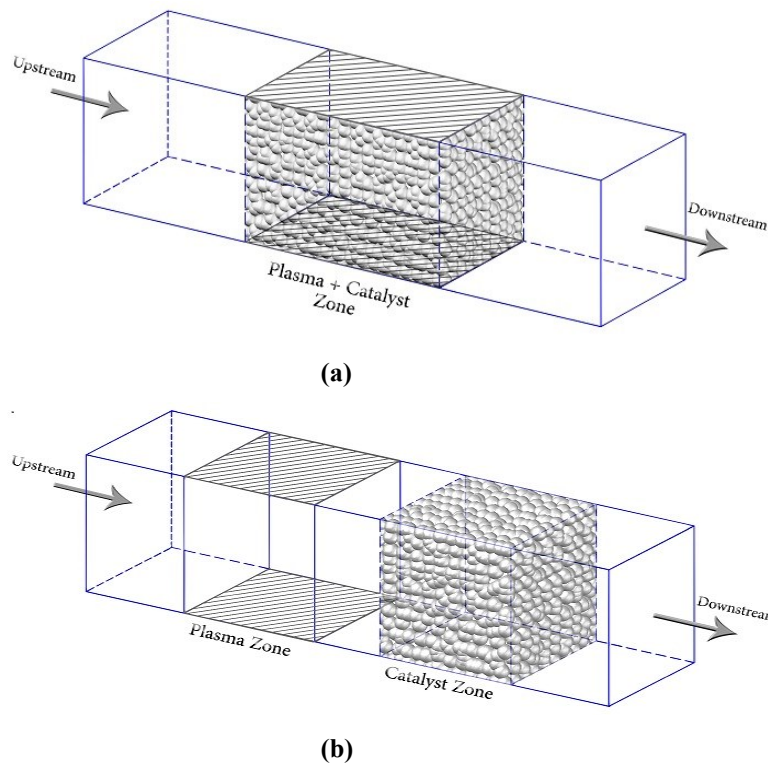


Figure 2.2 Schematic diagram of plasma reactors: (a) in plasma catalyst (IPC) reactor, and (b) post plasma catalyst

- **In plasma catalyst (IPC):** In this single-stage method, a catalyst is introduced to the discharge zone of the reactor (Figure 2.2.(a)). The catalyst can be used either as a packed bed or honey comb monolith, or it can be coated on the surface of electrode or the reactor walls [69], [80]. High levels of pollutants concentration demand higher level of energy for destruction of these compounds [81]: As the SIE increases it causes the rate of NO_x and ozone concentration increase [82]. The ozone coverage of the catalyst surface diminishes the catalyst activation and leads to the

formation of CO due to non-complete oxidation of pollutants [31]. In these conditions, IPC reactors, are more efficient, due to the lower demand of SIE and higher energy performance [83]. Though, in indoor environment applications, because of the low concentration of the VOCs, there is less demand for SIE. Therefore, the application of the second type of plasma reactor is discussed.

- **Post plasma catalyst (PPC):** In a two-stage plasma catalyst method, the catalyst can be placed either upstream or downstream of the discharge zone. However, the installation of the catalyst downstream of the plasma (PPC) is more efficient, since the generated reactive species in the plasma zone participate in oxidation reactions in the catalyst zone and complete the mineralization reactions (Figure 2.2.(b)). The result is an increase in CO₂ selectivity rather than CO formation, as well as abatement of ozone concentration in the effluent gas [84]. Due to the higher capability of PPC reactors in elimination of CO and ozone compared to IPC, these systems are more appropriate for indoor environment application [81].

2.1.4.1 Catalyst

Selecting an appropriate catalyst is an important challenge for enhancing the VOCs removal efficiency in a plasma catalyst process. The presence of the catalyst increases the probability of surface reactions between the reactants and reactive species, which leads to more selective reactions and higher removal efficiency of the system. Therefore, the catalyst surface textural properties including specific surface area, pore volume, pore size and size distribution, as well as particle size and shape have an important role on the plasma catalyst performance [85], [86]. The effect of the catalyst in altering the reaction mechanism is described in section 2.1.4.4.

The performance of a catalytic plasma process is also related to the catalyst storage capacity. To have a high VOC removal efficiency, VOCs should form strong bonds with the catalyst surface. Formation of these bonds becomes more important in low concentration levels [87]. A catalyst with a great ability of adsorbing VOCs as well as formed reactive species in the presence of plasma increases the removal efficiency of these compounds. Dual functional adsorbent/catalysts are favorable catalysts when generated reactive species under plasma catalyst conditions are not enough for decomposition of the pollutants. In fact, the storage materials capacity increases the reaction time as well as the probability of collision between the VOCs compounds and reactive species on the surface of the catalyst [81]. Earlier studies have reported the positive effect of

employing a dual functional adsorbent/catalyst on energy efficiency and eliminating the formation of harmful by-products [71], [88].

Porous adsorbents, including Al_2O_3 [28], [89], zeolites, and other molecular sieves [28], [31] were the first materials considered for such application [89]. Zeolites feature more permanently in the literature because of their greater storage capacity of VOCs.[30],[90]. The catalyst properties and plasma activity can be enhanced by coating the porous materials with metals (i.e. Ag, Pt, Pd, Rh, Ni, Cu, Co, Mg, Ti) or metal oxides (TiO_2 , V_2O_5 , WO_3 , etc.) as support [4], [31]–[33]. However, in some studies decreasing the removal efficiency was reported as a consequence of adding a support and decreasing the specific surface area of the catalyst[82], [83].

Titanium dioxide (TiO_2) has been used as the catalyst in plasma processes. Coating TiO_2 with other metals and metal oxides (i.e. Ag/TiO_2 , WO_3/TiO_2 , $\text{V}_2\text{O}_5/\text{TiO}_2$) [82], [83], [91] or using TiO_2 as a coat on AC filter [92] are different techniques of using this material as catalyst. The role of TiO_2 as a photocatalyst in plasma process is explained in section 4.6.

2.1.4.2 Catalyst Deactivation in Ambient Temperature

Earlier studies conducted at ambient temperature reported that gradual deactivation of the catalyst occurred due to covering the active sites by carbon containing materials [93], [94]. Hammer et al. [95] reported that applying plasma in IPC reactors increases the temperature of the catalyst about 10-15°C for applying 10 J L^{-1} input energy density. Accordingly, the catalyst surface temperature is less than 100°C [27], [82], [89], [90], [96]. This temperature is not sufficient to thermally activate the catalyst [27], [81]; however, it could still prevent the catalyst deactivation [97]. For PPC reactors, catalyst deactivation is more considerable [98]. A mild heating (about 70°C) may be required to prevent this problem [81], [98].

2.1.4.3 Plasma Catalyst Process Specifications

In a plasma catalyst process the interaction between the catalyst and plasma can be different based on the type of the employed reactor (IPC or PPC). The following sections describe the influences of plasma and catalyst and the effect of the reactor type on these interactions.

2.1.4.3.1 Catalyst and Plasma Interactions in IPC

2.1.4.3.1.1 Catalyst Effects

Introducing a catalyst into the discharge zone of an IPC reactor causes an increase in the energy level of the electric field, due to shortening the discharge gap [80]. This increase in the energy level results in more accelerated electrons and consequently, improvement of catalyst activity and energy efficiency [99]. Moreover, the physical properties of the discharge mode in the presence of the catalyst is changed, which results in generation of more reactive species in the pore volume of the catalyst [97]. Some studies reported this phenomenon for the oxidation of VOCs in the presence of silica gel, porous alumina, and metal oxides as catalysts [32], [69].

2.1.4.3.1.2 Plasma Effects

Guo et al. [100] employed $\text{MnO}_2/\gamma\text{-Al}_2\text{O}_3/\text{Ni}$ foam as a catalyst in a DBD system for decomposition of toluene and found a higher catalyst stability and oxidation capability. This result was due to increasing the catalyst specific surface area in the presence of the plasma. In contrast, a decrease in the specific surface area of γ -alumina, TiO_2 and HZSM-5 was observed when these catalysts were exposed to plasma zones [80]. Plasma exposure also causes a decrease in the particle size of the support metal or metal oxides on the surface of the catalyst, and enhances the impregnation of these supports on the catalyst [101], [102]. This results in an improved dispersion of catalyst active sites [100], as well as an enhanced activity and stability of their supported materials [103].

Changing the oxidation state of the catalyst surface is another observed effect of plasma on the catalyst [27]. Guo et al. [100] reported detection of Mn_3O_4 beside Mn_2O_3 catalyst in the presence of NTP.

2.1.4.3.2 Catalyst and Plasma Interactions in PPC

Separating plasma and catalyst zones in a PPC reactor results in relatively simpler function compared to IPC reactor. In a PPC reactor, short-living oxidizing species generated in plasma zone are not effective and disappear before reaching the catalyst zone [104]. According to the study of Wallis et al. [105], the dominant reactions in plasma zone are:

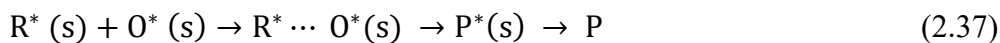
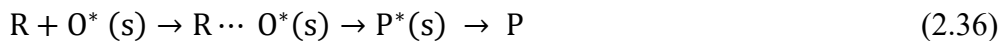
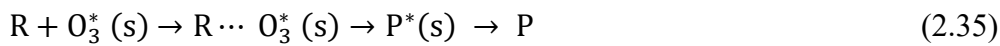
- Formation of reactive species with a longer life time from background gas

- Conversion of target VOCs to other compounds which are more easily treated by the catalyst.

Formation of ozone is one of the important concerns for indoor environment applications. By placing the catalyst downstream of the plasma, the generated plasma can participate in oxidation reactions of VOC molecules on the catalyst surface. Therefore, ozone concentration in the effluent gas in a PPC reactor is lower than IPC reactors. As oxygen atoms are more reactive than ozone [106], finding a method to convert ozone to oxygen atom before it reacts with VOCs on the surface of the catalyst is an effective way of improving the system performance [81]. Different catalysts (TiO_2 , $\gamma\text{-Al}_2\text{O}_3$, zeolites, and MnO_2) have been used in the presence of DBD as plasma discharge mode to successfully achieve ozone conversion and greater system performance [27], [107].

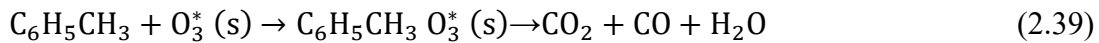
2.1.4.4 VOCs Abatement and Reaction Mechanism in Plasma Catalytic Reactors

Plasma reactions are very complicated processes both in the presence and in the absence of a catalyst. Several mechanisms may explain the formation of reactive species when accelerated electrons collide with background gaseous molecules [108], [109]. The nature of the catalyst plays an important role on the type of formed reactive species and reaction mechanisms, as well as the product selectivity [80], [105]. The formed reactive species either directly react with VOC molecules or are adsorbed on the catalyst surface and form superficial active structures (indicated by $^*(s)$ in the following reactions). The simultaneous presence of these reactive species and the target components (R) on the catalyst surface provides a bed for initiating chemical interactions between these components ($\text{R} \cdots \text{O}_3^*(s)$, $\text{R} \cdots \text{O}^*(s)$, *etc.*), followed by a series of complex chain reactions. The result is oxidation of components into products (P) in the form of mineralized molecules (CO_2 and H_2O) or new formed organic compounds, which eventually are desorbed from the catalyst surface.



Decomposition of formaldehyde (HCHO) in a PPC reactor in the presence of MnO_x/Al₂O₃ catalyst showed that destruction of this compound can occur not only by short-living reactive species in the discharge zone, but also by long-living species in the catalyst zone[84]. Ozone as a long-living species does not react directly with HCHO; however, after chemisorption of both ozone and target components, destructive reactions take place on the catalyst surface. It is postulated that the highly reactive oxygen species, which are mostly formed on the catalyst surface, are responsible for decomposition of HCHO in the catalyst presence.

Magureanu et al. [108] studied the decomposition of toluene in the presence of Ag/Al₂O₃ catalyst in a post plasma reactor. They found that, during the decomposition of toluene, ozone is chemisorbed on the catalyst surface without any change in the size and oxidation state of the catalysts. These interactions result in formation of activated ozone, which in the next step participates in toluene mineralization [108]:



Futamara et al. [106] reported a significant increase in benzene and CO decomposition and decrease in ozone concentration in a DBD reactor as the result of ozone decomposition in the presence of Manganese dioxide (MnO₂). On the other hand, the molar equivalent of ozone, which takes part in benzene decomposition, was smaller compared to that of stoichiometric required for a complete oxidation. They explained that a part of VOCs participate in an incomplete oxidation, resulting in CO formation and possibly other intermediates. The formed CO in the next step reacts with O₂ leading to a complete oxidation.

Figure 2.3 shows a schematic of the possible reactions in a PPC reactor. In a plasma zone, the dominant reactions for VOC removal include formation of reactive species (see also section 2.1.3.2). The presence of a catalyst suppresses these types of reactions and enhances the heterogeneous oxidation reactions, resulting in higher CO₂ selectivity. The same mechanism can be observed in IPC reactors.

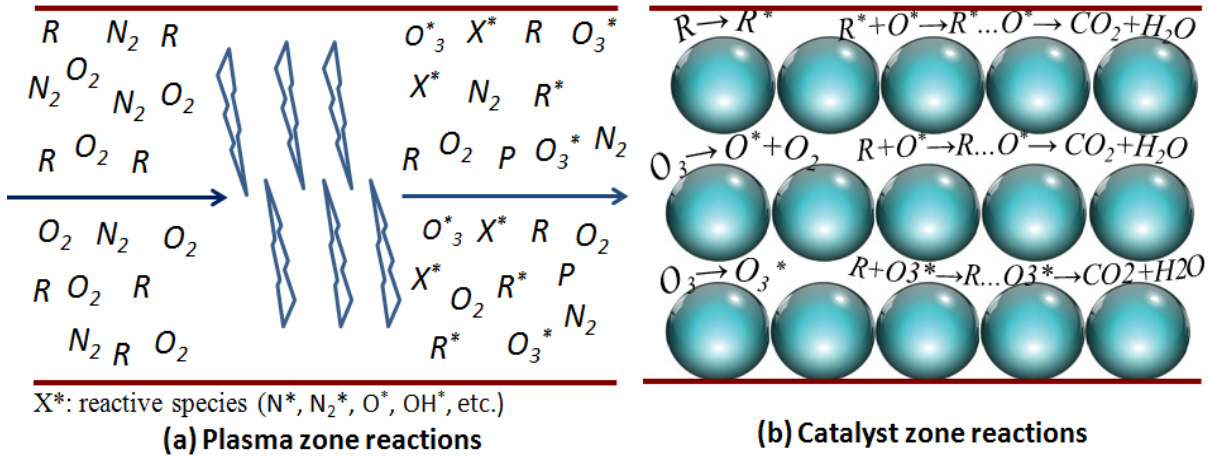
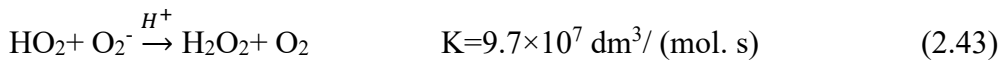
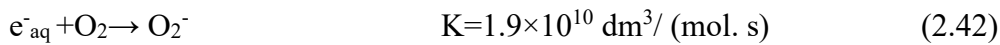
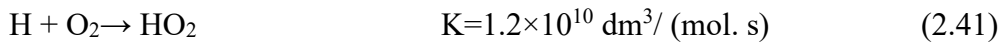


Figure 2.3 Scheme of the possible reactions in (a) plasma zone and (b) catalyst zone on the surface of the catalyst

2.1.4.5 Effect of Humidity in plasma catalyst

Relative humidity has an important role in plasma catalyst performance [32], [64], [81]. Yufang et al. [75] studied the effect of humidity on toluene decomposition efficiency in a PPC reactor at ambient temperature. The result of carrying out their experiments in the presence of Co₃O₄/Al₂O₃/nickel foam as catalyst showed the importance role of water molecules in completing the oxidation reactions. The proposed reactions are shown as follows:



These formed species facilitate complete VOCs oxidation reactions. A decrease in CO concentration along with an increase in CO₂ selectivity is the consequence of the following reaction:



However, the negative effect of high humidity level is that the catalyst surface is covered with water molecules, which leads to decrease in removal efficiency [75], [106]. This negative impact should be taken into account more seriously in case of an indoor environment application in which

the concentration of pollutants are in the order of ppb. Therefore the decrease in the system performance due to coverage of the catalyst surface by water molecules can be more significant.

Table 2.2 summarizes the residence time, VOCs removal, CO₂ selectivity, energy efficiency and by-product formation for different types of plasma catalyst reactors. Results show an increase in VOCs' removal efficiency, and CO₂ selectivity and an increase in the energy efficiency in plasma catalyst reactors compared to NTP (see Table 2.1).

2.1.4.6 Function of Photocatalyst in Plasma Reactions

2.1.4.6.1 Plasma Photocatalyst Combination

TiO₂ as a semiconductor is an ideal photocatalyst that is capable of electron-hole pair formation when absorbing UV light. Sano et al. [110] used two different catalysts, TiO₂ and γ -Al₂O₃, to investigate the effect of generated UV light by plasma in photocatalyst activation. For this purpose they used a PPC reactor for elimination of acetaldehyde (CH₃CHO) and CO. They reported a higher mineralization degree for acetaldehyde in the presence of γ -Al₂O₃ compared to TiO₂. Also, utilization of γ -Al₂O₃ improved the oxidation of CO twofold compared to the TiO₂. They proposed that the active oxygen species formed by the O₃ decomposition can be responsible for high activity of γ -Al₂O₃. These species are released due to the activation of lattice oxygen of either TiO₂ or γ -Al₂O₃ under plasma discharge. Finally, they postulated that employing a catalyst with the high ability of lattice oxygen and ozone utilization can enhance the VOC removal more efficiently than a photocatalyst that can be activated by weak UV light emitted from plasma [110]. Similar results were reported by [111], [112].

2.1.4.6.2 Plasma-UV Photocatalyst Combination

Huang et al. [111] performed an experiment, in the presence of a TiO₂/AC catalyst, to investigate the effect of combining plasma and external UV light for toluene decomposition. Their results showed a significant increase in the removal efficiency. In this condition, the generated ozone produces OH radicals which can participate in later reactions. They ascribed this outcome to the synergic effect of the plasma and UV light rather than to the synergic effect between plasma and photocatalyst.

Table 2.2 Results of VOC removal, CO₂ selectivity, residence time, energy efficiency and by-product formation in plasma catalyst reactors

Ref.	Reactor type	Catalyst	SSA (m ² g ⁻¹)	Target pollutant	Carrier gas	Conc. (ppm)	Flow rate (L min ⁻¹)	Residence time (Sec)	Removal efficiency (%)	CO ₂ yeild (%)	SIE (J L ⁻¹)	EEi (g kWh ⁻¹)	Reported by-product	Concentration
[74]	DBD/ PPC	MnO ₂ -FeO ₃	219	Toluene	20%O ₂ + 80%N ₂	240	0.315	N/A	76	23.5	172	14.4 ^c	O ₃ , CO	3.9 ppm , 16.5%
		MnO ₂ /γ-Al ₂ O ₃	169						88	18		16.7 ^c		14.6 ppm , 14.0%
		MnO/AC	1024						99.7	30.2		18.9 ^c		8 ppm , 24.8%
[90]	Surface Discharge /PPC	NaY	750	Toluene	80% N ₂ + 20% O ₂ + 0.5% H ₂ O	200	0.5	N/A	78	60	600 ^b	3.54 ^c	O ₃ /CO	0.2 * 10 ⁻³ mol, N/A
		HY	520						87	38		3.94 ^c		0.3 * 10 ⁻³ mol, N/A
[96]	DBD/IPC	γ -Al ₂ O ₃ α-Al ₂ O ₃	133 0.26	Carbowax ethane-1,2-ol (C ₂ H ₆ O ₂)	Air	200	0.1	N/A	77 100	96 61	2400 ^b	0.64 ^c 0.83 ^c	O ₃	0 N/A
	DBD/PPC	γ -Al ₂ O ₃ α-Al ₂ O ₃ + γ-Al ₂ O ₃	133 N/A						69 45	98 92		2400 ^b		0.57 ^c 0.37 ^c
[113]	DBD/IPC	Pt/Al ₂ O ₃	N/A	2-Heptanone	Dry air	180	0.42	1.5	98	64	34	87.4 ^c	CO, O ₃ , NO _x	36%, N/A, < 10ppm
					Air+ 3% H ₂ O				86	56		76.7 ^c		26%, N/A, < 10ppm
[114]	AC DBD/ IPC	3 wt% MnO _x /SMF ¹	N/A	Isopropanol	Air	100	0.5	N/A	100	100	195	4.55 ^c	O ₃	N/A
[75]	DBD/IPC	Co ₃ O ₄ /Al ₂ O ₃ /nickel	N/A	Toluene	N ₂ + 5%O ₂	50	0.1	N/A	96	75	500	1.30 ^c	CO	N/A
[64]	Positive DC Corona /PPC	MnO _x /Al ₂ O ₃	N/A	Formaldehyde	Air+ 30%RH	2.2	6	0.21	87	N/A	20	0.43 ^c	O ₃	14 ppm
[4]	Tooth wheel cylinder plasma-DC/ PPC	MnO _x /Al ₂ O ₃	200	BTX mix (Benzene Toluene p-Xylene)	Air +25% RH	1.5	6	0.21	94	100	10	1.63 ^c	O ₃ NO ₂	1.9 ppm 40 ppb
						1.4			97			1.85 ^c		
						1.2			95			1.80 ^c		

Ref.	Reactor type	Catalyst	SSA (m ² g ⁻¹)	Target pollutant	Carrier gas	Conc. (ppm)	Flow rate (L min ⁻¹)	Residence time (Sec)	Removal efficiency (%)	CO ₂ yield (%)	SIE (J L ⁻¹)	EEi (g kWh ⁻¹)	Reported by-product	Concentration
[69]	DC Corona /PPC	CuOMnO ₂ /TiO ₂	50	Toluene	Dry air	0.5	10.8	0.25	78	N/A	2.5	2.2 °	O ₃ NO NO ₂	24 ppm N/A 553 ppb
	DC Corona /IPC	TiO ₂	49		Dry air			1.12	82 ± 2	N/A	17	0.35 °	O ₃ NO NO ₂	3.6 ppm <10 ppb 1295 ppb ^a
[115]	DC tooth wheel cylinder Plasma/PPC	MnOx/Al ₂ O ₃ 5 wt.% Mn	N/A	Benzen	Air+ 30%RH Air+ 50%RH	0.470	6	0.21	100 ~0.63 ^a	~20-35 ^a	10	0.54 ° 0.34 °	O ₃ CO	27.3- 30ppm N/A
				Toluene	Air+ 30%RH Air+ 50%RH	0.810			100 ~0.95 ^a			1.1 ° 1.05 °		
				<i>p</i> -Xylene	Air+ 30%RH Air+ 50%RH	0.730			95 ~95 ^a			1.08 ° 1.08 °		
[32]	Positive DC corona / PPC	Pd/Al ₂ O ₃	230-280	Toluene	Air	0.5ppm	10 L	N/A	94	N/A	10	0.64 ° 0.27 °	O ₃	2.9 ppm
					Air+ 74%RH				39					2.0 ppm

^a Approximate amounts extracted from graphs

^b Calculated by equation (28) data extracted from reference.

^c Calculated by equation (29) data extracted from reference.

SSA: specific surface area

¹SMF: sintered metal fiber

According to Maciucă et al. [109] the synergic effect of plasma, UV and TiO₂ in VOC removal enhancement is the outcome of TiO₂ activation in the presence of UV light, and formation of electron-hole pairs on the surface of the catalyst. They suggested that the activated TiO₂ decomposes ozone in plasma zone, under the UV light radiation ($\lambda = 254\text{nm}$):



When the highly reactive species ($\text{O}^{\bullet -}$) is in contact with the conduction band of UV-irradiated TiO₂, it captures the electrons which results in the formation of holes and in the following reactions [109]:



$\text{O}^{\bullet -}$ and OH^{\bullet} have a key role in the oxidation reaction process [109]. Table 2.3 shows the VOC conversion during the post-plasma process in the presence of UV/TiO₂, TiO₂ and UV.

Results of Table 2.3 show the positive effects of ozone decomposition in the destruction of toluene. Moreover, the combination of Plasma/UV/TiO₂ enhances the toluene conversion. Considering the fact that all earlier studies have been performed at VOC concentration much higher than those which can be found in indoor environment more studies are needed to demonstrate the applicability of this technique for indoor environment.

Table 2.3 Comparison of VOC Conversion (50 ppm) by UV/TiO₂, TiO₂ and UV in a PPC Reactor

Ref.	Reactor Type	Target component	SIE (J/L)	Flow rate (L/min)	Method	%X _{VOC}
[111]	PPC	Toluene	N/A	0.2	Plasma/UV/TiO ₂	82.2
					Plasma/TiO ₂	77.6
					Plasma/UV	40.5
					Plasma	1.2
					UV/ TiO ₂	N/A
[109]	IPC	Isovaleraldehyde	5.4	5	Plasma/UV/TiO ₂	85.1
					Plasma/TiO ₂	44.2
					Plasma/UV	N/A
					Plasma	39.2
					UV/ TiO ₂	33.2

2.1.4.7 Cycled Storage–Discharge (CSD) Plasma Catalytic Process

Energy consumption is an important element in the application of plasma-based techniques for indoor environment. Although catalyst implementation in plasma reactors has made this method more cost-effective, optimization of these systems to decrease the expenses is still a goal in developing plasma processes. One promising technique to decrease the energy consumption is using CSD plasma catalytic reactors as reactive adsorption processes. Kim et al. [116] reported the application of adsorption-plasma cycle method, for the first time, for complete oxidation of absorbed benzene by an Ag/TiO₂ catalyst: Other studies also reported this application [30], [84], [87], [107].

A CSD plasma catalytic reactor acts in a two-stage cycle. In the first step (storage stage) the target component is adsorbed on the catalyst while plasma is off. In the second step (discharge stage), plasma is applied in the reactor to oxidize the adsorbed VOCs [87]. Figure 2.4 shows a schematic diagram of a semi-batch CSD plasma catalytic reactor. In this figure, Q₁ and Q₂ are the polluted and clean airflow rates in the storage stage and discharge stage, respectively; t₁ is the storage period, and t₂ is the discharge period of the CSD process.

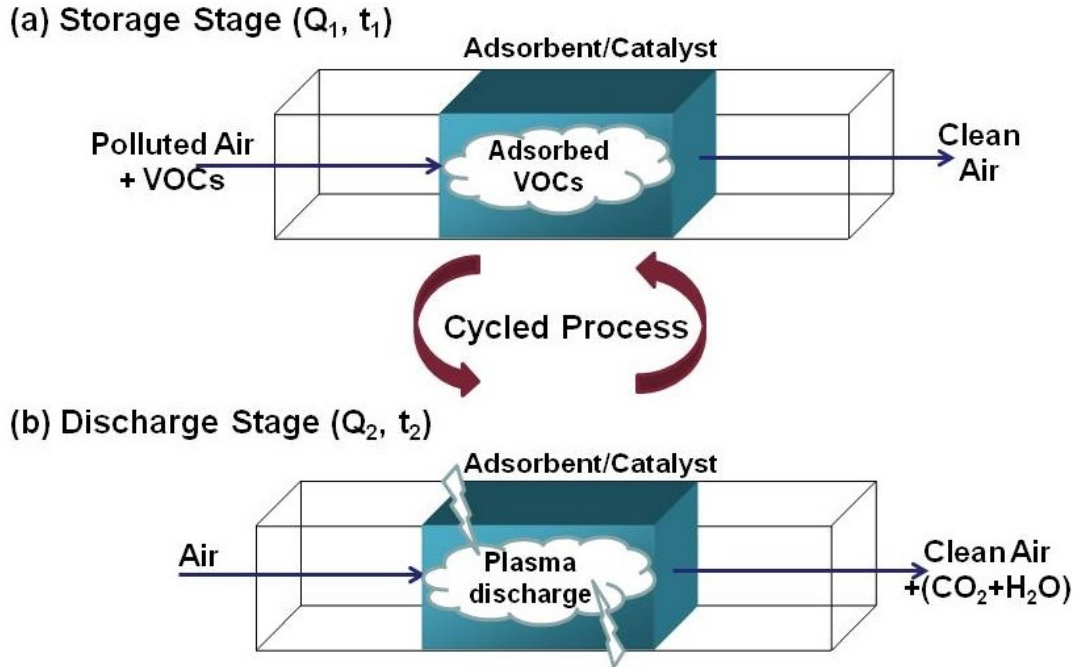


Figure 2.4 Schematic diagram for a CSD plasma catalytic reactor

Energy cost (kWhm^{-3}) in a CSD plasma catalyst reactor can be calculated by:

$$E_c^{CSD} = \frac{P_{discharge} \times t_2}{Q_1 \times t_1} \quad (2.53)$$

where, $P_{discharge}$ (kWh) is the discharge power, Q_1 (m^3h^{-1}) is the flow rate in the storage step and t_1 and t_2 are the storage and discharge periods (h), respectively.

Figure 2.5 shows the operating diagram of a CSD process. This diagram shows that decreasing the discharge time during a CSD plasma catalytic process can decrease the energy consumption of the system significantly. High surface area and storage capacity are two important factors for the catalyst to increase the storage time (t_1) and consequently the energy cost. Furthermore, in high levels of relative humidity, the existing water molecules compete with the target components for adsorbing on the catalyst surface and limit the access of these molecules to the catalyst surface. The outcome is that the removal efficiency of VOCs diminishes. Thereby, an appropriate catalyst should provide an excellent adsorbent characteristics as well as hydrophobic properties.

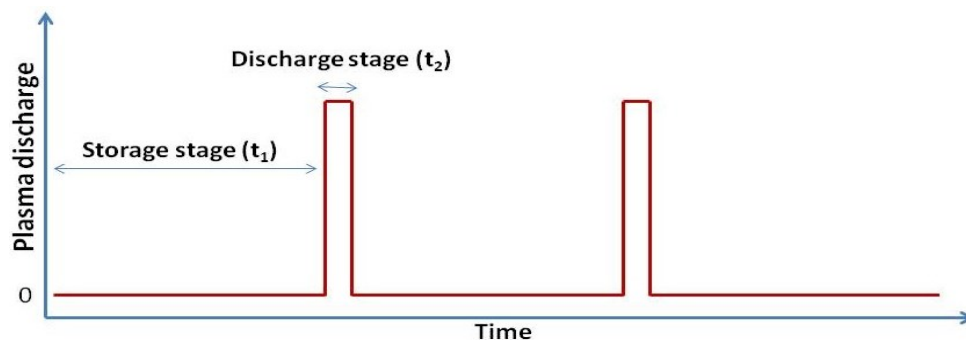


Figure 2.5 Operating diagram of plasma discharge- time in a CSD plasma reactor

Kim et al. [107] employed different types of catalysts to investigate the effect the catalyst type on VOCs removal and CO₂ selectivity. They found that TiO₂-based catalysts have a high removal efficiency; although, their low storage capacity make them inappropriate for utilizing in CSD processes. Hydrophobic zeolite-based materials, as dual functional absorbent/catalysts, exhibit high storage capacity and high surface area along with excellent humidity tolerance, which make them favorable candidates for application in CSD processes [30], [87], [117]. The oxidation properties of these catalysts can be enhanced by loading metals or metal oxides on the surface of these materials. However, specific surface area and pore volume are generally decreased by loading the support materials on the surface of the catalyst [118]. Employing an AgCu/HZSM-5 catalyst for HCHO removal in a CSD plasma catalyst showed that this method is capable of HCHO removal even in ppb levels [87]. Moreover, the hydrophobic properties of HZSM-5 help to increase the adsorption of the target component which results in high removal efficiency. Table 2.4 presents an overview of the studies on the CSD plasma process.

Despite the advantages of hydrophobic zeolites, the relatively small pore sizes of these materials make them improper for adsorption of large size molecules [119]. Therefore, selecting an appropriate catalyst with high storage capacity and oxidation capability of different sizes of VOCs is one of the important challenges in developing the catalyst.

It has been shown that CSD plasma process is a cost-effective and high performance technique for VOCs removal in low concentration levels when it was tested in semi-batch system. However, to be used for indoor environment application (ambient temperature, high relative humidity, high air flow rate, mixture of contaminant, etc.), and to assess its energy efficiency, further systematic research is required.

Table 2.4 An overview of studies on the CSD plasma process

Ref	plasma Type	Catalyst	SSA (m ² /g)	Target Pollutant	Carrier Gas	Conc. (ppm)	Flow Rate (ml/min)	t (min)	R* (S)	Target Conversion (%)	CO ₂ Select. (%)	P _{dis.} (W)/SIE(J/L)	EEc (kWhm ⁻³)
[117]	DBD	Ag/HZSM-5	334	Benzene	Air+50%RH	4.7	Q ₁ =600 Q ₂ =60	t ₁ = 60 t ₂ = 10	N/A	100	99.8	4.7 W	3.7e ⁻³
[87]	DBD	AgCu/HZSM-5		HCHO	Air+50%RH	5.3	Q ₁ =300 Q ₂ =60	t ₁ = 780 t ₂ = 14	0.3	100	> 99 ^a	2.3 W	10 ⁻⁵ – 10 ⁻⁴
[107]	DBD	1%Ag/TiO ₂	≤ 68	Benzene	Air (50%O ₂ PP)	200	4000-5000	N/A	0.16	100a	N/A	169J/L	N/A
		4%Ag/TiO ₂	≤ 68		Air (60%O ₂ PP)	200	10 000	N/A		75 ^a	80 ^a	136 J/L	
		0.5%Ag/γ-Al ₂ O ₃	≤ 210		Air (60%O ₂ PP)					90 ^a	75 ^a	160 J/L	
		H-Y	520		Air (80%O ₂ PP)					100	>70 ^a	160 J/L	
		2%Ag/H-Y	520		Air (80%O ₂ PP)					100	65 ^a	140 J/L	
[120]	DBD	0.8 wt%Ag/HZSM-5	334	Benzene	Air+50% RH	4.7	Q ₁ =600 Q ₂ =60	T ₁ = 60 T ₂ = 15	N/A	100	100	4.7 W	

^a Approximate amounts extracted from graphs

* R: Residence time

2.2 Part 2: Metal Organic Frameworks

2.2.1 Introduction

Selecting an appropriate dual functional adsorbent/catalyst (DFA/C) is an important challenge for a plasma-driven catalyst process. As previously mentioned, high adsorption capacity, swift adsorption rate and hydrophobicity, especially at low concentration levels of VOCs, are essential characteristics of an employed catalyst in a plasma system. Furthermore, the oxidation ability of the catalyst plays an important role in the VOC removal performance. Due to the variety of VOCs regarding their structural, chemical properties, and molecular sizes, finding a proper DFA/C suitable for degradation of all types of these compounds is not easy.

Activated carbon (AC) is one of the most common porous materials used as the adsorbent. The large micropore size distribution along with its high surface area results in high adsorption capacity of VOCs [121]. The low price of AC makes it more favorable than other adsorbents. However, due to the highly amorphous structure of AC and the lack of the presence of metal active sites in its structure, adsorption on AC is uncontrollable [122]. Also, difficulty in its regeneration due to the risk of firing at high temperature restricts the application of AC as a DFA/C [121].

Hydrophobic zeolites, on the other hand, are highly crystalline materials with an extremely uniform framework. These properties along with their stable structure in the presence of humidity and high temperature propose zeolites as excellent DFA/Cs. Several studies have conducted plasma catalytic experiments in the presence of zeolites [30], [82], [83], [30], [87], [117]. However, the small size of their micropores (≤ 2 nm) is hardly tunable due to their highly stable structure. This barrier inhibits the adsorption ability of zeolites for large size VOCs [121] as well as their catalytic characteristics.

As an alternative, metal organic frameworks (MOFs) are a new class of porous organic-inorganic polymers with phenomenal flexibility in tuning their networks and adjustability in their internal surface [36], [122], [123], [124]. The flexible framework of these porous materials causes some unusual patterns in adsorption isotherms for small inorganic molecules (i.e., H₂O, N₂, O₂, Ar, CO₂, CH₄), as well as large organic compounds (i.e., ethylene oxide, acetonitrile, benzene, xylene isomers, tetrahydrothiophene, cyclohexane and thiophene etc.) [36], [122], [125].

Up to now, the application of MOFs has been studied in many different fields, including ion exchange, sensor, gas and liquid separations, molecular sieves, size-selective separation, polymerization, nonlinear optics, conductors and semi-conductors [36] [126], [127], [128].

Table 2.5 compares the general properties of MOFs with other adsorbents and/or catalysts that have been used in plasma catalytic systems.

Table 2.5 General characteristic of different adsorbents and/or catalysts in plasma studies

	AC	Metal Oxides	Zeolites	MOFs
Structure	Amorphous	Crystalline	Highly Crystalline	Highly Crystalline
Surface area	High	Limit	High	Extra high
Pore size	Not Fixed	Small	Relatively small	Tunable
Adsorption capacity	High	Limit	High	High
Catalytic properties	No	Yes	Yes	Yes
Thermal stability	Weak	Highly Stable	Highly Stable	Stable
Chemical stability	Weak	Highly Stable	Highly Stable	Stable
Diversity	Limit	Limit	Limit	Infinite

Despite the superior properties of MOFs, to the best knowledge of the author, the potential catalytic capacity of these materials for oxidation of VOCs has not been investigated so far. Accordingly, the following section is a review on MOFs characteristics, synthesis methods, and their application in the adsorption of VOCs. As the studies in catalytic properties field are limited to the role of MOFs in catalytic conversion of organic compounds rather than their total oxidation, general properties of these materials as catalysts are explained.

2.2.2 Structure of MOFs

MOFs are classified as microporous and mesoporous materials with the pore size between the range of an angstrom to nanometers [129]. These highly porous materials are composed of inorganic metal ions or metal clusters and organic linkers [128], [130], coordinated together with strong covalent bonds [122]. This organic-inorganic topology allows MOFs to have an adjustable framework by changing the organic linkers as well as metal clusters [131]. The structure and properties of a MOF is predictable based on the metal node and the linker in its building units [132].

The metal nodes in the structure of MOFs is commonly a transition metal, s /p group, or the lanthanides group, which are supplied in the form of a salt including, nitrate, chloride, acetate, etc. [133]. The organic linker has an important role in construction of the synthesized MOF. Linkers can induce diverse properties in MOFs and tailor their structures according to the type of their functional group [134]. Accordingly, based on the type of linkers the structure of MOFs can be classified as:

Carboxylate framework: In the structure of these types of MOFs polycarboxylic acids such as terephthalic acid or complex polyaromatic molecules are used as linkers [131], [133], [135]. Carboxylate-based MOFs exhibit remarkable functional properties as well as chemical and thermal stability [126]. Therefore, increasing the temperature in order to remove the solvent from their pores without any change or destruction of their structure is possible[126]. However, the metal-carboxylate bond in some of these MOFs can be hydrolyzed. Also, strong coordinative water-unsaturated metal center bonds is a disadvantage for some of these MOFs especially for application in a humid environment [125].

Phosphonate framework: Phosphonate ligands are used less than carboxylates in MOFs. The reason is because of the different steps of deprotonation, which results in complexity in the coordination chemistry of the phosphonate ligands. These ligands form dense layered and less ordered materials [136].

Sulphonate framework: Commonly, sulfonate structural MOFs do not have enough reactivity and the formed framework contains lower dimensionality and less coordinated crystalline framework [137]. There are very limited inorganic counterions able to be joined to the sulphonates. After synthesis, the structure of the formed MOF is not strong enough and pores can collapse [136].

Polyazolate Framework: Polyazolate-based MOFs (polyazolate: tetrazolate, triazolate, imidazolate, and pyrazolate), exhibit similar stereochemistry to carboxylate materials but they possess a higher basicity along with a more robust network which potentially make them more selective adsorbents and better catalysts [125]. Zeolitic imidazolate frameworks, known as ZIFs, are the most common sub-class of this framework. The symmetry and porosity of ZIFs is less than other MOFs[136]. However, they are thermally and chemically robust and exhibit higher catalytic properties [136].

Porphyrin frameworks: Porphyrins have rigid networks, and acceptable thermal and chemical stability, which make them capable to withstand in severe conditions[136]. Different types of metal ions can be coordinated in the center of their ring[136].

Carbonate-based frameworks: These MOFs show rigid network, thermal stability up to 400°C, and chemical stability which make them capable to withstand in severe solvothermal conditions[136]. The pore size of these MOFs is smaller than formed pores based on phenyl [136].

A very advantageous characteristic of MOFs is that using an organic linker with a longer length can increase the opening size and extend the specific surface area of the formed MOF without any negative effect on its stability [138]. For instance, employing 1,4-benzene-dicarboxylate, biphenyl-dicarboxylate and terphenyl dicarboxylate in the synthesise of UiO-66, UiO-67 and UiO-68, respectively, resulted in about two to three times increase in the surface area [138]. Furthermore, the dimensions of a unit cell can be changed by changing the organic linker while the crystal structure does not change (See Table 2.6) [132].

Table 2.6 The effect of the length of organic linker on the specific surface area and opening size of the synthesized MOF [138]

MOF	Organic Linker	Number of benzene molecules in the linker	Langmuir surface area (m ² /g)	Opening size (Å)
UiO-66	1,4-benzene-dicarboxylate	One -	1187	6
UiO-67	Biphenyl-dicarboxylate	Two -	3000	8
UiO-68	Terphenyl-dicarboxylate	Three-	4170	10

2.2.3 MOFs as Adsorbent

MOFs have large porosity, high surface area, tunable pore size and shape, that can be variable in the range of microporous to mesoporous scale based on the nature of the organic linkers and the connectivity of the inorganic moiety [139]. Unlike other porous materials (i.e. AC and zeolites) MOFs have no dead volume or non-accessible pores in their structure for guest molecules [35]. Although, these properties make MOFs potential candidates for adsorption of different sizes of molecules, other factors including the presence of free active sites, adsorption activation energy, reactivity, physicochemical stability, fast kinetics and high reversibility, can critically affect the adsorption properties of these porous materials.

As of now, several studies have investigated the adsorption properties of different types of hazardous and non-hazardous gases on MOFs [140], [36], [141], [142]. Due to our focus on VOCs elimination, here, the characteristics of some MOFs and their potential for adsorbing VOCs are discussed.

2.2.3.1 MOF-5 or IRMOF-1 and its Relatives

IRMOF-1, also known as MOF-5 ($Zn_4O(C_8H_4O_4)$), contains 15 Å cages that are connected by pore openings of 7.5 Å [123]. The structure of MOF-5 is introduced as a parent for a series of other MOFs with large cubic pores [143]. This MOF has a highly nanoporous structure with at least two different types of adsorption sites [36], [115]. The adsorption capacity of MOF-5 is reported in different studies. For instance, the adsorption of more than 30 VOCs including alkanes, alkenes, aromatics, ketones, and halogenated compounds on IRMOF-1 were investigated in the study of Luebbers et al. [123]. They demonstrated that the interaction between the guest molecule and inorganic vertex of the IRMOF-1 framework for aromatic compounds is stronger than that of light molecules such as hydrogen or methane [143]. The flexibility in the structure of this MOF allows it to be adapted according to the size and the shape of host organic compounds [144]. However, the framework of IRMOF-1 is unstable when exposed to humidity in the ambient atmosphere, which causes a remarkable loss of its activity [145].

Britt et al. [122] studied the adsorption behavior of four different VOCs (tetrahydrothiophene, benzene, dichloromethane, ethylene oxide) on six different MOFs. All of these MOFs had the same basic structural framework as IRMOF-1. Table 2.7 presents the characteristics of the tested MOFs.

Table 2.7 Characteristics of the benchmark MOFs, [122]

MOF	Open Metal Site	BET Surface area (m ² /g)	Pore Volume (cm ³ /g)
MOF-5		2205	1.22
IRMOF-3		1568	1.07
MOF-74	■	632	0.39
MOF-177		3875	1.59
MOF-199	■	1264	0.75
IRMOF-62		1814	0.99

A comparison between the breakthrough curves of the selected VOCs on these MOF and a commercial type of AC (Calgon BPL), showed that the dynamic adsorption capacity of some

MOFs surpasses AC capacity up to 35% (Figure 2.6). The curves show that MOF-177 does not show a high VOC uptake, despite its extra high specific surface area. The same trend is observed in MOF-5 behavior. On the other hand, MOF-199 (HKUST-1) and MOF-74 are the most effective MOFs in IRMOF-1 family for capturing vaporous VOCs.

MOF-199 possesses open copper (II) sites in its structure. Also, MOF-74 contains the highly reactive 5-coordinate zinc species and potentially reactive oxo groups. These unsaturated metal sites in MOF-74 and MOF-199 act as reactive Lewis acids. Thus, they could be proposed as highly effective adsorbents with high dynamic adsorption capacity. The lack of open metal sites in the framework of other MOFs (IRMOF-3, IRMOF-5, MOF-177, and IRMOF-62) incapacitates them to act as a Lewis acid. Therefore, the uptake properties are very poor [122].

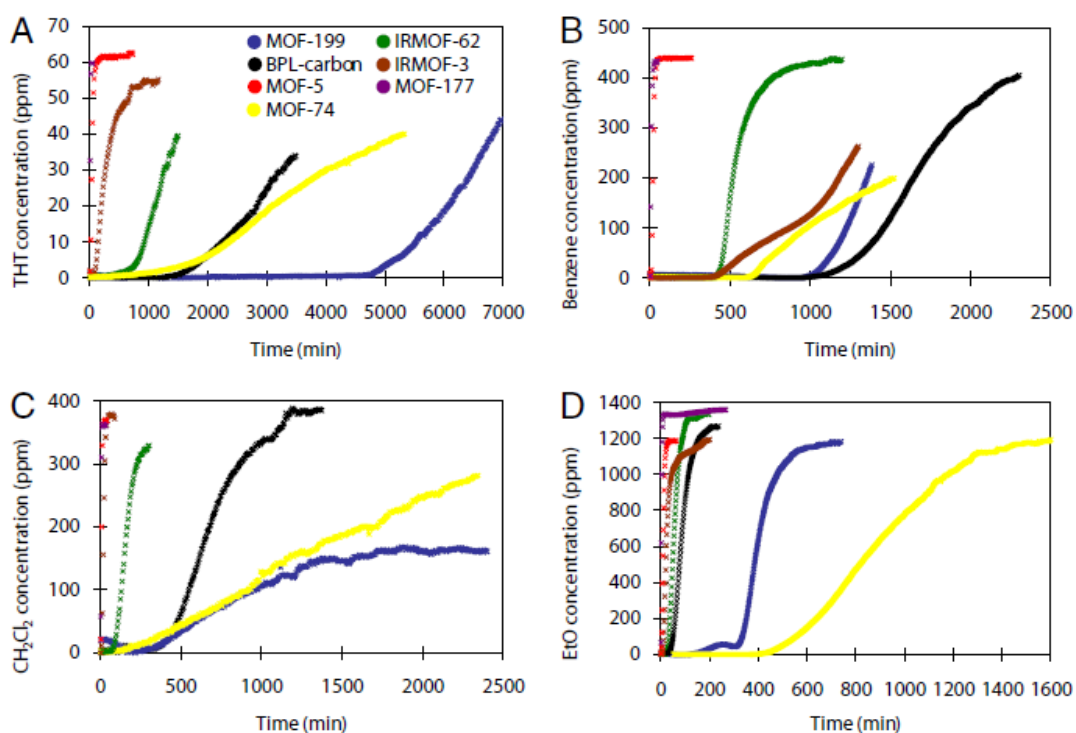


Figure 2.6 Breakthrough curves of (A) tetrahydrothiophene (THT), (B) benzene, (C) dichloromethane (CH₂Cl₂), ethylene oxide (EtO) adapted from [122]

Not only MOF-199, Cu₃(btc)₂ (btc=benzene-1,3,5-tricarboxylate) shows a high capacity of adsorption for the mentioned VOCs, but it is also one of the most effective MOFs for adsorption of organo-sulphur compounds. This MOF exhibits an excellent permanent adsorption of

tetrahydrothiophene, which is desirable for protective applications. Changing the color is an indicator that shows the progress of its saturation [122]. However, the irreversible coordination of water or organic compounds and open metal sites makes MOF-199 inappropriate for adsorption applications [122], [125].

2.2.3.2 Bis-pyrazolate-based MOFs

Ni(bpb) and Zn(bpb), (bpb: 1,4-Bis (4-pyrazolyl)- benzene), are two flexible bis-pyrazolate based MOFs. These thermally stable MOFs have highly porous structures and specific surface areas of 1600 and 2200m²/g, respectively. The accessible channels in their frameworks make these MOFs suitable for capturing organic compounds. During the synthesis, based on the thermal conditions, the solvent is trapped in their porous polymeric network. This solvent can be removed by treating the MOF at higher temperatures [125].

Galli et al. [125] studied the adsorption behavior of benzene and cyclohexane and thiophene on Ni(bpb) and Zn(bpb). Results showed a quasi-reversible isotherm adsorption of cyclohexane on both MOFs at 303 K, while benzene followed an almost irreversible adsorption isotherm. A comparison between the breakthrough curves of these MOFs and MOF-199 in the presence of 60% moisture at 298 K showed that Zn(bpb) and MOF-199 are totally inefficient for the adsorption of thiophene in the presence of humidity. Zn(bpb) does not allow the direct interaction between the metal center ions and the S-donor atoms. In contrast, the one-dimensional hydrophobic channels in Ni(bpb) structure makes its network flexible for interaction between the metal center ions and the S-donor. Ni(bpb) has high thermal stability and surpasses other carboxylate-based MOFs, which cannot be applied in air filters because of their sensitivity to humid air [125]. The low performance of CH₄ and CO₂ adsorption indicates weak interaction between these molecules and MOFs. This suggests that Ni(bpb) and Zn(bpb) are not suitable adsorbents for small size molecules under atmospheric pressure. However, these MOFs can form strong static and dynamic bonds with benzene, cyclohexane, and thiophene [125].

2.3.3.3 Lanthanide-based MOFs

Lanthanide-based MOFs (Ln-MOFs) especially Tb³⁺ and Eu³⁺ have versatile coordination geometry, unique luminescent and magnetic properties, which are useful in selective gas adsorption [126]. Europium-based MOFs (Eu-MOF) can act as efficient photocatalysts in the presence of UV light [145]. Their framework is highly stable in the presence of solvents. For

instance, two La(III) complexes, $\{\text{La}(\text{cpia})(2\text{H}_2\text{O})_3 \cdot 4\text{H}_2\text{O}\}_n$ and $\{\text{La}(\text{cpia})(\text{H}_2\text{O})(2\text{DMF})\}_n$, (cpiaH₃=5-(4-carboxy-phenoxy)-isophthalic acid, are insoluble in organic solvents (acetone, ethanol, and pyridine), as well as water. Their structure is also stable in the air and high temperature (up to 400°C). Therefore, the guest solvent trapped in their framework can be evacuated by heating without collapsing their framework [126]. Nevertheless, the specific surface area of these MOFs is very low compared to other MOFs. For the $\{\text{La}(\text{cpia})(2\text{H}_2\text{O})_3 \cdot 4\text{H}_2\text{O}\}_n$, Langmuir surface area of is $\sim 147 \text{ m}^2 \text{ g}^{-1}$ and BET surface area at 77K for N₂ is less than $1 \text{ m}^2 \text{ g}^{-1}$ [126]. The difficulty in controlling the design of their structure due to a variety of coordination numbers [126] make them unfavorable candidates for adsorption application.

2.2.3.4 Crystalline Porous Material-5 (CPM-5)

CPM-5, $[(\text{CH}_3)_2\text{NH}_2][\text{In}_3\text{O}(\text{BTC})_2(\text{H}_2\text{O})_3]_2 \cdot [\text{In}_3(\text{BTC})_4] \cdot 7\text{DMF} \cdot 23\text{H}_2\text{O}$, is a crystalline porous material with a highly symmetrical framework [146]. In CPM-5 the structure consists of a large Archimedean cage which is made up of 24 mononuclear In³⁺ sites, known as In₂₄ cage. These big sodalite cages encapsulate smaller Archimedean cages (In₁₂ cage) at their center (Figure 2.6). The framework of CPM-5 constitutes of In₃O clusters as metal centers which are connected together by means of 1,3,5-benzenetricarboxylate (BTC) linkers [146].

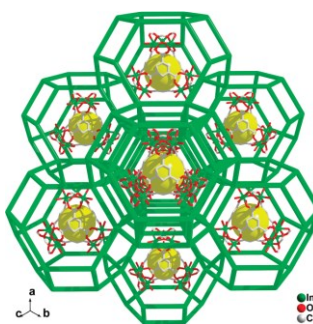


Figure 2.7 A view of the three dimensional, cage-within-cage architecture of CPM-5, Adapted from [146]

CPM-5 is thermally, hydrothermally and photochemically stable. [129]. The unique cage-within-cage structure of CPM-5 increases the potential of its adsorption capacity. Different studies have reported the high adsorption capacity of CO₂ on CPM-5 [141], [146]. Yet, VOCs adsorption on this MOF has not been studied.

2.2.3.5 Material Institute Lavoisier

Material institute Lavoisier (MIL) frameworks are a common group of metal carboxylate MOFs in which their framework consists of linear organic linkers, especially terephthalic acid [135]. The properties of two important MOFs in this group are explained in the following sections.

2.2.3.5.1 MIL-53

MIL-53 consists of trivalent cations, Cr^{3+} , Fe^{3+} or Al^{3+} , which are connected together by means of benzene dicarboxylic acid (terphthalic acid). This MOF shows a highly flexible framework and high thermal stability up to 500°C [135]. The flexible structure of MIL-53 causes a transition in its structural phase (shrinking or expansion of frameworks) upon the adsorption/desorption process based on the polarity of guest molecules [147]. This phenomenon is described as the breathing phenomenon, which is shown in Figure 2.7 for hydration-dehydration of MIL-53 (Al, Cr) [148]. Deformation of the structure in the presence of water molecules is the result of interactions between hydrogens in H_2O and oxygens in carboxylate and hydroxo group. The formed hydrogen-bond is easily destroyed by heating the MIL-53[148].

Application of MIL-53 is studied in liquid-liquid separation, gas sorption, and drug delivery [135].

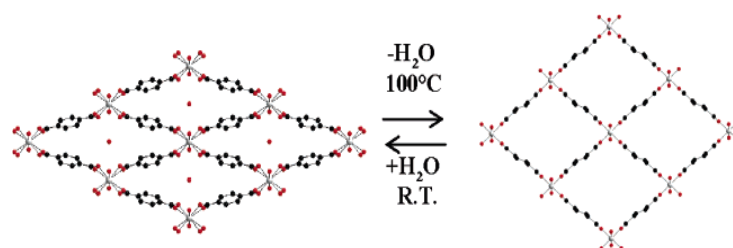


Figure 2.8 Breathing phenomenon upon the hydration/ dehydration of MIL-53. Left: MIL-53 (hydrated), and Right: MIL-53 (dehydrated), Adapted from [148]

2.2.3.5.2 MIL-101

MIL-101 is a chromium terphthalate-based MOF [35] with cubic structure, huge porosity, and exceptionally high specific surface area. The Langmuir surface area of MIL-101 can reach up to $5900 \pm 300 \text{ m}^2/\text{g}$, which is the highest reported surface area for porous materials till date [149].

MIL-101 has a zeotype topology with crystals in the sizes of around 100 nm, and pore volume $1.9 \text{ cm}^3/\text{g}$. MIL-101 possesses two types of mesoporous cages, 2.9 nm and 3.4 nm (29 and 34 Å) in

its structure [131], [34]. The smaller cages exhibit pentagonal windows with free openings of ~ 12 Å, while the large cages possess both pentagonal and larger hexagonal windows with approximately 14.5 Å and 16 Å free aperture, respectively [35]. This causes easy mass transport via its microporous pentagonal and hexagonal windows [150]. Figure 2.8 illustrates the structure of this MOF.

The structure of MIL-101 is stable in the presence of both organic solvents and water as well as high temperature[35]. Several studies have reported rapid adsorption of different types of VOCs, including benzene, n-hexane, toluene, methanol, butanone, dichloromethane and n-butylamine on MIL-101. [35], [34], [150], [151]. Results demonstrated that this MOF is an excellent candidate for VOCs removal from air. However, the effect of change in ambient conditions such as humidity especially in low concentration of VOCs has not been intensively considered in the adsorption behavior of this MOF.

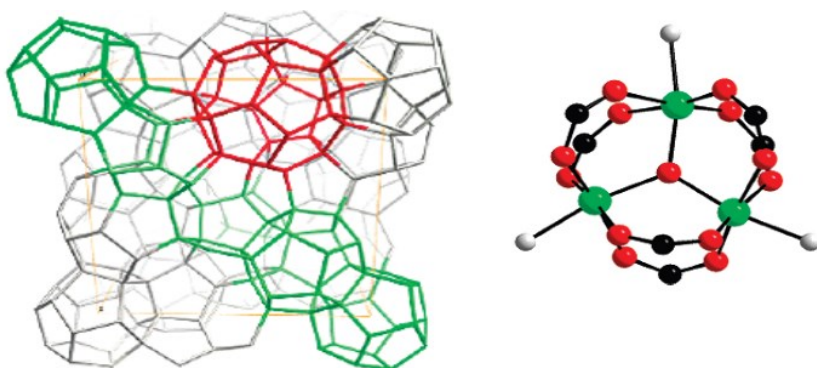


Figure 2.9 Left: Structure of the MIL-101(Cr), Right: The corresponding inorganic subunit of MIL-53. Metal, oxygen, and carbon atoms are shown in green, red, and black, respectively, terminal water molecules and fluorine are shown in gray. Adapted from [140]

Table 2.8 shows a comparison between the equilibrium amounts of adsorbed benzene on MIL-101 and other adsorbents. The adsorption uptake is calculated as follows [35]:

$$Q_e = \frac{1000(W_e - W_a)}{W_a M_{benzene}} \quad (2.54)$$

Where Q_e (mmol/g) is the amount of adsorbed per gram at equilibrium time, M_{benzene} (g/mol) is the molecular weight of benzene, W_e (g) is the amount of adsorbent (MIL-101) at equilibrium, W_a is the initial weight of the adsorbent.

Results of Table 2.8 show a superior capacity of benzene adsorption on MIL-101 compared to all other adsorbents[35]. The large pore sizes and extra high surface area are the reasons for this transcendent capacity [35].

Table 2.8 Comparison between the equilibrium amount of adsorbed benzene on MIL-101 and other adsorbents; adapted from [35]

adsorbent	Q_e (mmol/g)	temperature (K)	pressure (mbar)
MIL-101	15.02	298	55.0
MIL-101	15	303	56.1
ACF	2.56	303	—
Ajax	5.23	303	—
carbon monolith	12.69	303	57.2
silicalite-1	8.39	295	54.0
SBA-15	7.1	303	56.0

A comparison between the diffusion coefficient of benzene in different adsorbents in Table 2.9 also shows that the diffusivity is nearly fivefold higher compared to activated carbon and around four to ten-fold higher than zeolites [35]. The same result was obtained in another study for adsorption equilibrium of p-xylene on MIL-101 [34]. The maximum capacity of p-xylene adsorption on the MIL-101 was reported to be 3–8 times more than other adsorbents including γ -Al₂O₃, active carbon, and zeolites. This higher diffusivity is due to the mesoporous cavities and large apertures, which supply high storage possibility for gases [34]. The extra-high surface area provides a vast area of adsorption sites available for p-xylene [34]. Also, the existence of benzenes, as functional groups, in the microporous framework of MIL-101, increases the electrostatic interaction between the adsorbent and the target aromatic compound [34]. The result is a faster adsorption kinetics [34], [35].

Table 2.9 Comparison between the diffusion parameters of benzene within the MIL-101 and other adsorbents, adapted from [35]

adsorbent	diffusivity (10^{-10} cm ² /s)	temp (K)	activation energy (kJ/mol)
MIL-101	42.6	298	2.41
activated carbon	8.7	303	—
ACF	—	303	18.1
Ajax	—	303	17.8
ZSM-5	1.5–4.5	338	40.2
HZSM-5	10	400	25.92
silicalite-1	5.2	303	28.8
silicalite	6	400	28.01

The adsorption isotherms exhibit a decrease in the adsorption capacity by increasing the temperature from 288 to 318K, which demonstrates that the interaction between the VOC, benzene/p-Xylene, and MIL-101 is a physisorption phenomenon [34], [35]. A study of five consecutive cycles of benzene adsorption-desorption on MIL-101 at 298 K/303 K, and 0.04 mbar also showed that desorption rate is nearly as fast as the adsorption rate and the efficiency reaches 97% for benzene. [35].

2.2.3 MOFs as Catalyst

Crystal size and size distribution are two important factors when a material is considered as a catalyst [152], [139]. Zeolites are an important class of commercial heterogeneous catalysts due to their highly crystalline, uniform framework, and highly robust structure under extreme conditions [131]. However, as mentioned earlier, their relatively small pore sizes restrict their application for the removal of large size molecules. MOFs, on the other hand, possess diverse structure, hybrid nature with high to extra high porosity and surface area, tunable pore size, and very low density of framework [132], [153]. These characteristics facilitate the mass transport phenomena, including adsorption of target components, diffusion into pores and desorption of the products, and provide a favorable condition for catalyzing a reaction [132]. MOFs also have abundant amounts of metal content, around 20–40 wt% in the form of metal nodes, with free and exchangeable active sites [152]. The presence of these metal sites induces heterogeneous catalytic properties [154].

Up to now, several studies have reported the successful employment of MOFs as catalyst. For instance, MOFs act as catalysts in isomerization reactions, because of the presence of Lewis acid sites in their structures [155], [132]. MOFs have been used as semiconductor in photocatalytic

reactions [156], Brønsted acid catalysts in the hydration of alkenes, esterification, and alkylation, and also base catalysts [134]. Results show very high catalytic performance of the applied MOFs. Some MOFs show the ability for CO oxidation [157]. To the best knowledge of the author, total oxidation of VOCs on MOFs has not been investigated yet.

Despite the pointed transcendent characteristics of MOFs as catalyst, it is noteworthy that the maximum temperature that MOFs can stand is roughly 400°C and rarely 500°C for very few of them [138]. Therefore they cannot be used in catalytic reactions that requires high temperature, as their network collapses [132].

2.2.4 Synthesis of MOFs

Generally, MOFs are formed in the presence of a metal salt (i.e. nitrate, chloride, acetate, etc. [133] and an organic linker [132]. The self-assembly of a MOF is usually performed in a few hours between room temperature up to 200°C [152]. During the synthesis process, variety of moieties including fragile organic molecules are encapsulated in the MOF framework, leading to the formation of various types of MOFs [127]. After the synthesis, there is an accumulation of solvent in the framework (up to 150 wt%), which causes a decrease in the porosity and surface area [152]. This trapped solvent should be removed prior to using MOF in gas-phase adsorption and reaction processes. Since the solvent removal may result in collapsing the MOF structure, this evacuation should be processed in a gentle operational condition [152].

The pH value rules the stability of the formed MOF [152]. Commonly, the synthesis is performed in acidic environment [150]. However, for the formation of MOFs, the organic ligand should be deprotonated. The presence of a base (for instance NaOH) can accelerate this deprotonation at room temperature [153], [158]. The result of the presence of a base is the formation of nanometer size crystals (up to 200 times smaller than the ones obtained in the absence of any base) with higher yield [153]. The role of the solvent in MOF synthesis is not only to dissolve the reactants, but it is also to act as an agent in directing the structure [153]. Due to the milder operational conditions of MOFs synthesis, these catalysts seem to be more cost effective for preparation in industrial scale, compared to many other catalysts.

2.2.4.1 Synthesis Methods

Generally, the synthesis of MOFs is performed under solvothermal method in pressurized autoclaves, which is also known as the conventional electrical (CE) heating method. Recently, microwave (MW) and ultrasound (US) synthesis methods, have also been reported for this purpose [129], [139], [159]. It is demonstrated that in MW irradiation and US, the obtained size is usually smaller compared to the CE heating method (i.e. 10 times smaller in MW compared to the CE method) [35], [139]. Furthermore, the obtained crystals in the MW method are more uniform compared to the CE method [35].

2.3 Summary and Research Direction

The shortcomings of the presently available air purifiers, including incomplete oxidation of VOCs, generation of hazardous by-products, low reaction rates, inability of removing different sizes of existing VOCs, and the negative effects of humidity in the indoor environment necessitate the introduction of an alternative method to eliminate these deficiencies to improve the air quality of indoors. Although literature states that plasma-driven catalyst methods are capable of improving these problems to some extent, these methods are not economical when the concentration of VOCs is very low.

The critical role of the catalyst to achieve a high performance of VOCs removal opens a new field of study for the development of novel dual functional adsorbent/catalysts (DFA/Cs), with excellent storage and oxidation capacity. The excellent adsorption capacity and high potential catalytic properties of MOFs makes these materials potential DFA/Cs. However, many unstudied areas should be considered prior to utilizing these materials in plasma systems.

The main objective of this research is defined to utilize MOFs as DFA/Cs for a plasma-catalyst system. After an intensive literature review on different plasma-based methods and also several MOFs:

- DBD plasma was selected as the applied plasma system for this research. The set-up was designed, implemented and the impact of design parameters on the energy density and the rate of ozone generation were studied.

- Three different MOFs, MIL-101, MIL-53, and CPM-5, were chosen as DFA/Cs. These MOFs were synthesized and characterized to identify their type, specific surface area and thermal stability.
- Adsorption isotherms and breakthrough behaviors of the synthesized MOFs were intensively studied for adsorption of one ppm toluene and isobutanol.
- The target MOFs were used as catalyst in a plasma reactor and their VOCs removal efficiencies were studied.
- Formation of ozone and organic by-products and also the ability of catalyst regeneration after a plasma-oxidation reaction were investigated.
- The effect of the presence of 30% relative humidity on the adsorption behavior and oxidation ability of each MOF was investigated.
- Feasibility of regeneration of the targeted MOFs after adsorption and oxidation processes were studied.

Chapter 3

3. Impact of Design Parameters on the Performance of Non-Thermal Plasma Air Purification System

Connecting Statement

Design and implementation of a plasma set-up was the first defined sub-objective of this research. For this purpose, a dielectric barrier discharge (DBD) micro reactor was selected as non-thermal plasma set-up. Different forms and types of metals including silver paste, aluminum foil and two different meshes of stainless steel were applied as ground electrodes. The area of plasma active zone was changed via changing the length of the inner electrode. Also the gap between the electrodes was altered by changing the reactor diameter. The impact of the above mentioned design parameters on the energy consumption and the rate of ozone generation in the plasma set-up were investigated.

The outcome of this research is published in “Chemical Engineering Journal” (*Bahri, M., Haghghat, F., Rohani, S., & Kazemian, H., (2016), Chemical Engineering Journal, 302, 204-212*).

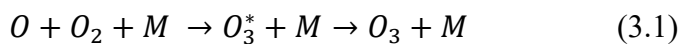
3.1 Introduction

Over the past decade, non-thermal plasma (NTP) systems have been considered as indoor air treatment methods for removal of volatile organic compounds (VOCs) [32], [77], [160], [161], as well as particulate matters [65], [68] and bacteria [66], [67]. In this method, acceleration of electrons takes place in the presence of a high voltage discharge. The collision of these high energy electrons with the molecules in the air causes the formation of different types of reactive species,

ions and radicals (R^* , R^+ , $R\cdot$), which contribute to oxidation reactions of organic pollutants as well as removal of particulate matters and bacteria [50], [160].

The advantages of NTP systems include destruction of VOCs for a wide range of concentration, especially concentrations lower than 100 ppm [81], and also their relatively high removal efficiency for particulate matters [65], [68]. However, there are some concerns, which restrict the application of these systems for the indoor environment. One of these concerns is related to the high level of energy consumption in plasma-based systems [50], [162]. To overcome this problem, different types of plasma systems have been studied for utilization in indoor environment [49], [50]. Among them, dielectric barrier discharge (DBD) systems have attracted significant attention due to their facile implementation and scale up, and higher energy efficiency [52], [53]. A DBD reactor consists of one or two dielectric barriers between the two electrodes. The discharge which is initiated on the surface of the inner electrode produces large volume of micro-discharges [163], [164]. The characteristics of micro-discharges depend on different parameters including reactor configuration, composition of the gap-gas, as well as its pressure, the field polarity, and the frequency of the applied voltage [164].

The second and very important concern of plasma-based method is formation of large amounts of ozone molecules as one of the reactive species [56], [62]. Formation of ozone is a consequence of dissociation of oxygen and nitrogen molecules [52]. The main part of the ozone formation is the result of a reaction, which takes place in a few microseconds, in the presence of micro-discharges in a DBD system, as follows:



M is described as a third collision partner including O_2 , O_3 , O or N_2 in the case of air [52]. In addition, dissociation of nitrogen molecules in the air initiates a series of reactions that eventuates to generation of more O_3 molecules due to the formation of oxygen atoms [52] according to the reactions (3.2) to (3.5):





The presence of large volumes of ozone in the treatment of drinking water or flue gas with high concentration levels of pollutants is an advantage, as it can play a significant role in the decomposition of pollutants [57], [62]. Yet, when it comes to its application for indoor air treatment, due to very low concentration levels of VOCs, generation of high amounts of ozone is not necessary. In addition, this highly reactive molecule has been recognized as a hazardous compound for occupants' health [165]–[167]. One approach to reduce the ozone concentration is introducing a catalyst downstream of the plasma reactor [106]. The catalyst not only removes the residual ozone from the downstream, but also initiates a series of heterogeneous catalytic reactions in the presence of the ozone which eventually results in enhancement of VOCs removal performance [160].

Several studies have reported destruction of VOCs with concentrations around two ppm successfully using the ozone level of less than 60 ppm in the presence of a catalyst [32], [69]. For instance, while the removal efficiency of 2.2 ppm formaldehyde in a NTP reactor was 36%, utilizing MnO_x/Al_2O_3 as catalyst enhanced this amount to 87%, and the amount of the outlet ozone was decreased from 58 ppm to 14 ppm due to decomposition of ozone on the surface of the catalyst [64]. In another study, removal of a mixture of benzene, toluene and p-xylene with the concentration of 1.5, 1.4 and 1.2 ppm, respectively in the presence of 46.7 ppm of ozone and MnO_x/Al_2O_3 as the catalyst showed a conversion of 94%, 97% and 95% , as well as reducing the outlet ozone concentration to 1.9 ppm [4]. It should be noted that even the catalyst cannot totally remove the generated ozone and the ozone level in the outlet is still much higher than 20 ppb specified by the Health Canada's Residential Indoor Air Quality Guideline [168], for a long-term exposure.

The reaction kinetic of ozone formation can be optimized by controlling the operating parameters including the power density, pressure, air-gap width between the electrodes, electrodes' configuration and the properties of the dielectric barrier in a plasma system [52]. Up to now, various types of the reactors with different sizes, as well as electrode configurations and types have been utilized and the removal efficiency of VOCs is investigated in these reactors [32], [76], [103], [113], [114], [117]. However, despite the importance of controlling the ozone level for indoor applications, the impact of design parameters on the ozone generation along with energy

consumption in a DBD system has not been specifically investigated. Accordingly, this paper reports the outcomes of a series of experimental studies, which investigated the impact of residence time, type and configuration of the ground electrode, and reactor size on the energy density and the rate of ozone generation of a DBD micro-reactor.

3.2 Experimental Setup and Apparatus

Figure 3.1 illustrates the schematic diagram of the set-up.

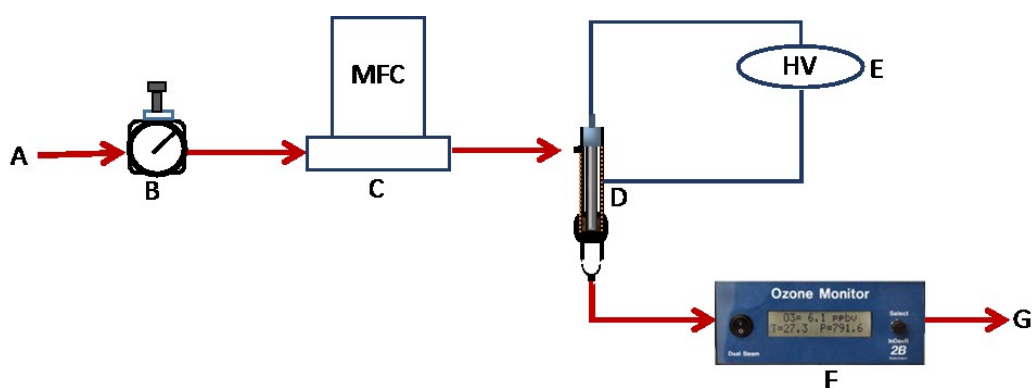


Figure 3.1 Schematic diagram of the plasma set-up; (A) Compressed air, (B) pressure regulator, (C) mass flow controller (MFC), (D) DBD reactor, (E) high voltage generator array, (F) ozone monitor, and (G) Exhaust

Figure 3.1 shows that compressed air (A) passes through a pressure regulator (B) to adjust the pressure to 10 psig. The airflow rate is set and controlled by a mass flow controller (MFC) (C) and passes through a DBD reactor (D). The applied voltage is provided by a high voltage generator array (E) which is explained later. The airflow rate is set at 0.6 L/min and the experiment is performed at ambient temperature ($21\pm 1^\circ\text{C}$). The concentration of generated ozone in the reactor is measured downstream of the reactor using a Model 202 Ozone Monitor (F) (2B Technologies, An InDevR Company), which is capable of measuring ozone concentration in a linear dynamic range of 1.5 ppb -250 ppm with resolution of 0.1 ppb. The measurement principle is based on the absorption of UV light at 254 nm. The measurement interval is set to 10 s. For each test, at least 20 readings of the ozone concentration are recorded and the average amount is used as the ozone concentration.

In this study, two sizes of the quartz tubes were employed as a reactor. Specification of these reactors is summarized in Table 3.1. The concentric geometry of reactors consists of a centered stainless steel-316 rod (D: 5mm, L: 150mm) as an inner electrode.

Table 3.1 Specification of the reactors

	ID (mm)	OD (mm)	L(mm)
Reactor#1	9.9	12.0	250.0
Reactor#2	10.4	12.8	250.0

The ground electrode consists of three metals in four different configurations, including stainless steel with two mesh sizes of 600 μ m (SS-T) and 90 μ m (SS-F), aluminum foil (Al), and silver paste (Ag). To prepare silver as the ground electrode, the outer surface of quartz tube is covered with a thick layer of silver paste (Aldrich, $\rho= 5-6 \mu\Omega.cm$). The reactor is then cured at 180 $^{\circ}$ C for three hours. The electrode configurations are shown in Figure 3.2.

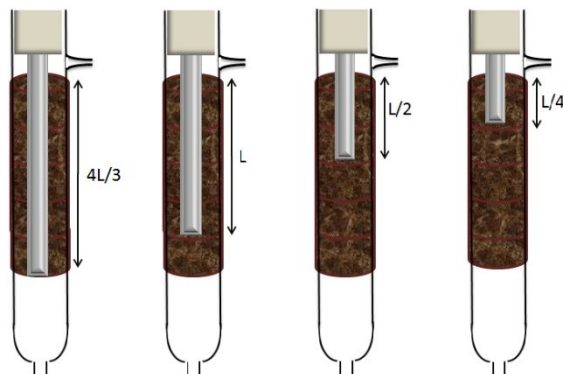


Figure 3.2 Configuration of the inner electrodes

The schematic of the high voltage power supply, indicated by HV in Figure 3.1, is illustrated in Figure 3.3.

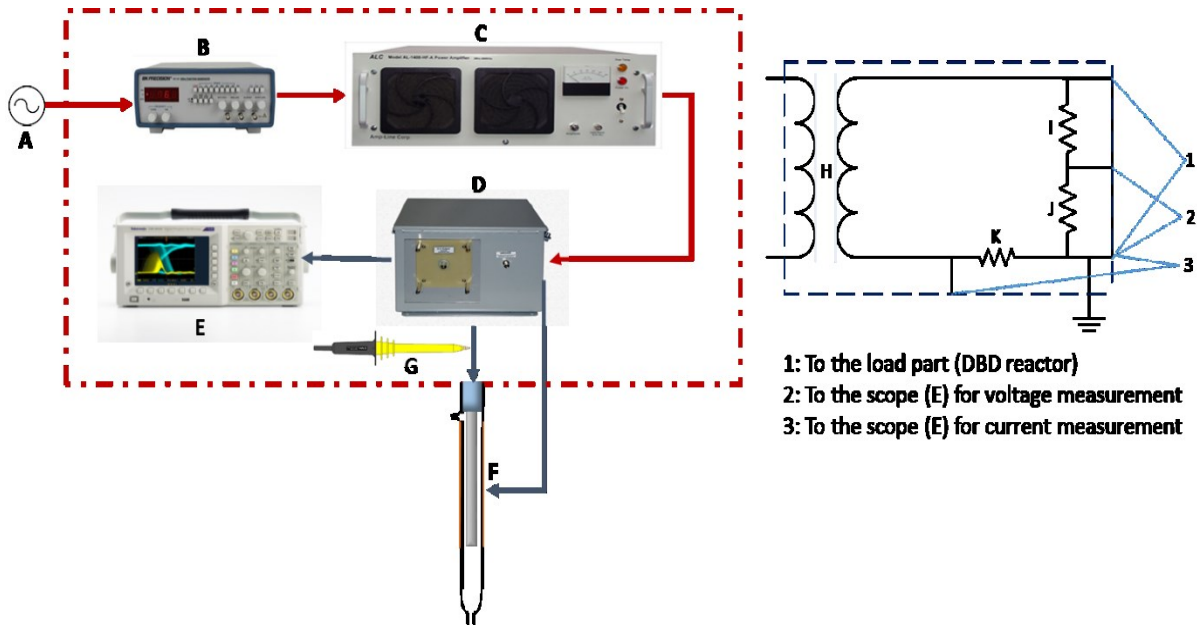


Figure 3.3 Left panel: The schematic diagram of the high voltage power supply; (A) AC power, (B) function generator, (C) AC power amplifier, (D) high voltage transformer box, (E) oscilloscope, (F) DBD reactor, and (G) high voltage probe. Right panel: The block diagram of the high voltage transformer box; (H) Coil, (I) 10 k Ω resistor, (J) 530 k Ω resistor, (K) 1 k Ω resistor.

The function generator (B) (BK PRECISION, Model 4011A), shown in the left panel of Figure 3.3, uses AC power (A) as input and generates sinusoidal waveform with the adjustable frequency between 50Hz and 2kHz. The output of the function generator is applied to a wideband AC power amplifier (C) (Model AL-600-HF-A, Amp-Line Corp.), which transforms the input signal of 0-2 V_{rms} to an adjustable voltage in the range of 0-28 V_{rms} and frequency between 20 Hz and 800 kHz, with an output power of maximum 600 W. Afterward, a high voltage transformer box (D) (Model AL-T250-V25/10K-F50/2K, Amp-Line Corp.), transforms the primary voltage to a secondary voltage up to 30 kV_{p-p} . The output power and the bandwidth of the transformer are 250 W, and 50 Hz to 2 kHz, respectively. The block diagram of the high voltage transformer and the added resistors (I, J, and K), are illustrated in the right panel of Figure 3.3. The coil (H) intensifies the input voltage by 440 times. The high voltage output is loaded by the DBD reactor (F) via resistor I, while the outputs of resistors J and K are sent to a digital oscilloscope (E) (Tektronix, TBS1052B-EDU, 50MHZ, 2CHANNEL) to monitor the voltage and current signals of the system over time. To make sure about the voltage which is delivered to the reactor, the high voltage in the

load part is also measured by a 30 kV high voltage probe (G) (Keysight N2771B). All parts of the set-up are connected using high voltage wires.

The measured data are used to evaluate the energy consumption of the system. For a plasma system the applied energy density into the reactor, known as specific input energy (SIE, JL^{-1}), is an indicator of the energy consumption, which is defined as:

$$\text{SIE} = \frac{60VI}{Q} \quad (3.6)$$

where, V is the applied voltage (kV); I is the discharge current (mA); Q is the gas flow rate (L min^{-1}), and 60 is the conversion factor ($1 \text{ W.h} = 3600 \text{ J}$). The frequency for all experiments is set to 60 Hz. Prior to the main tests, a series of experiments are performed to investigate the repeatability of the system. Results are provided in Appendix A.

3.3. Results and Discussion

3.3.1 Effect of residence time

To study the effect of residence time on the consumed power, as well as on the volume of generated ozone, a series of experiments were performed in which the effective volume of plasma zone was changed by changing the lengths of the inner electrodes: L, L/2, and L/4 using Reactor#1 (see Table 3.1). The experiments were performed for four different configurations of ground electrodes including, SS-T, SS-F, Al and Ag. Results are displayed in Figures 3.4 and 3.5.

Figure 3.4 shows an increase in power consumption as the length of the inner electrode increases for all configurations of ground electrodes. This result is explicitly related to an expansion in the effective volume of the plasma zone, and consequent requirement of higher levels of energy for ionization of the existing air molecules between the two electrodes. On the other hand, according to Figure 3.4, by decreasing the effective length of the inner electrode, a higher amount of voltage is required to achieve the plasma ignition.

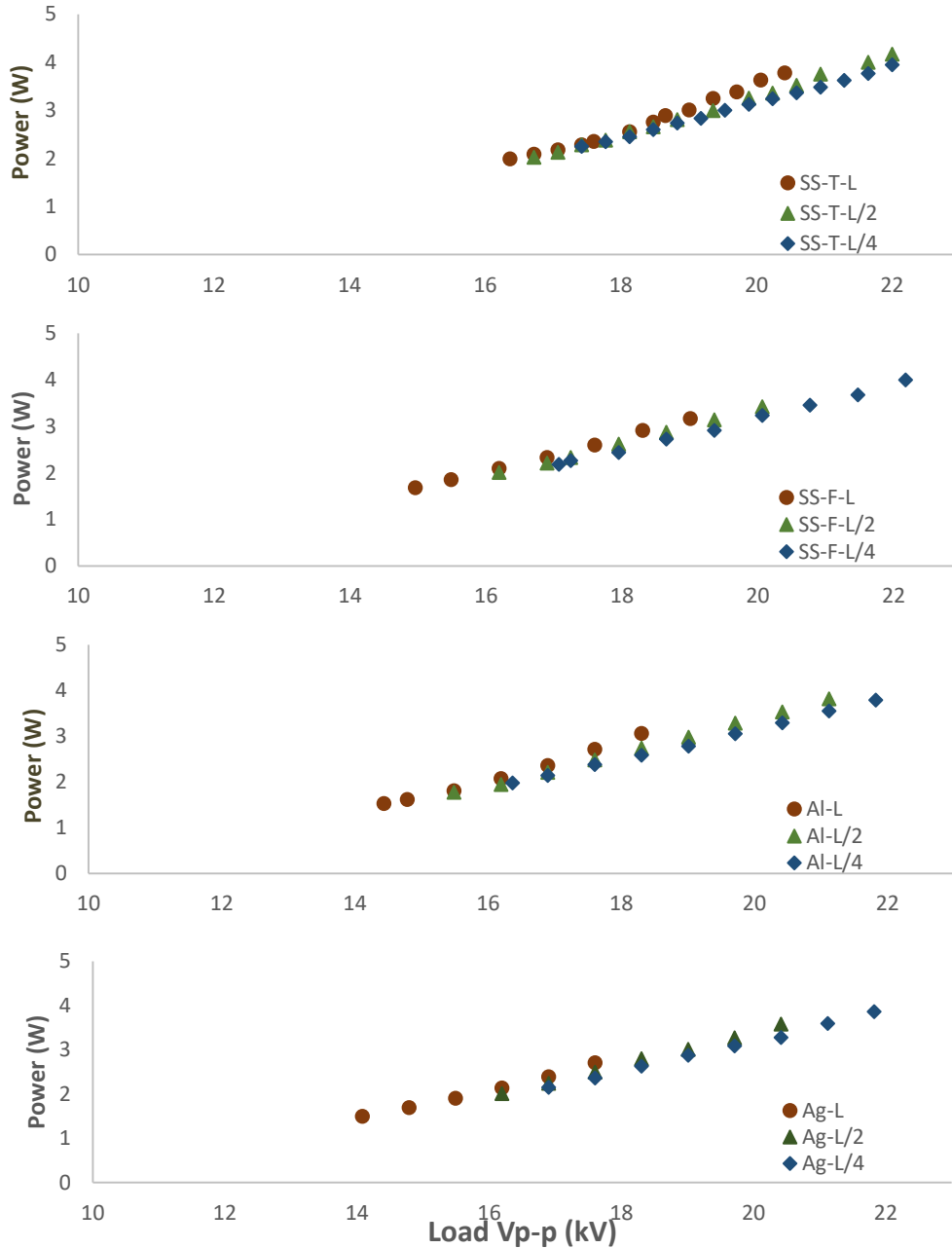


Figure 3.4 Effect of increasing the residence time (IE size: L, L/2 and L/4) on the required power; GE: SS-T, SS-F, Al, and Ag; Reactor#1

According to the Townsend definition, plasma ignition is a self-sustaining discharge, which is independent of an external source of free electrons [169]. Ignition is a function of pressure and the air gap distance between the electrodes. Since the pressure and the air-gap are kept constant in all experiments, it is postulated that by decreasing the inner electrode length, the effective electrode surface, which is exposed to the air molecules decreases. The decrease in the effective electrode

surface results in formation of less micro-discharges in the active plasma zone inside the reactor [164], [170], which leads to a decrease in the chance of breakdown of the gas. Similar trends were observed for all types of ground electrodes (SS-T, SS-F, Al, and Ag), (Figure 3.4). While the amount of the SIE according to Equation (3.6) is proportional to the power, increasing the residence time by increasing the inner electrode length, eventually gives rise to larger rate of ozone generation.

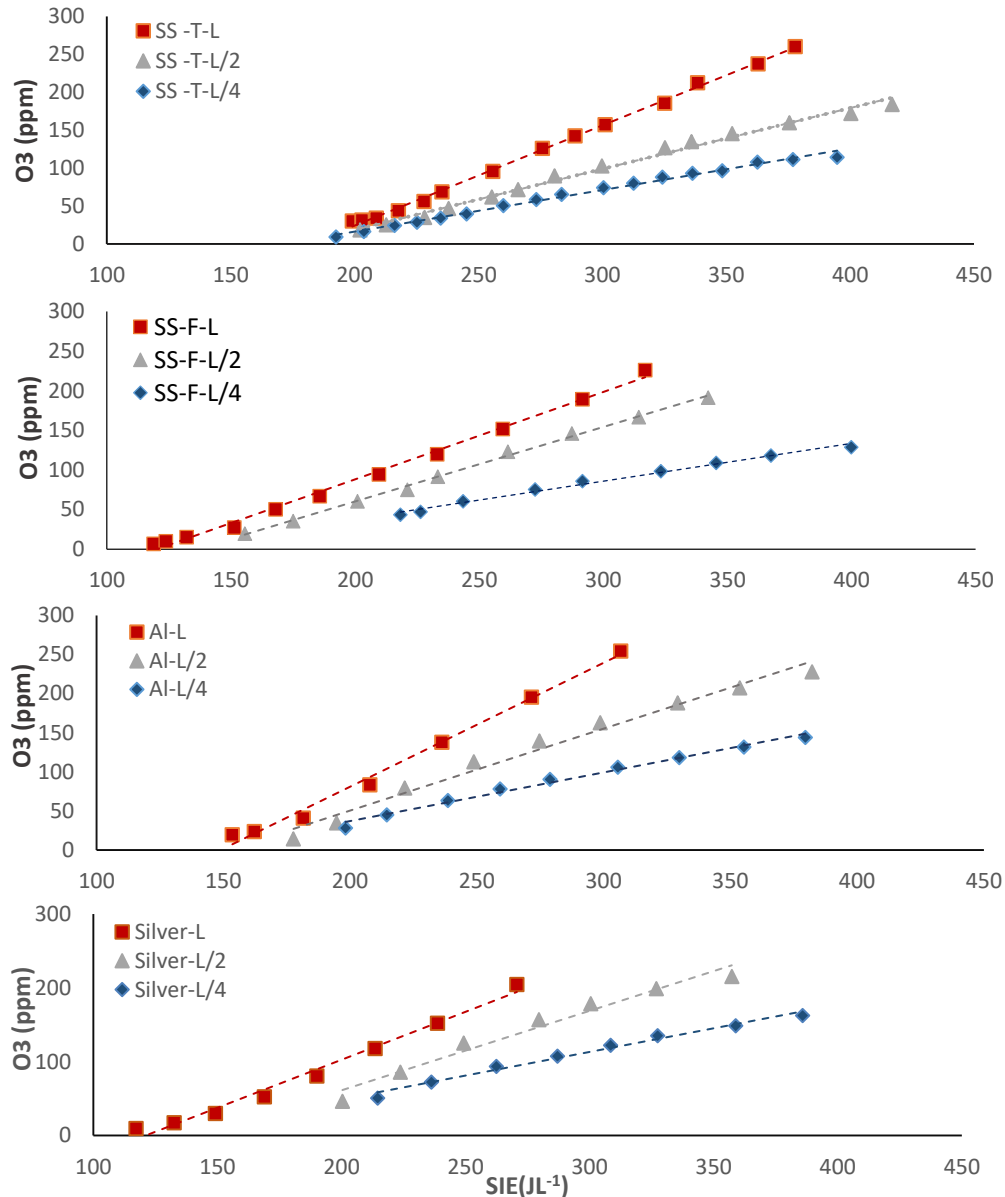


Figure 3.5 Effect of increasing the residence time (IE size: L, L/2, and L/4) on the ozone generation; GE: SS-T, SS-F, Al, and Ag; Reactor#1

Figure 3.5 shows that using a longer length of inner electrode not only ignites plasma at a lower voltage, but also increases the rate of ozone generation for a given SIE. The detailed values of standard deviation (STD) for generated ozone in different specific input energies are presented in appendix B.

3.3.2 Effect of electrode configuration

Figure 3.6 shows that for a given effective inner electrode length and a given SIE, the rate of the ozone generation changes by changing the ground electrode. The sequence of ozone generation rates for different electrodes is Ag>Al>SS-F>SS-T. It should be noted that the ground electrode is a passive electrode (it does not touch the electric field directly); thus its conductivity cannot be an effective parameter in the ozone generation. However, the difference between the amounts of the generated ozone for two different meshes of stainless steel (600 μ m (SS-T) and 90 μ m (SS-F)) confirms that the configuration of the ground electrodes is the more dominant factor on the ozone generation than its type (applied metal).

The effect of ground electrode configuration on the decomposition of benzene was explained by Kim and his colleagues [170]. When the AC voltage is applied to the reactor, accumulation of ions with the same charges on the surface of the dielectric barrier during the first half-cycle is followed by an increase in the charges of the air-gap between the electrodes during the second half-cycle [170], [171]. This results in generation of micro-discharges and enhancement of an electric field in the air-gap in the reactor. The presence of any small gap between the dielectric barrier and the ground electrode results in the dust-enhanced streamers or corona discharges outside of the reactor [164], [170]. Figure 3.7 (A) illustrates the perspective of micro-discharges in the air-gap inside a DBD reactor, as well as corona discharges outside of the reactor.

In this case, the dielectric (DE) layer, the air-gap inside of the reactor (Air), and the void between the ground electrode and the dielectric layer (Air*) act as capacitances. Figure 3.7 (B) shows the equivalent electrical circuit during plasma generation. The total capacity of the system is calculated as:

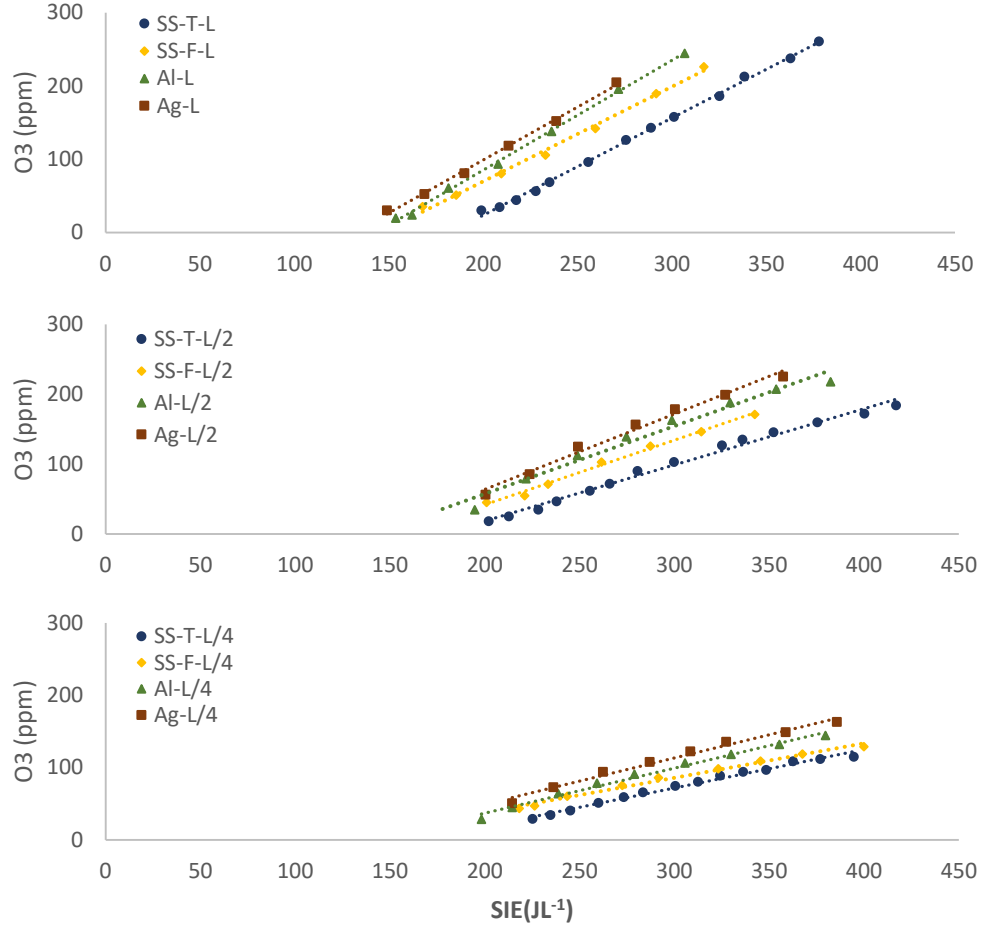


Figure 3.6 Effect of the specific input energy on the rate of ozone generation; IE size: L, L/2 and L/4, GE: SS-T, SS-F, Al, and Ag; Reactor#1

$$\frac{1}{C_{Total}} = \frac{1}{C_{Air}} + \frac{1}{C_{DE}} + \frac{1}{C_{Air*}} \quad (3.7)$$

$$C_{Total} = \frac{C_{Air} \cdot C_{DE} \cdot C_{Air*}}{C_{Air*} \cdot C_{DE} + C_{Air} \cdot C_{Air*} + C_{Air} \cdot C_{DE}} \quad (3.8)$$

where C_{Air} is the capacitance of air-gap inside the reactor between the electrodes, C_{DE} is the capacitance of dielectric layer, C_{Air*} is the capacitance of the void outside the reactor. $R(t)$ and $R'(t)$, shown in Figure 3.7 (B), are the equivalent discharge resistances of the DBD. The applied voltage in this case is divided between all these capacitors, and the energy which is used to ionize the air in the outer layer of the reactor: it can be considered as “wasted energy” [170]. When Ag is pasted and cured, the ground electrode is uniformly attached on the surface of the dielectric barrier.

Therefore, the void between the dielectric barrier and the ground electrode is eliminated. Thereby, the total capacitance is simplified to:

$$\frac{1}{C_{Total}} = \frac{1}{C_{Air}} + \frac{1}{C_{DE}} \quad (3.9)$$

$$C_{Total} = \frac{C_{Air} \cdot C_{DE}}{C_{DE} + C_{Air}} \quad (3.10)$$

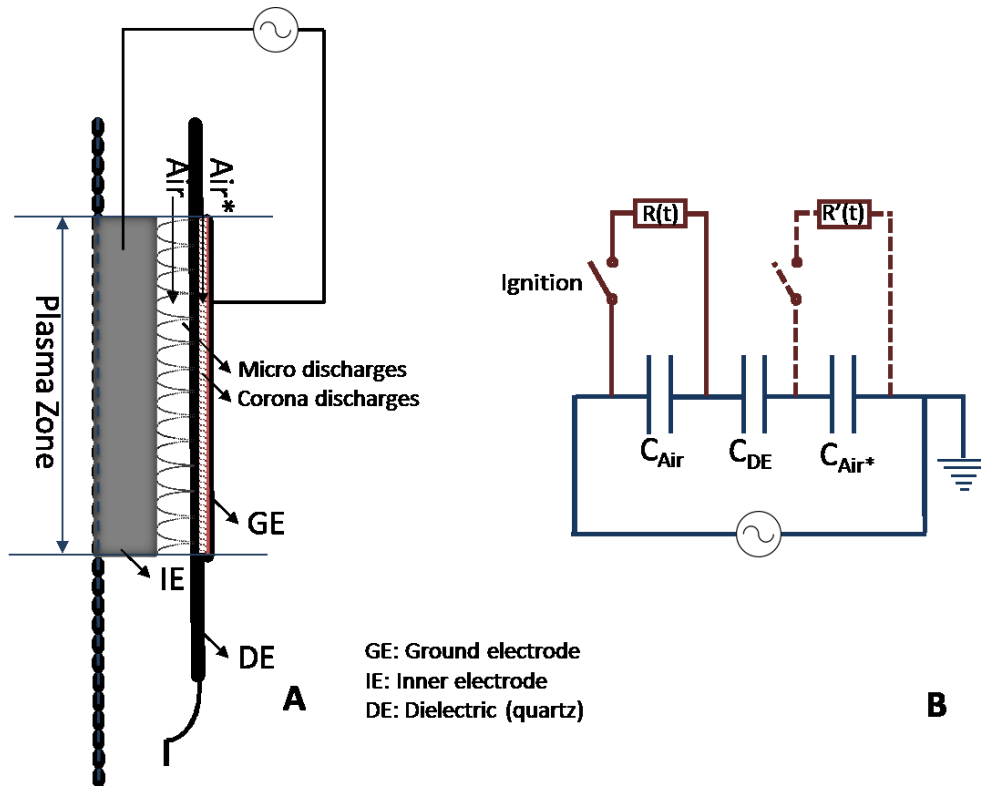


Figure 3.7 Formation of micro-discharges in the air-gap inside the reactor, as well as corona discharges outside of the reactor (A), and the equivalent electrical circuit (B) during plasma generation in a DBD reactor

The result of eliminating the C_{Air*} is saving that part of the energy that is wasted in the form of parasite discharges out of the reactor. This saved energy could participate in the ionization reactions that take place in the air-gap and result in a higher rate of ozone generation. This could explain why Ag electrode shows a higher performance. The application of SS-T as the ground electrode provides an uneven field containing several voids and thus increases the amount of the wasted energy (Figure 3.6). The performance of Al foil and SS-F are between these two electrodes.

3.3.3 Effect of reactor size

To investigate the effect of the reactor size on the rate of the generated ozone, the size of reactor was increased by means of changing the diameter of the quartz tube that caused an increase in the gap between the electrodes by approximately 5%, as well as 12.5% of increase in the quartz thickness. Figure 3.8 shows a decrease in the rate of ozone generation for a given amount of consumed power in Reactor#2 compared to Reactor#1, see Table 3.1.

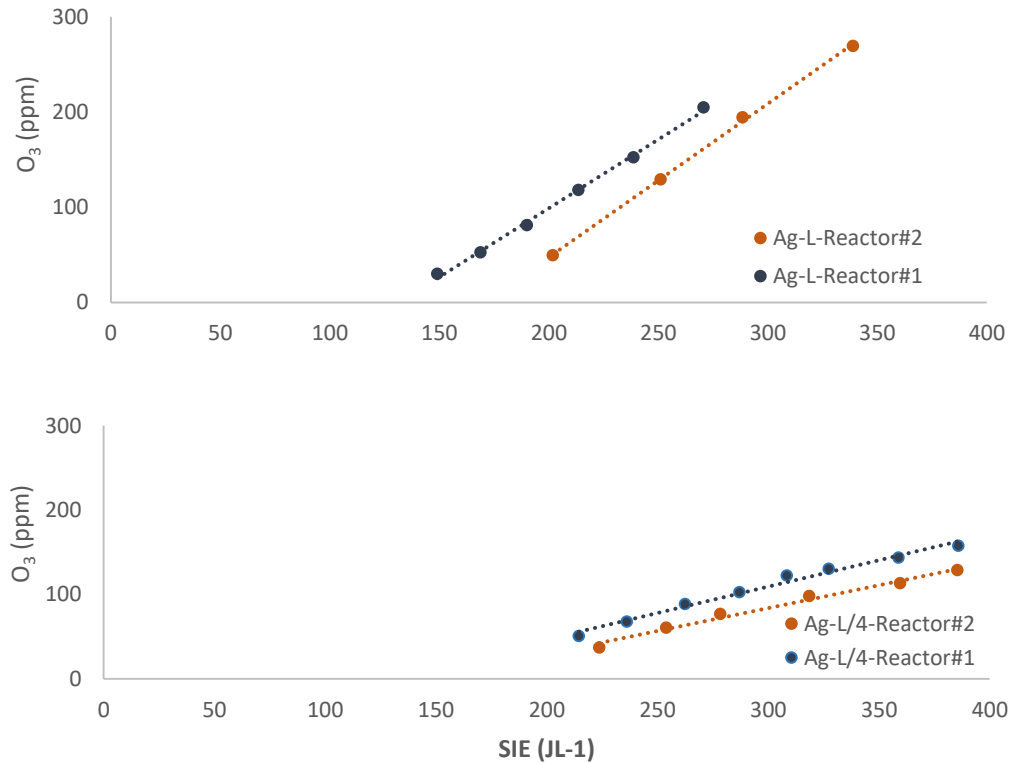


Figure 3.8 Effect of increasing the size of reactor on the rate of ozone generation; IE size: L, and L/4, GE: Ag

Obviously, properties of the dielectric barrier including permittivity and thickness can affect its capacitance [52]. Quartz as a dielectric ($\epsilon = 3.8$) plays an important role in stabilizing the NTP system by reducing the field strength in the discharge area, and constricting the discharge channels [52], [54]–[56]. Yet, a reduction in the air-gap voltage is the consequence of increasing the thickness of the dielectric, which causes a decrease on its capacitance [164]. Furthermore, increasing the air-gap between the two electrodes is another effective factor that suppresses the ignition voltage [169]. The passing air through the reactor acts as a weak dielectric. Therefore,

more energy is required for reaching the ignition voltage. The presence of larger amounts of air molecules between the gaps causes the dilution of the reactive species including ozone.

Figure 3.9 summarizes the effect of changing the length of the inner electrode on the amount of ozone generation for Reactor#2, when Aluminum and Silver were used as ground electrodes. The result follows similar patterns for Reactor#1: for each applied length of the inner electrode, an increase in the amount of ozone generation can be seen by an increase in the SIE.

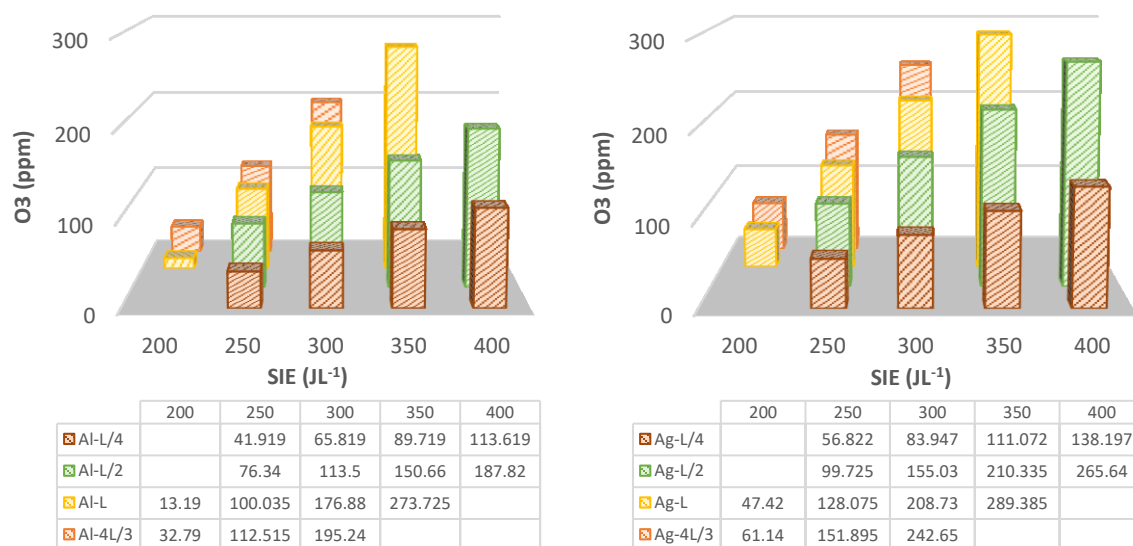


Figure 3.9 Effect of the specific input energy on the amount of generated ozone; IE: 4L/3, L, L/2 and L/4; GE: Al and Ag, Reactor#2

Figure 3.9 shows that providing a longer length of inner electrode leads to the enhancement of plasma zone, residence time. According to Figure 3.9, for a given amount of SIE the amount of ozone is increased. A quantitative comparison between the rates of generated ozone for Al and Ag ground electrodes (Figure 3.10), confirms that regardless of the size of the reactor, utilizing Ag as ground electrode forms a larger amount of ozone. Obviously, while the objective of this research is providing the concentration of ozone for treatment of indoor VOCs, formation of large amounts of ozone is unnecessary. According to the results, utilizing either silver or aluminum as the ground electrode, and also an inner electrode with the length of $\geq L$, and the SIE levels of ~ 200 to 250 JL^{-1} seem to provide the sufficient amount of ozone, which is required for decomposition of VOCs in indoor environment [4], [32], [69].

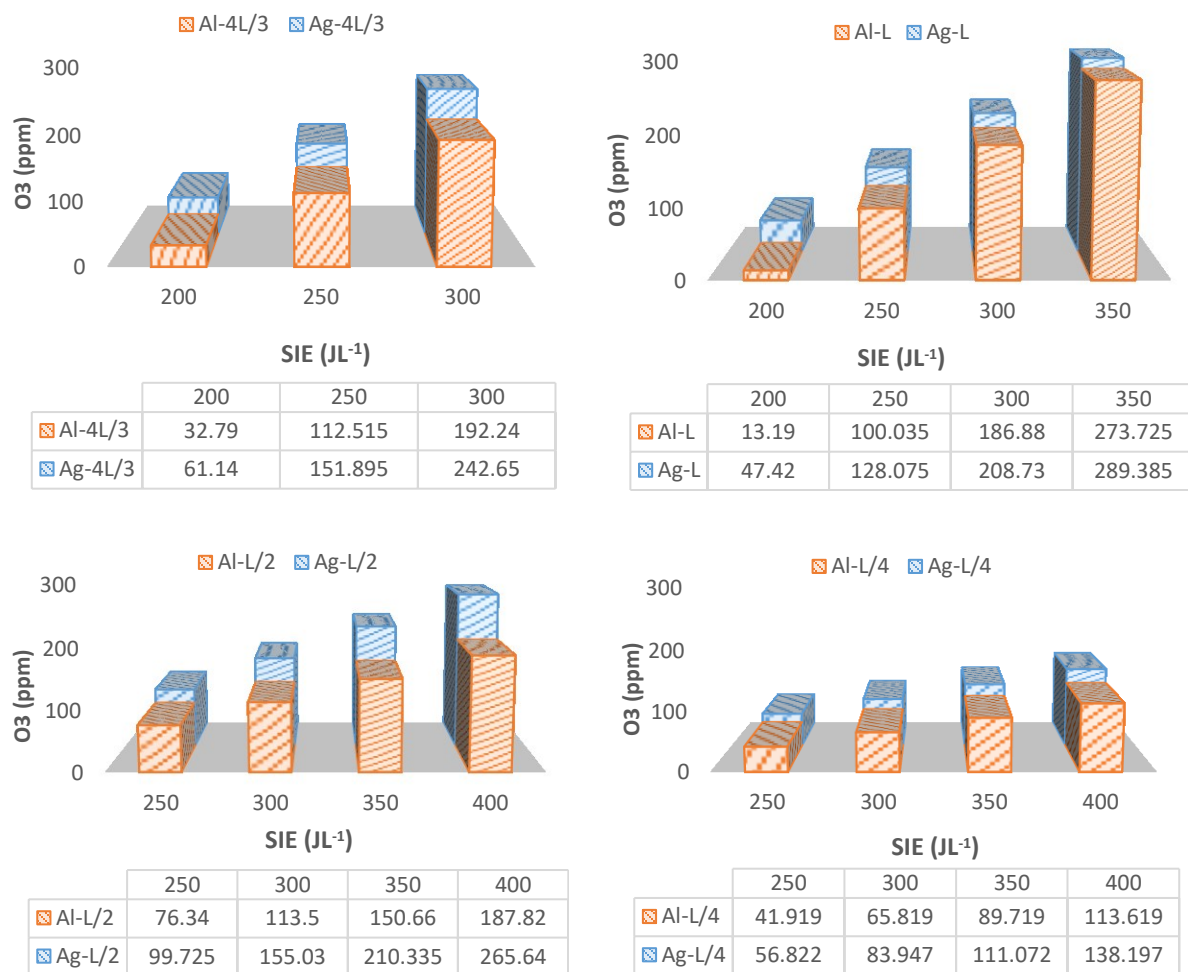


Figure 3.10 Comparison between the amounts of ozone generation in reactors; IE: 4L/3, L, L/2 and L/4; GE: Al and Ag; Reactor#2

3.4 Conclusion

In this study the effect of design parameters including the configuration and type of electrodes as well as the size of the reactor on the rate of ozone generation and also SIE were investigated. The application of the designed set-up is considered for an indoor environment; thus, controlling the rate of ozone is critical. Results showed that:

- Although the energy yield, for different forms and types of electrodes varies ($Ag_{\text{paste}} > Al_{\text{foil}} > SS-F_{\text{mesh}} > SS-T_{\text{mesh}}$), configuration of ground electrode is a dominant parameter on ozone generation, rather than its type.

- Increasing the active zone of plasma by means of utilizing a longer inner electrode results in an earlier plasma ignition, as well as formation of larger amounts of ozone in the same SIE. This result is valid regardless of the type and configuration of the applied ground electrode.

- Increasing the size of the reactor by increasing the gap between the electrodes, gives rise to the requirement of larger SIE amounts to reach the same level of ozone concentration. This point should be considered very carefully in the plasma reactor scale- up.

- For the implemented set-up, applying SIE $\sim 200 \text{ JL}^{-1}$ along with the size of L when silver paste or aluminum foil are applied as ground electrodes, generate the required level of ozone for indoor application when Reactor#2 is used. The same range of ozone generation can be achieved by applying approximately 150 JL^{-1} of SIE in Reactor#1, when the effective size of the inner electrode is L.

- Further studies are required to optimize the energy level and ozone concentration for decomposition of VOCs in an indoor condition when a catalyst is applied in the reactor.

Chapter 4

4. Mechanochemical synthesis of CPM-5: A Green Method

Connecting Statement

Synthesis of three different MOFs as DFACs was the second sub-objective of this research. To prepare the catalysts, different methods have been reported. An important issue in preparation of these MOFs with conventional methods is the use of an abundant amount of N, N-dimethylformamide (DMF), which is a hazardous solvent. Therefore, the development of green technologies has been considered as an approach to address some of the environmental issues of commercializing these materials. Accordingly, in this study, the first attempt was to develop a new green method for the synthesis of at least one of the selected MOFs.

So far, no environmentally friendly method has been reported for the preparation of Crystalline Porous Material-5 (CPM-5). Therefore, a mechanochemical method was developed to synthesize this MOF. For this purpose, a mixer mill was used to pulverize and thoroughly mix the precursors and to eliminate the use of an organic solvent during the course of catalyst preparation.

Different numbers of stainless steel balls (3.2mmØ, ~0.134g each) were used for grinding. The oscillation frequency was varied from 30 to 90 Hz, and the oscillation time was ranged from 15 to 60 min. After grinding, thermal treatment and washing of the samples were used to complete the synthesis process. The resulting samples were characterized by different methods including X-ray diffraction (XRD), scanning electron microscopy (SEM), thermogravimetric analysis (TGA), and BET surface area analysis.

The outcome of this research is accepted as a research paper in "Journal of Chemical Engineering & Technology" (*Bahri, M., Kazemian, H., Rohani, S., & Haghghat, F., (2017), Journal of Chemical Engineering & Technology, 40, No.1, 88–93*).

4.1 Introduction

Metal organic frameworks (MOFs) are a new class of organic-inorganic polymers with phenomenal flexibility in tuning their porous structure and adjusting their internal surface properties [36], [123], [124]. These highly porous materials are composed of inorganic metal ions or metal clusters and organic linkers, in the form of mono-, di-, tri-, or tetravalent ligand molecules [128], [130], coordinated together with strong covalent bonds [122]. This organic-inorganic topology allows MOFs to have numerous types of adjustable open framework structures by changing the organic linkers, as well as metal clusters [131], [172]. Crystalline Porous Material-5 (CPM-5) with a typical chemical formula of $[(\text{CH}_3)_2\text{NH}_2][\text{In}_3\text{O}(\text{BTC})_2(\text{H}_2\text{O})_3]_2\text{-}[\text{In}_3(\text{BTC})_4]\cdot 7\text{DMF}\cdot 23\text{H}_2\text{O}$ is a MOF with a highly symmetric framework [146]. The framework of CPM-5 consists of In_3O clusters as metal centers, which are connected by means of 1,3,5-benzenetricarboxylate (BTC) linkers [146]. The unique cage-within-cage structure of CPM-5, along with its luminosity and hydrothermal, thermal, and photochemical stability, make this MOF a great potential candidate for many applications including adsorption, catalysis, gas separation, and oxygen sensing [141], [146], [173], [174].

Zheng et al [146] were the first group to report the synthesis of CPM-5 using a solvothermal method at 120°C in 5 days. Later on, this MOF was synthesized using different synthesizing approaches including a hybrid technique by means of microwave (MW) and ultrasound energies [129]. The latter method is advantageous in terms of time and energy efficiency. However, during the synthesis and the treatment processes of CPM-5, a substantial amount of N, N-dimethylformamide (DMF) is used, which is a hazardous solvent from an environmental point of view. Furthermore, the solvent used must be removed after synthesis/treatment steps. Therefore, a separation unit has to be utilized downstream and this adds to the costs of the entire process. These concerns, therefore, hinder industrial scale application for the preparation of CPM-5. To eliminate or minimize the solvent consumption, application of solvent-free methods such as mechanochemical (MC) and thermal methods has been proposed [175]–[178]. However, solvent-free methods are challenging for the preparation of MOFs, as the precursors are generally solid materials [179].

Generally, in a MC method, grinding of powdered precursors takes place due to violent shaking of media in the presence of stainless-steel balls in a metal jar [180], [181]. This rapid movement

results in a series of physical and chemical phenomena and an increase in the temperature of the reactants. Usually, the mechanical grinding initializes the reaction, after which the reaction continues spontaneously [182]. This then results in the formation of the desired product either during or after the grinding step [180]. It has been demonstrated that using a MC method not only eliminates the use of solvent during the synthesis process, but it also decreases the reaction time compared to conventional methods [178], [181], [183], [184]. Nonetheless, it should be noted that in some cases the use of a solvent for purification of the formed sample by a MC method is necessary [184], [185].

This paper is the first to report a green MC method using a ball mill for the synthesis of CPM-5. The effects of several mechanical parameters, including oscillation frequency and time, and the proportion of balls to precursors for grinding, were investigated. Furthermore, two post-synthesis treatment techniques, including thermal treatments and washing with different solvents, were performed to study the effect of these operational parameters on the final product.

4.2 Materials and Methods

A MC procedure was developed in a Mixer Mill (RETSCH MM2 Pulverizer, 110 Volt, 60Hz, 40 Watt, Germany) for the synthesis of the CPM-5 and the effect of mechanical blending on the formed sample was investigated by changing the oscillation frequency and time, and the number of metal balls used for milling. For this purpose, the solid precursors including indium (III) nitrate hydrate ($\text{In}(\text{NO}_3)_3 \cdot x\text{H}_2\text{O}$; 99.5%, Philipsburg, USA) and 1,3,5-benzenetricarboxylic acid ($\text{C}_9\text{H}_6\text{O}_6$), known as trimesic acid (BTC, MW=210.14, Caledon Laboratory Chemicals, Georgetown, Ontario, Canada), were mixed together. The ratio of these precursors ($\text{In}(\text{NO}_3)_3 \cdot x\text{H}_2\text{O}$ / BTC: 0.4 g/ 0.34g) was the same as those reported by Sabouni et al. [129]. The blended solid was then placed in a 10 mL capacity Tungsten Carbide (WC) jar to pulverize and thoroughly mix the precursors in the Mixer Mill. Different numbers of balls (stainless steel, 3.2mm \varnothing , ~0.134g) were used during the synthesis. The oscillation frequency and time were changed from 30 to 90 Hz, and 15 to 60 min, respectively.

After grinding, the resulting material was placed in an oven (DKN 400, Yamato Scientific America, Inc., Santa Clara, CA) at 150°C for three hours. For those samples, in which a washing

treatment was used, the solid-liquid separation process was performed in a centrifuge (Du Pont Instruments Sorvall RC-5B Refrigerated Super-speed). Characterization of the obtained samples was performed by means of X-ray diffraction (XRD), scanning electron microscopy (SEM), thermogravimetric analysis (TGA), and Brunauer-Emmett-Teller (BET) analysis.

An XRD instrument (Rigaku-MiniFlex, Japan), using CuK α (k for K α =1.54059 Å) and the Jade 7 software, was used for the X-ray diffraction of samples. The analysis was performed between the ranges of $5 < \theta < 40^\circ$ with a step width of 0.04° . The XRD results were compared with the simulated PXRD pattern of the single-crystal structured CPM-5 obtained from the Cambridge Crystallographic Data Centre (CCD). A thermogravimetric analyzer (Mettler Toledo TGA/SDTA851e, Switzerland) with the Stare software version 6.1 was used for performing thermal analysis of samples. The analysis was performed in the range of 25-600°C under nitrogen purge ($50 \text{ mL}\cdot\text{min}^{-1}$) at a heating rate of $10^\circ\text{C}/\text{min}$ in a $100\mu\text{L}$ aluminum container. To compare the TGA results of the sample with other studies, the exact procedure and the same amount of precursors presented in Sabouni et al. [129] were used for the preparation of CPM-5 with microwave energy. The BET/Langmuir surface areas of samples were measured using a surface area analyzer (Micrometrics ASAP 2010 BET Surface Area Analyzer, USA). For this purpose, each sample was first degassed in the vacuum (10^{-5} Torr) at 150°C . The specific surface area was measured according to nitrogen adsorption/desorption isotherms using the Analysis Bath at 77.35 K. The micrographs of the synthesized samples were obtained using a SEM instrument (JEOL instrument, Hitachi Variable Pressure S3400N, Japan), in conjunction with an Oxford EDS system, operating at an acceleration voltage of 15 keV.

4.3. Results and Discussion

4.3.1 The effect of metal balls/reactant ratio

To investigate the effect of the mass ratio of metal balls to the precursors, the number of balls used for grinding was changed from 10 to 20 and 30 in samples #B-1, #B-2, and #B-3. Grinding conditions, including oscillation frequency and time, were adjusted to 90 Hz and 60 min, respectively. The XRD patterns that are illustrated in Figure 4.1 show very similar peaks for all of the samples. Nevertheless, the intensity of the desired peak at $2\theta = 8.4^\circ$ is improved by increasing

the number of balls. This can be explained by the fact that by increasing the ball numbers, the mechanical and thermal energies generated through collision and friction is more intense, and this enhances the reaction rate. Although increasing the number of balls improved the intensity of the desired peaks, we did not include more than 30 balls due to the restriction dictated by the volume of the jar and the difficulty of separation of the sample and the balls.

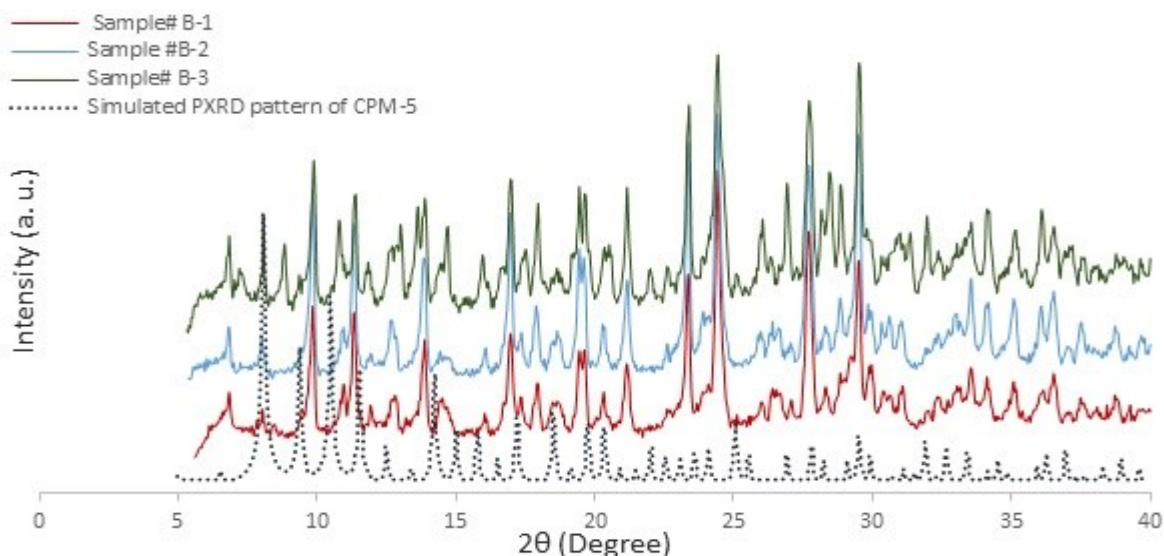


Figure 4.1 Effect of ball numbers in the intensity of the formed peaks; comparison between XRD patterns of samples #B-1, #B-2 and #B-3, and the simulated XRD pattern of CPM-5

4.3.2 The effect of oscillation parameters

In the second series of the tests, the number of balls was set to 30 and the oscillation parameters, including the frequency and time, were varied. These conditions are summarized in Table 4.1.

Table 4.1 Specification of the applied method for the MC synthesis of CPM-5; Effect of oscillation frequency and time, ball number: 30, Thermal treatment:150°C/3h

SAMPLE	Grinding Condition	
	Oscil. frequency(Hz)	Oscil. time (min)
#O-1	90	60
#O-2	90	30
#O-3	90	15
#O-4	30	30

A comparison between XRD patterns of the obtained samples and the simulated XRD pattern of CPM-5, which is presented in Figure 4.2, shows that decreasing the frequency or grinding time

diminishes the desired peak that appears at $2\theta < 10^\circ$. As demonstrated in previous studies [178], the frequency provides the required energy for shaking and grinding of the precursors, and eventually the product is crystallized. Decreasing the frequency, either by limiting the time or oscillation, hinders the precursors from reacting due to the lack of activation energy in the reaction medium. This eventuates to losing the main peak at around $2\theta = 8.4^\circ$, which is one of the characteristic peaks of CPM-5.

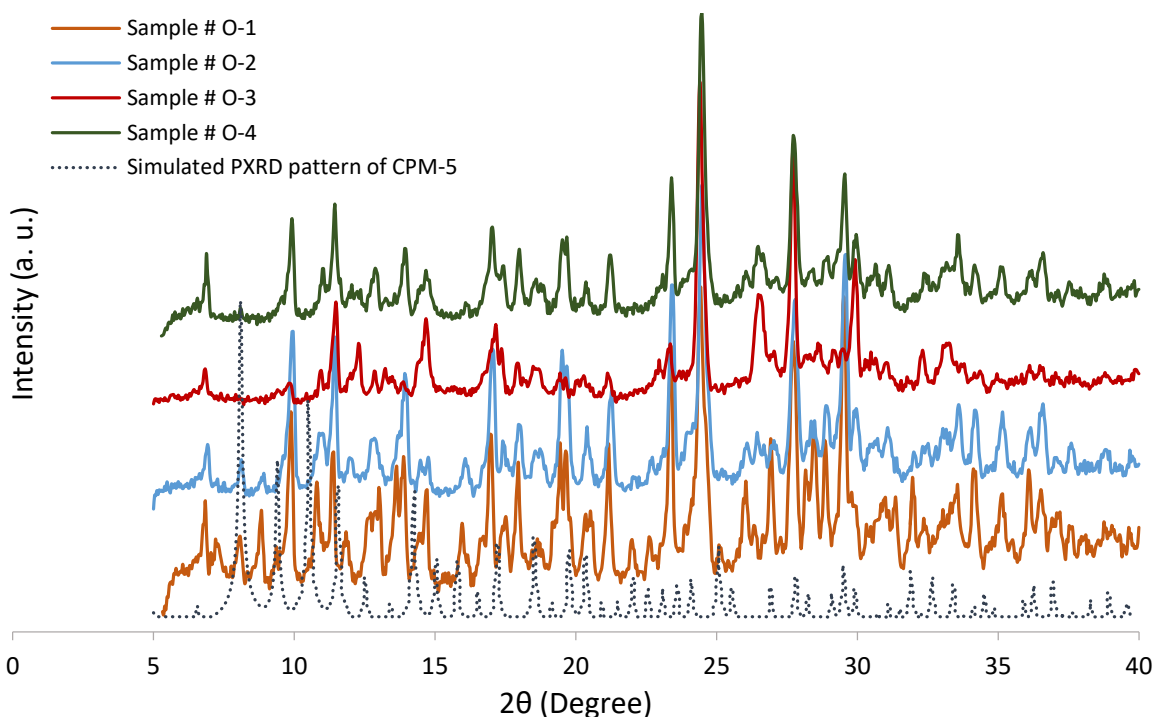


Figure 4.2 Effect of ball numbers in the intensity of the formed peaks in the resulted samples; comparison between XRDs of samples #O-1, #O-2, #O-3, and #O-4, and the simulated XRD pattern of CPM-5

4.3.3 Effect of thermal condition

In all of the previously mentioned tests, the resulting products following grinding were subjected to thermal conditioning at 150°C for three hours. To study the effect of thermal treatment on transforming the precursors towards CPM-5 formation, five different post-synthesis treatments were tested. The products were characterized using XRD technique. The experimental conditions are presented in Table 4.2.

Table 4.2 Specification of the applied method for the MC synthesis of CPM-5; Effect of thermal condition; Oscillation frequency: 90 Hz, oscillation time: 30 min, ball number: 30

SAMPLE*	Ball Number	Thermal Condition	
		Temperature (°C)	Time (h)
#T-As	30	N/A	N/A
#T-3h	30	20	3
#T-15h	30	50	15
#T-Fin	30	50/150	15/1
#T-*	30	150	2

Sample #T-As: As synthesized, just after grinding; #T-3hr: Sample was kept at 20°C (ambient temperature) for 3hr; #T-15hr: Sample was heat treated at 50°C for 15hr; #T-Fin: The previous sample (Sample#T-15hr) was heat treated again at 150°C for 1h; #T-: Sample was heat treated at 150°C for 2h directly after grinding.

XRD patterns of the prepared samples are also compared with the XRD pattern of the pure precursors (i.e. Indium (III) nitrate hydrate and trimesic acid) in Figure 4.3.

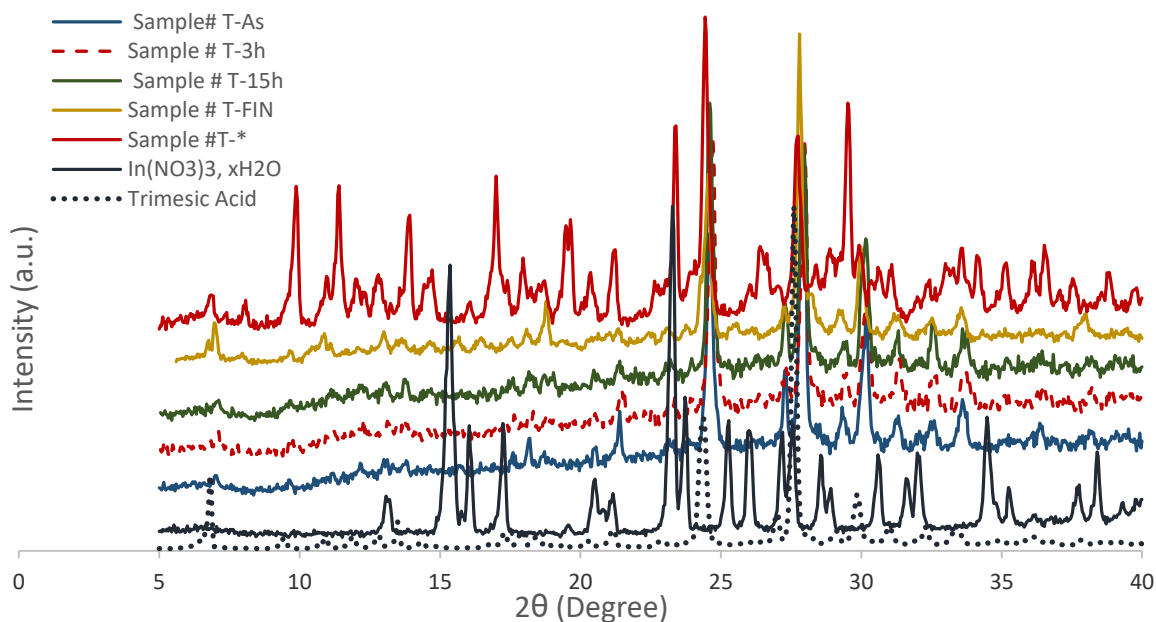


Figure 4.3 Effect of thermal condition in change phase of precursors; comparison between XRDs of formed samples in 5 different stages: Samples #T-As, #T-3hr, #T-15h #T-Fin, and #T-*, and precursors: (In(NO3)3.xH2O, and trimesic acid)

The XRD patterns reveal that the structures of $\text{In}(\text{NO}_3)_3 \cdot x\text{H}_2\text{O}$, and trimesic acid are demolished during the course of grinding. However, no evidence of formation of CPM-5 is observed in the first three samples, in which the applied temperature was either roughly 20°C (Sample #T-As & #T-3h) or 50°C (sample #T-15h). Applying a temperature of 150°C for samples

#T-15h and #T-* initiates the formation of desired peaks. Nevertheless, even after two hours of heat treatment, CPM-5 characteristic peaks were not fully developed and the main peak at $2\theta=8.4^\circ$ is not noticeable. It can be postulated that grinding initiates the reaction; yet, a thermal treatment for at least three hours (the same as described in the previous tests) is required to reach the CPM-5 phase with proper crystallinity

4.3.4 Effect of washing

In order to remove un-reacted precursors from the synthesized CPM-5 products, different solvents were used to study the effect of washing as a post-synthesis treatment. The samples were washed with 10 mL of a specified solvent (i.e. de-ionized water (DW), dimethylformamide (DMF) and mixture of these solvents). In order to do so, samples were filtered following a dispersion in the solvent lasting five minutes using an ultrasonic bath. In the next step, 10 mL of fresh solvent was added to the filtered sample and mixed thoroughly. The mixture was then centrifuged for 15 min at 20,000 rpm. The washing procedure was repeated three times. Before characterization, the sample was dried in an oven at 100°C overnight and then at 150°C for three hours. The specifications of the experiments and the description of solvents are summarized in Table 4.3.

Table 4.3 Specification of the method applied for the MC synthesis of CPM-5; Effect of washing with different solvents; Oscillation frequency: 90 Hz, , Thermal treatment:150°C/3h

SAMPLE	Ball Number	Oscil. time (min)	Solvent Properties	
			Solvent	Ratio
#W-1	20	60	DMF	---
#W-2	30	60	DW	---
#W-3	30	15	DMF-DW	1:1
#W-4	30	30	DMF-DW	1:1

XRD patterns of the washed samples are compared with the simulated XRD pattern of CPM-5 in Figure 4.4. Broader peaks at different intensities of the synthesized samples in comparison to the simulated pattern can be related either to the different particle sizes under the employed method [178], or to the presence of impurities in the MC-synthesized samples.

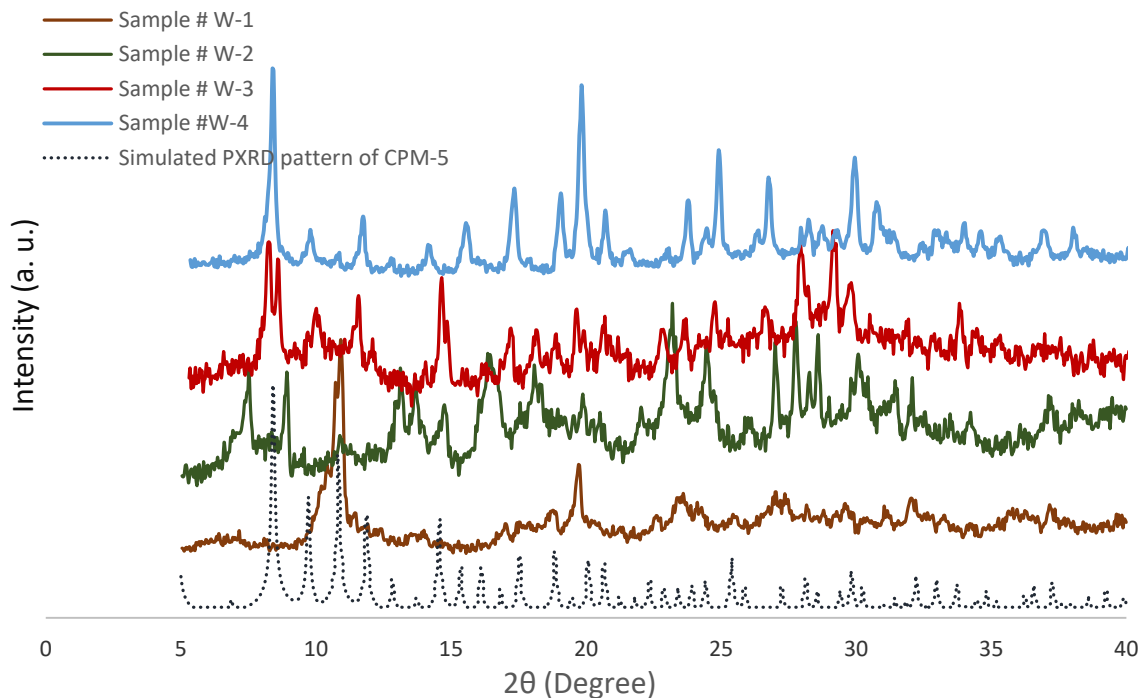


Figure 4.4 Comparison between XRDs of washed samples #W-1, #W-2, #W-3, #W-4, and the simulated XRD pattern of CM-5; Effect of washing treatment with different solvents on the formed CPM-5

According to the experimental data, it can be seen that using pure DMF or distilled water to wash the products resulted in either the disappearance or decrease of the intensity of main peaks at 2θ between 8.4° and 10.9° and in the creation of some amorphous phase. On the other hand, a mixture of DMF and distilled water with the ratio of 1:1 as a solvent resulted in more or less the same situation for both #W-3 and #W-4 samples. However, for the #W-4 sample, in which the oscillation time was twofold compared to #W-3, the formed peaks are more intense and bold which indicates a CPM-5 product with higher crystallinity. Results also show a good agreement between the XRD pattern for sample #W-4 and the hydrothermally synthesized sample by Zheng et al [146].

4.3.5 Further characteristic analysis

Specific surface areas of a typical CPM-5 sample, before and after washing treatment, measured using the BET technique are summarized in Table 4.4. From this data, it can be seen that washed samples show a roughly six-fold increase in the BET and Langmuir surface area. This increase in the surface area can be ascribed to the removal of unreacted precursors from the surface and pores of the CPM-5 by washing the samples. It is noteworthy that the resulting surface area of

the produced CPM-5 is still lower than that of the CPM-5 samples prepared via other methods [129]. XRD and SEM results for the MW-synthesized CPM-5 can be also found in section 5.3.1.

Table 4.4 The BET/ Langmuir surface area of the synthesized CPM-5 before and after washing

SAMPLE	BET Surface Area (m ² /g)	Langmuir Surface Area (m ² /g)
Before Washing	15.4	21.4
After Washing	79.9	112.1

The SEM micrographs of a typical MC synthesized CPM-5 are illustrated in Figure 4.5. A comparison between the formed crystals using the MC method and other methods [129] shows an asymmetric morphology and different sizes of the crystals. While the structure of the formed crystallites by the solvothermal method is cubic [129], such a structure was not distinguished in samples made via MC method. Indeed, the diversity in the morphology and/or the size of the crystals by changing the synthesis technique (e.g. using microwave or ultrasound instead of solvothermal method) has been reported [129], [144]. The different morphology of the MC-synthesized sample might be explained as a result of the applied mechanical stress during the course of grinding in the MC method. During the rapid shaking of the precursors, local heating/melting may deform or dislocate the crystal lattice or agglomerate the crystals [186].

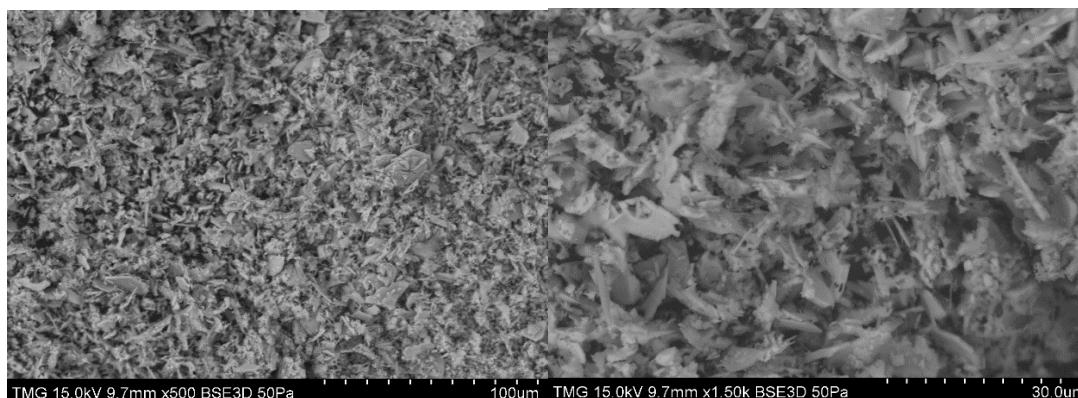


Figure 4.5 The SEM micrographs of crystallized CPM-5 synthesized by MC method: Sample #W-4

Thermal curve of the MC-synthesized sample (CPM-5, MC) obtained by thermogravimetric analysis (TGA) technique is shown in Figure 4.6. The result is compared with a CPM-5 reference sample that was synthesized by means of the microwave method (CPM-5, MW) [129]. According

to the TGA curves, the overall trend of weight loss for both samples is the same. The lower amount of weight loss of CPM-5 of the MC sample compared to the MW sample is attributed to the disuse of solvent in the MC technique. The first derivative curve of the MC sample also reveals three distinguished weight losses at roughly 100°C, 270°C, and 480°C. The first and second stages are related to the loss of roughly 25% of the weight due to the evaporation of the trapped H₂O and DMF molecules inside the porous structure of CPM-5. The weight loss at 480°C corresponds to around 42% due to the decomposition of the CPM-5 structure.

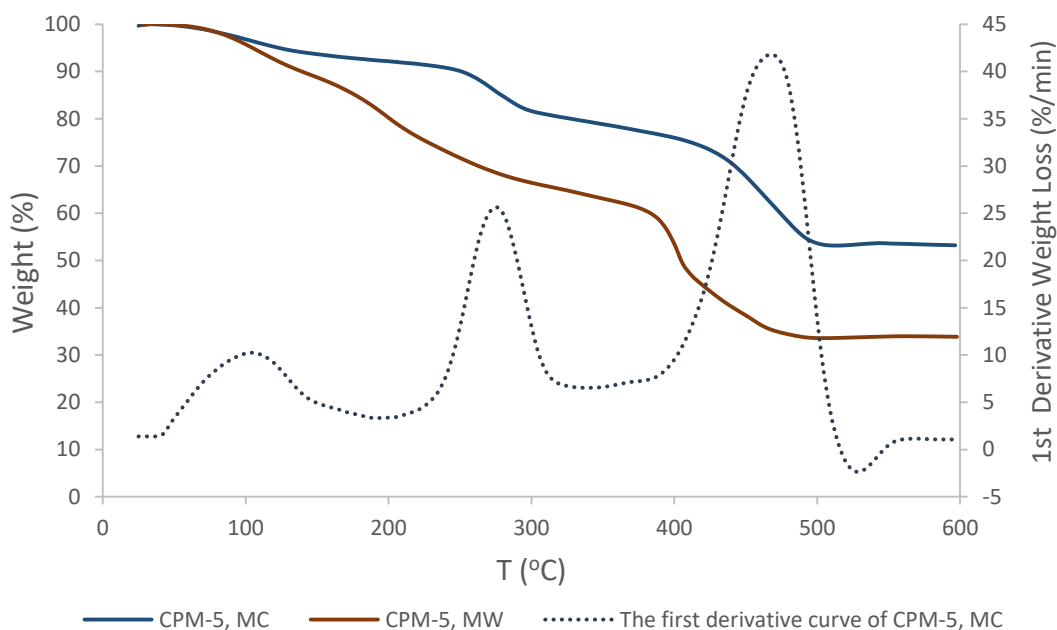


Figure 4.6 Comparing the TGA curves of the CPM-5 samples prepared by MC and MW methods

4.4 Conclusion

In this study, a mechanochemical (MC) synthesis of CPM-5 was developed using a mixer mill; the effects of different parameters on the synthesized products including grinding conditions, thermal treatment, as well as washing with different solvents were studied. Successful formation of the CPM-5 structure was ascertained under the following reaction condition: oscillation frequency of 90Hz in 30 min followed by three hours of heat treatment at 150°C and washing with a 1:1 (DMF: DW) as the solvent. The TGA analysis showed that the thermal stability was similar to the CPM-5 synthesized by the microwave energy. However, the SEM micrographs showed the formation of a different morphology of crystallites. The surface area of the MC-synthesized CPM-

5 was lower than the CPM-5 synthesized by the microwave method. This indicates the necessity of further studies to understand the exact effect of ball milling on the morphology of the product, and to optimize the reaction parameters in order to obtain a product with a higher surface area.

Chapter 5

5. A Comparative Study on Metal Organic Frameworks for Indoor Environment Application: Adsorption Evaluation

Connecting statement

In Chapter 3, a new mechanochemical method was successfully developed for the synthesis of CPM-5. However, the surface area of the obtained sample was lower than the CPM-5 synthesized by other reported methods. Due to the critical role of the surface area in the adsorption and catalytic reactions, in the present chapter other methods were used to prepare the target MOFs.

Chapter 4 reports the results of a study in which three MOFs, MIL-101, MIL-53 and CPM-5 were synthesized and characterized. Selection of these MOFs was based on a comprehensive literature review on several different MOFs and considering their structure and stability, as it has been described in part 2.2. Preparation of these MOFs was performed using solvothermal and microwave methods. These methods are selected based on those reported in other studies, with some minor modifications. Properties of the obtained samples were tested by means of different characterization methods including X-ray diffraction (XRD), Scanning electron microscopy (SEM), thermogravimetric analysis (TGA), Dynamic Vapor sorption (DVS), and BET surface area analyzer. Adsorption isotherms and breakthrough behaviors of these MOFs were studied for two volatile organic compounds: toluene and isobutanol. The effect of the presence of 0% and 30% relative humidity on the adsorption capacity of one (1) ppm toluene and isobutanol on each MOF was investigated. The feasibility of the regeneration of these MOFs was also investigated.

The outcome of this research is in press in “Chemical Engineering Journal” (*Bahri, M., Haghghat, F., Kazemian, H., & Rohani, S., (2016), Chemical Engineering Journal, DOI: <http://dx.doi.org/10.1016/j.cej.2016.10.004>*).

5.1 Introduction

Volatile organic compounds (VOCs) are a group of biogenic and/or anthropogenic compounds that are emitted from several sources in indoor environment [187], [188]. The negative effect of these compounds is proven for various health problems [9], [10], [189]. To eliminate VOCs from indoor environment, different physical and chemical methods have been developed. For instance, adsorption is a physical phenomenon in which the removal of VOCs is performed in the presence of an appropriate adsorbent like activated carbon (AC) and zeolites [6], [14], [190], [191]. Photocatalytic oxidation (PCO) and non-thermal plasma (NTP) methods, on the other hand, are two proposed chemical methods for the removal of VOCs from indoor air environment [22], [192].

Although the ability of VOCs degradation using chemical techniques provides many advantages compared to adsorption, the application of chemical techniques alone in indoor environment is not cost effective due to very low concentration of VOCs [29]. Therefore, developing reactive adsorption processes has become a new approach to improve VOCs removal efficiency of air purification systems [30]. In a reactive adsorption process, a combination of chemical reactions coupled with the adsorption process is performed simultaneously, in a single unit operation [29], [193]. Utilizing such an adsorber-reactor is not only favorable from an economic point of view, but it is also advantageous due to higher removal efficiency of the reactor [29].

When a reactive adsorption process is considered for indoor air treatment, selecting an appropriate dual functional adsorbent/catalyst (DFA/C) becomes a challenge. This is because the employed DFA/C should not only possess high oxidation capability, but it should also have a high adsorption capacity. Furthermore, due to the presence of humidity in the indoor environment and the competition between VOCs and water molecules for adsorption on DFA/C, hydrophobicity of the media is a crucial factor, especially at very low levels of VOCs (ppb range) [160]. Another important aspect in selecting an appropriate DFA/C is the ability to regenerate the DFA/C after being saturated with adsorbate. Therefore, sorption of VOCs should be physisorption rather than chemisorption. Surface area, pore size and availability of pores are other determining factors in adsorbent efficiency [194]. Due to the structural and chemical diversities of VOCs, finding a suitable DFA/C with the ability of adsorbing and degrading these compounds is a challenging issue.

Hydrophobic zeolites are highly crystalline materials with extremely uniform frameworks [195], [196]. These properties, along with their stable structure in the presence of humidity, make zeolites excellent DFA/Cs. However, the hardly tunable and relatively small size of zeolite micropores (≤ 2 nm) inhibit their application for removal of large size VOCs [121].

Metal organic frameworks (MOFs), on the other hand, are a new class of porous materials with large pore volume and uniform structures [34], [35]. These materials possess a diverse structure, high to extra high porosity and surface area, tunable pore size, and very low density of framework [132], [153]. The flexible framework of these porous materials causes some unusual patterns in their adsorption isotherms for small inorganic molecules (i.e., H₂O, N₂, O₂, Ar, CO₂, CH₄), as well as larger organic compounds (i.e., ethylene oxide, acetonitrile, benzene, xylene isomers, tetrahydrothiophene, cyclohexane and thiophene etc.) [122], [125]. Furthermore, high adsorption capacity, fast kinetics and high reversibility of MOFs suggest that these materials can be applied as DFA/Cs in a reactive adsorption process [197]. Thus far, the application of MOFs has been studied in many areas including catalysis, ion exchange, gas storage, molecular sieves, size-selective separation, etc. [127], [128], [198], [199]. Several studies have also reported adsorption of some VOCs on MOFs [35], [36], [200], [201]. However, very few have discussed the effect of relative humidity (RH) on the adsorption behavior of MOFs, especially in the presence of low VOCs concentrations [202]–[205]. Thus, further research is required in this area.

In this study three MOFs, a chromium (Cr) based MIL-101 (MIL: Materials of Institute Lavoisier), an iron (Fe) based MIL-53 and an indium (In) based CPM-5 (CPM: Crystalline Porous Material), are selected. CPM-5, with chemical formula of $[(\text{CH}_3)_2\text{NH}_2][\text{In}_3\text{O}(\text{BTC})_2(\text{H}_2\text{O})_3]_2 \cdot [\text{In}_3(\text{BTC})_4] \cdot 7\text{DMF} \cdot 23\text{H}_2\text{O}$, is a crystalline porous material with a highly symmetric framework. This framework consists of In₃O metal centers which are connected together by means of 1,3,5-benzenetricarboxylate (BTC) linkers [146]. The average pore size of this microporous material is estimated to be around 4.9 Å [146]. CPM-5 is thermally, hydrothermally and photochemically stable. Different studies have demonstrated high adsorption capacity of CO₂ on CPM-5 [141]. Yet, to the authors' best knowledge, no study has been reported on the removal of organic compounds on CPM-5.

MIL-53 $[\text{M}^{\text{III}}(\text{OH}) \cdot (\text{O}_2\text{C}-\text{C}_6\text{H}_4-\text{CO}_2) \cdot \text{H}_2\text{O}]$ consists of trivalent cations, $\text{M} = \text{Cr}^{3+}$, Fe^{3+} or Al^{3+} , which are cross-linked by means of benzene dicarboxylic acid (terphthalic acid). This microporous

material possesses one-dimensional pore channels in the range of $\sim 8 \text{ \AA}$ [206]. The highly flexible structure of MIL-53 allows for a transition in its structural phase, upon the adsorption/desorption of guest molecules [147], [148]. The change in the flexible geometry of MIL-53 family during the swelling of organic molecules is reported to be between 50 to 230% [206], [207]. MIL-53 shows a thermal stability up to 500°C and its application is studied in liquid-liquid separation, gas sorption, and drug delivery [135], [206].

MIL-101, $\text{Cr}_3\text{F}(\text{H}_2\text{O})_2\text{O}[(\text{O}_2\text{C})\text{-C}_6\text{H}_4\text{-}(\text{CO}_2)]_3\cdot n\text{H}_2\text{O}$, is a mesoporous chromium terephthalate-based MOF with cubic structure, huge porosity, and exceptionally high specific surface area [35]. Its Langmuir surface area can reach up to $5900 \text{ m}^2/\text{g}$ [149], which is the highest reported surface area for porous materials. MIL-101 possesses micropores in the size of 8.6 \AA , as well as mesoporous cages of about 29 and 36 \AA [34], [131], [200]. Its structure is stable in the presence of organic solvents, water, and high temperatures [201], [203]. MIL-101 exhibits a much higher capacity than conventional adsorbents including AC and zeolites for adsorption of VOCs such as benzene, n-hexane, toluene, methanol, butanone, dichloromethane and n-butylamine [150], [151], [208].

This paper first describes methods used to synthesize three above-mentioned MOFs and their characterization using different analytical techniques. Then it presents the adsorption isotherms and breakthrough behaviors of these MOFs when they are challenged with one ppm of a non-polar compound (toluene) and a polar compound (isobutanol). The paper also reports the adsorption behaviors of MOFs when they are exposed to a mixture of the targeted VOC and humid air.

5.2 Experimental

5.2.1 Synthesis and Preparation of Materials

The synthesis method for MIL-101, MIL-53 and CPM-5 was based on previously reported methods [129], [144], [150], [151], with some minor modifications. The properties of precursors and solvents used for the preparation of these MOFs are summarized in Table 5.1.

Table 5.1 Properties of chemical compounds used to synthesize the MOFs

MOF	Precursors	Formula	Supplier	Properties
MIL-101	Chromic nitrate nonahydrate	$\text{Cr}(\text{NO}_3)_3, 9\text{H}_2\text{O}$	Caledon	$\geq 98\%$ Mw: 400.14 g/mol
	Benzene-1,4 dicarboxylic acid (H ₂ BDC)	$\text{C}_8\text{H}_6\text{O}_4$	Alfa Aesar	$\geq 98\%$ Mw: 166.13 g/mol
	N,N- dimethylformamide (DMF)	$\text{C}_3\text{H}_7\text{NO}$	Caledone	$\geq 99.8\%$ Mw: 73.09g/mol
	Ethanol	$\text{C}_2\text{H}_6\text{O}$	Sigma Aldrich	$>99.9\%$ Mw: 46.07 g/mol
	Distilled water (DW)	H_2O		
MIL-53	Ferric chloride (III) hexahydrate	$\text{FeCl}_3, 6\text{H}_2\text{O}$	Caledon,	97-102%, Mw: 270.3g/mol
	Benzene-1,4 dicarboxylic acid (H ₂ BDC)	$\text{C}_8\text{H}_6\text{O}_4$	Alfa Aesar	$\geq 98\%$ Mw: 166.13g/mol
	N,N- dimethylformamide (DMF)	$\text{C}_3\text{H}_7\text{NO}$	Caledone	$\geq 99.8\%$, Mw: 73.09g/mol
	Distilled water (DW)	H_2O		
CPM-5	Indium (III) nitrate hydrate	$\text{In}(\text{NO}_3)_3, x\text{H}_2\text{O}$	Sigma Aldrich	99.9 %
	1,3,5-Benzenetricarboxylic acid ((BTC)	$\text{C}_9\text{H}_6\text{O}_6$	Caledone	$\geq 99\%$ Mw=210.14
	N,N-dimethylformamide (DMF)	$\text{C}_3\text{H}_7\text{NO}$	Caledone	$\geq 99.8\%$, Mw: 73.09g/mol
	Distilled water (DW)	H_2O		

In most studies, the network of MIL-101 is formed in the presence of hydrofluoric acid (HF) [149]. However, to avoid the safety hazards of working with hydrofluoric acid, recently, researchers are focused on developing HF-free methods. Efforts were made to use a method that not only eliminates HF consumption, but also to reduce the presence of other hazardous solvents during the synthesis and treatment steps. The selected HF free synthesis procedure in this study was a solvothermal method, developed according to the earlier studies [150], [151].

The required precursors consisted of chromic nitrate nonahydrate ($\text{Cr}(\text{NO}_3)_3, 9\text{H}_2\text{O}$), benzene-1,4 dicarboxylic acid (H₂BDC), and distilled water (DW). These compounds were added together

according to the ratio suggested by Bromberg [150], and mixed in an ultrasonic bath for 10 min. The acquired mixture was placed in a 25 mL Teflon-lined par bomb. The reactor then underwent a thermal treatment in the oven at 218°C for 18 hours. After cooling, the sample was washed to separate the green crystals from unreacted white terephthalic acid crystals. The washing procedure was performed three times with dimethylformamide (DMF). After each step, the process of separating the sample from DMF was carried out by means of a centrifuge at 20,000 rpm for 15 min. The sample was then dispersed in ethanol using an ultrasonic bath, for one hour. After sonication and separation of the sample, the whole washing procedure (DMF washing, ethanol dispersion, separation) was repeated three times.

The synthesis of MIL-53 followed Gordon and his colleagues' technique [144], according to a microwave (MW) method. Ferric Chloride (III) hexahydrate ($\text{FeCl}_3 \cdot 6\text{H}_2\text{O}$), benzene-1,4 dicarboxylic acid (H_2BDC), and N,N- dimethylformamide (DMF) were used as precursors. These materials were added and mixed by means of an electromagnetic mixer to completely dissolve the solid precursors in DMF as solvent. The acquired mixture was then poured in a 40 ml pressurized glass tube and placed in a microwave (CEM Focused Microwave™ Synthesis System, Model Discover) at the temperature and power of 150°C and 300 watt, respectively. The 30 min synthesis time was followed by 20 min of cooling. The formed sediment was then washed three times with DMF followed by separation by centrifugation at 20,000 rpm for 20 min.

Preparation of CPM-5 was also a MW method based on the study of Sabouni and her colleagues [129]. Indium (III) nitrate hydrate ($\text{In}(\text{NO}_3)_3 \cdot x\text{H}_2\text{O}$), 1,3,5-benzenetricarboxylic acid (BTC), N,N- dimethylformamide (DMF), and distilled water (DW) were added as precursors and stirred with a magnetic stirrer for 10 min. The solution was then put in the microwave, for 10 min at 150°C and 300 watt power. The cooling time of the MW was 20 min. After reaching ambient temperature, the solvent was decanted and the obtained sample was washed with a 1:1 solution of DW and DMF. The washing process was repeated three times and after each step, the separation of the solution and sample was done using a centrifuge at 20,000 rpm for 20 min.

All three samples (MIL-101, MIL-53, and CPM-5) were dried at 100°C overnight, following by a three-hour heating treatment at 150°C. The thermal operation was performed in an oven (DKN 400, Yamato Scientific America, Inc., Santa Clara, CA).

5.2.2 Materials characterization

A Rigaku-MiniFlex XRD model (Japan), using CuK α (k for K α =1.54059 Å), was used to collect X-ray diffraction (XRD) pattern of the synthesized samples. Analysis was performed in the ranges of $5 < \theta < 40^\circ$ with a step of 0.04° . The micrographs of the synthesized samples were also obtained using a scanning electron microscopy (SEM) instrument (Joel instrument, JSM 600F model, Japan) operating at an acceleration voltage of 5 keV.

The surface characteristics of samples were measured by means of a Brunauer-Emmett-Teller (BET) Surface Area Analyzer (Micrometircs ASAP 2010 BET, USA). For this purpose, each sample was first degassed under the vacuum (10^{-5} Torr) at 150°C , and then the specific surface area was measured according to nitrogen adsorption/desorption isotherms at 77.35 K.

A thermo-gravimetical analyzer (TGA, Mettler Toledo, 851e model, Switzerland), with Stare software version 6.1, was used for thermal analysis of samples before adsorption and after saturation of each sample with toluene. The analysis was performed in the range of $25\text{-}700^\circ\text{C}$ at a heating rate of $10^\circ\text{C}/\text{min}$ in a $70\mu\text{l}$ alumina crucible.

5.2.3 Apparatus and method

The schematic diagram of the adsorption set-up is illustrated in Figure 5.1. Compressed air passes through a pressure regulator to adjust the pressure. The air flow rate is controlled by means of a mass flow controller. The target compound is injected into the system at a constant rate via an injection pump (KD Scientific, Model KDS-210, made in USA). Polluted air containing the target VOC passes through the adsorbent in the reactor. The micro reactor, enlarged in the right panel of Figure 5.1, is a packed bed reactor, which consists of a quartz tube (ID: 10mm; OD: 12 mm; L: 250mm). The VOC concentrations at the upstream and downstream of the reactor are measured using a PID detector (ppb3000 RAE, Made in USA). The desired relative humidity is provided using a bottle of distilled water, which is placed at the upstream. The relative humidity is controlled by means of an ETS electro-tech systems humidity controller (Model 514, Made in USA). This system has the capability of providing a fast response with an accuracy of $\pm 2\%$ R.H. from 0-90% RH. It is noteworthy that since the presence of humidity could affect the reading of PID detector, for each test PID detector was calibrated separately.

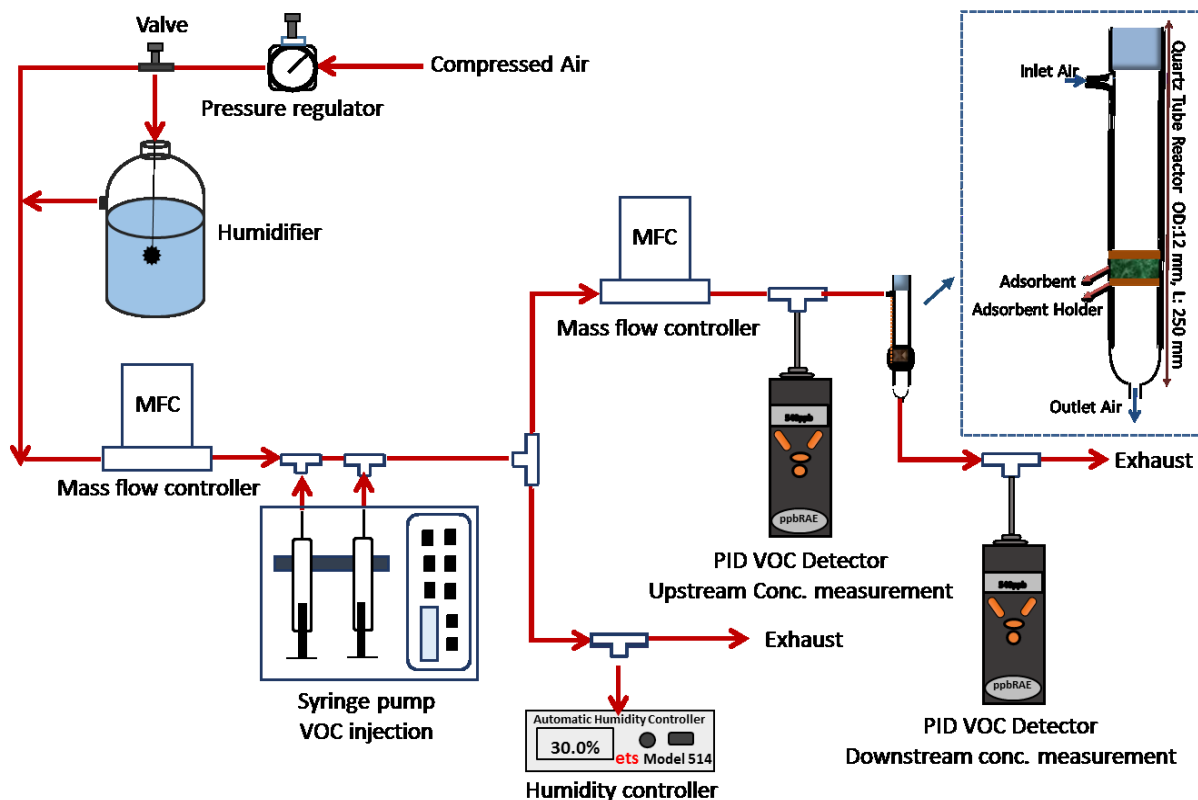


Figure 5.1 Schematic diagram of the adsorption apparatus

Toluene and isobutanol were selected as target VOCs in this study. Both of these compounds are commonly found in indoor environment. The properties of these compounds are summarized in Table 5.2. Experiments were performed to develop breakthrough curves for toluene at one ppm concentration on three MOFs at two different levels of relative humidity of 0% and 30%. Similar experiments were conducted at one ppm concentration of isobutanol as well. Each experiment was continued till the adsorbent was completely saturated with the target VOC at 23°C. The experimental parameters of the adsorption are listed in Table 5.3.

To prepare the adsorbents for each experiment, a hydraulic press (Carver, Model C12 Ton Benchtop, Laboratory Press), was first used to form thin pellets with an approximate thickness of 0.5 mm. These pellets were then crashed and sieved to the size of 35 to 60 meshes (250 to 500 μm). Prior to any test, all samples were heated at 150°C for two hours to remove any potential adsorbed water vapor molecules from the air. For each experiment, 0.2 g of MOF was placed into

the micro reactor on the top of fiberglass, as an adsorbent holder. The residence time for this condition is calculated as follows:

$$\tau = \frac{\text{Bed Volume}}{\text{Gas Flow Rate}} = \frac{V}{F} = \frac{(\pi r^2 L)}{F} \quad (5.1)$$

The calculated residence time for different media varies between ~ 0.06 to 0.09 s.

Table 5.2 Some physicochemical properties of the selected VOCs

Compound	Supplier	Category	Formula	Molar mass (g/mol)	Boiling point (°C)	Polarity	Kinetic Diameter (Å)	Dipolar moment (D)
Toluene	Fisher Scientific 99.9%	Aromatic	C ₇ H ₈	92.14	110.6	Non-polar	5.8	0.36
Isobutanol	Fisher Scientific 99.9%	Alcohol	C ₄ H ₁₀ O	74.12	80.2	Polar	5.4	1.79

Table 5.3 Experimental parameters of the adsorption tests

Compound	Concentration (ppm)	Flow rate (mLmin ⁻¹)	Temperature (°C)	Relative humidity (%)
Toluene	1	600±2%	23±1	0 and 30%±1
Isobutanol	1	600±2%	23±1	0 and 30%±1

Evaluating dynamic sorption isotherms of toluene and isobutanol on MOFs was performed by means of a dynamic vapor sorption system (DVS-Advantage, Surface Measurement Systems Ltd. UK) using a DVS Advanced Analysis Suite software. For each test, approximately 10 mg (±0.1 µg) of MOF sample was exposed to the target VOC vapor in the DVS system. A two-hour pre-heating of the sample was performed before starting the sorption test. To determine the pore characteristics of adsorbents, sorption-desorption cycles were carried out by monitoring the percentage change in the reference mass of the sample versus the increase in the P/P₀ ratio of target VOC. Furthermore, N₂ sorption-desorption evaluation of MOFs was also conducted via the same BET surface area analyzer which was used for the sample characterization (Micrometircs ASAP 2010 BET, USA).

In this study, a one-cycle isobutanol sorption-desorption experiment was performed for MIL-101, MIL-53 and CPM-5 at a time-step of two hours. A waiting time of 48 hours between the half-cycles was applied to ensure that the system reaches the equilibrium. In addition, a two-cycle toluene sorption-desorption, at a time-step of two hours and a two-hour of waiting between the half cycles, was performed to study the general sorption-desorption trend of the targeted MOFs. All experiments were performed at $23\pm 1^\circ\text{C}$ and the relative pressure was changed within the range of $0 < P/P_0 < 95\%$.

5.2.4 Efficiency Evaluation

The sorbent saturation capacity (C_s ; $\text{mg}_{(\text{VOC})}/\text{g}_{(\text{s})}$; %) is the total mass of the adsorbed VOC per unit weight of adsorbent, which is calculated as follows:

$$C_s = \frac{\int_0^{t_s} (C_{up}(t) - C_{down}(t)) \times Q \times dt}{M_s} \times 100 \quad (5.2)$$

where $C_{up}(t)$ and $C_{down}(t)$ are the target VOC concentrations (mg m^{-3}) measured at the upstream and downstream of the reactor, respectively. Q is the volumetric airflow rate ($\text{m}^3\text{min}^{-1}$), M_s is the total mass of sorbent (mg), and t_s (min) is the time required to reach 100% breakthrough.

5.3 Result and Discussion

5.3.1 MOF Characterization

The XRD patterns of CPM-5, MIL-53, and MIL-101 are illustrated in Figure 5.2. The peaks for all samples are in good agreement with those reported in previous studies [52–54]. The sharp intensities of diffraction peaks also demonstrate good crystallinity of synthesized MIL-101, MIL-53 and CPM-5 samples.

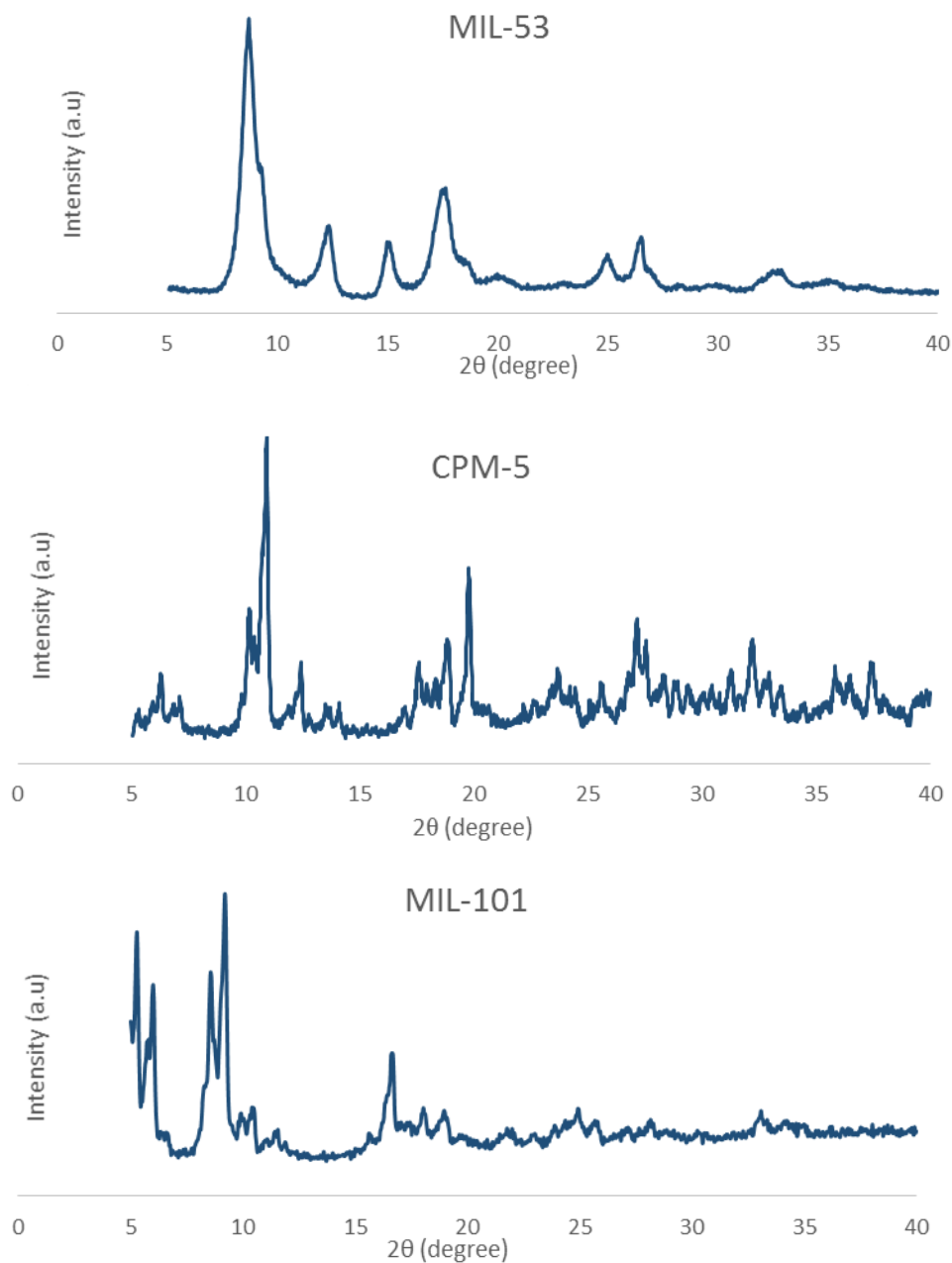


Figure 5.2 XRD patterns of MIL-53, CPM-5, and MIL-101

Figure 5.3 illustrates the SEM images of crystallized CPM-5, MIL-53 and MIL-101. According to the SEM pictures, MIL-53 sample contains two different morphologies: the large sized prism with rectangular base crystals of smaller than $50\ \mu\text{m}$ and the small sized hexagonal bipyramidal crystals of approximately $10\ \mu\text{m}$. These morphologies are almost in accordance to the ones reported by Gordon and his colleagues [144].

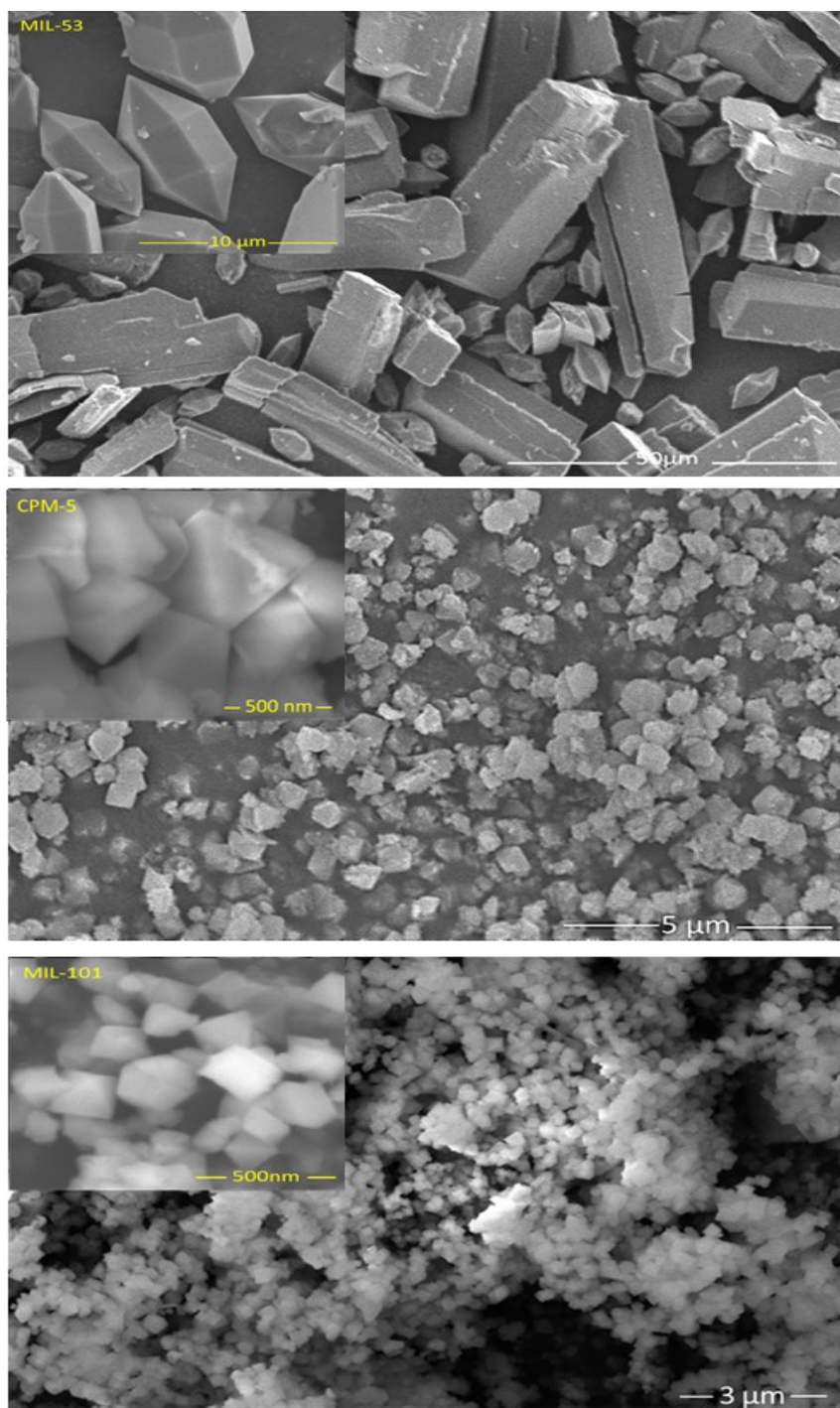


Figure 5.3 SEM images of fully crystallized synthesized particles; MIL-53 (up) scale: 10 μm, CPM-5 (middle), scale: 5 μm; MIL-101 (down), scale: 3 μm

CPM-5 pictures also show a homogeneous morphology with crystals in the size of approximately 500 nm. This morphology is comparable with that of reported earlier [129]. Also,

SEM results of MIL-101 in Figure 5.3 illustrate an almost uniform morphology of crystallites with particle size of around 100 nm, which was also reported by Wee et al. [210].

Table 5.4 summarizes the pore structure specifications of the synthesized CPM-5, MIL-53, and MIL-101. According to Table 5.4 the specific surface area of MIL-101 is significantly higher than MIL-53 and CPM-5. The structure parameters are comparable with those in other studies [139], [144], [148], [209].

Table 5.4 Pore Structure parameters of the synthesized CPM-5, MIL-53, and MIL-101

Sample	SSA* _{BET} ^a (m ² /g)	SSA _{Langmuir} ^a (m ² /g)	Micropore area ^a (m ² /g)	External area ^a (m ² /g)	Micropore volume ^a (cm ³ /g)
MIL-53	951	1275	606	345	0.279
MIL-101	2728	3747	780	1948	0.289
CPM-5	1140	1560	656	484	0.284

* SSA: Specific surface area

^a All data are determined from nitrogen adsorption isotherms (t-plot).

5.3.2 Adsorption isotherms

N₂ adsorption isotherms for CPM-5, MIL-53, and MIL-101 at 77 K and relative pressure of 0 < P/P₀ < 1 obtained by BET analyzer are illustrated in Figure 5.4. This figure shows a much higher N₂ adsorption capacity of MIL-101 in both low and high pressures. A comparison between MIL-53 and CPM-5, also shows that the N₂ adsorption capacity of CPM-5 at low pressures (~P/P₀ < 0.10) is slightly higher than that of MIL-53. However, this amount for MIL-53 surpasses at higher pressures (~P/P₀ > 0.80).

According to Figure 5.4, in CPM-5 sample, adsorption rises steeply by a small increase in the adsorbate pressure and is followed by a plateau at higher pressures. This trend is in accordance with Type I isotherm based on Brunauer, Deming, Deming, and Teller (BDDT) isotherm theory [211]. Type I isotherm, follows the Langmuir isotherm pattern, which signifies monolayer adsorption and it usually occurs in microporous materials with pore diameter of smaller than 2 nm [212].

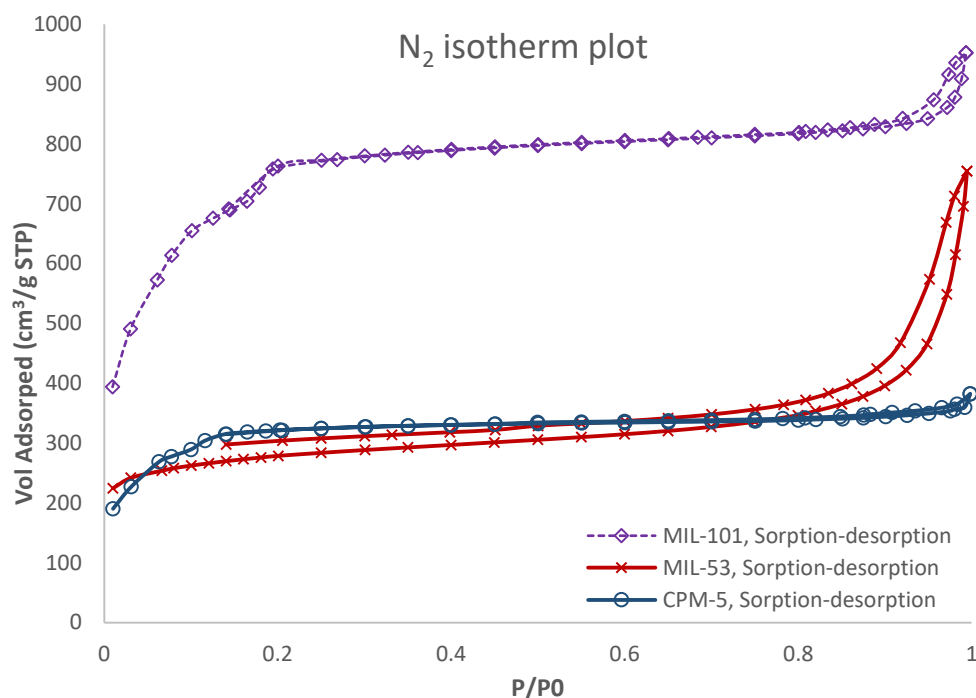


Figure 5.4 N₂ adsorption isotherms of CPM-5, MIL-53 and MIL-101. Data obtained by a BET Analyzer

For MIL-101, as seen in Figure 5.4, a fast increase in the adsorption before $P/P_0 < 0.20$ is followed by a plateau. The curve then continues by another sharp increase in adsorption for the relative pressure of more than $\sim P/P_0 \geq 0.90$. The first increase is due to the monolayer adsorption in micropores of MIL-101, with a diameter of 8.6 Å. The second increase takes place in 29 Å and 36 Å mesopores [150], [200]. Here, the adsorption isotherms follow Type II or IV isotherms based on BDDT classification [211]. This type of isotherm is an evidence of capillary condensation during the multilayer adsorption that appears in a mesoporous material [212]–[214].

Although MIL-53 is a microporous material, the isotherm behavior of this Fe based MIL-53 follows Type II according to BDDT classification (see Figure 5.4). Nevertheless, previous studies have shown a different adsorption behavior for chromium (Cr) and aluminum (Al) based MIL-53. For instance, N₂ adsorption isotherm of Cr based MIL-53 has shown a type I adsorption–desorption isotherm, demonstrating its microporous characteristic [215].

As previously mentioned, MIL-53 has a flexible structure with the ability of shrinking or expansion in its framework upon host-guest interactions [135], [147]. The framework transition, which is described as the “breathing phenomenon”, is strongly affected when the metal center is

altered in MIL-53[216]. While the Cr and Al based MIL-53 reveal micropore characteristics even in their anhydrous forms, Fe based MIL-53 displays closed pores which are not accessible for most gases, when it is anhydrous [216]. It can be postulated that the second steep increase in the adsorption curve of MIL-53 (Fe), stems from the opening of a part of the closed micropores in $P/P_0 \geq 0.90$ due to an increase in N_2 concentration.

The adsorption isotherms of isobutanol on MIL-101, MIL-53 and CPM-5 at 23°C and relative pressure between $0 < P/P_0 < 95\%$ are illustrated in Figure 5.5. An isobutanol adsorption capacity for MIL-101 is observed to be approximately four times higher than MIL-53 and CPM-5.

According to Figure 5.5, CPM-5 demonstrates Type I isotherm behavior, based on BDDT isotherm theory. The increase in the mass of CPM-5 reaches around 27% at 95% relative pressure. Also, hysteresis appears at relative pressures less than 10%, and the curve does not return to zero. This gap between the adsorption-desorption curves in the first cycle is due to the trapped vapor, which is a characteristic of microporous materials.

As previously mentioned, anhydrous MIL-53 (Fe) possess inaccessible pores that are reopened when MIL-53 is exposed to an organic molecule [216]. The maximum adsorption capacity of MIL-53 reaches roughly 34% at 95% relative pressure. The increase in the adsorbed amount, however, continues due to the increase in the pressure, demonstrating an expansion in the structure upon exposure to isobutanol.

In the case of MIL-101, while the general adsorption trend is expected to follow Type II or IV isotherms due to its mesoporous structure, a Type I isotherm behavior is observed. Similar findings are reported for organic compounds' adsorption on MIL-101 [201], [217]–[219], where Type I isotherms are reported. According to Figure 5.5, in low concentrations (at $0 < P/P_0 < 20\%$), a steep increase in adsorbed amount of isobutanol occurs due to the monolayer adsorption of isobutanol in both micropores and mesopores. The adsorption capacity then slowly increases by an increase in the relative pressure up to 95%, which demonstrates the multilayer adsorption in mesopores; however, there is no evidence of another sharp increase in this curve at high pressure to indicate a shift from type I to II or IV.

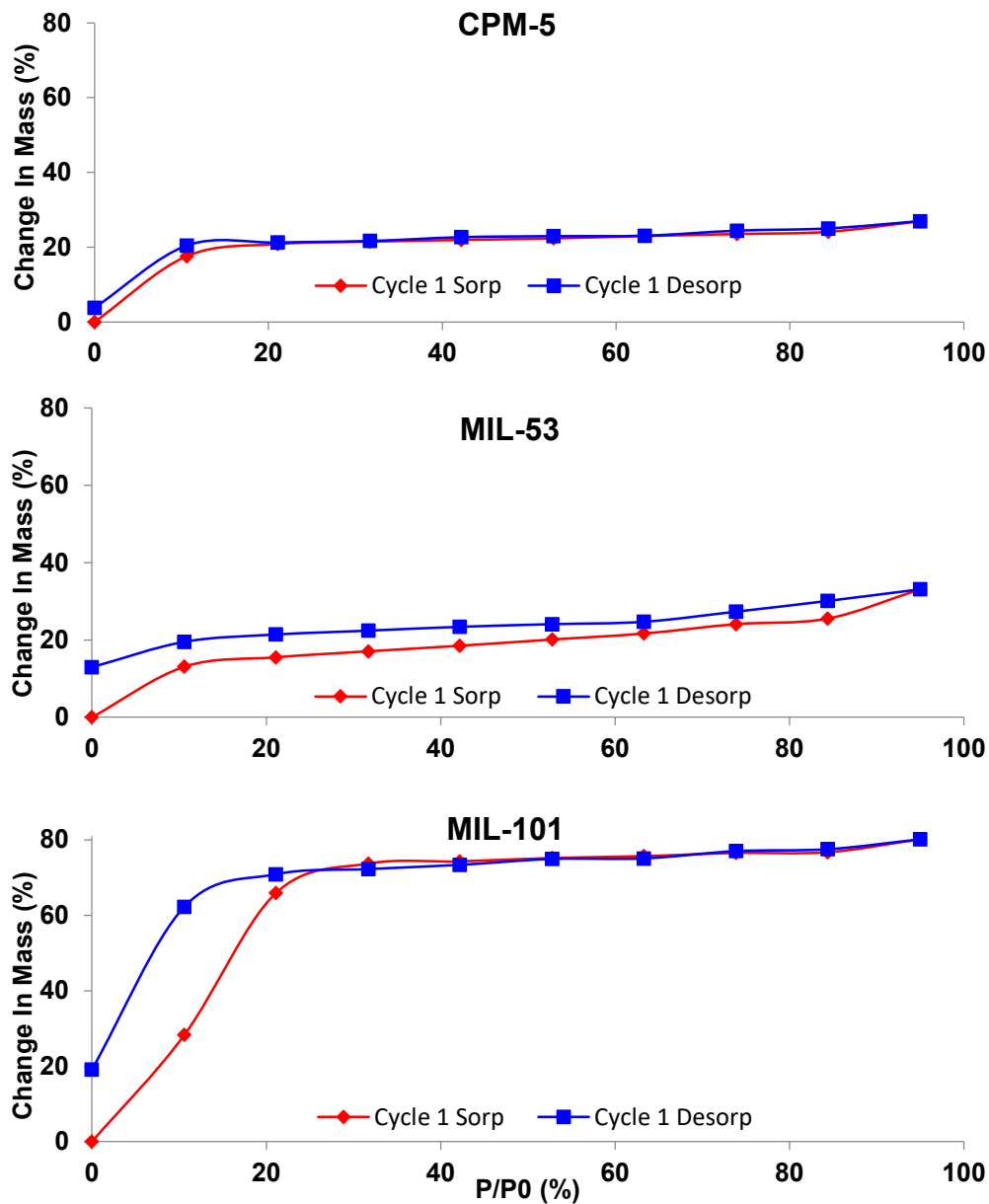


Figure 5.5 Dynamic adsorption-desorption isotherms of isobutanol over CPM-5, MIL-53, and MIL-101. Results are obtained by DVS, one (1) cycle, and step size: 2h. 48 hours of wait is applied before desorption to reach equilibrium.

A study of two consecutive cycles of toluene adsorption-desorption on MIL-101, MIL-53 and CPM-5 at 23°C is illustrated in Figure 5.6. Figure 5.6 shows that adsorption isotherms follow Type I behavior. Furthermore, desorption curves in the first cycles do not return to zero, which is an indication of the existence of micropores in all MOFs. In the second cycle, however, the general trends of adsorption-desorption demonstrate that the adsorbed molecules on the solid surface

interact by weak (electrostatic) forces and are removed as the pressure is reduced [194]. Hence, the sorption is a reversible physisorption, also known as van der waals adsorption, and the removal efficiency reaches almost 100%.

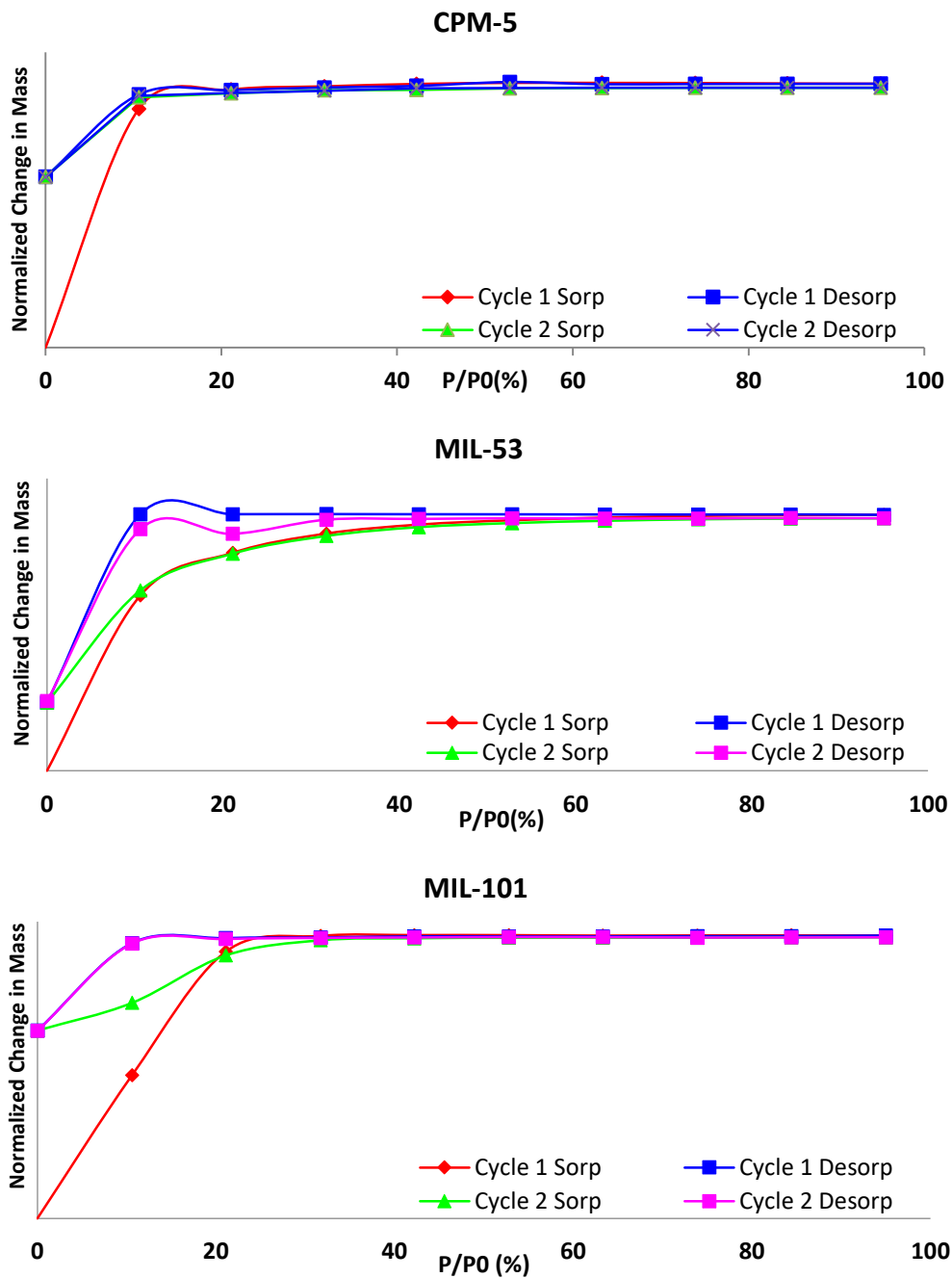


Figure 5.6 Dynamic adsorption-desorption isotherms of isobutanol over CPM-5, MIL-53, and MIL-101; results are obtained by DVS; 2 cycles, step size: 2h, and 2h of wait after each adsorption.

5.3.3 Breakthrough curves and influence of relative humidity on adsorption capacity

Figures 5.7 and 5.8 show the adsorption breakthrough curves of one ppm toluene and isobutanol over CPM-5, MIL-53 and MIL-101 in dry air. C/C_0 shows the ratio of the VOC concentration at the reactor upstream and downstream.

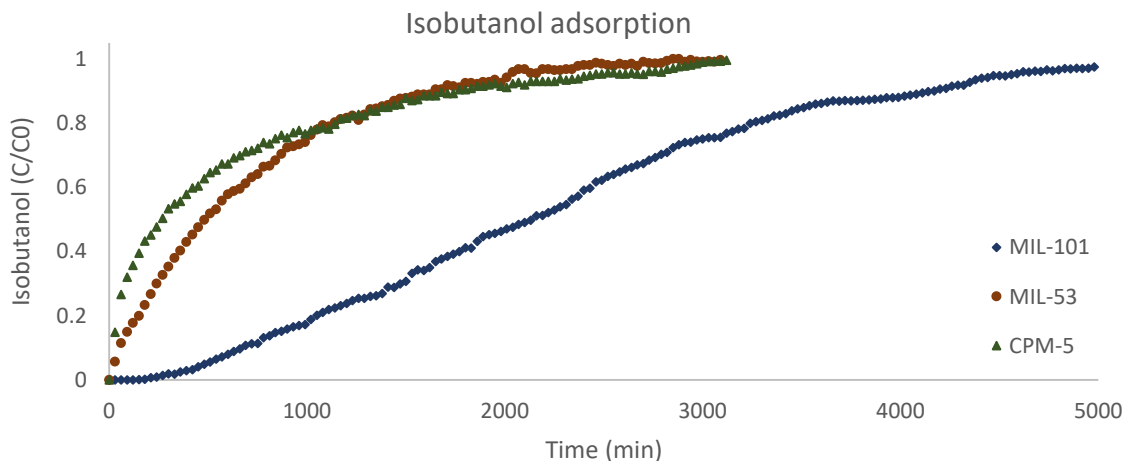


Figure 5.7 Adsorption breakthrough curves of isobutanol over MIL-101, MIL-53 and CPM-5 in dry air

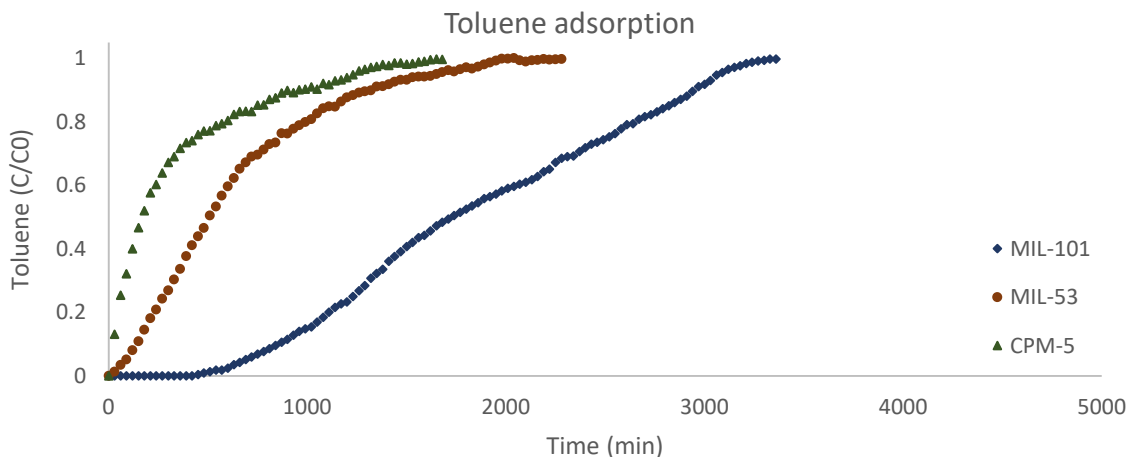


Figure 5.8 Adsorption breakthrough curves of toluene over MIL-101, MIL-53 and CPM-5 in dry air

Results show that the adsorption capacity of both toluene and isobutanol on MIL-101 is superior to the adsorption capacities of these compounds on MIL-53 and CPM-5. Adsorption of VOC on MOF occurs due to the interaction between the organic linker in the MOF structure and target VOC [35]. Besides, the trivalent metal cation sites (Cr^{3+} in MIL-101, Fe^{3+} in MIL-53 and

In⁺³ in CPM-5) act as strong sites for VOC adsorption. In the case of MIL-101, the adsorption capacity of both toluene and isobutanol is significantly higher than MIL-53 and CPM-5, as seen in Figures 5.7 and 5.8. This is due to the extra-high surface area (see Table 5.4) and large mesoporous cavities of MIL-101, which provide high storage capacity for these molecules. Due to the fact that toluene is a heavier compound with kinetic diameter larger than isobutanol (see Table 5.2), toluene adsorption breakthrough curve reaches the equilibrium faster than isobutanol. This trend is observed for all three MOFs.

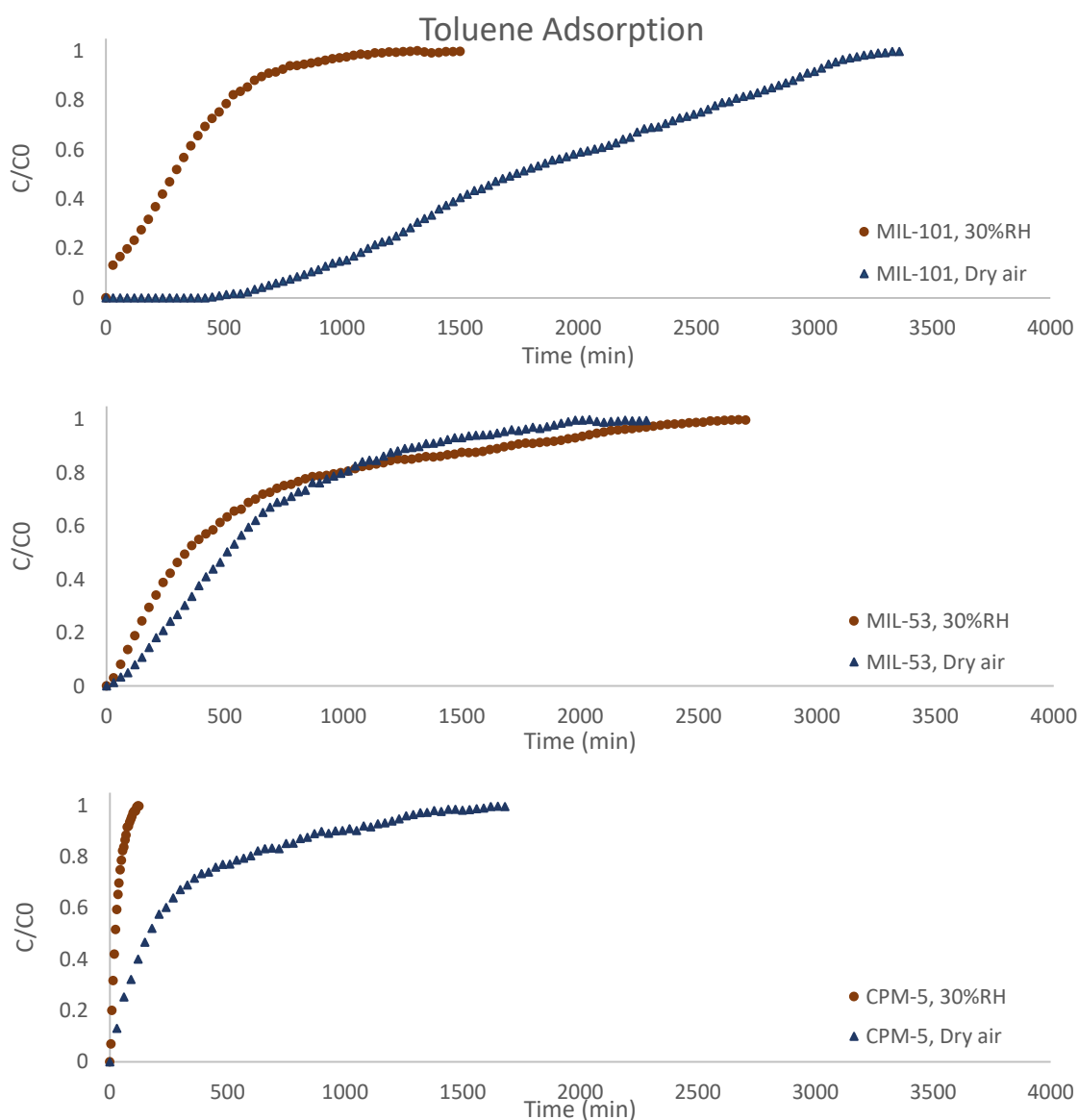


Figure 5.9 Breakthrough behavior of toluene on MIL-101, MIL-53, and CPM-5 in the absence of humidity (dry air) and the presence of humidity (RH: 30%); T: 21°C, flow rate: 0.6L/min, cat: 0.2g.

It can be observed from Figures 5.7 and 5.8 that MIL-53 exhibits a higher adsorption capacity for both toluene and isobutanol, compared to CPM-5. Since the specific surface area of CPM-5 is higher than MIL-53, this parameter is not a determining factor. The result can be linked to the breathing phenomenon and reopening of inaccessible pores, when MIL-53 is exposed to an organic molecule [216].

Figures 5.9 and 5.10 show a comparison between breakthrough curves of isobutanol and toluene on three MOFs in dry and humid air. Table 5.5 also quantifies the adsorption capacity of toluene and isobutanol on MIL-101, MIL-53, and CPM-5, in dry air and humid air.

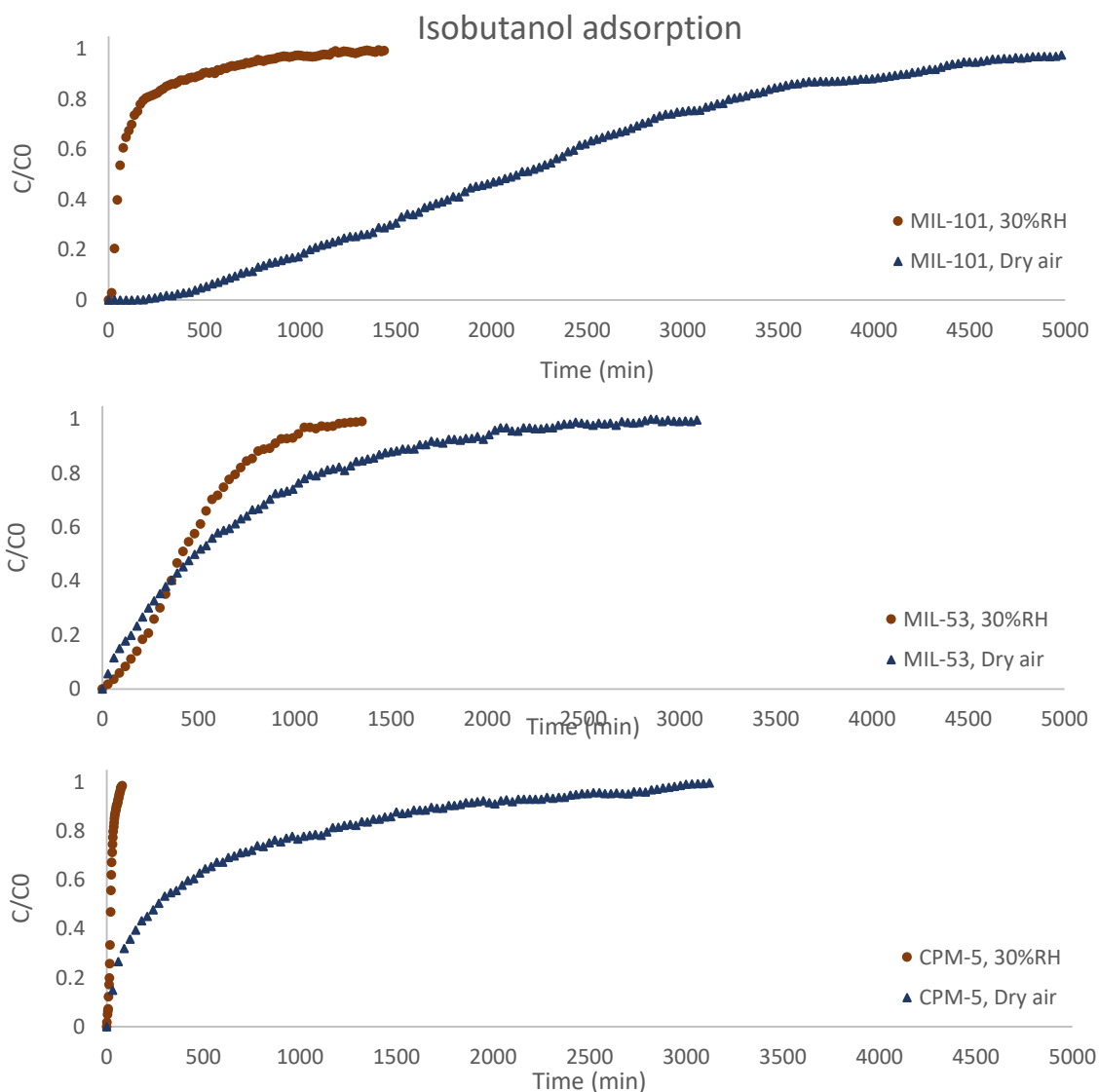


Figure 5.10 Breakthrough behavior of isobutanol on MIL-101, MIL-53, and CPM-5 in the absence of humidity (dry air) and the presence of humidity (RH: 30%); T: 21°C, flow rate: 0.6L/min, cat: 0.2 g.

Table 5.5 shows that the adsorption capacity of MIL-101 is almost three times higher than MIL-53 and around five times more than CPM-5 for both isobutanol and toluene. However, the relative humidity intensively influences this result. It is clear from Figures 5.9 and 5.10 that the presence of humidity has a considerable negative impact on the rate of VOC adsorption on CPM-5 and MIL-101. This negative effect is however less in the case of MIL-53. While the amount of sorption capacity for MIL-53 decreases slightly in the presence of 30% RH, this amount for MIL-101 and CPM-5, drops to around 20% and 10%, respectively.

Table 5.5 The maximum sorption capacity of toluene and isobutanol on CPM-5, MIL-53 and MIL-101 in dry air (RH=0%) and humid air (RH=30%) calculated according to equation (2)

Adsorbent	Cs (mg toluene/gr cat)		Cs (mg isobutanol /gr cat)	
	RH=0%	RH=30%	RH=0%	RH=30%
CPM-5	388.5	39.9	569.5	20.4
MIL-53	730.4	691.8	643.2	444.7
MIL-101	2115.7	395.1	2060.3	157.5

MOFs are amphiphilic porous materials with both hydrophilic and lipophilic properties. The inorganic part of MOFs including unsaturated metal sites and oxygen anions possess hydrophilic properties, while the organic linker exhibit the lipophilic properties due to the presence of benzene ring as the functional group [202]. Benzene rings increase the electrostatic interaction between the adsorbent and the target organic compound, resulting in faster adsorption kinetics [34], [35]. However, the sharp decrease in adsorption capacity of targeted VOCs on MOF samples in the presence of relative humidity proves that bonds formed between water molecules and the MOFs are stronger than those formed between VOCs and MOFs. The competitive adsorption behavior of water and VOCs on MIL-101 surface has also reported by Xian and his colleagues [202]. It is explained that when adsorption takes place in the presence of relative humidity, Cr^{+3} metal sites favorably adsorb polar molecules of H_2O rather than VOCs. These H_2O molecules can form clusters on the surface of the solid and prevent VOC molecules to reach the active sites; this results in a sharp decrease in the adsorption capacity of MIL-101 in the presence of relative humidity. The same phenomenon can be seen in the adsorption behavior of toluene and isobutanol on CPM-5, in the presence of relative humidity.

On the other hand, in the case of MIL-53, the presence of H₂O molecules causes interactions between hydrogens in H₂O and oxygens in carboxylate and hydroxo group and deformation of the structure [148]. While a part of the pores are filled with H₂O molecules in the hydrated form of MIL-53 (Fe), the flexible framework of this MOF allows more expansion of its structure and adsorption of VOCs in those pores which are still closed and empty [216]. Therefore, the adsorption capacity of MIL-53 even in the presence of relative humidity is subject to change less than those of MIL-101 and CPM-5.

5.3.4 Thermo-gravimetric analysis (TGA) characterization

TGA results of the synthesized samples is illustrated in Figure 5.11. The curves reveal different stages of weight loss as the temperature is increased. The first and second weight losses in all samples attribute to evaporation of the trapped solvents -water and DMF molecules- from the structure of MOFs. These weight losses occur between about 70 to 260°C. The following sharp weight loss corresponds to the decomposition of the MOF structure. Results are in good agreement with those reported earlier [135], [141], [209].

A comparison between first derivative curves before and after toluene adsorption reveals that structures of CPM-5, MIL-53, and MIL-101 do not show any remarkable change in the peak positions. This implies physisorption of toluene and stable structure of all three MOFs after adsorption.

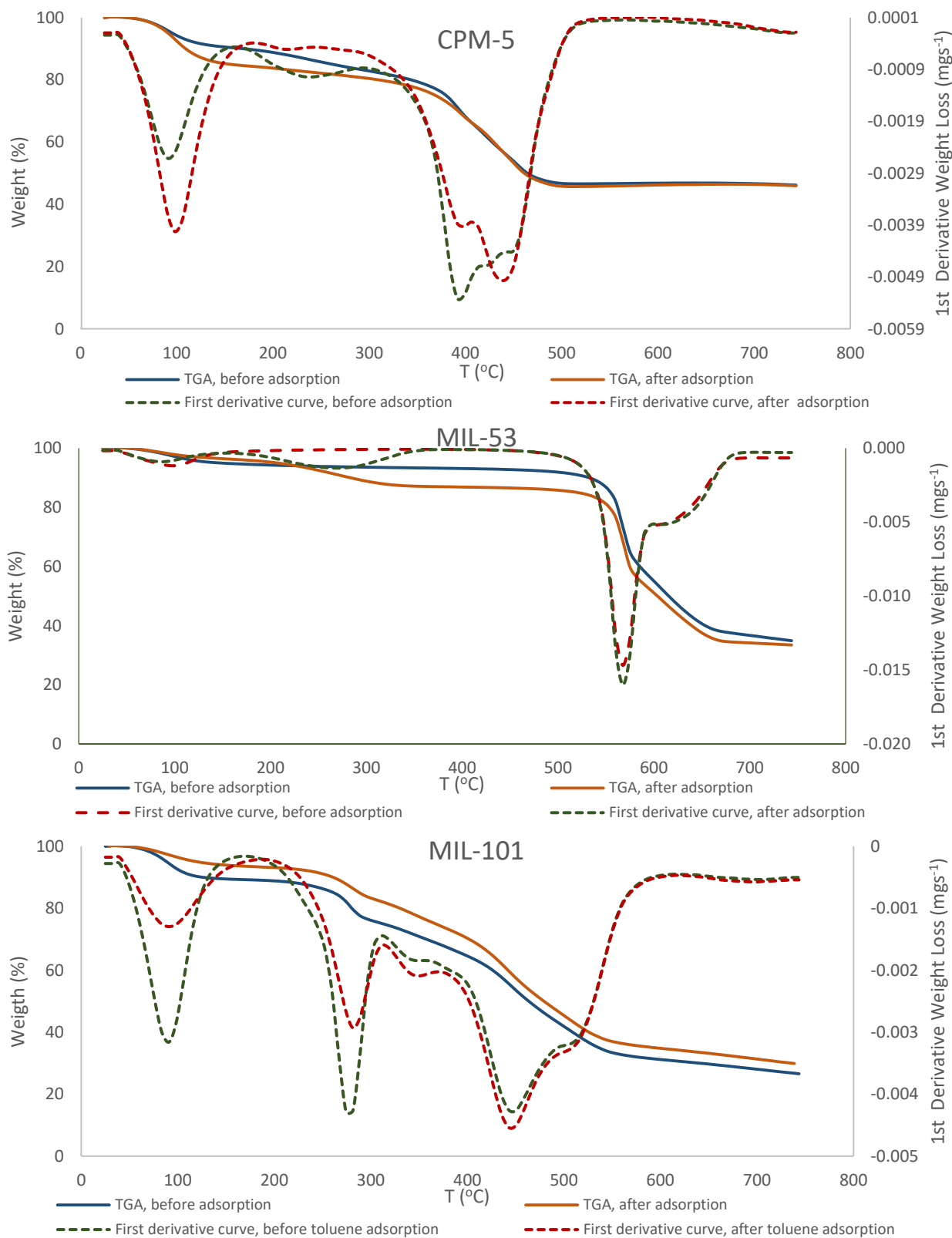


Figure 5.11 TGA and first derivative curves of CPM-5, MIL-53, and MIL-101 before and after toluene adsorption

5.4 Conclusion

In this study, three different MOFs including CPM-5, MIL-101, and MIL-53 were synthesized successfully. The obtained XRD, BET, SEM, and TGA characteristics of these samples were in good agreement with the research work. The adsorption isotherm behaviors of two VOCs, toluene and isobutanol, on these MOFs indicated the physisorption process. This result was also confirmed by TGA characterization of samples before and after toluene adsorption.

A comparison between the adsorption capacity of MIL-101, MIL-53, and CPM-5 showed that MIL-101 exhibited a much higher capacity for both toluene and isobutanol compared to MIL-53 and CPM-5. Nevertheless, in the presence of relative humidity, adsorption capacity steeply declined for MIL-101 and CPM-5. While in this study, the application of these MOFs is considered for removal of VOCs in indoor environment, and due to the inevitable presence of relative humidity in such an environment, MIL-53 is the best candidate for this purpose. Utilizing MIL-101 is applicable only if a dehumidifier can be implemented before this MOF.

The experimented MOFs in this study will be studied as DFA/Cs in a NTP system in the future work.

Chapter 6

6. Metal Organic Frameworks for Gas-Phase VOCs Removal in a NTP-Catalytic Reactor

Connecting statement

In Chapter 5, three different MOFs, MIL-101, MIL-53, and CPM-5, were synthesized, characterized, and the feasibility of their regeneration and also their adsorption behaviors were studied in dry and humid air. In Chapter 6, the ultimate objective of this research is addressed. For this purpose, the synthesized and characterized samples were used as dual functional adsorbent/catalysts in a non-thermal plasma (NTP) catalytic reactor. The adsorption and oxidation evaluations of these MOFs for the removal of one (1) ppm toluene and isobutanol were performed at both dry and humid air (RH=30%).

To eliminate the interference of the oxidation performance and the adsorption capacity of MOFs, the catalyst was saturated with VOC prior to any plasma-catalytic test. Formation of organic by-products and ozone was also studied. The structural characteristics of utilized catalysts were studied before and after NTP-catalytic reactions via FTIR spectroscopy to investigate the feasibility of the catalyst regeneration after a plasma-oxidation reaction.

The obtained results of this chapter is reported as a manuscript which is submitted for possible publication in “Chemical Engineering Journal”.

6.1 Introduction

Development of non-thermal plasma (NTP) technology and its remarkable capacity for VOCs destruction has opened a new field of study in the area of air treatment [31], [160]. In a NTP

process, applying a high electrical voltage results in the formation of reactive species, ions and radicals due to the collision of highly energetic electrons with molecules in the air [220], [221]. As a result, destruction of pollutants including VOCs happens at ambient temperature [76]. However, incomplete oxidation and formation of harmful by-products such as O₃, CO, NO_x and other VOCs are the main disadvantages of this technology [40], [192], [222]. Furthermore, due to a high level of energy consumption, utilizing NTP technology is not cost effective, especially when this technique is considered for the abatement of low concentration levels of VOCs in indoor environment [192], [222]. As a solution, utilizing a catalyst in NTP reactor is proposed [222], [223].

Implementation of catalyst in a NTP reactor enhances VOCs removal efficiency and decreases the by-products formation due to the synergic effect of plasma and catalyst. Despite a reduction in the demand of electricity in such a system, energy efficiency is still a concern when the concentration of pollutants is very low. In such conditions, utilizing an adsorbent for pre-concentrating pollutants becomes attractive due to lower energy consumption [194]. Therefore, as a new approach, reactive adsorption process was developed [29], [193], [214]. This method specifically attracted the interests of researchers for economizing energy consumption in the plasma catalyst field [30], [84], [87], [107], [224]. In this method, the VOC removal performance is a function of both the adsorption characteristics and oxidation ability of the media, which is used as the adsorbent/catalyst [225]. Therefore, selecting an appropriate dual functional adsorbent/catalyst (DFA/C) is a crucial aspect if this method is considered for indoor air treatment.

In addition to oxidation capability, an employed DFA/C should possess high adsorption capacity and hydrophobicity especially at low concentration levels of VOCs and in the presence of humidity. The higher the capacity of the media for VOCs storage, the greater the amount of pollutants that can be adsorbed on its surface. As a result, energy consumption is decreased during a reactive adsorption process. Several studies have been conducted on NTP-catalyst in the presence of different types of DFA/Cs, including metals^{and}/or metal oxides, which are used as a support for porous materials such as activated carbon and zeolites [30], [83], [87], [90], [226], [227]. Due to their excellent characteristics, zeolite based media show high removal efficiency for most VOCs. However, the relatively small pore sizes of these materials limit the application of zeolites for removal of large VOCs [119].

Metal organic frameworks (MOFs) as a new class of porous materials exhibit excellent specifications, such as exceptionally large surface area, high gas adsorption, substantial storage capacity, and extra-high porosity[35], [36], [228], [229]. The uniform crystal size and size distribution of MOFs [139], [152] facilitate mass transport phenomena, including adsorption of target compounds, diffusion into pores and desorption of the products, and provide a favorable condition for catalyzing a reaction [132], [142], [230]. MOFs also have an abundant amount of metal content (~20–40 wt%) in the form of metal nodes, with free and exchangeable active sites [152]. The presence of these metal sites induces heterogeneous catalytic properties in MOFs [154]. The above-mentioned specifications of MOFs suggest that these materials can be potential candidates as DFA/Cs for the removal of VOCs in a NTP-catalytic reactor. However, the potential performance of these materials for the degradation of VOCs has not been yet investigated in any plasma catalytic.

In this study three different MOFs - MIL-101 (MIL: Materials of Institute Lavoisier), MIL-53, and CPM-5 (CPM: Crystalline Porous Material) - are used as catalysts in a NTP-catalytic system. All of these MOFs have been previously synthesized, characterized, and their VOCs adsorption behaviors have been investigated in dry air and in the presence of humidity [231]. In the current study, the removal efficiency of these MOFs for the degradation of one (1) ppm of toluene and isobutanol in dry air and at 30% relative humidity (RH) is explored. In addition, formation of organic by-products and ozone is studied. Finally, the structural characteristics of utilized catalysts before and after NTP-catalytic reactions are studied.

6.2 Experimental

6.2.1 Experimental set-up and measurement apparatus

VOC removal efficiency of the selected MOFs is evaluated at a total flow rate of 1 Lmin⁻¹ and ambient temperature (23±1°C). The experimental set-up is illustrated in Figure 6.1.

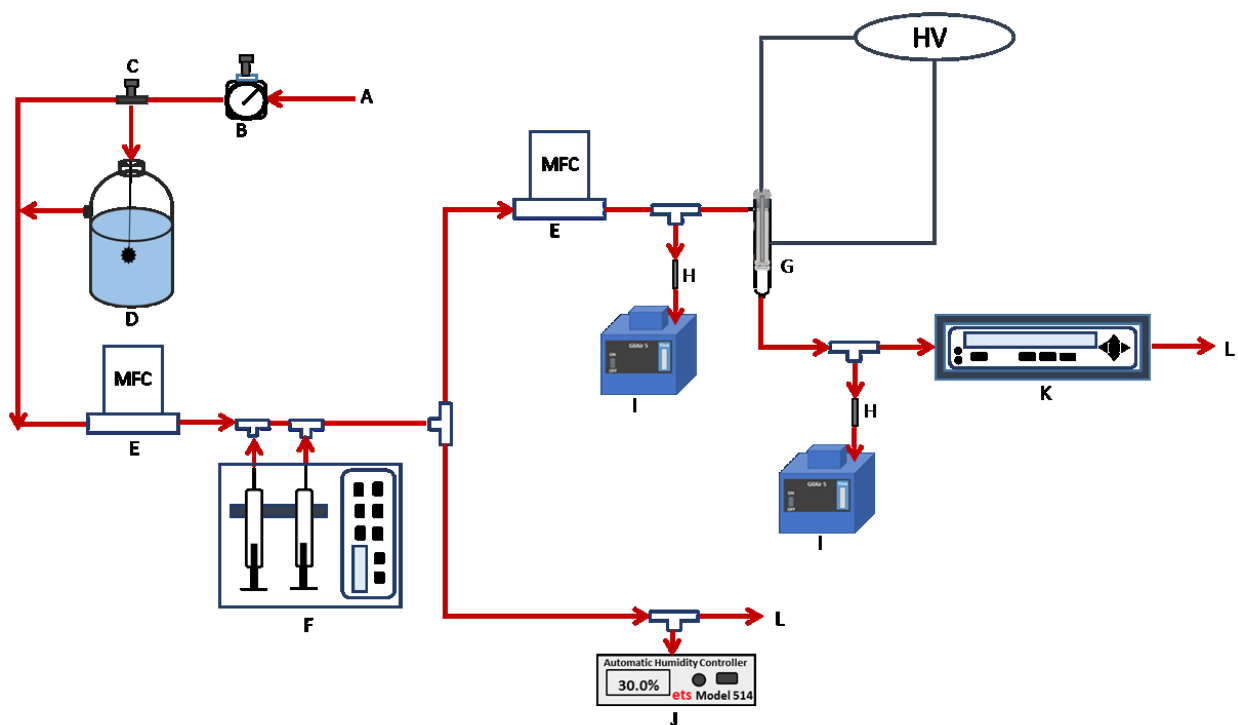


Figure 6.1 Schematic diagram of the set-up; (A) Compressed air, (B) regulator, (C) control valve, (D) water bubbler, (E) mass flow controllers, (F) syringe pump, (G) reactor, (H) adsorption tubes, (I) sampling pump, (J) humidity controller, (K) ozone monitor

In this continuous system, dry air is supplied from a compressed air reservoir (A) and passes through a regulator (B) to adjust the pressure. A water bubbler (D) is utilized upstream to provide the required relative humidity (RH). The amount of the humidity is adjusted via a control valve (C) and the air flow rate is controlled by means of mass flow controllers (Matheson, Model 8274) (E). A syringe pump (KD Scientific, Model KDS-210) (F) injects the target VOC at the desired rate into the system. Afterward, the air stream containing the target VOC passes through the catalyst in the reactor (G). The upstream and downstream samples are collected from the reactor in stainless steel adsorption sampling tubes (Supelco Air Toxics, packed with Tenax-TA 49) (H) by means of sampling pumps (17G9 GilAir-3 Sampler) (I) in an adjusted flow rate of 50 mLmin^{-1} . The duration of each sampling is 20 minutes. These samples are analyzed using a gas chromatograph/mass spectrometer (GC/MS, Perkin Elmer, Clarus 500) coupled with an automatic thermal desorber (ATD, Perkin Elmer, model TurboMatrix 350). The RH is controlled via a humidity controller (Electro-Tech Systems (ETS), Model 514) (I) upstream of the reactor.

Concentration of the generated O_3 is measured with an ozone monitor (Model 202, 2B Technologies, An InDevR Company) (K) downstream of the reactor.

The micro reactor, depicted in Figure 6.2, is a fixed-bed catalytic reactor containing a coaxial cylindrical quartz tube (ID: 10.4 mm; OD: 12.8 mm; L: 250 mm), with a centered stainless steel-316 rod (D: 5mm) as an inner electrode. The resulting discharge gap of the reactor is 2.7 mm. Ten (10) centimeter of an aluminum foil is wrapped around the reactor as a ground electrode. The inner electrode is connected to a high voltage (HV) supplier which has been explained in details elsewhere [192]. Briefly, this HV power supply, illustrated in Figure 6.3, constitutes a function signal generator (BK PRECISION, Model 4011A) (B), a wideband AC power amplifier (Model AL-600-HF-A, Amp-Line Corp.) (C), and a high voltage transformer box (Model AL-T250-V25/10K-F50/2K, Amp-Line Corp.) (D). This HV AC power supply provides an adjustable voltage and frequency in the range of 0 –30 kV_{p-p} , and 50Hz to 2 kHz, respectively, which is applied to the DBD reactor (F). A digital oscilloscope (Tektronix, TBS1052B-EDU, 50MHZ, 2CHANNEL) (E) monitors the voltage and current signals of the system. A 30 kV high voltage probe (Keysight N2771B) (G) measures the delivered voltage to the reactor. In this study, the frequency is set to 60 Hz and the applied voltage is 16.8 ± 0.1 kV_{p-p} for isobutanol and 17.6 ± 0.3 kV_{p-p} for toluene. Selection of the input voltage was based on a series of preliminary tests in order to reach the lowest amount of voltage in which a stable discharge along with a minimum amount of ozone generation in both dry and humid conditions is formed in the plasma reactor.

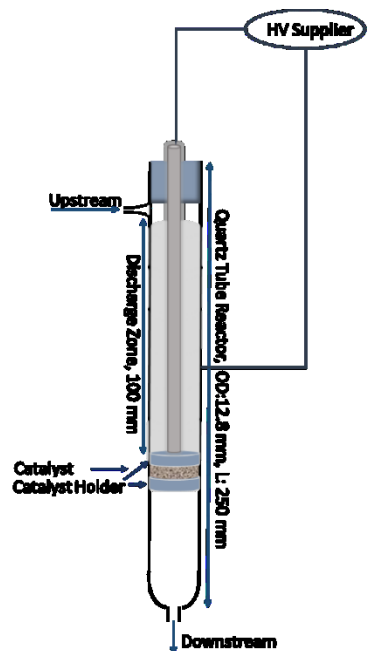


Figure 6.2 The DBD reactor

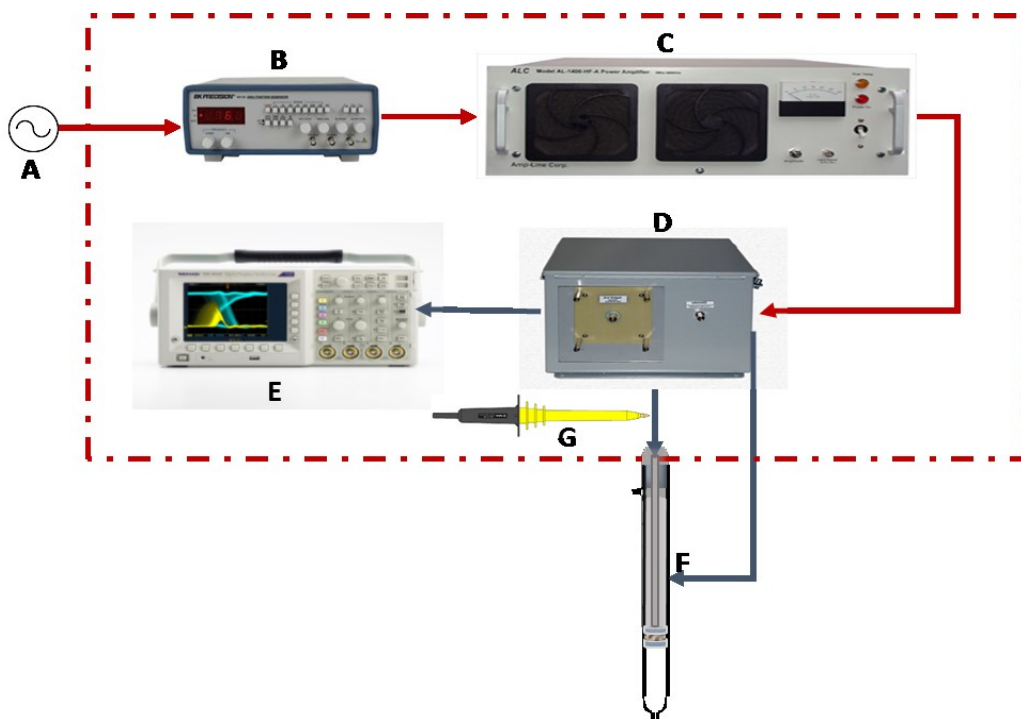


Figure 6.3 Schematic of the high voltage apparatus; (A) AC power, (B) function generator, (C) AC power amplifier, (D) high voltage transformer box, (E) oscilloscope, (F) DBD reactor, and (G) high voltage probe.

6.2.2 Catalysts and reagents

MIL-101, MIL-53 and CPM-5 are the three selected MOFs, which are used as DFA/Cs in this study. These MOFs have been previously synthesized and characterized [231]. For each test, 0.2 g of the catalyst is prepared in the size of 35 to 60 meshes (250 to 500 μm). The preparation is reported in reference [231]. The catalyst is loaded in the reactor, and placed between two layers of fiber glass, which are used as catalyst holders. The residence time on the catalyst zone is calculated as follows:

$$\tau = \frac{\text{Bed Volume}}{\text{Gas Flow Rate}} = \frac{V}{F} = \frac{(\pi r^2 L)}{F} \quad (6.1)$$

The calculated residence time for different media varies between ~ 0.01 to 0.015 s. Toluene and isobutanol are two selected VOCs as target pollutants in this study. Both of these reagents were purchased from Fisher Scientific and were of analytical grade with purity higher than 99.9%.

6.2.3 Catalytic performance evaluation for VOCs adsorption and oxidation

Experiments are performed to determine the adsorption and oxidation efficiency of MIL-101, MIL-53 and CPM-5 for the removal of toluene and isobutanol. In the first step, the selected catalyst is saturated with one (1) ppm of the target VOC and the adsorption capacity is evaluated in the depicted set-up in Figure 6.1 while plasma is off. All tests are carried out at two different conditions: dry air (RH=0%), and in the presence of humidity (RH=30%). The adsorption capacity (η_b , mmol) and normalized adsorption capacity per area (q_s , mmol.m⁻²) are calculated according to equations (2) and (3) [232]:

$$n_{ad} = \frac{\int_0^{t_s} (C_{up,t} - C_{down,t}) \times Q \times dt}{24.4 \times 1000} \quad (6.2)$$

$$q_s = \frac{n_{ad}}{m \times S_{BET}} \quad (6.3)$$

In these equations, Q (L.min⁻¹) is the air flow rate, t_s (min) is the time required to reach the defined breakthrough, 24.4 (L.mol⁻¹) is the molar volume of gas at standard temperature (T=298 K), 1000 is the unit conversion coefficient, m (g) is the weight of the catalyst and finally, S_{BET} (m².g⁻¹) is the BET surface area of the applied catalyst in the reactor. Breakthrough time in this

study is when the downstream concentration reaches the same amount as the upstream (100% saturation) at ambient temperature ($T \sim 21^\circ\text{C}$).

The oxidation performance of the pollutant is evaluated for isobutanol and toluene at two levels of humidity (RH=0% and 30%). For this purpose, prior to any NTP-catalytic oxidation test, the catalyst is saturated with one (1) ppm of the target VOC, while the plasma is off. When the downstream concentration of VOC reaches 100% breakthrough, the plasma is applied into the reactor. The injection of targeted VOC is continued during the course of experiments. The single pass removal efficiency of the pollutant, η_t (%), is calculated according to the following equation:

$$\eta_t(\%) = \frac{C_{Up,t} - C_{Down,t}}{C_{Up,t}} \times 100\% \quad (6.4)$$

where, $C_{Up,t}$ and $C_{Down,t}$ are concentrations of target VOC (ppm) at the upstream and downstream of the reactor as a function of time. Since prior to any test the catalyst is saturated with VOC, equation (4) gives the oxidation performance and the interference of the adsorption removal is deducted.

6.2.4 Catalyst Characterization

Fourier transform infrared (FTIR) experiment was done using Nicolet 6700 (Thermo Scientific, made in USA) in the range of $525\text{-}4000\text{ cm}^{-1}$. Measurements were performed by ATR (Attenuated Total Reflectance), using a Smart iTR module. Catalysts were analyzed at three different conditions: (a) the fresh catalyst, (b) after 4 days (96 hours) of NTP-catalytic reaction of one (1) ppm of isobutanol and 30%RH, and (c) after its regeneration by passing dry air through the reactor at ambient temperature for 48 hours. For each catalyst, results of these three cases were compared to detect the presence of certain functional groups and to identify any probable change in the structure of MOFs during the oxidation processes.

6.3 Results and Discussion

6.3.1 Adsorption capacities of catalysts

Toluene and isobutanol adsorption capacities of MIL-101, MIL-53 and CPM-5 are determined in dry air (RH=0%), as well as in the presence of humidity (RH=30%), see Figure 6.4.

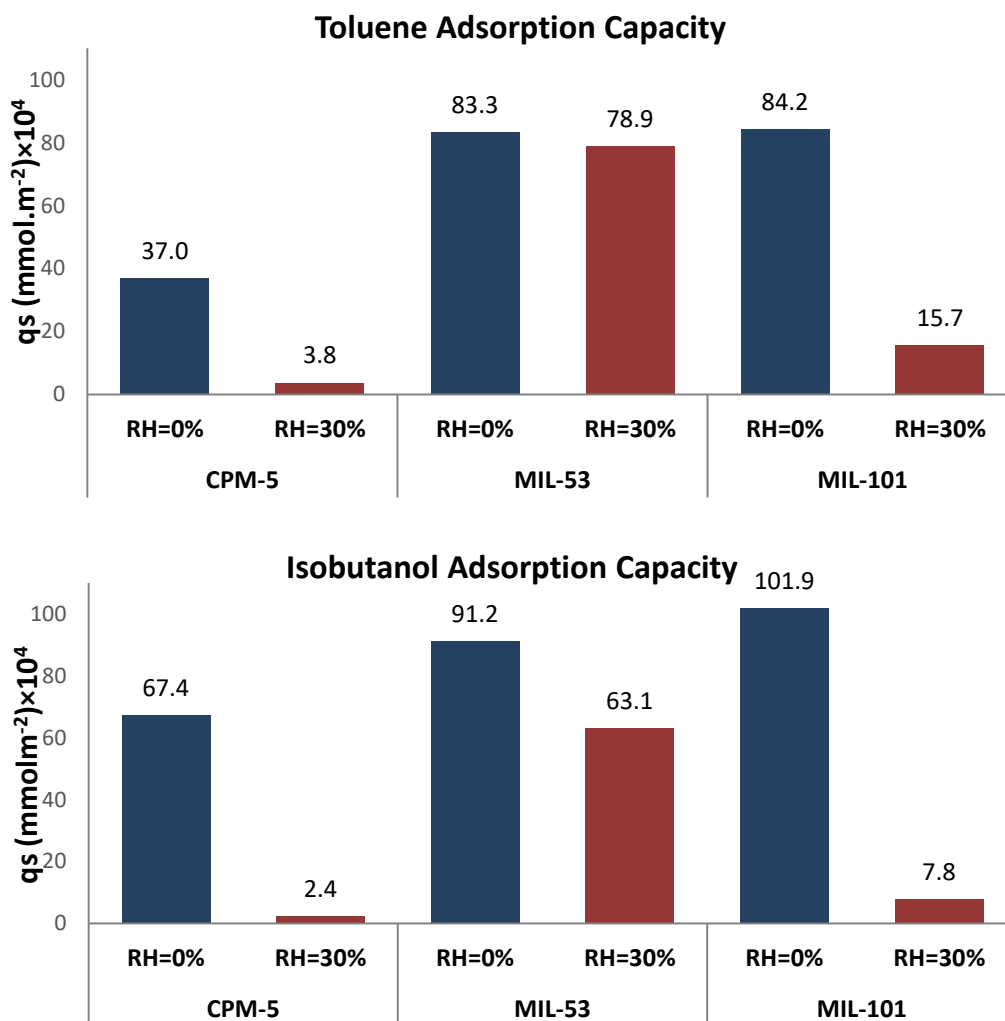


Figure 6.4 Adsorption capacity of toluene and isobutanol over CPM-5, MIL-53 and MIL-101 in: dry air (RH=0%), and humid air (RH=30%).

Figure 6.4 shows a high adsorption capacity of VOCs over the examined MOFs in dry air conditions. The large adsorption capacity of these MOFs is related to the electrostatic interaction between the adsorbed VOC and the organic linker in the structure of the MOF [34], [35]. From

Figure 6.4 it can also be seen that MIL-101 possesses the highest adsorption capacity of both toluene and isobutanol in dry condition. An extra-high surface area of MIL-101, combined with the presence of large mesopores in its structure, explain the higher storage capacity of this MOF compared to MIL-53 and CPM-5 (Langmuir surface area of MIL-101~ 3750 m²/g, MIL-53~1275 m²/g, CPM-5: 1560 m²/g) [231].

Another observation from Figure 6.4 is that the adsorption capacity of MIL-53 is much higher for isobutanol and toluene than CPM-5, despite the larger surface area of the latter catalyst. This can be due to the expansion of the framework of MIL-53 (as host) upon exposure to an organic compound (as guest), which is known as breathing phenomenon [216]. This host-guest interaction results in the opening of inaccessible pores in the anhydrate form of the MIL-53 [140], [231], [233].

On the other hand, from Figure 6.4, it is clearly evident that the presence of humidity (RH=30%) has a negative impact on the adsorption capacity of all MOFs. The order of adsorption capacity in this condition is MIL-53>> MIL-101> CPM-5. The decrease in the adsorption capacity results from the formation of water clusters on the surface of the catalyst. This prevents target organic molecules from reaching the active sites, including the trivalent metal cation sites (In⁺³ in CPM-5, Cr³⁺ in MIL-101, and Fe⁺³ in MIL-53), as well as the benzene rings of organic linkers in the structure of the MOF. The result is a sharp decrease in the adsorption capacity of MIL-101 and CPM-5. The decrease in the adsorption capacity is, however, much less in the case of MIL-53. Although the hydrated form of MIL-53 contains some pores that are filled with water molecules, there are still closed pores that can be opened for adsorption of more amounts of VOCs [231].

6.3.2 VOCs removal efficiency at dry condition

Using a series of experiments to investigate the removal efficiency of toluene and isobutanol over MIL-53, MIL-101 and CPM-5 at dry condition, and comparing it with that of non-thermal plasma alone, the selected catalyst is saturated with one (1) ppm of the targeted VOC. The experiment is then started by applying the discharge to the reactor. The experiment is performed for six hours and the removal efficiency is reported based on the average of 10 samples, which are collected in the course of the experiment. Results show 100% removal efficiency (η_t (%)) of

isobutanol over all three MOFs. This amount decreases to 56.6% when NTP alone (no catalyst) is used in the reactor.

Figure 6.5 compares the removal efficiency of toluene in the absence of the catalyst (NTP), and also over MIL-53, MIL-101 and CPM-5. Results show almost the same amounts of toluene removal efficiency for MIL-101 and MIL-53 (~93%), while this amount for CPM-5 is slightly lower (89%). Also, regardless of the type of catalysts used, a twofold increase in toluene removal efficiency is observed compared to the removal efficiency of NTP alone.

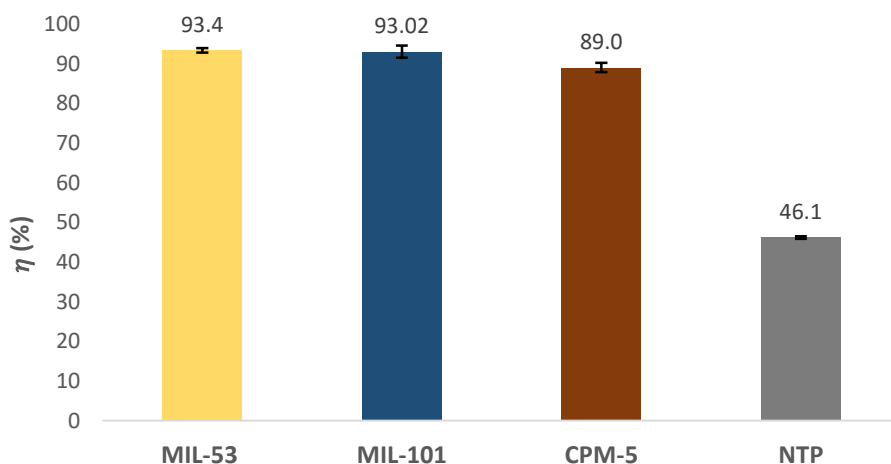


Figure 6.5 Removal efficiency of toluene over MIL-53, MIL-101, CPM-5, and in the absence of catalyst (NTP)

Since the catalyst is saturated by the target VOC prior to each experiment, the reported removal efficiencies are purely based on the oxidation capacity rather than the adsorption capacity of these VOCs over the MOFs. Therefore, it is concluded that at a dry condition (RH=0%), the selected MOFs demonstrate a high removal performance during a NTP-catalytic process. It is notable that the performance of the catalyst remained constant for both isobutanol removal and for toluene removal during the six-hour test.

6.3.3 Effect of relative humidity on VOCs removal efficiency

To investigate the effect of humidity on the removal performance of the catalysts, a series of tests were conducted for removal of one (1) ppm target VOC in humid air (RH=30%). Experiments were continued for four days (96 hours) for MIL-101 and CPM-5 to determine whether or not the

performance of the catalyst is affected during the time. In the case of MIL-53, the duration of the experiment was extended to 11 days (264 hours). Results are illustrated in Figures 6.6 and 6.7.

Figure 6.6 shows that toluene removal efficiency for all catalysts increases with time. The reason is that at the beginning of the tests, the catalyst is saturated with one ppm of toluene and 30% RH. It has been demonstrated in the previous section (6.3.1) that the presence of H₂O molecules limits the access of VOC molecules to the surface of the catalyst and decreases the VOC adsorption capacity of the MOFs. Therefore, when plasma is applied in the reactor at the beginning of the reaction, the removal efficiency is low. As the time passes, due to the oxidation reactions, toluene and water concentration decrease on the catalyst surface. Therefore, the remaining toluene molecules have more access to the active sites of the catalyst. The result is an increase in the removal performance over time. From Figure 6.6, it can be also seen that after four days of reaction, the removal efficiency reaches to 72.6%, 82.0% and 53.0% for MIL-101, MIL-53 and CPM-5, respectively. The very low removal performance of CPM-5 is likely due to its small pore sizes. The small size of H₂O, favors its access to the surface of CPM-5, compared to toluene. Therefore, the efficiency is lower than MIL-101 and MIL-53. A comparison between the removal efficiency of MIL-101 and MIL-53 also shows that despite a significantly higher adsorption capacity of MIL-53 in the presence of humidity, this catalyst has a slightly higher removal efficiency than MIL-101.

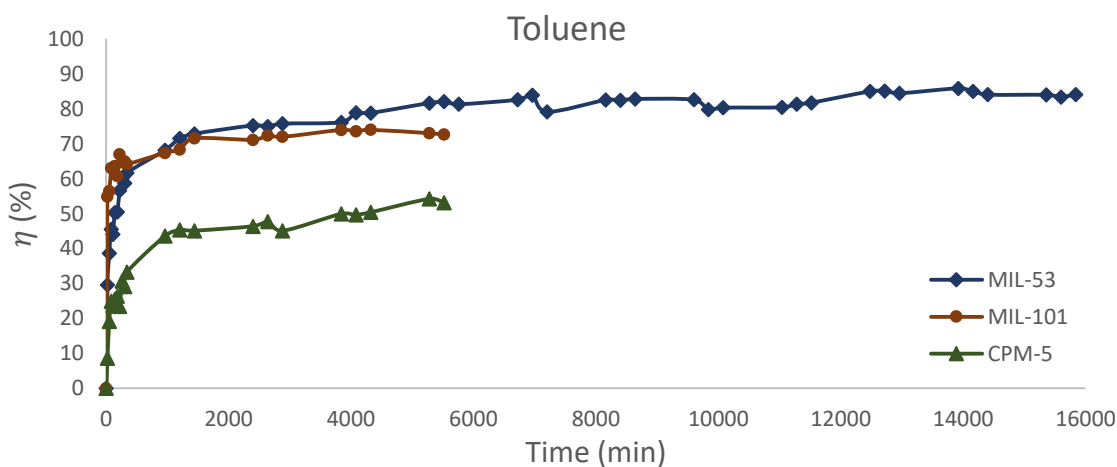


Figure 6.6 Removal efficiency of one ppm toluene over MIL-53, MIL-101, CPM-5 as catalyst in humid air (RH=30%).

Figure 6.7 compares isobutanol removal efficiency over MIL-53, MIL-101, and CPM-5 in the presence of 30%RH. The figure shows 97% isobutanol removal efficiency for MIL-101 at the beginning of NTP-catalyst process. This is the highest observed toluene removal efficiency between the three studied MOFs. However, this amount drops after the first five hours of the test by almost 10%. On the other hand the performance of MIL-53 and CPM-5 increases with time. The removal efficiencies after four days are 95.3%, 84.6% and 88.6% for MIL-53, MIL-101, CPM-5, respectively. It can be postulated that the decrease in the removal efficiency of MIL-101 is due to some changes in the catalyst structure. Characterization of the catalyst is described further.

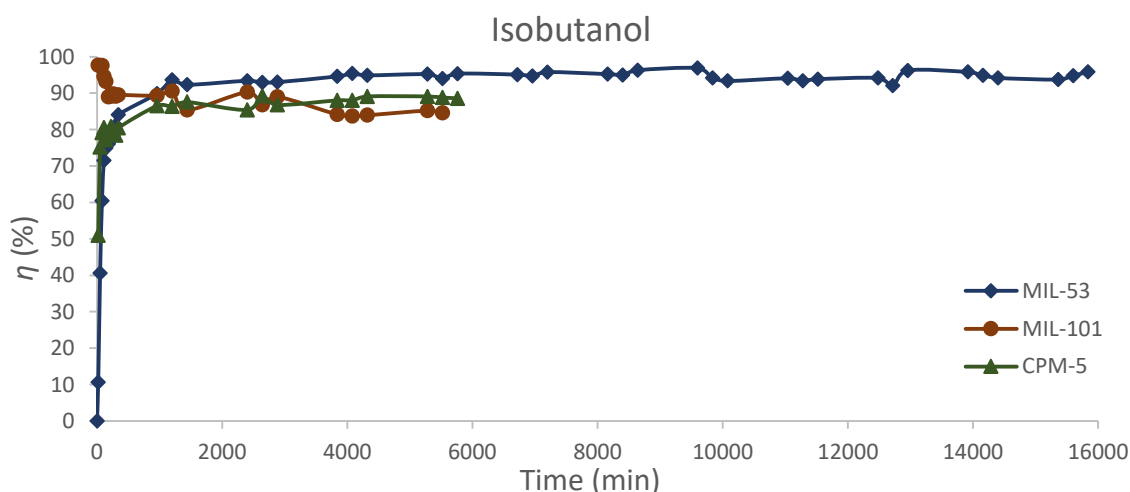


Figure 6.7 Removal efficiency of one ppm isobutanol over MIL-53, MIL-101, CPM-5 as catalyst in humid air (RH=30%).

Figures 6.6 and 6.7 also demonstrate that in the case of MIL-53, for toluene and isobutanol oxidation, continuing the test for 11 days does not reveal any decrease in its removal performance.

A comparison between the removal efficiency of MIL-101, MIL-53 and CPM-5 in dry and humid conditions shows that the performance of all catalysts decreases in the presence of the humidity. Yet, some studies have reported an increase in catalyst performance in the presence of humidity due to the formation of hydroxyl radicals and atomic oxygen [234]. OH radicals are one of the long life span reactive species, more active than ozone for VOCs decomposition. This radical also plays an important role in the destruction of organic compounds [64], [75], [234], [235].

However, increasing the level of relative humidity can quench reactive species and limit their activity, resulting in a decrease in removal efficiency [75]. Furthermore, the catalyst is saturated with 30%RH and one (1) ppm of the target VOC ($C_{\text{VOC}}/C_{\text{H}_2\text{O}} \sim 1/5000$). Considering the abundance of water molecules together with the amphiphilic nature of MOFs, formation of water clusters on the surface of the catalyst is unavoidable [202]. The result is the limited access of organic compounds to the catalyst surface and a decrease in its removal performance.

In a different test a fresh MIL-53 was used as the catalyst and once injection of isobutanol and humidity started, the plasma was applied in the reactor. The experiment continued for four days. Results, showed 100% removal efficiency in the course of the test, which demonstrates the effect of adsorption capacity in the VOC removal performance of the catalyst.

6.3.4 Organic by-products formation and effect of humidity

Formation of organic by-products is one of the most important concerns when a NTP- catalytic method is utilized for VOCs removal. The selected MOFs have demonstrated ability for removal of toluene and isobutanol. However, a determining factor to decide about the excellence of the catalyst also depends on the by-product formation. Figures 6.8 illustrates formation of organic by-products during the plasma treatment of toluene and isobutanol over MIL-53, MIL-101, CPM-5, and also NTP alone. Since the detected by-products by GC/MS analysis for both humid and dry air were very similar, the chromatograms are reported just for experiments, which are conducted in the presence of 30%RH.

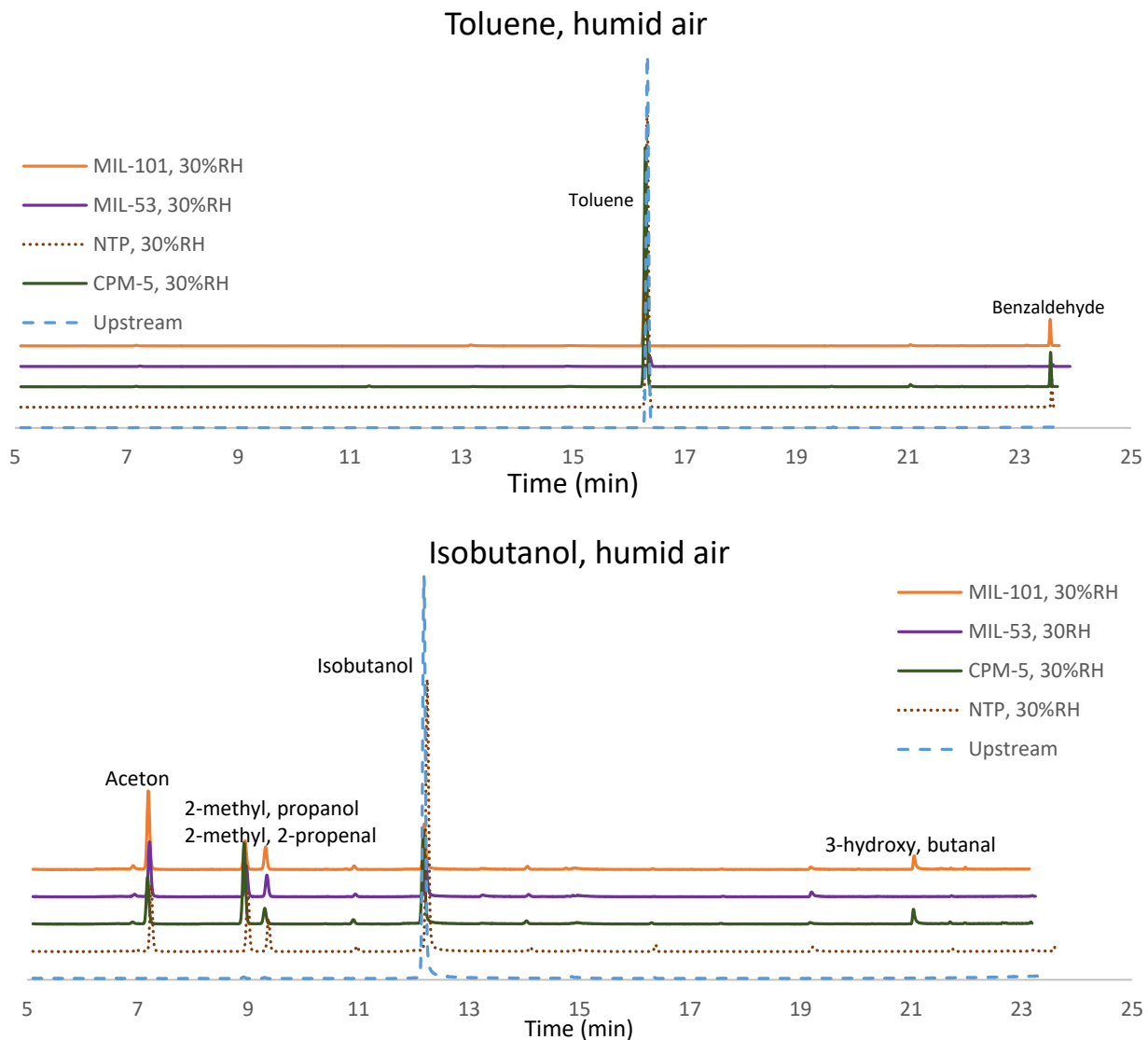


Figure 6.8 GC/MS chromatograms of organic by-products during plasma-catalyst treatment of toluene (up) and isobutanol (down) over MIL-53, MIL-101, CPM-5, and NTP alone.

The results show formation of almost the same by-products for three different catalysts during the oxidation process. From Figure 6.8, benzaldehyde is the major organic compound formed during the toluene plasma-catalytic oxidation test. However, during the plasma-catalytic oxidation of isobutanol, different types of by-products are formed. Table 6.1 specifies the detected organic by-products during the plasma-catalytic oxidation of isobutanol and toluene.

Table 6.1 Detected organic compounds downstream of the plasma reactor during the oxidation of toluene and isobutanol in dry condition (RH=0%) and humid condition (RH=30%)

Target VOC	By-products	RT*(min) ^a
Isobutanol	Isopropyl alcohol	6.8
	Acetone	7.1
	2-methyl, propanol	8.9
	2-methyl, 2-propenal	9.3
	Acetic acid	13.1
	1-butanol	14.1
	2-methyl, propionic acid	19.2
	3-hydroxy, butanal	21.7
Toluene	Acetic acid	13.2
	Benzaldehyde	23.6

*Retention time

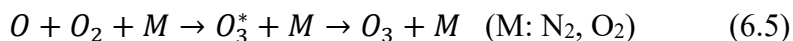
^a Background peaks appear at RT: 11.3, 15.0, 16.3, 21.1, and 22.2 min in almost all isobutanol and toluene chromatograms.

6.3.5 Ozone as by-product and the effect of humidity

To investigate the performance of the selected catalysts for removal of ozone, in a series of tests, the targeted VOC was injected in the plasma reactor and ozone concentration was measured downstream of the reactor in the absence of the catalyst for both dry condition (RH=0%) and humid air (RH=30%). Afterwards, the catalyst was inserted into the reactor and ozone concentration was monitored, in the presence of 30%RH. The applied input voltage for toluene and isobutanol was set at 17.6 ± 0.3 kVp-p and 16.8 ± 0.1 kVp-p, respectively.

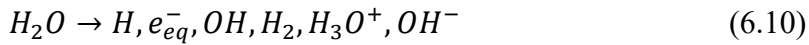
It was observed that while the average concentrations of ozone during the decomposition of toluene and isobutanol in dry air were 37.8 ppm and 33.3 ppm, respectively; in the presence of 30%RH these amounts declined to 13.8 ppm and 5.0 ppm for these compounds, respectively. A considerable decline in the ozone concentration is also reported in other studies, when humidity is introduced into the system [64], [234].

In a DBD system, dissociation of O₂ and N₂ molecules in dry air results in the formation of reactive species including ozone (O₃) and oxygen atoms (O) according to equations (5) to (9) [52], [192]:





When humidity is introduced into the reactor, other types of reactive species are formed from the following decomposition reactions [75]:



It has been reported that formation of ozone in the presence of humidity is suppressed, as the energetic electrons are extinguished by H₂O molecules [235]. In addition, ozone molecules can act as a source of hydroxyl radical formation, according to equations (6.14) to (6.19) [234]:



Figures 6.9 and 6.10 compare the amount of ozone when MIL-101, MIL-53 and CPM-5 are utilized as the catalysts downstream of the reactor.

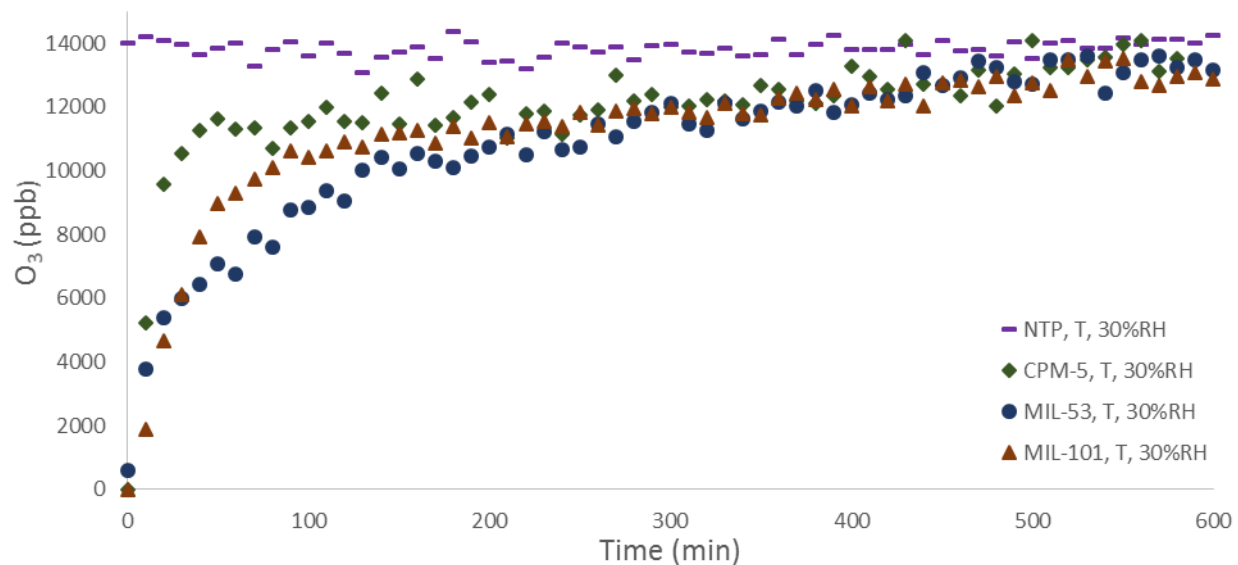


Figure 6.9 Ozone concentration downstream of the reactor during the plasma-catalyst treatment of toluene over MIL-53, MIL-101, CPM-5, and NTP; input voltage: 17.6 ± 0.3 kVp-p

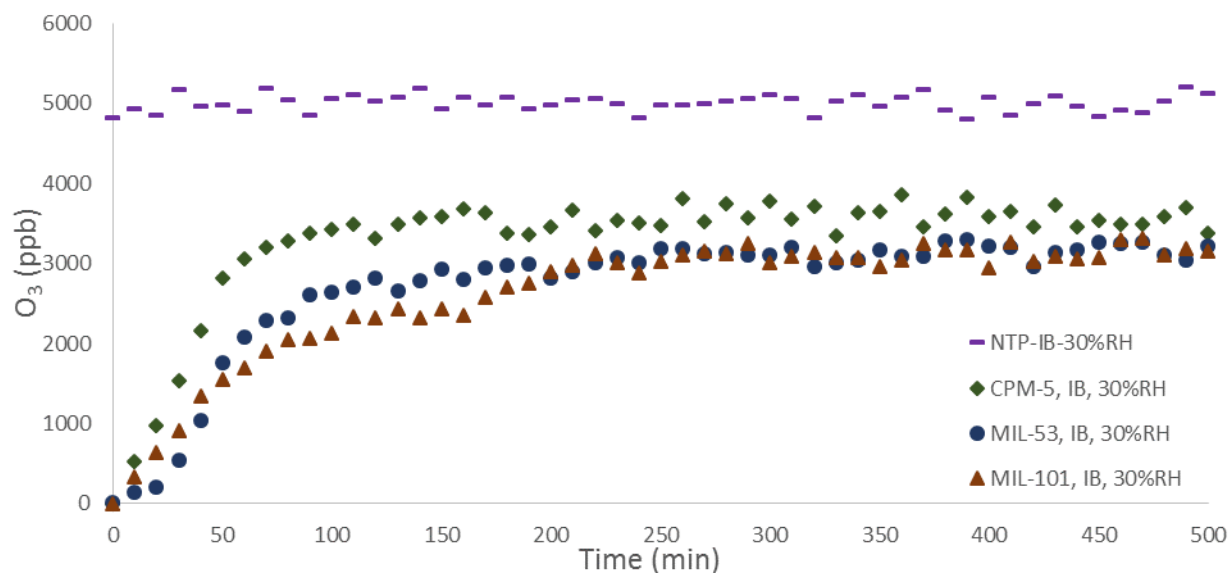


Figure 6.10 Ozone concentration downstream of the reactor during plasma-catalyst treatment of isobutanol over MIL-53, MIL-101, CPM-5, and NTP; input voltage: 16.8 ± 0.1 kVp-p

The first observation from Figures 6.9 and 6.10 is that the amount of downstream ozone in the case of toluene oxidation is almost threefold of isobutanol oxidation. Since the applied voltage in the reactor for toluene oxidation experiments is on average 0.9 kVp-p higher than isobutanol oxidation tests, this increase in the ozone generation is rational. As mentioned earlier, the minimum

voltages for each compound were selected in order to minimize the ozone concentration, while a stable discharge takes place in the reactor. In the case of isobutanol, plasma generation requires a lower applied discharge to reach this stable point.

According to Figures 6.9 and 6.10, in the first three hours, the ozone removal performance of MIL-53 and MIL-101 are almost the same and slightly higher than that of CPM-5. After three hours, however, the concentration of ozone reaches a stable amount for all catalysts.

It is noteworthy that in all the above-mentioned experiments; the catalyst was saturated with one ppm of the target compound and 30%RH prior to applying discharge and monitoring the amount of ozone. Figure 6.11 compares the performance of the saturated MIL-53 with the fresh MIL-53 for ozone removal. In the latter test, injection of isobutanol and 30% RH, and also applying discharge into the reactor started simultaneously. It can be seen that after 700 minutes, the ozone removal performance for the fresh catalyst is 72.7%, which is roughly twofold more than the saturated catalyst with a removal performance of 35.3%.

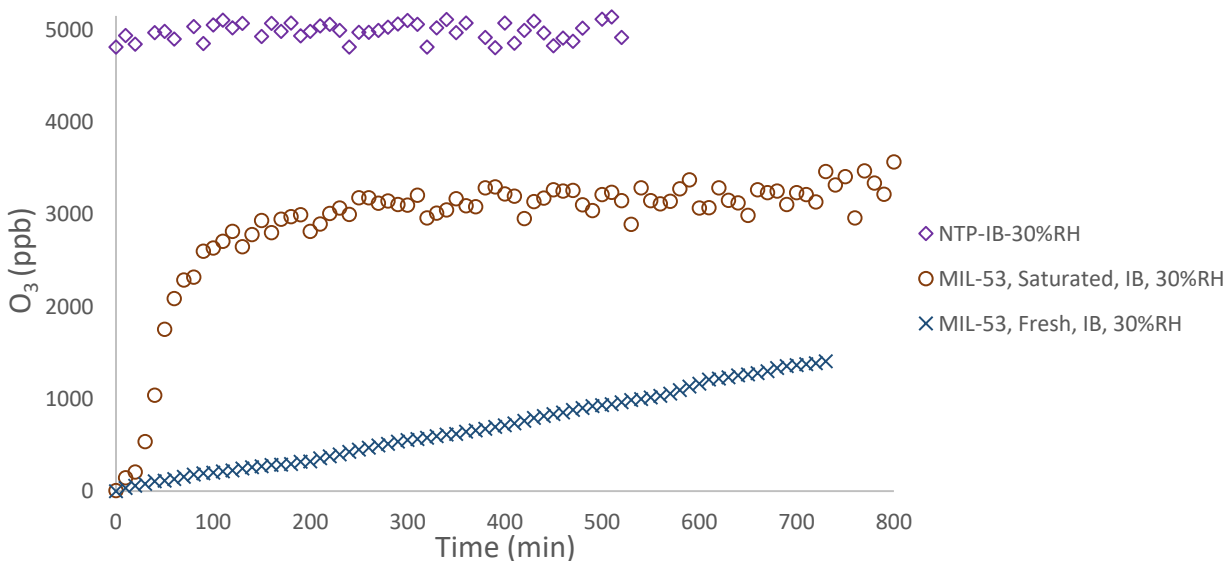


Figure 6.11 A comparison between the ozone removal performance of fresh and saturated MIL-53 during a plasma-catalyst treatment of isobutanol, RH=30%, input voltage: 16.8 ±0.1 kVp-p

6.3.6 Catalyst characterization

FTIR spectroscopy was performed to identify the possibility of any change in the molecular structure and functional groups of MIL-101, MIL-53 and CPM-5 during the NTP-catalytic reaction. Figures 6.12 to 6.14 illustrate the FTIR results of the utilized MOFs. For each catalyst, the analysis is carried out for three different states: before catalytic reaction (fresh), after four days (96 hours) of NTP-catalyst treatment of isobutanol in the presence of 30%RH (saturated), and finally after regeneration of the catalyst by passing dry air throughout the reactor for 48 hours (regenerated). From the results, the FTIR spectra of all fresh samples are in good agreement with other studies [129], [236]–[238].

The results of MIL-53 spectroscopy, illustrated in Figure 6.12, show two prominent bands at 1534 cm^{-1} and 1385 cm^{-1} , corresponding to the asymmetric $\nu_{\text{as}}(\text{COO}^-)$ and symmetric $\nu_{\text{s}}(\text{COO}^-)$ vibrations of carboxylic groups. These bands indicate the presence of dicarboxylic acid as a linker in the structure of MIL-53 [233], [239]. The intense peaks at 1017 and 751 cm^{-1} are associated with C-H bonding vibration of the benzene rings [233]. The appeared peak at 545 cm^{-1} is attributed to Fe-O vibration in the structure of MIL-53 [240]. A comparison of the FTIR spectra of fresh catalyst with the saturated and regenerated ones reveals no change in the functional groups of MIL-53.

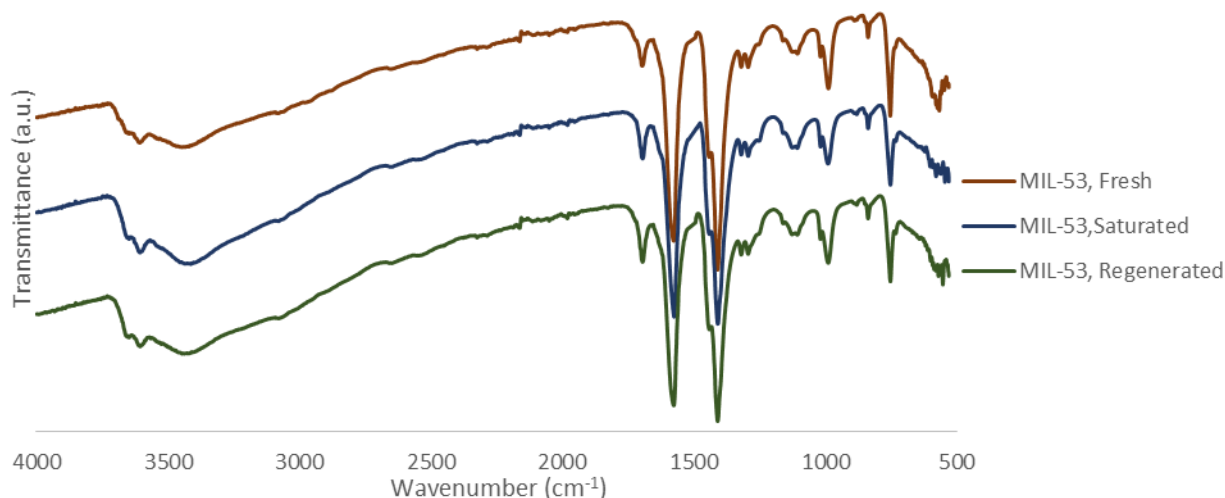


Figure 6.12 FTIR spectra of MIL-53 before catalytic reaction (Fresh), after 96 hours NTP-catalyst treatment of isobutanol in the presence of 30%RH (Saturated), and after regeneration for 48 hours (Regenerated)

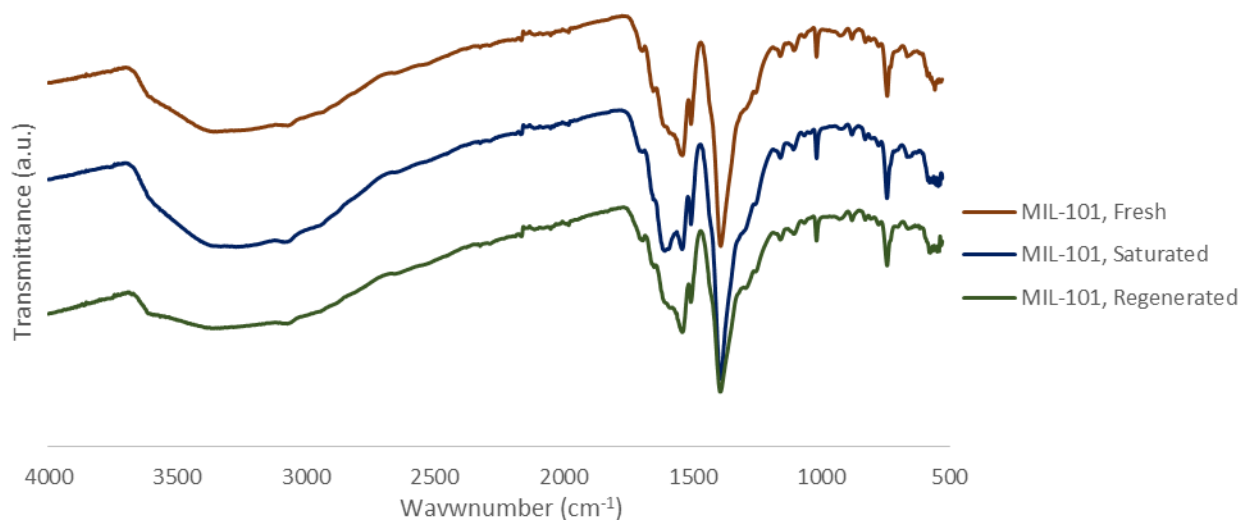


Figure 6.13 FTIR spectra of MIL-101 before catalytic reaction (Fresh), after 96 hours NTP-catalyst treatment of isobutanol in the presence of 30%RH (Saturated), and after regeneration for 48 hours (Regenerated)

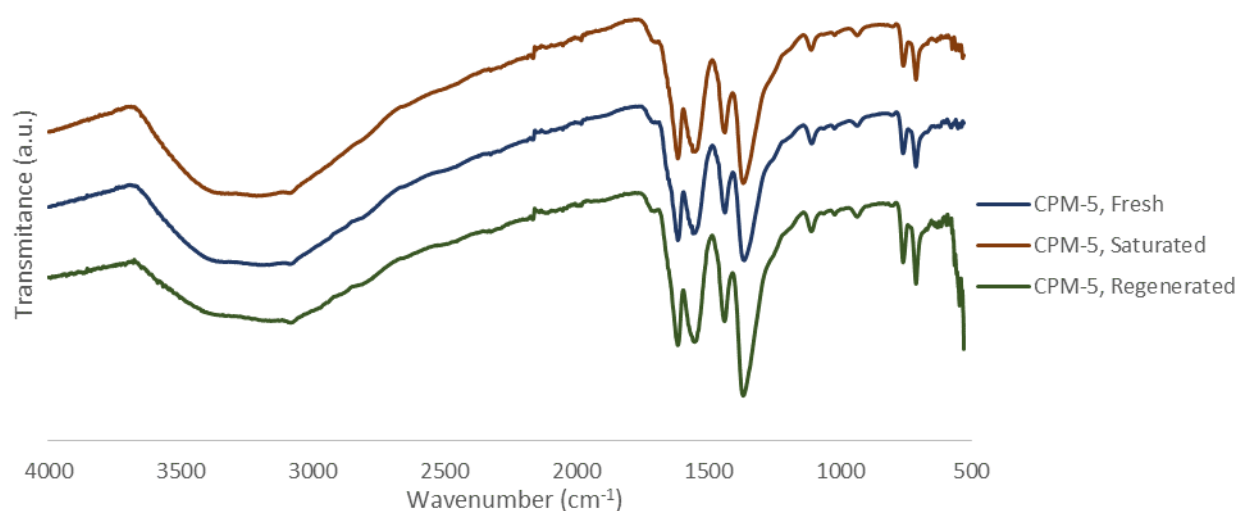


Figure 6.14 FTIR spectra of CPM-5 before catalytic reaction (Fresh), after 96 hours NTP-catalyst treatment of isobutanol in the presence of 30%RH (Saturated), and after regeneration for 48 hours (Regenerated)

For MIL-101, as it can be seen from Figure 6.13, the related bands, which correspond to the asymmetric $\nu_{as}(\text{COO}^-)$ and symmetric $\nu_s(\text{COO}^-)$ groups of terephthalate linkers, appear at 1537 cm^{-1} and 1389 cm^{-1} , respectively [241]. Also, the visible bands at 1017 and 743 cm^{-1} are associated with vibration of C-H in aromatic rings [242]. The presence of weak bands at 538 cm^{-1} corresponds to the formation of metal-oxo bond between the carboxylate group in terephthalic linker and Cr(III) [237]. A comparison of the FTIR spectra of MIL-101 in three states shows the

appearance of a peak at 1640 cm^{-1} , which is due to the stretching of C=O vibrations. This peak disappears after regeneration of the catalyst.

In the case of CPM-5, as illustrated in Figure 6.14, the stretched bands in the spectral region of $1800\text{--}1300\text{ cm}^{-1}$ represent the presence of different carboxylate groups vibrations in benzene rings [129]. This is almost the same characteristic vibration band that was observed in the spectra of MIL-53 and MIL-101. The same vibration band as MIL-101 and MIL-53 is also detected at 533 cm^{-1} , which can be related to the bond between the (COO^-) group and In (III) in the framework of CPM-5. Results do not show any change in the functional groups of CPM-5 during the oxidation reaction of isobutanol.

In all three MOFs, the wide peak which is centered at 3440 cm^{-1} is assigned to vibration of O-H, which is due to the presence of adsorbed water on the surface of the catalysts [146], [237], [240]. Increasing the O-H vibrations in the saturated state of all catalysts can imply protonation of COO^- groups [146], [242], which is removed upon regeneration of the catalysts.

6.4 Conclusion

The importance of optimizing NTP-catalytic systems for air purification application has led researchers to employ dual functional adsorbent/catalysts in these systems. In the current study, the adsorption and oxidation abilities of MIL-101, MIL-53, and CPM-5 were studied for the removal of one (1) ppm isobutanol and toluene in a DBD plasma-catalytic reactor. The effect of the presence of humidity on the performance of these MOFs was investigated. Results demonstrated a high adsorption capacity of both VOCs over the examined MOFs in dry condition in decreasing order of: $\text{MIL-101} \geq \text{MIL-53} \gg \text{CPM-5}$. However, the presence of 30% RH, changed this order to $\text{MIL-53} \gg \text{MIL-101} > \text{CPM-5}$.

During a six-hour NTP-catalytic oxidation experiment using catalysts saturated with one ppm targeted VOCs, 100% isobutanol removal efficiency was observed for all catalysts. For toluene, the obtained removal efficiencies were 93%, 93% and 89%, for MIL-101, MIL-53 and CPM-5, respectively. Performing NTP catalytic tests using catalysts saturated with one (1) ppm targeted VOC and 30% RH for a period of 96 hours showed the negative effect of humidity on the removal

performance of all catalysts. However, when a fresh MIL-53 was utilized, 100% of removal performance was obtained even in the presence of humidity, indicating the effect of adsorption capacity on the performance of the catalyst.

During a NTP-catalytic reaction, different organic by-products were detected either in dry or humid conditions for both toluene and isobutanol. Also, the downstream concentration of ozone reaches equilibrium over saturated MIL-53 at least two times faster than over fresh MIL-53, even in the presence of humidity. Finally, the FTIR spectroscopy signifies no change in the functional groups of MIL-53 and CPM-5. For MIL-101 a slight change in the band related to the stretching of C=O vibrations was observed. However, the disappearance of the peak upon regeneration of the catalyst indicates a facile regeneration of the catalyst, by passing dry air through it.

In conclusion, the present study demonstrated the potential of utilizing the three selected MOFs as dual functional adsorbent/catalysts (DFA/Cs) in a NTP system. Specifically, MIL-101 and MIL-53 exhibited higher adsorption and oxidation capacities compared to CPM-5 in most of the experiments. Further studies are required on each catalyst to quantify the amount of organic by-products. Also, energy optimization is necessary, when these MOFs are utilized as DFA/C in a NTP-catalytic system.

Chapter 7

7. Conclusions and Recommendations

7.1 Conclusion

The ultimate objective of this research was to develop metal organic frameworks (MOFs) as dual functional adsorbent/catalysts (DFA/Cs), with high adsorbent capacities and catalytic properties, for a plasma-driven catalyst reactor. This objective was accomplished in four different steps as follows:

1. A dielectric barrier discharge (DBD) micro reactor was designed and implemented as a non-thermal plasma (NTP) set-up.
2. Three different MOFs, MIL-101 (MIL: Metal institute Lavoisier), MIL-53, and CPM-5 (CPM: Crystalline Porous Material-5), were selected and synthesized. Preparation of these MOFs was performed using mechanochemical, solvothermal, and microwave methods.
3. Adsorption isotherms and breakthrough behaviors of the synthesized MOFs were studied for one (1) ppm of two different VOCs including an aromatic compound (toluene) and an alcohol (isobutanol).
4. The removal efficiency of the prepared MOFs was studied for the degradation of toluene and isobutanol during a plasma-catalytic reaction.

During the adsorption and catalytic-oxidation tests, the effect of the presence of humidity on the adsorption capacity and oxidation ability of each MOF was investigated. Different characterization and analytical instruments such as X-ray Diffraction (XRD), Scanning Electron microscopy (SEM), thermogravimetric analysis (TGA), BET surface area analyzer, Fourier Transform Infrared Spectroscopy (FTIR), Gas Chromatograph/Mass Spectrometer (GC/MS), Ozone Monitor, and VOC Photoionization Detector (PID) were utilized during the experiments.

The conclusive outcomes of the research are:

1) Set-up design and implementation:

The study on the impact of different parameters on the required specific input energy (SIE) and the rate of ozone generation showed that:

- The energy yield for different forms and types of ground electrodes changed in the decreasing order of: $Ag_{\text{paste}} > Al_{\text{foil}} > SS-F_{\text{mesh}} > SS-T_{\text{mesh}}$. Nevertheless configuration of the ground electrode was a dominant parameter on the amount of generated ozone, rather than its type.
- The result of enlarging the active zone of the plasma reactor by means of a longer inner electrode was an earlier plasma ignition along with larger amounts of ozone in the same SIE. This result was valid regardless of the type and configuration of the applied ground electrode.
- By increasing the gap between the electrodes larger SIE amounts was required to reach the same level of ozone concentration.

2) MOFs synthesis and characterization:

Three different MOFs including CPM-5, MIL-101, and MIL-53 were synthesized:

- CPM-5 was synthesized by means of mechanochemical and microwave methods. MIL-53 was prepared using a microwave method, and a solvothermal method was performed for preparation of MIL-101.
- A mechanochemical (MC) method for CPM-5 synthesis showed a successful formation of the CPM-5 structure under the following reaction conditions: oscillation frequency of 90Hz in 30 min followed by three hours of heat treatment at 150°C, and washing with a 1:1 (DMF: DW) as the solvent. The TGA analysis showed that the thermal stability of the synthesized sample was similar to the CPM-5 synthesized by the microwave method. However, the SEM micrographs showed the formation of a different morphology of crystallites. Also, the surface area of the MC-synthesized CPM-5 was lower than the CPM-5 synthesized by the microwave method.
- For the synthesized CPM-5 and MIL-53 samples by microwave method and also the prepared MIL-101 using solvothermal method, the obtained XRD, BET, SEM, and TGA characteristics were in good agreement with other reported studies.

3) Adsorption Evaluation:

The synthesized and characterized MIL-101, MIL-53, and CPM-5 samples were used for adsorption of one (1) ppm of isobutanol and toluene at dry (RH=0%) and humid (RH=30%) conditions.

- The adsorption isotherm behaviors of toluene and isobutanol indicated the physisorption of these VOCs on all the examined MOFs. This result was also confirmed by TGA characterization of samples before and after toluene adsorption.
- MIL-101 exhibited a superior capacity for adsorption of toluene and isobutanol compared to MIL-53 and CPM-5 in dry air.
- In the presence of 30% relative humidity (RH), the adsorption capacities of MIL-101 and CPM-5 steeply declined. MIL-53 showed the highest adsorption capacity in this condition (RH=30%).

4) Oxidation Evaluation:

The synthesized and characterized MIL-101, MIL-53, and CPM-5 samples were used as dual functional adsorbent/catalysts in NTP-catalytic reactor. To eliminate the interference of the oxidation performance and the adsorption capacity of MOFs, the catalyst was saturated with the target VOC prior to any plasma-catalytic test. The adsorption and oxidation evaluations of these MOFs for the removal of one (1) ppm toluene and isobutanol were performed at both dry air and humid air (RH=30%) conditions.

- During a six-hour experiment using catalysts saturated with one ppm targeted VOCs, 100% isobutanol removal efficiency was observed for all catalysts. For toluene, the obtained removal efficiencies were 93%, 93% and 89%, for MIL-101, MIL-53 and CPM-5, respectively.
- Performing the tests using catalysts saturated with one (1) ppm VOC and 30% RH for a period of 96 hours showed the negative impact of humidity on the removal performance of all catalysts. Isobutanol removal efficiencies were 95.3%, 84.6% and 88.6% for MIL-53, MIL-101, CPM-5, respectively. For toluene 72.6%, 82.0% and 53.0% efficiencies were observed on MIL-101, MIL-53 and CPM-5, respectively.

- A fresh sample of MIL-53 as catalyst showed 100% of removal performance even in the presence of humidity. This indicated the effect of adsorption capacity on the performance of the catalyst.
- The FTIR spectroscopy signified no change in the functional groups of MIL-53 and CPM-5. For MIL-101, a slight change in the band related to the stretching of C=O vibrations was observed. However, the disappearance of the peak upon regeneration of the catalyst indicated a facile regeneration of the catalyst, by passing dry air through it.
- Different organic by-products and also ozone were detected downstream of the reactor either in dry or humid conditions for toluene and isobutanol.
- The downstream concentration of ozone reached equilibrium over saturated MIL-53 at least two times faster than over fresh MIL-53.
- After 700 minutes, when MIL-53 was applied for the plasma-catalytic oxidation of isobutanol in the presence of 30% humidity, the ozone removal performance for the fresh catalyst was approximately twofold more than the saturated catalyst (72.7% for fresh catalysts vs. 35.3% for saturated catalyst).

To conclude, this research demonstrated the potential capacity of MOFs as dual functional adsorbent/catalysts (DFA/Cs) in a NTP system. Specifically, MIL-101 and MIL-53 exhibited higher adsorption and oxidation ability compared to CPM-5 in most of the experiments. Results showed a higher adsorption capacity and almost the same oxidation efficiency for MIL-101 compared to MIL-53. Nevertheless, the negative influence of RH on adsorption and oxidation efficiency of MIL-101 was much higher than that of MIL-53. Therefore, due to the inevitable presence of relative humidity in indoor environment, MIL-53 is the best candidate for this purpose. Utilizing MIL-101 is applicable only if a dehumidifier can be implemented in the system before this MOF.

7.2 Recommendation for Future Work

The importance of optimizing the performance of NTP-catalytic systems for air purifying applications has led researchers to employ DFA/Cs in these systems. Based on the course of the

presented research and its findings, the following aspects are recommended to be addressed before this technology can be applied to an indoor environment:

1. This study was conducted on a small scale plasma set-up for degradation of one (1) ppm of target VOC. Evaluating the performance of a full scale plasma set-up for the removal of VOCs in the range of concentration which exists in indoor environment (sub ppm) is a subject that needs further research.
2. Qualitative analysis of generated organic by-products and quantitative analysis of formed ozone were performed in this study. While formation of by-products is a crucial factor in employing any air cleaning system, more study is required on the amount of formed inorganic by-products (i.e. O₃, NO_x, CO), as well as other probable organic by-products.
3. The presence of a variety of VOCs in indoor environment brings a complexity in their oxidation mechanism, which may lead to formation of more unwanted by-products. Studying the VOCs' removal performance in the presence of a mixture of organic pollutants and the possible interference in their oxidation reaction pathways should be taken into account intensively.
4. In this research, experiments were performed at dry air (RH=0%) and in the presence of 30% RH. The impact of higher RH should be considered, especially for removal of VOCs in ppb levels, due to the coverage of the catalyst surface with water molecules, and limited access of the target pollutants to the catalyst.
5. The critical role of the catalyst to achieve a high removal performance in a plasma catalyst system opens a new field of study to develop novel DFA/Cs. This study demonstrated the excellent storage and oxidation capacity of MOFs as DFA/Cs. However, the negative effect of humidity on these materials should be improved using post-synthetic modification of MOFs.
6. Finally, in the context of energy optimization, a reactive adsorption plasma system is more capable of energy optimization than other plasma-based methods. Yet, a comprehensive study is needed to evaluate the energy cost when a MOF is utilized as a DFA/C in such system.

Bibliography

- [1] World Health Organization (WHO), “Burden of disease from the joint effects of Household and Ambient Air Pollution for 2012.” 2014.
- [2] F. Farrokhian and M. Bahri, “Study of the Effects of Climatic Parameters on the Pollutants CO, SO₂, NO_x, and O₃ through Regression Models,” *Bull. Env. Pharmacol. Life Sci*, vol. 4, pp. 139–145, 2014.
- [3] World Bank and Institute for Health Metrics and Evaluation, “The Cost of Air Pollution: Strengthening the Economic Case for Action.” Washington, DC: World Bank. License: Creative Commons Attribution CC BY 3.0 IGO, 2016.
- [4] X. Fan, T. L. Zhu, M. Y. Wang, and X. M. Li, “Removal of low-concentration BTX in air using a combined plasma catalysis system,” *Chemosphere*, vol. 75, no. 10, pp. 1301–1306, 2009.
- [5] D. Farhanian, F. Haghghat, C.-S. Lee, and N. Lakdawala, “Impact of Design Parameters on the Performance of Ultraviolet Photocatalytic Oxidation Air Cleaner,” *Building and Environment*, 2013.
- [6] F. I. Khan and A. Kr Ghoshal, “Removal of volatile organic compounds from polluted air,” *Journal of Loss Prevention in the Process Industries*, vol. 13, no. 6, pp. 527–545, 2000.
- [7] W. P. L. Carter, J. A. Pierce, D. Luo, and I. L. Malkina, “Environmental chamber study of maximum incremental reactivities of volatile organic compounds,” *Atmospheric Environment*, vol. 29, no. 18, pp. 2499–2511, 1995.
- [8] P. H. Fischer *et al.*, “Traffic-related differences in outdoor and indoor concentrations of particles and volatile organic compounds in Amsterdam,” *Atmospheric Environment*, vol. 34, no. 22, pp. 3713–3722, 2000.
- [9] H. Guo, S. C. Lee, L. Y. Chan, and W. M. Li, “Risk assessment of exposure to volatile organic compounds in different indoor environments,” *Environmental Research*, vol. 94, no. 1, pp. 57–66, 2004.
- [10] Y. Zhao, S. Wang, K. Aunan, H. Martin Seip, and J. Hao, “Air pollution and lung cancer risks in China—a meta-analysis,” *Science of the total environment*, vol. 366, no. 2, pp. 500–513, 2006.

- [11] L. Mølhave, B. Bach, and O. F. Pedersen, "Human reactions to low concentrations of volatile organic compounds," *Environment International*, vol. 12, no. 1, pp. 167–175, 1986.
- [12] D. W. VanOsdell, M. K. Owen, L. B. Jaffe, and L. E. Sparks, "VOC removal at low contaminant concentrations using granular activated carbon," *Journal of the Air & Waste Management Association*, vol. 46, no. 9, pp. 883–890, 1996.
- [13] L. Zhong, F. Haghghat, P. Blondeau, and J. Kozinski, "Modeling and physical interpretation of photocatalytic oxidation efficiency in indoor air applications," *Building and Environment*, vol. 45, no. 12, pp. 2689–2697, 2010.
- [14] F. Haghghat, C. S. Lee, B. Pant, G. Bolourani, N. Lakdawala, and A. Bastani, "Evaluation of various activated carbons for air cleaning—Towards design of immune and sustainable buildings," *Atmospheric Environment*, vol. 42, no. 35, pp. 8176–8184, 2008.
- [15] A. Bastani, C. S. Lee, F. Haghghat, C. Flaherty, and N. Lakdawala, "Assessing the performance of air cleaning devices—A full-scale test method," *Building and Environment*, vol. 45, no. 1, pp. 143–149, 2010.
- [16] X. S. Zhao, Q. Ma, and G. (Max) Lu, "VOC removal: comparison of MCM-41 with hydrophobic zeolites and activated carbon," *Energy & fuels*, vol. 12, no. 6, pp. 1051–1054, 1998.
- [17] J. Zhao and X. Yang, "Photocatalytic oxidation for indoor air purification: a literature review," *Building and Environment*, vol. 38, no. 5, pp. 645–654, 2003.
- [18] S. Wang, H. M. Ang, and M. O. Tade, "Volatile organic compounds in indoor environment and photocatalytic oxidation: State of the art," *Environment international*, vol. 33, no. 5, pp. 694–705, 2007.
- [19] J. Mo, Y. Zhang, Q. Xu, J. J. Lamson, and R. Zhao, "Photocatalytic purification of volatile organic compounds in indoor air: A literature review," *Atmospheric environment*, vol. 43, no. 14, pp. 2229–2246, 2009.
- [20] A. T. Hodgson, H. Destailats, D. P. Sullivan, and W. J. Fisk, "Performance of ultraviolet photocatalytic oxidation for indoor air cleaning applications," *Indoor air*, vol. 17, no. 4, pp. 305–316, 2007.
- [21] W. A. Jacoby *et al.*, "Heterogeneous photocatalysis for control of volatile organic compounds in indoor air," *Journal of the Air & Waste Management Association*, vol. 46, no. 9, pp. 891–898, 1996.

- [22] D. Farhanian and F. Haghghat, "Photocatalytic oxidation air cleaner: Identification and quantification of by-products," *Building and Environment*, vol. 72, pp. 34–43, 2014.
- [23] S. B. Kim and S. C. Hong, "Kinetic study for photocatalytic degradation of volatile organic compounds in air using thin film TiO₂ photocatalyst," *Applied Catalysis B: Environmental*, vol. 35, no. 4, pp. 305–315, 2002.
- [24] A. K. Boulamanti, C. A. Korologos, and C. J. Philippopoulos, "The rate of photocatalytic oxidation of aromatic volatile organic compounds in the gas-phase," *Atmospheric Environment*, vol. 42, no. 34, pp. 7844–7850, 2008.
- [25] F. Holzer, U. Roland, and F. D. Kopinke, "Combination of non-thermal plasma and heterogeneous catalysis for oxidation of volatile organic compounds: Part 1. Accessibility of the intra-particle volume," *Applied Catalysis B: Environmental*, vol. 38, no. 3, pp. 163–181, 2002.
- [26] W. Mista and R. Kacprzyk, "Decomposition of toluene using non-thermal plasma reactor at room temperature," *Catalysis Today*, vol. 137, no. 2, pp. 345–349, 2008.
- [27] U. Roland, F. Holzer, and F. D. Kopinke, "Combination of non-thermal plasma and heterogeneous catalysis for oxidation of volatile organic compounds: Part 2. Ozone decomposition and deactivation of γ -Al₂O₃," *Applied catalysis B: environmental*, vol. 58, no. 3, pp. 217–226, 2005.
- [28] Y. H. Song, S. J. Kim, K. I. Choi, and T. Yamamoto, "Effects of adsorption and temperature on a nonthermal plasma process for removing VOCs," *Journal of electrostatics*, vol. 55, no. 2, pp. 189–201, 2002.
- [29] M. Sharma, R. K. Vyas, and K. Singh, "A review on reactive adsorption for potential environmental applications," *Adsorption*, vol. 19, no. 1, pp. 161–188, 2013.
- [30] K. Inoue, H. Okano, Y. Yamagata, K. Muraoka, and Y. Teraoka, "Performance tests of newly developed adsorption/plasma combined system for decomposition of volatile organic compounds under continuous flow condition," *Journal of Environmental Sciences*, vol. 23, no. 1, pp. 139–144, 2011.
- [31] M. Magureanu, N. B. Mandache, P. Eloy, E. M. Gaigneaux, and V. I. Parvulescu, "Plasma-assisted catalysis for volatile organic compounds abatement," *Applied catalysis B: environmental*, vol. 61, no. 1, pp. 12–20, 2005.

- [32] J. Van Durme, J. Dewulf, K. Demeestere, C. Leys, and H. Van Langenhove, "Post-plasma catalytic technology for the removal of toluene from indoor air: Effect of humidity," *Applied Catalysis B: Environmental*, vol. 87, no. 1–2, pp. 78–83, 2009.
- [33] T. Zhu, J. Li, W. Liang, and Y. Jin, "Synergistic effect of catalyst for oxidation removal of toluene," *Journal of hazardous materials*, vol. 165, no. 1–3, pp. 1258–1260, 2009.
- [34] Z. Zhao, X. Li, and Z. Li, "Adsorption equilibrium and kinetics of p-xylene on chromium-based metal organic framework MIL-101," *Chemical Engineering Journal*, vol. 173, no. 1, pp. 150–157, 2011.
- [35] Z. Zhao, X. Li, S. Huang, Q. Xia, and Z. Li, "Adsorption and diffusion of benzene on chromium-based metal organic framework MIL-101 synthesized by microwave irradiation," *Industrial & Engineering Chemistry Research*, vol. 50, no. 4, pp. 2254–2261, 2011.
- [36] W.-G. Shim *et al.*, "Adsorption and thermodesorption characteristics of benzene in nanoporous metal organic framework MOF-5," *Advanced Powder Technology*, 2011.
- [37] K. M. Choi, K. Na, G. A. Somorjai, and O. M. Yaghi, "Chemical environment control and enhanced catalytic performance of platinum nanoparticles embedded in nanocrystalline metal–organic frameworks," *Journal of the American Chemical Society*, vol. 137, no. 24, pp. 7810–7816, 2015.
- [38] Y.-Z. Chen *et al.*, "A seed-mediated approach to the general and mild synthesis of non-noble metal nanoparticles stabilized by a metal–organic framework for highly efficient catalysis," *Materials Horizons*, vol. 2, no. 6, pp. 606–612, 2015.
- [39] F. Alvarez, K. Topudurti, M. Keefe, C. Petropoulou, and T. Schlichting, "Field Evaluation of High Voltage Electron Beam Technology for Treating VOC-Contaminated Groundwater Part I: VOC Removals and Treatment Costs," *JOURNAL OF ADVANCED OXIDATION TECHNOLOGIES*, vol. 3, pp. 98–106, 1998.
- [40] T. Oda, "Non-thermal plasma processing for environmental protection: decomposition of dilute VOCs in air," *Journal of Electrostatics*, vol. 57, no. 3, pp. 293–311, 2003.
- [41] T. Hammer, "Application of plasma technology in environmental techniques," *Contributions to Plasma Physics*, vol. 39, no. 5, pp. 441–462, 1999.

- [42] H. Kohno *et al.*, “Destruction of volatile organic compounds used in a semiconductor industry by a capillary tube discharge reactor,” *Industry Applications, IEEE Transactions on*, vol. 34, no. 5, pp. 953–966, 1998.
- [43] A. Fridman and L. A. Kennedy, *Plasma physics and engineering*, Second. CRC, 2011.
- [44] J. Heberlein and A. B. Murphy, “Thermal plasma waste treatment,” *Journal of Physics D: Applied Physics*, vol. 41, p. 053001, 2008.
- [45] J. Heberlein, “New approaches in thermal plasma technology,” *Pure and applied chemistry*, vol. 74, no. 3, pp. 327–336, 2002.
- [46] D. C. Schram, “The use of thermal plasmas for processing and relevance to environmental use,” *Proc. 8th Int. Conf. on Switching Arc Phenomena with satellite Int. Symp. on Electrical Technologies for Environmental Protection, Lodz, Poland*, pp. 135–142, 1997.
- [47] E. Pfender, “Thermal plasma technology: Where do we stand and where are we going?,” *Plasma Chemistry and Plasma Processing*, vol. 19, no. 1, pp. 1–31, 1999.
- [48] K. P. Francke, H. Miessner, and R. Rudolph, “Plasmacatalytic processes for environmental problems,” *Catalysis Today*, vol. 59, no. 3–4, pp. 411–416, 2000.
- [49] H. H. Kim, “Nonthermal Plasma Processing for Air-Pollution Control: A Historical Review, Current Issues, and Future Prospects,” *Plasma Processes and Polymers*, vol. 1, no. 2, pp. 91–110, 2004.
- [50] A. M. Vandenbroucke, R. Morent, N. De Geyter, and C. Leys, “Non-thermal plasmas for non-catalytic and catalytic VOC abatement,” *Journal of hazardous materials*, vol. 195, pp. 30–54, 2011.
- [51] K. Urashima and J. S. Chang, “Removal of volatile organic compounds from air streams and industrial flue gases by non-thermal plasma technology,” *Dielectrics and Electrical Insulation, IEEE Transactions on*, vol. 7, no. 5, pp. 602–614, 2000.
- [52] U. Kogelschatz, “Dielectric-barrier discharges: Their history, discharge physics, and industrial applications,” *Plasma chemistry and plasma processing*, vol. 23, no. 1, pp. 1–46, 2003.
- [53] J. O. Chae, V. Demidiouk, M. Yeulash, I. C. Choi, and T. G. Jung, “Experimental study for indoor air control by plasma-catalyst hybrid system,” *Plasma Science, IEEE Transactions on*, vol. 32, no. 2, pp. 493–497, 2004.

- [54] H. Ma, P. Chen, M. Zhang, X. Lin, and R. Ruan, "Study of SO₂ removal using non-thermal plasma induced by dielectric barrier discharge (DBD)," *Plasma Chemistry and Plasma Processing*, vol. 22, no. 2, pp. 239–254, 2002.
- [55] V. I. Gibalov and G. J. Pietsch, "The development of dielectric barrier discharges in gas gaps and on surfaces," *Journal of Physics D: Applied Physics*, vol. 33, p. 2618, 2000.
- [56] U. Kogelschatz, "Filamentary, patterned, and diffuse barrier discharges," *Plasma Science, IEEE Transactions on*, vol. 30, no. 4, pp. 1400–1408, 2002.
- [57] R. McAdams, "Prospects for non-thermal atmospheric plasmas for pollution abatement," *Journal of Physics D: Applied Physics*, vol. 34, p. 2810, 2001.
- [58] C. Wang and X. He, "Effect of atmospheric pressure dielectric barrier discharge air plasma on electrode surface," *Applied Surface Science*, vol. 253, no. 2, pp. 926–929, 2006.
- [59] W. Liang, J. Li, J. Li, and Y. Jin, "Abatement of toluene from gas streams via ferroelectric packed bed dielectric barrier discharge plasma," *Journal of hazardous materials*, vol. 170, no. 2, pp. 633–638, 2009.
- [60] A. Ogata, N. Shintani, K. Mizuno, S. Kushiya, and T. Yamamoto, "Decomposition of benzene using a nonthermal plasma reactor packed with ferroelectric pellets," *Industry Applications, IEEE Transactions on*, vol. 35, no. 4, pp. 753–759, 1999.
- [61] U. Roland, F. Holzer, and F. D. Kopinke, "Improved oxidation of air pollutants in a non-thermal plasma," *Catalysis Today*, vol. 73, no. 3–4, pp. 315–323, 2002.
- [62] B. Eliasson and U. Kogelschatz, "Nonequilibrium volume plasma chemical processing," *Plasma Science, IEEE Transactions on*, vol. 19, no. 6, pp. 1063–1077, 1991.
- [63] M. B. Chang and C. C. Chang, "Destruction and removal of toluene and MEK from gas streams with silent discharge plasmas," *AIChE journal*, vol. 43, no. 5, pp. 1325–1330, 1997.
- [64] Y. Wan, X. Fan, and T. Zhu, "Removal of low-concentration formaldehyde in air by DC corona discharge plasma," *Chemical Engineering Journal*, vol. 171, no. 1, pp. 314–319, 2011.
- [65] A. Mizuno *et al.*, "Indoor air cleaning using a pulsed discharge plasma," *Industry Applications, IEEE Transactions on*, vol. 35, no. 6, pp. 1284–1288, 1999.

- [66] Y. Liang *et al.*, “Rapid Inactivation of Biological Species in the Air using Atmospheric Pressure Nonthermal Plasma,” *Environmental science & technology*, vol. 46, no. 6, pp. 3360–3368, 2012.
- [67] G. Fridman *et al.*, “Comparison of Direct and Indirect Effects of Non-Thermal Atmospheric-Pressure Plasma on Bacteria,” *Plasma Processes and Polymers*, vol. 4, no. 4, pp. 370–375, 2007.
- [68] J. H. Park, J. H. Byeon, K. Y. Yoon, and J. Hwang, “Lab-scale test of a ventilation system including a dielectric barrier discharger and UV-photocatalyst filters for simultaneous removal of gaseous and particulate contaminants,” *Indoor air*, vol. 18, no. 1, pp. 44–50, 2008.
- [69] J. Van Durme, J. Dewulf, W. Sysmans, C. Leys, and H. Van Langenhove, “Efficient toluene abatement in indoor air by a plasma catalytic hybrid system,” *Applied Catalysis B: Environmental*, vol. 74, no. 1–2, pp. 161–169, 2007.
- [70] K. Urashima, J. S. Chang, and T. Ito, “Destruction of volatile organic compounds in air by a superimposed barrier discharge plasma reactor and activated carbon filter hybrid system,” presented at the Industry Applications Conference, Thirty-Second IAS Annual Meeting, IAS’97, New Orleans, US, 1997, vol. 3, pp. 1969–1974.
- [71] V. Demidiouk, S. I. Moon, and J. O. Chae, “Toluene and butyl acetate removal from air by plasma-catalytic system,” *Catalysis Communications*, vol. 4, no. 2, pp. 51–56, 2003.
- [72] M. Sugawara, G. Annadurai, and S. Futamura, “Reaction Behavior of Toluene–Dichloromethane Mixture in Nonthermal Plasma,” *Industry Applications, IEEE Transactions on*, vol. 45, no. 4, pp. 1499–1505, 2009.
- [73] H. Quoc An, T. Pham Huu, T. Le Van, J. M. Cormier, and A. Khacef, “Application of atmospheric non thermal plasma-catalysis hybrid system for air pollution control: Toluene removal,” *Catalysis Today*, vol. 176, no. 1, pp. 474–477, 2011.
- [74] S. Delagrangé, L. Pinard, and J.-M. Tatibouët, “Combination of a non-thermal plasma and a catalyst for toluene removal from air: Manganese based oxide catalysts,” *Applied Catalysis B: Environmental*, vol. 68, no. 3–4, pp. 92–98, 2006.
- [75] G. Yu-fang, Y. Dai-qi, T. Ya-feng, and C. Ke-fu, “Humidity effect on toluene decomposition in a wire-plate dielectric barrier discharge reactor,” *Plasma chemistry and plasma processing*, vol. 26, no. 3, pp. 237–249, 2006.

- [76] H. Wang, D. Li, Y. Wu, J. Li, and G. Li, "Removal of four kinds of volatile organic compounds mixture in air using silent discharge reactor driven by bipolar pulsed power," *Journal of electrostatics*, vol. 67, no. 4, pp. 547–553, 2009.
- [77] J. Van Durme, J. Dewulf, W. Sysmans, C. Leys, and H. Van Langenhove, "Abatement and degradation pathways of toluene in indoor air by positive corona discharge," *Chemosphere*, vol. 68, no. 10, pp. 1821–1829, 2007.
- [78] H. Einaga, T. Ibusuki, and S. Futamura, "Performance evaluation of a hybrid system comprising silent discharge plasma and manganese oxide catalysts for benzene decomposition," *Industry Applications, IEEE Transactions on*, vol. 37, no. 5, pp. 1476–1482, 2001.
- [79] V. Demidiouk and J. O. Chae, "Decomposition of volatile organic compounds in plasma-catalytic system," *Plasma Science, IEEE Transactions on*, vol. 33, no. 1, pp. 157–161, 2005.
- [80] A. E. Wallis, J. C. Whitehead, and K. Zhang, "The removal of dichloromethane from atmospheric pressure nitrogen gas streams using plasma-assisted catalysis," *Applied Catalysis B: Environmental*, vol. 74, no. 1–2, pp. 111–116, 2007.
- [81] H. L. Chen, H. M. Lee, S. H. Chen, M. B. Chang, S. J. Yu, and S. N. Li, "Removal of volatile organic compounds by single-stage and two-stage plasma catalysis systems: a review of the performance enhancement mechanisms, current status, and suitable applications," *Environmental science & technology*, vol. 43, no. 7, pp. 2216–2227, 2009.
- [82] H. H. Kim, A. Ogata, and S. Futamura, "Effect of different catalysts on the decomposition of VOCs using flow-type plasma-driven catalysis," *Plasma Science, IEEE Transactions on*, vol. 34, no. 3, pp. 984–995, 2006.
- [83] A. M. Harling, V. Demidyuk, S. J. Fischer, and J. C. Whitehead, "Plasma-catalysis destruction of aromatics for environmental clean-up: Effect of temperature and configuration," *Applied Catalysis B: Environmental*, vol. 82, no. 3, pp. 180–189, 2008.
- [84] X. Fan, T. Zhu, Y. Sun, and X. Yan, "The roles of various plasma species in the plasma and plasma-catalytic removal of low-concentration formaldehyde in air," *Journal of hazardous materials*, vol. 196, pp. 380–385, 2011.
- [85] V. I. Parvulescu, M. Magureanu, and P. Lukes, *Plasma Chemistry and Catalysis in Gases and Liquids*. John Wiley & Sons, 2012.

- [86] A. Rousseau, O. Guaitella, J. Röpcke, L. V. Gatilova, and Y. A. Tolmachev, "Combination of a pulsed microwave plasma with a catalyst for acetylene oxidation," *Applied Physics Letters*, vol. 85, no. 12, p. 2199, 2004.
- [87] D. Z. Zhao, X. S. Li, C. Shi, H. Y. Fan, and A. M. Zhu, "Low-concentration formaldehyde removal from air using a cycled storage–discharge (CSD) plasma catalytic process," *Chemical Engineering Science*, vol. 66, no. 17, pp. 3922–3929, 2011.
- [88] A. Ogata, H. Einaga, H. Kabashima, S. Futamura, S. Kushiya, and H. H. Kim, "Effective combination of nonthermal plasma and catalysts for decomposition of benzene in air," *Applied Catalysis B: Environmental*, vol. 46, no. 1, pp. 87–95, 2003.
- [89] A. Ogata, K. Yamanouchi, K. Mizuno, S. Kushiya, and T. Yamamoto, "Oxidation of dilute benzene in an alumina hybrid plasma reactor at atmospheric pressure," *Plasma chemistry and plasma processing*, vol. 19, no. 3, pp. 383–394, 1999.
- [90] S. M. Oh, H. H. Kim, A. Ogata, H. Einaga, S. Futamura, and D. W. Park, "Effect of zeolite in surface discharge plasma on the decomposition of toluene," *Catalysis letters*, vol. 99, no. 1, pp. 101–104, 2005.
- [91] T. Oda, K. Yamaji, and T. Takahashi, "Decomposition of dilute trichloroethylene by nonthermal plasma processing–gas flow rate, catalyst, and ozone effect," *Industry Applications, IEEE Transactions on*, vol. 40, no. 2, pp. 430–436, 2004.
- [92] H. B. Huang, D. Q. Ye, M. L. Fu, and F. D. Feng, "Contribution of UV light to the decomposition of toluene in dielectric barrier discharge plasma/photocatalysis system," *Plasma Chemistry and Plasma Processing*, vol. 27, no. 5, pp. 577–588, 2007.
- [93] H. Einaga and S. Futamura, "Catalytic oxidation of benzene with ozone over alumina-supported manganese oxides," *Journal of Catalysis*, vol. 227, no. 2, pp. 304–312, 2004.
- [94] H. Einaga and S. Futamura, "Oxidation behavior of cyclohexane on alumina-supported manganese oxides with ozone," *Applied Catalysis B: Environmental*, vol. 60, no. 1, pp. 49–55, 2005.
- [95] T. Hammer, T. Kappes, and M. Baldauf, "Plasma catalytic hybrid processes: gas discharge initiation and plasma activation of catalytic processes," *Catalysis today*, vol. 89, no. 1, pp. 5–14, 2004.

- [96] F. Holzer, U. Roland, and F. D. Kopinke, "Combination of non-thermal plasma and heterogeneous catalysis for oxidation of volatile organic compounds:: Part 1. Accessibility of the intra-particle volume," *Applied Catalysis B: Environmental*, vol. 38, no. 3, pp. 163–181, 2002.
- [97] J. Van Durme, J. Dewulf, C. Leys, and H. Van Langenhove, "Combining non-thermal plasma with heterogeneous catalysis in waste gas treatment: A review," *Applied Catalysis B: Environmental*, vol. 78, no. 3–4, pp. 324–333, 2008.
- [98] H. Einaga and S. Futamura, "Catalytic oxidation of benzene with ozone over Mn ion-exchanged zeolites," *Catalysis Communications*, vol. 8, no. 3, pp. 557–560, 2007.
- [99] H. L. Chen, H. M. Lee, S. H. Chen, Y. Chao, and M. B. Chang, "Review of plasma catalysis on hydrocarbon reforming for hydrogen production—Interaction, integration, and prospects," *Applied Catalysis B: Environmental*, vol. 85, no. 1, pp. 1–9, 2008.
- [100] Y. F. Guo, D. Q. Ye, K. F. Chen, J. C. He, and W. L. Chen, "Toluene decomposition using a wire-plate dielectric barrier discharge reactor with manganese oxide catalyst in situ," *Journal of Molecular Catalysis A: Chemical*, vol. 245, no. 1, pp. 93–100, 2006.
- [101] C. Liu *et al.*, "Plasma application for more environmentally friendly catalyst preparation," *Pure and applied chemistry*, vol. 78, no. 6, pp. 1227–1238, 2006.
- [102] D. Cheng and X. Zhu, "Reduction of Pd/HZSM-5 using oxygen glow discharge plasma for a highly durable catalyst preparation," *Catalysis Letters*, vol. 118, no. 3, pp. 260–263, 2007.
- [103] Y. Guo, D. Ye, K. Chen, and J. He, "Toluene removal by a DBD-type plasma combined with metal oxides catalysts supported by nickel foam," *Catalysis today*, vol. 126, no. 3–4, pp. 328–337, 2007.
- [104] C. Subrahmanyam, M. Magureanu, A. Renken, and L. Kiwi-Minsker, "Catalytic abatement of volatile organic compounds assisted by non-thermal plasma: Part 1. A novel dielectric barrier discharge reactor containing catalytic electrode," *Applied Catalysis B: Environmental*, vol. 65, no. 1, pp. 150–156, 2006.
- [105] A. E. Wallis, J. C. Whitehead, and K. Zhang, "The removal of dichloromethane from atmospheric pressure air streams using plasma-assisted catalysis," *Applied Catalysis B: Environmental*, vol. 72, no. 3, pp. 282–288, 2007.

- [106] S. Futamura, A. Zhang, H. Einaga, and H. Kabashima, "Involvement of catalyst materials in nonthermal plasma chemical processing of hazardous air pollutants," *Catalysis Today*, vol. 72, no. 3–4, pp. 259–265, 2002.
- [107] H. H. Kim, A. Ogata, and S. Futamura, "Oxygen partial pressure-dependent behavior of various catalysts for the total oxidation of VOCs using cycled system of adsorption and oxygen plasma," *Applied Catalysis B: Environmental*, vol. 79, no. 4, pp. 356–367, 2008.
- [108] M. Magureanu *et al.*, "In situ study of ozone and hybrid plasma Ag-Al catalysts for the oxidation of toluene: Evidence of the nature of the active sites," *Applied Catalysis B: Environmental*, vol. 104, no. 1–2, pp. 84–90, 2011.
- [109] A. Maciucă, C. Batiot-Dupeyrat, and J.-M. Tatibouët, "Synergetic effect by coupling photocatalysis with plasma for low VOCs concentration removal from air," *Applied Catalysis B: Environmental*, vol. Volume 125, pp. 432–438, 2012.
- [110] T. Sano, N. Negishi, E. Sakai, and S. Matsuzawa, "Contributions of photocatalytic/catalytic activities of TiO₂ and γ -Al₂O₃ in nonthermal plasma on oxidation of acetaldehyde and CO," *Journal of Molecular Catalysis A: Chemical*, vol. 245, no. 1, pp. 235–241, 2006.
- [111] H. Huang and D. Ye, "Combination of photocatalysis downstream the non-thermal plasma reactor for oxidation of gas-phase toluene," *Journal of hazardous materials*, vol. 171, no. 1, pp. 535–541, 2009.
- [112] S. Chavadej, K. Saktrakool, P. Rangsunvigit, L. L. Lobban, and T. Sreethawong, "Oxidation of ethylene by a multistage corona discharge system in the absence and presence of Pt/TiO₂," *Chemical engineering journal*, vol. 132, no. 1, pp. 345–353, 2007.
- [113] C. Ayrault *et al.*, "Oxidation of 2-heptanone in air by a DBD-type plasma generated within a honeycomb monolith supported Pt-based catalyst," *Catalysis today*, vol. 89, no. 1, pp. 75–81, 2004.
- [114] J. Karuppiah, L. Sivachandiran, R. Karvembu, and C. Subrahmanyam, "Catalytic nonthermal plasma reactor for the abatement of low concentrations of isopropanol," *Chemical Engineering Journal*, vol. 165, no. 1, pp. 194–199, 2010.
- [115] X. Fan, T. Zhu, Y. Wan, and X. Yan, "Effects of humidity on the plasma-catalytic removal of low-concentration BTX in air," *Journal of hazardous materials*, vol. 180, no. 1, pp. 616–621, 2010.

- [116] H.-H. Kim, S.-M. Oh, A. Ogata, and S. Futamura, "Decomposition of Gas-Phase Benzene Using Plasma Driven Catalyst Reactor: Complete Oxidation of Adsorbed Benzene Using Oxygen Plasma," *Journal of Advanced Oxidation Technologies*, vol. 8, no. 2, pp. 226–233, 2005.
- [117] H. Y. Fan, C. Shi, X. S. Li, D. Z. Zhao, Y. Xu, and A. M. Zhu, "High-efficiency plasma catalytic removal of dilute benzene from air," *Journal of Physics D: Applied Physics*, vol. 42, no. 22, p. 225105, 2009.
- [118] C. Shi, B. Chen, X. Li, M. Crocker, Y. Wang, and A. Zhu, "Catalytic formaldehyde removal by 'storage-oxidation' cycling process over supported silver catalysts," *Chemical Engineering Journal*, vol. 200–202, pp. 729–737, 2012.
- [119] Y.-H. Chu *et al.*, "Preparation of mesoporous silica fiber matrix for VOC removal," *Catalysis today*, vol. 74, no. 3, pp. 249–256, 2002.
- [120] H. Y. Fan *et al.*, "Plasma Catalytic Oxidation of Stored Benzene in a Cycled Storage-Discharge (CSD) Process: Catalysts, Reactors and Operation Conditions," *Plasma Chemistry and Plasma Processing*, vol. 31, no. 6, pp. 799–810, 2011.
- [121] D. Das, V. Gaur, and N. Verma, "Removal of volatile organic compound by activated carbon fiber," *Carbon*, vol. 42, no. 14, pp. 2949–2962, 2004.
- [122] D. Britt, D. Tranchemontagne, and O. M. Yaghi, "Metal-organic frameworks with high capacity and selectivity for harmful gases," *Proceedings of the National Academy of Sciences*, vol. 105, no. 33, pp. 11623–11627, 2008.
- [123] M. T. Luebbbers, T. Wu, L. Shen, and R. I. Masel, "Trends in the Adsorption of Volatile Organic Compounds in a Large-Pore Metal-Organic Framework, IRMOF-1," *Langmuir*, vol. 26, no. 13, pp. 11319–11329, 2010.
- [124] H. Qu *et al.*, "Structures and photocatalytic activities of metal-organic frameworks derived from rigid aromatic dicarboxylate acids and flexible imidazole-based linkers," *Inorganic Chemistry Communications*, vol. 14, no. 9, pp. 1347–1351, 2011.
- [125] S. Galli *et al.*, "Adsorption of harmful organic vapors by flexible hydrophobic bis-pyrazolate based MOFs," *Chemistry of Materials*, vol. 22, no. 5, pp. 1664–1672, 2010.
- [126] P. Lama, A. Aijaz, S. Neogi, L. J. Barbour, and P. K. Bharadwaj, "Microporous La (III) Metal-Organic Framework Using a Semirigid Tricarboxylic Ligand: Synthesis, Single-Crystal to Single-Crystal Sorption Properties, and Gas Adsorption Studies," *Crystal Growth & Design*, vol. 10, no. 8, pp. 3410–3417, 2010.

- [127] J. Juan-Alcañiz, J. Gascon, and F. Kapteijn, "Metal–organic frameworks as scaffolds for the encapsulation of active species: state of the art and future perspectives," *Journal of Materials Chemistry*, vol. 22, no. 20, pp. 10102–10118, 2012.
- [128] A. A. Adeyemo, I. O. Adeoye, and O. S. Bello, "Metal organic frameworks as adsorbents for dye adsorption: overview, prospects and future challenges," *Toxicological & Environmental Chemistry*, vol. 94, no. 10, pp. 1846–1863, 2012.
- [129] R. Sabouni, H. Kazemian, and S. Rohani, "Microwave Synthesis of the CPM-5 Metal Organic Framework," *Chemical Engineering & Technology*, vol. 35, no. 6, pp. 1085–1092, 2012.
- [130] Y. Liu, Z. Ng, E. A. Khan, H.-K. Jeong, C. Ching, and Z. Lai, "Synthesis of continuous MOF-5 membranes on porous α -alumina substrates," *Microporous and Mesoporous Materials*, vol. 118, no. 1, pp. 296–301, 2009.
- [131] J. Lee, O. K. Farha, J. Roberts, K. A. Scheidt, S. T. Nguyen, and J. T. Hupp, "Metal–organic framework materials as catalysts," *Chemical Society Reviews*, vol. 38, no. 5, pp. 1450–1459, 2009.
- [132] A. Dhakshinamoorthy, M. Alvaro, and H. Garcia, "Commercial metal–organic frameworks as heterogeneous catalysts," *Chemical Communications*, vol. 48, no. 92, pp. 11275–11288, 2012.
- [133] L. Alaerts, M. Maes, P. A. Jacobs, J. F. Denayer, and D. E. De Vos, "Activation of the metal–organic framework MIL-47 for selective adsorption of xylenes and other difunctionalized aromatics," *Physical Chemistry Chemical Physics*, vol. 10, no. 20, pp. 2979–2985, 2008.
- [134] J. Gascon, U. Aktay, M. D. Hernandez-Alonso, G. P. van Klink, and F. Kapteijn, "Amino-based metal-organic frameworks as stable, highly active basic catalysts," *Journal of Catalysis*, vol. 261, no. 1, pp. 75–87, 2009.
- [135] T. Ahnfeldt *et al.*, "Synthesis and modification of a functionalized 3D open-framework structure with MIL-53 topology," *Inorganic chemistry*, vol. 48, no. 7, pp. 3057–3064, 2009.
- [136] S. Natarajan and P. Mahata, "Non-carboxylate based metal-organic frameworks (MOFs) and related aspects," *Current Opinion in Solid State and Materials Science*, vol. 13, no. 3, pp. 46–53, 2009.

- [137] C. N. R. Rao, J. N. Behera, and M. Dan, "Organically-templated metal sulfates, selenites and selenates," *Chemical Society Reviews*, vol. 35, no. 4, pp. 375–387, 2006.
- [138] J. H. Cavka *et al.*, "A new zirconium inorganic building brick forming metal organic frameworks with exceptional stability," *Journal of the American Chemical Society*, vol. 130, no. 42, pp. 13850–13851, 2008.
- [139] N. A. Khan, I. J. Kang, H. Y. Seok, and S. H. Jung, "Facile synthesis of nano-sized metal-organic frameworks, chromium-benzenedicarboxylate, MIL-101," *Chemical Engineering Journal*, vol. 166, no. 3, pp. 1152–1157, 2011.
- [140] L. Hamon *et al.*, "Comparative study of hydrogen sulfide adsorption in the Mil-53 (Al, Cr, Fe), MIL-47 (V), MIL-100 (Cr), and MIL-101 (Cr) metal-organic frameworks at room temperature," *Journal of the American Chemical Society*, vol. 131, no. 25, pp. 8775–8777, 2009.
- [141] R. Sabouni, H. Kazemian, and S. Rohani, "Carbon Dioxide Adsorption in Microwave-Synthesized Metal Organic Framework CPM-5: Equilibrium and Kinetics study," *Microporous and Mesoporous Materials*, 2013.
- [142] J. L. Rowsell, E. C. Spencer, J. Eckert, J. A. Howard, and O. M. Yaghi, "Gas adsorption sites in a large-pore metal-organic framework," *Science*, vol. 309, no. 5739, pp. 1350–1354, 2005.
- [143] S. Amirjalayer and R. Schmid, "Adsorption of Hydrocarbons in Metal–Organic Frameworks: A Force Field Benchmark on the Example of Benzene in Metal–Organic Framework 5," *The Journal of Physical Chemistry C*, vol. 116, no. 29, pp. 15369–15377, 2012.
- [144] J. Gordon, H. Kazemian, and S. Rohani, "Rapid and efficient crystallization of MIL-53 (Fe) by ultrasound and microwave irradiation," *Microporous and Mesoporous Materials*, 2012.
- [145] J. R. Choi, T. Tachikawa, M. Fujitsuka, and T. Majima, "Europium-Based Metal–Organic Framework as a Photocatalyst for the One-Electron Oxidation of Organic Compounds," *Langmuir*, vol. 26, no. 13, pp. 10437–10443, 2010.
- [146] S.-T. Zheng *et al.*, "Pore Space Partition and Charge Separation in Cage-within-Cage Indium-Organic Frameworks with High CO₂ Uptake," *Journal of the American Chemical Society*, vol. 132, no. 48, pp. 17062–17064, 2010.

- [147] D. Farrusseng, S. Aguado, and C. Pinel, "Metal–organic frameworks: opportunities for catalysis," *Angewandte Chemie International Edition*, vol. 48, no. 41, pp. 7502–7513, 2009.
- [148] S. Bourrelly, P. L. Llewellyn, C. Serre, F. Millange, T. Loiseau, and G. Férey, "Different adsorption behaviors of methane and carbon dioxide in the isotypic nanoporous metal terephthalates MIL-53 and MIL-47," *Journal of the American Chemical Society*, vol. 127, no. 39, pp. 13519–13521, 2005.
- [149] G. Férey *et al.*, "A chromium terephthalate-based solid with unusually large pore volumes and surface area," *Science*, vol. 309, no. 5743, pp. 2040–2042, 2005.
- [150] L. Bromberg, Y. Diao, H. Wu, S. A. Speakman, and T. A. Hatton, "Chromium (III) Terephthalate Metal Organic Framework (MIL-101): HF-Free Synthesis, Structure, Polyoxometalate Composites, and Catalytic Properties," *Chemistry of Materials*, vol. 24, no. 9, pp. 1664–1675, 2012.
- [151] C.-Y. Huang, M. Song, Z.-Y. Gu, H.-F. Wang, and X.-P. Yan, "Probing the Adsorption Characteristic of Metal–Organic Framework MIL-101 for Volatile Organic Compounds by Quartz Crystal Microbalance," *Environmental science & technology*, vol. 45, no. 10, pp. 4490–4496, 2011.
- [152] A. U. Czaja, N. Trukhan, and U. Müller, "Industrial applications of metal–organic frameworks," *Chemical Society Reviews*, vol. 38, no. 5, pp. 1284–1293, 2009.
- [153] D. Peralta, G. Chaplais, A. Simon-Masseron, K. Barthelet, and G. D. Pirngruber, "Synthesis and adsorption properties of ZIF-76 isomorphs," *Microporous and Mesoporous Materials*, vol. 153, pp. 1–7, 2012.
- [154] A. Corma, H. Garcia, and F. X. Llabrés i Xamena, "Engineering metal organic frameworks for heterogeneous catalysis," *Chemical reviews*, vol. 110, no. 8, pp. 4606–4655, 2010.
- [155] L. Alaerts, E. Séguin, H. Poelman, F. Thibault-Starzyk, P. A. Jacobs, and D. E. De Vos, "Probing the Lewis Acidity and Catalytic Activity of the Metal–Organic Framework [Cu₃ (btc)₂](BTC= Benzene-1, 3, 5-tricarboxylate)," *Chemistry-A European Journal*, vol. 12, no. 28, pp. 7353–7363, 2006.
- [156] P. Mahata, G. Madras, and S. Natarajan, "Novel photocatalysts for the decomposition of organic dyes based on metal-organic framework compounds," *The Journal of Physical Chemistry B*, vol. 110, no. 28, pp. 13759–13768, 2006.

- [157] H.-L. Jiang, B. Liu, T. Akita, M. Haruta, H. Sakurai, and Q. Xu, "Au@ ZIF-8: CO oxidation over gold nanoparticles deposited to metal-organic framework," *Journal of the American Chemical Society*, vol. 131, no. 32, pp. 11302–11303, 2009.
- [158] Y.-S. Li, H. Bux, A. Feldhoff, G.-L. Li, W.-S. Yang, and J. Caro, "Controllable synthesis of metal–organic frameworks: From MOF nanorods to oriented MOF membranes," *Advanced Materials*, vol. 22, no. 30, pp. 3322–3326, 2010.
- [159] S. Aguado, J. Canivet, and D. Farrusseng, "Facile shaping of an imidazolate-based MOF on ceramic beads for adsorption and catalytic applications," *Chemical Communications*, vol. 46, no. 42, pp. 7999–8001, 2010.
- [160] M. Bahri and F. Haghghat, "Plasma-Based Indoor Air Cleaning Technologies: The State of the Art-Review," *CLEAN–Soil, Air, Water*, vol. 42, no. 12, pp. 1667–1680, 2014.
- [161] S. Sultana, A. M. Vandenbroucke, C. Leys, N. De Geyter, and R. Morent, "Abatement of VOCs with Alternate Adsorption and Plasma-Assisted Regeneration: A Review," *Catalysts*, vol. 5, no. 2, pp. 718–746, 2015.
- [162] M. Bahri and F. Haghghat, "Plasma Based Methods, New Air Cleaner Technologies for VOCs Removal in Non-Industrial Buildings."
- [163] A. Chirokov, A. Gutsol, and A. Fridman, "Atmospheric pressure plasma of dielectric barrier discharges," *Pure and applied chemistry*, vol. 77, no. 2, pp. 487–495, 2005.
- [164] T. N. Das and G. R. Dey, "Cold Plasma: simple tool for convenient utilitarian chemistry in homogeneous and heterogeneous environments," Bhabha Atomic Research Centre, 2015.
- [165] E. Giovanis, "Evaluation of the 'Clean Air Works' program on actual ozone concentrations: a case study in North Carolina," *International Journal of Environmental Technology and Management*, vol. 18, no. 5–6, pp. 465–477, 2015.
- [166] Z. Qian *et al.*, "Ambient air pollution and preterm birth: a prospective birth cohort study in Wuhan, China," *International Journal of Hygiene and Environmental Health*, 2015.
- [167] A. W. Reitze Jr, "The National Ambient Air Quality Standards for Ozone," *Ariz. J. Env'tl. L. & Pol'y*, vol. 6, pp. 421–421, 2015.
- [168] "Residential Indoor Air Quality Guidelines," 22-Dec-2015. [Online]. Available: <http://healthycanadians.gc.ca/healthy-living-vie-saine/environnement-environnement/air/guidelines-lignes-directrices-eng.php>.

- [169] M. A. Lieberman and A. J. Lichtenberg, "Principles of plasma discharges and materials processing," *MRS Bulletin*, vol. 30, pp. 899–901, 1994.
- [170] H.-H. Kim, S.-M. Oh, A. Ogata, and S. Futamura, "Decomposition of benzene using Ag/TiO₂ packed plasma-driven catalyst reactor: influence of electrode configuration and Ag-loading amount," *Catalysis letters*, vol. 96, no. 3–4, pp. 189–194, 2004.
- [171] K. G. Kostov, R. Y. Honda, L. M. S. Alves, and M. E. Kayama, "Characteristics of dielectric barrier discharge reactor for material treatment," *Brazilian Journal of Physics*, vol. 39, no. 2, pp. 322–325, 2009.
- [172] B. Li, M. Chrzanowski, Y. Zhang, and S. Ma, "Applications of Metal-Organic Frameworks Featuring multi-Functional Sites," *Coordination Chemistry Reviews*, 2015.
- [173] Z. Dou *et al.*, "Luminescent Metal-Organic Framework Films as Highly Sensitive and Fast-Response Oxygen Sensors," *Journal of the American Chemical Society*, 2014.
- [174] D. J. Wales *et al.*, "Gas sensing using porous materials for automotive applications," *Chemical Society Reviews*, 2015.
- [175] K. Fujii *et al.*, "Direct structure elucidation by powder X-ray diffraction of a metal-organic framework material prepared by solvent-free grinding," *Chemical Communications*, vol. 46, no. 40, pp. 7572–7574, 2010.
- [176] K. Müller-Buschbaum and Y. Mokaddem, "MOFs by solvent free high temperature synthesis exemplified by $3 \infty [\text{Eu}_3(\text{Tz}^*)_6(\text{Tz}^*\text{H})_2]$," *Solid State Sciences*, vol. 10, no. 4, pp. 416–420, 2008.
- [177] E. Pérez-Mayoral, R. M. Martín-Aranda, A. J. López-Peinado, P. Ballesteros, A. Zukal, and J. Čejka, "Green synthesis of acetals/ketals: Efficient solvent-free process for the carbonyl/hydroxyl group protection catalyzed by SBA-15 materials," *Topics in Catalysis*, vol. 52, no. 1–2, pp. 148–152, 2009.
- [178] A. Pichon, A. Lazuen-Garay, and S. L. James, "Solvent-free synthesis of a microporous metal-organic framework," *CrystEngComm*, vol. 8, no. 3, pp. 211–214, 2006.
- [179] A. L. Garay, A. Pichon, and S. L. James, "Solvent-free synthesis of metal complexes," *Chemical Society Reviews*, vol. 36, no. 6, pp. 846–855, 2007.

- [180] T. Friščić *et al.*, “Real-time and in situ monitoring of mechanochemical milling reactions,” *Nature chemistry*, vol. 5, no. 1, pp. 66–73, 2013.
- [181] K. D. Harris, “Mechanochemical synthesis: How grinding evolves,” *Nature chemistry*, vol. 5, no. 1, pp. 12–14, 2013.
- [182] N. K. Singh, M. Hardi, and V. P. Balema, “Mechanochemical synthesis of an yttrium based metal–organic framework,” *Chemical Communications*, vol. 49, no. 10, pp. 972–974, 2013.
- [183] Y. Sun and H.-C. Zhou, “Recent progress in the synthesis of metal–organic frameworks,” *Science and Technology of Advanced Materials*, vol. 16, no. 5, p. 054202, 2015.
- [184] S. L. James *et al.*, “Mechanochemistry: opportunities for new and cleaner synthesis,” *Chemical Society Reviews*, vol. 41, no. 1, pp. 413–447, 2012.
- [185] T.-X. Métro, J. Bonnamour, T. Reidon, J. Sarpoulet, J. Martinez, and F. Lamaty, “Mechanosynthesis of amides in the total absence of organic solvent from reaction to product recovery,” *Chemical Communications*, vol. 48, no. 96, pp. 11781–11783, 2012.
- [186] S. Tanaka, K. Kida, T. Nagaoka, T. Ota, and Y. Miyake, “Mechanochemical dry conversion of zinc oxide to zeolitic imidazolate framework,” *Chemical Communications*, vol. 49, no. 72, pp. 7884–7886, 2013.
- [187] F. Haghghat and L. De Bellis, “Material emission rates: literature review, and the impact of indoor air temperature and relative humidity,” *Building and Environment*, vol. 33, no. 5, pp. 261–277, 1998.
- [188] A.-L. Tiffonnet, P. Blondeau, F. Allard, and F. Haghghat, “Sorption isotherms of acetone on various building materials,” *Indoor and Built Environment*, vol. 11, no. 2, pp. 95–104, 2002.
- [189] G. Wieslander, D. Norbäck, E. Björnsson, C. Janson, and G. Boman, “Asthma and the indoor environment: the significance of emission of formaldehyde and volatile organic compounds from newly painted indoor surfaces,” *International archives of occupational and environmental health*, vol. 69, no. 2, pp. 115–124, 1996.
- [190] Y. Bai, Z.-H. Huang, and F. Kang, “Synthesis of reduced graphene oxide/phenolic resin-based carbon composite ultrafine fibers and their adsorption performance for volatile organic compounds and water,” *Journal of Materials Chemistry A*, vol. 1, no. 33, pp. 9536–9543, 2013.

- [191] Y. Bai, Z.-H. Huang, and F. Kang, "Electrospun preparation of microporous carbon ultrafine fibers with tuned diameter, pore structure and hydrophobicity from phenolic resin," *Carbon*, vol. 66, pp. 705–712, 2014.
- [192] M. Bahri, F. Haghghat, S. Rohani, and H. Kazemian, "Impact of design parameters on the performance of non-thermal plasma air purification system," *Chemical Engineering Journal*, vol. 302, pp. 204–212, 2016.
- [193] A. Stankiewicz, "Reactive separations for process intensification: an industrial perspective," *Chemical Engineering and Processing: Process Intensification*, vol. 42, no. 3, pp. 137–144, 2003.
- [194] J. Richards, *Control of gaseous emissions: Student manual, APTI Course 415*. North Carolina State University, 1995.
- [195] M. Delkash, B. E. Bakhshayesh, and H. Kazemian, "Using zeolitic adsorbents to cleanup special wastewater streams: A review," *Microporous and Mesoporous Materials*, vol. 214, pp. 224–241, 2015.
- [196] Z. G. L. V. Sari, H. Younesi, and H. Kazemian, "Synthesis of nanosized ZSM-5 zeolite using extracted silica from rice husk without adding any alumina source," *Applied Nanoscience*, vol. 5, no. 6, pp. 737–745, 2015.
- [197] S. I. Garcés-Polo, J. Villarroel-Rocha, K. Sapag, S. A. Korili, and A. Gil, "A comparative study of CO₂ diffusion from adsorption kinetic measurements on microporous materials at low pressures and temperatures," *Chemical Engineering Journal*, vol. 302, pp. 278–286, 2016.
- [198] C.-C. Wang, X.-D. Du, J. Li, X.-X. Guo, P. Wang, and J. Zhang, "Photocatalytic Cr(VI) reduction in metal-organic frameworks: A mini-review," *Applied Catalysis B: Environmental*, vol. 193, pp. 198–216, 2016.
- [199] L. Qin, Z. Li, Z. Xu, X. Guo, and G. Zhang, "Organic-acid-directed assembly of iron-carbon oxides nanoparticles on coordinatively unsaturated metal sites of MIL-101 for green photochemical oxidation," *Applied Catalysis B: Environmental*, vol. 179, pp. 500–508, 2015.
- [200] N. Klein, A. Henschel, and S. Kaskel, "n-Butane adsorption on Cu₃(btc)₂ and MIL-101," *Microporous and Mesoporous Materials*, vol. 129, no. 1, pp. 238–242, 2010.
- [201] J. Shi, Z. Zhao, Q. Xia, Y. Li, and Z. Li, "Adsorption and diffusion of ethyl acetate on the chromium-based metal-organic framework MIL-101," *Journal of Chemical & Engineering Data*, vol. 56, no. 8, pp. 3419–3425, 2011.

- [202] S. Xian *et al.*, “Competitive adsorption of water vapor with VOCs dichloroethane, ethyl acetate and benzene on MIL-101 (Cr) in humid atmosphere,” *RSC Advances*, vol. 5, no. 3, pp. 1827–1834, 2015.
- [203] P. Küsgens *et al.*, “Characterization of metal-organic frameworks by water adsorption,” *Microporous and Mesoporous Materials*, vol. 120, no. 3, pp. 325–330, 2009.
- [204] Z. Zhao, S. Wang, Y. Yang, X. Li, J. Li, and Z. Li, “Competitive adsorption and selectivity of benzene and water vapor on the microporous metal organic frameworks (HKUST-1),” *Chemical Engineering Journal*, vol. 259, pp. 79–89, 2015.
- [205] N. Al-Janabi *et al.*, “Mapping the Cu-BTC metal–organic framework (HKUST-1) stability envelope in the presence of water vapour for CO₂ adsorption from flue gases,” *Chemical Engineering Journal*, vol. 281, pp. 669–677, 2015.
- [206] P. Horcajada *et al.*, “Flexible porous metal-organic frameworks for a controlled drug delivery,” *Journal of the American Chemical Society*, vol. 130, no. 21, pp. 6774–6780, 2008.
- [207] C. Serre, C. Mellot-Draznieks, S. Surblé, N. Audebrand, Y. Filinchuk, and G. Férey, “Role of solvent-host interactions that lead to very large swelling of hybrid frameworks,” *Science*, vol. 315, no. 5820, pp. 1828–1831, 2007.
- [208] K. Yang, Q. Sun, F. Xue, and D. Lin, “Adsorption of volatile organic compounds by metal–organic frameworks MIL-101: Influence of molecular size and shape,” *Journal of hazardous materials*, vol. 195, pp. 124–131, 2011.
- [209] J. Tang, M. Yang, M. Yang, J. Wang, W. Dong, and G. Wang, “Heterogeneous Fe-MIL-101 catalysts for efficient one-pot four-component coupling synthesis of highly substituted pyrroles,” *New Journal of Chemistry*, vol. 39, no. 6, pp. 4919–4923, 2015.
- [210] L. H. Wee, F. Bonino, C. Lamberti, S. Bordiga, and J. A. Martens, “Cr-MIL-101 encapsulated Keggin phosphotungstic acid as active nanomaterial for catalysing the alcoholysis of styrene oxide,” *Green Chemistry*, vol. 16, no. 3, pp. 1351–1357, 2014.
- [211] S. Brunauer, L. S. Deming, W. E. Deming, and E. Teller, “On a theory of the van der Waals adsorption of gases,” *Journal of the American Chemical Society*, vol. 62, no. 7, pp. 1723–1732, 1940.

- [212] A. J. Fletcher, K. M. Thomas, and M. J. Rosseinsky, “Flexibility in metal-organic framework materials: Impact on sorption properties,” *Journal of Solid State Chemistry*, vol. 178, no. 8, pp. 2491–2510, 2005.
- [213] W. Xuan, C. Zhu, Y. Liu, and Y. Cui, “Mesoporous metal–organic framework materials,” *Chemical Society Reviews*, vol. 41, no. 5, pp. 1677–1695, 2012.
- [214] D. Romero *et al.*, “Removal of toluene over NaX zeolite exchanged with Cu²⁺,” *Catalysts*, vol. 5, no. 3, pp. 1479–1497, 2015.
- [215] F. Millange, C. Serre, and G. Férey, “Synthesis, structure determination and properties of MIL-53as and MIL-53ht: the first Cr iii hybrid inorganic–organic microporous solids: Cr iii (OH)· $\frac{1}{2}$ C₆H₄–CO₂· $\frac{1}{2}$ C₆H₄–CO₂ H₂O,” *Chemical Communications*, no. 8, pp. 822–823, 2002.
- [216] P. L. Llewellyn *et al.*, “Complex adsorption of short linear alkanes in the flexible metal-organic-framework MIL-53 (Fe),” *Journal of the American Chemical Society*, vol. 131, no. 36, pp. 13002–13008, 2009.
- [217] L. Song *et al.*, “Mesoporous metal–organic frameworks: design and applications,” *Energy & Environmental Science*, vol. 5, no. 6, pp. 7508–7520, 2012.
- [218] T. K. Trung *et al.*, “Adsorption of C₅–C₉ hydrocarbons in microporous MOFs MIL-100 (Cr) and MIL-101 (Cr): A manometric study,” *Microporous and Mesoporous Materials*, vol. 134, no. 1, pp. 134–140, 2010.
- [219] S. H. Jhung, J.-H. Lee, J. W. Yoon, C. Serre, G. Férey, and J.-S. Chang, “Microwave Synthesis of Chromium Terephthalate MIL-101 and Its Benzene Sorption Ability,” *Advanced Materials*, vol. 19, no. 1, pp. 121–124, 2007.
- [220] J. Van Durme, J. Dewulf, C. Leys, and H. Van Langenhove, “Combining non-thermal plasma with heterogeneous catalysis in waste gas treatment: A review,” *Applied Catalysis B: Environmental*, vol. 78, no. 3–4, pp. 324–333, 2008.
- [221] A. M. Vandembroucke *et al.*, “TCE abatement with a plasma-catalytic combined system using MnO₂ as catalyst,” *Applied Catalysis B: Environmental*, vol. 156, pp. 94–100, 2014.
- [222] H.-H. Kim, A. Ogata, and S. Futamura, “Atmospheric plasma-driven catalysis for the low temperature decomposition of dilute aromatic compounds,” *Journal of Physics D: Applied Physics*, vol. 38, no. 8, p. 1292, 2005.

- [223] R. Huang *et al.*, “Enhancement of the non-thermal plasma-catalytic system with different zeolites for toluene removal,” *RSC Advances*, vol. 5, no. 88, pp. 72113–72120, 2015.
- [224] S. W. Baek, J. R. Kim, and S. K. Ihm, “Design of dual functional adsorbent/catalyst system for the control of VOC’s by using metal-loaded hydrophobic Y-zeolites,” *Catalysis Today*, vol. 93, pp. 575–581, 2004.
- [225] B. Dou, Q. Hu, J. Li, S. Qiao, and Z. Hao, “Adsorption performance of VOCs in ordered mesoporous silicas with different pore structures and surface chemistry,” *Journal of hazardous materials*, vol. 186, no. 2, pp. 1615–1624, 2011.
- [226] J. Fang, X. Chen, Q. Xia, H. Xi, and Z. Li, “Effect of Relative Humidity on Catalytic Combustion of Toluene over Copper Based Catalysts with Different Supports,” *Chinese Journal of Chemical Engineering*, vol. 17, no. 5, pp. 767–772, 2009.
- [227] Q. H. Trinh and Y. S. Mok, “Effect of the adsorbent/catalyst preparation method and plasma reactor configuration on the removal of dilute ethylene from air stream,” *Catalysis Today*, 2015.
- [228] M. Bahri, H. Kazemian, S. Rohani, and F. Haghghat, “Mechanochemical synthesis of CPM-5: A Green Method,” *Chemical Engineering & Technology*, 2016.
- [229] Y. Hu, H. Kazemian, S. Rohani, Y. Huang, and Y. Song, “In situ high pressure study of ZIF-8 by FTIR spectroscopy,” *Chemical Communications*, vol. 47, no. 47, pp. 12694–12696, 2011.
- [230] H.-L. Jiang *et al.*, “From Metal–Organic Framework to Nanoporous Carbon: Toward a Very High Surface Area and Hydrogen Uptake,” *Journal of the American Chemical Society*, vol. 133, no. 31, pp. 11854–11857, 2011.
- [231] M. Bahri, F. Haghghat, H. Kazemian, and S. Rohani, “A Comparative Study on Metal Organic Frameworks for Indoor Environment Application: Adsorption Evaluation.” *Chemical Engineering Journal*, Jul-2016.
- [232] W. Wang, H. Wang, T. Zhu, and X. Fan, “Removal of gas phase low-concentration toluene over Mn, Ag and Ce modified HZSM-5 catalysts by periodical operation of adsorption and non-thermal plasma regeneration,” *Journal of hazardous materials*, vol. 292, pp. 70–78, 2015.
- [233] T. A. Vu *et al.*, “Arsenic removal from aqueous solutions by adsorption using novel MIL-53 (Fe) as a highly efficient adsorbent,” *RSC Advances*, vol. 5, no. 7, pp. 5261–5268, 2015.

- [234] J. Karuppiah, R. Karvembu, and C. Subrahmanyam, "The catalytic effect of MnO_x and CoO_x on the decomposition of nitrobenzene in a non-thermal plasma reactor," *Chemical Engineering Journal*, vol. 180, pp. 39–45, 2012.
- [235] B. R. Raju, E. L. Reddy, J. Karuppiah, P. M. K. Reddy, and C. Subrahmanyam, "Catalytic non-thermal plasma reactor for the decomposition of a mixture of volatile organic compounds," *Journal of Chemical Sciences*, vol. 125, no. 3, pp. 673–678, 2013.
- [236] L. Ai, L. Li, C. Zhang, J. Fu, and J. Jiang, "MIL-53 (Fe): A Metal–Organic Framework with Intrinsic Peroxidase-Like Catalytic Activity for Colorimetric Biosensing," *Chemistry–A European Journal*, vol. 19, no. 45, pp. 15105–15108, 2013.
- [237] R. Liang, F. Jing, L. Shen, N. Qin, and L. Wu, "MIL-53 (Fe) as a highly efficient bifunctional photocatalyst for the simultaneous reduction of Cr (VI) and oxidation of dyes," *Journal of hazardous materials*, vol. 287, pp. 364–372, 2015.
- [238] X. Zhou *et al.*, "A novel MOF/graphene oxide composite GrO@ MIL-101 with high adsorption capacity for acetone," *Journal of Materials Chemistry A*, vol. 2, no. 13, pp. 4722–4730, 2014.
- [239] L. Ai, C. Zhang, L. Li, and J. Jiang, "Iron terephthalate metal–organic framework: Revealing the effective activation of hydrogen peroxide for the degradation of organic dye under visible light irradiation," *Applied Catalysis B: Environmental*, vol. 148, pp. 191–200, 2014.
- [240] C. Zhang, L. Ai, and J. Jiang, "Solvothermal synthesis of MIL–53 (Fe) hybrid magnetic composites for photoelectrochemical water oxidation and organic pollutant photodegradation under visible light," *Journal of Materials Chemistry A*, vol. 3, no. 6, pp. 3074–3081, 2015.
- [241] X. Sun, Q. Xia, Z. Zhao, Y. Li, and Z. Li, "Synthesis and adsorption performance of MIL-101 (Cr)/graphite oxide composites with high capacities of n-hexane," *Chemical engineering journal*, vol. 239, pp. 226–232, 2014.
- [242] N. V. Maksimchuk *et al.*, "Heterogeneous selective oxidation catalysts based on coordination polymer MIL-101 and transition metal-substituted polyoxometalates," *Journal of Catalysis*, vol. 257, no. 2, pp. 315–323, 2008.

Appendix A

A. Repeatability of the system

To investigate the repeatability of the test, the inner electrode was set in two different length, L and L/2, respectively. The applied voltage into the system was increased and the changes in the rate of ozone generation were monitored. The collected data were used to quantify the statistical significance of repeatability of the test. Figure A-1 shows the results of the repeatability of these tests. A comparison between the amounts of the generated ozone in two series of tests shows the p-value of 2.65E-03 and 2.57E-05 for the two lengths of L and L/2, respectively. Since the P-values <0.05 indicate the data are statically significant; it can be definitely said that the tests are repeatable.

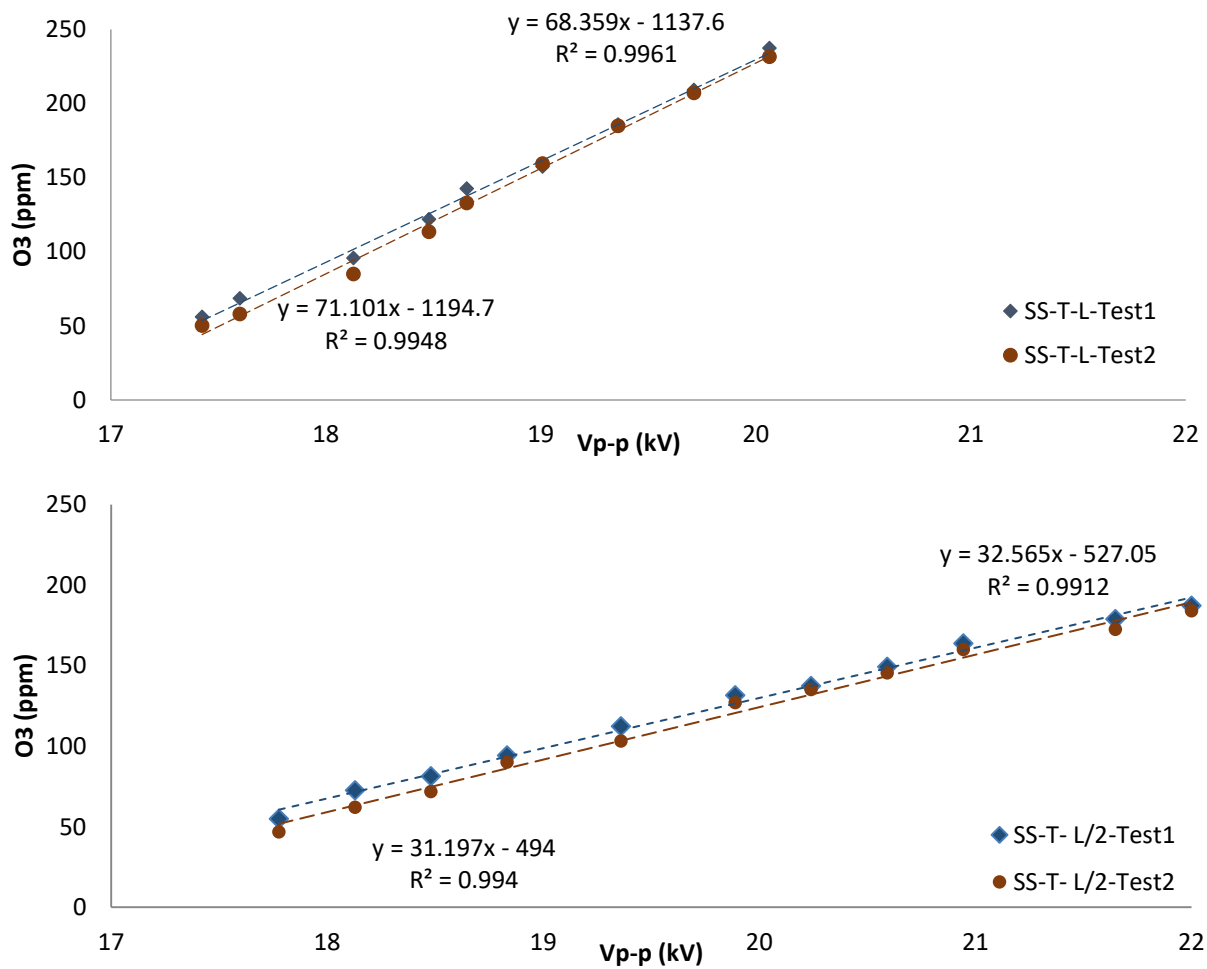


Figure A.1 The results of the repeatability of tests; Reactor#1; SS-T mesh as ground electrode; IE: L & L/2

Appendix B.

B.Detailed values of standard deviation

In Table B-1 the amounts of standard deviations (SD) quantify the dispersion of ozone concentration in a given specific input energy (SIE) for each experiment. The standard deviation is calculated using: $SD = \sqrt{\frac{\sum(x-\bar{x})^2}{n-1}}$, where x represents each ozone value in the population, \bar{x} is the mean value of the ozone concentration, and n is the number of values in the sampling. The amount of standard deviation is calculated according to at least 20 reading of ozone concentration during the test.

Table B.1 Standard deviation of ozone for different SIE (JL-1); IE size: L, L/2, and L/4; GE: SS-T, SS-F, AI, and Ag; Reactor#1

SS-T-L			SS-T-L/2			SS-T-L/4			SS-F-L			SS-F-L/2			SS-F-L/4		
SIE (J/L)	O3 (ppm)	SD															
199.1	30.3	0.70	202.2	18.5	1.75	225.2	28.6	0.86	167.9	35.4	0.70	200.9	45.4	2.54	218.2	41.1	1.30
208.7	34.3	1.44	212.8	25.3	1.72	234.7	34.2	0.88	185.6	50.8	1.07	221.0	55.3	0.99	226.2	47.0	1.27
217.6	44.0	0.94	228.2	34.7	2.66	245.2	39.9	1.07	209.5	80.2	1.13	233.3	71.5	1.45	243.4	60.3	1.57
227.9	56.0	1.85	237.9	46.6	1.80	260.0	50.7	0.98	233.0	104.9	1.19	261.5	101.4	1.61	272.4	75.1	2.51
235.2	68.6	1.91	255.4	62.0	2.04	273.3	58.5	0.72	259.5	142.1	2.73	287.3	126.1	1.02	291.6	85.8	1.65
255.7	95.8	1.58	265.9	71.8	1.73	283.5	65.7	2.04	291.5	189.3	2.14	314.2	146.4	0.86	323.1	98.3	3.06
288.9	142.8	2.29	299.8	102.0	4.34	300.5	74.4	2.04	316.9	226.0	2.74	342.3	171.4	1.25	345.5	106.3	3.52
301.1	158.5	3.30	325.2	127.0	4.77	312.6	81.6	2.23							367.4	118.2	5.60
338.4	212.2	8.58	352.4	145.4	2.28	324.2	88.4	3.80							399.9	127.2	4.18
362.8	237.6	6.59	375.4	160.0	5.08	348.4	96.7	3.04									
AI-L			AI-L/2			AI-L/4			Ag-L			Ag-L/2			Ag-L/4		
SIE (J/L)	O3 (ppm)	SD															
153.6	19.8	2.11	194.6	32.8	1.57	198.2	28.1	1.20	149.1	29.9	1.11	200.4	56.4	2.42	214.5	50.5	0.86
162.3	23.7	1.26	221.6	79.2	1.71	214.5	44.8	1.06	168.8	52.4	1.08	223.7	85.7	1.62	236.1	67.4	0.84
181.5	61.0	2.45	248.9	112.6	1.00	238.6	63.5	0.73	190.0	80.7	1.20	249.2	125.1	1.11	262.4	88.4	0.51
207.8	92.5	2.61	274.7	139.7	1.22	259.2	78.1	0.63	213.5	118.2	1.07	279.6	157.5	1.10	287.0	102.6	0.72
236.3	137.7	2.45	298.7	162.9	1.75	278.9	90.4	0.75	238.6	152.1	1.07	300.4	178.5	1.01	308.4	122.0	0.74
271.6	195.4	3.89	329.3	187.9	2.17	305.6	105.9	0.73	270.7	204.4	1.05	326.9	199.1	0.82	327.3	130.2	0.92
306.7	244.4	3.61	353.7	207.4	0.94	329.9	117.8	0.73				357.3	235.2	1.40	358.8	143.6	0.68
			382.3	217.9	1.77	355.4	131.9	0.53							385.8	157.5	0.73
						379.6	144.0	0.74									